The Three Methyls: the function and therapeutic potential of histone H3K36 trimethylation

DPhil Thesis
Supervised by Dr Timothy Humphrey

Sophia Xiao Pfister



CRUK MRC Institute for Radiation Oncology
Department of Oncology, University of Oxford

Green Templeton College

10th October 2014

All the projects in this thesis were supervised by Dr Timothy Humphrey, who has supervised the last two and a half years of my DPhil. Professor Thomas Helleday supervised the first one and a half years of my DPhil until he relocated to Sweden.

Acknowledgement

This work could not have been accomplished without my supervisor Dr Timothy Humphrey, who is very patient, caring and humorous. He guided me out of the difficult period of my DPhil and eventually helped to make my 'synthetic lethality' dream come true.

Many thanks to my previous supervisor Professor Thomas Helleday and all the wonderful members of the Helleday lab, Annette, Guy, Oliver, Bastiaan, Tina, Timi, Csanád, Sook and more who taught me many valuable research skills and made the lab life so exciting.

I am grateful for the funding provided by the Clarendon scholarship and the Department of Oncology.

I very much appreciate all the collaborators for the two papers, Enni, Sara, Sovan, Andy, Yanyan, Songmin, Vincenzo, Panos, Giulia, Mick and more. Many thanks to Songmin, an intelligent young group leader and a friend, who taught me how to ask good questions. I really admire the knowledge, efficiency and precision of Enni, who is also starting a lab of her own. The kindness, dedication

and integrity of the collaborators have set a role model for my future career.

I will always remember Sir Alan and Lady Marilyn Fersht, who met me in a conference during my A-Levels. Instead of thinking my questions about p53 were stupid, Alan encouraged me to study in Cambridge. Without them, I would not have achieved anything like this today.

I feel blessed to have my husband and my parents by my side during the DPhil journey. In addition to listening to my daily mourning over experiments that didn't work, my husband Tomas has also proof-read all 20 versions of my paper drafts and thesis. Despite doing a DPhil in engineering, he can explain SETD2 and synthetic lethality better than me. Their love taught me how to trust, hope, persevere and to rejoice with the truth.

Finally, I would like to dedicate this thesis to my grandma, a loving and intelligent woman: her fight with kidney cancer motivated me to seek cures for cancer, in the past and in the years to come. When hope seems so far away, I know I am not alone, she is with me.

Abstract

DNA is wrapped around proteins called histones, whose modification regulates numerous cellular processes. Therefore it is not surprising that mutations in the genes that modify the histones are frequently associated with human cancer. For example, mutations in *SETD2*, encoding the sole enzyme that catalyses histone H3 lysine 36 trimethylation (H3K36me3), occur frequently in multiple cancer types. This identifies H3K36me3 loss as an important event in cancer development, and also as a potential therapeutic target.

This thesis investigates the following questions: (1) how does the loss of H3K36me3 contribute to cancer development; and (2) what therapy can be used to kill cancers that have already lost H3K36me3.

To answer the first question, this thesis shows that H3K36me3 facilitates the accurate repair of DNA double-stranded breaks (DSBs) by homologous recombination (HR). H3K36me3 promotes HR by recruiting CtIP to the site of DSBs to carry out resection, allowing the binding of HR proteins (such as RPA and RAD51) to the damage sites. Thus it is proposed that error-free HR repair within H3K36me3-decorated transcriptionally active genomic regions suppresses genetic mutations which could promote tumourigenesis.

To answer the second question, this thesis reveals a clinically relevant synthetic lethal interaction between H3K36me3 loss and WEE1 inhibition. WEE1 inhibition selectively kills H3K36me3-deficient cells by inhibiting DNA replication, and subsequent fork stalling results in MUS81 endonuclease-dependent DNA damage and cell death. The mechanism is found to be synergistic depletion of RRM2 (ribonucleotide reductase small subunit), the enzyme that generates deoxyribonucleotides (dNTPs). This work reveals two pathways that regulate RRM2: one involves transcriptional activation of RRM2 by H3K36me3, and the other involves RRM2 degradation regulated by Cyclin-Dependent Kinase, CDK1 (which is controlled by WEE1, CHK1 and ATR). Based on this mechanism, the synthetic lethal interaction is expanded, from between two genes, to between two pathways. Supported by *in vivo* experiments, the study suggests that patients with cancers that have lost H3K36me3 could benefit from treatment with the inhibitors of WEE1, CHK1 or ATR.

Contents

1 Introduction **11**

1.1 Cancer and genome instability 11

1.1.1 Genome instability as a hallmark of cancer 12

1.1.2 Synthetic lethality as a cancer therapy 13

1.2 DNA Repair 15

1.2.1 Overview of DNA damage 15

1.2.2 Repair of DNA double-stranded breaks 16

1.3 Cell cycle checkpoints 23

1.3.1 DNA damage checkpoints 23

1.3.2 The intra-S checkpoint 25

1.3.3 Checkpoint kinase inhibitors as a cancer therapy 26

1.4 SETD2 and histone H3K36 trimethylation 27

1.4.1 Histone H3K36 modifications in DNA repair 32

1.4.2 Histone H3K36 modifications in DNA replication 33

1.4.3 Histone H3K36 modifications in transcription 34

1.4.4 Other functions of SETD2 36
1.4.5 The evolution of SETD2 36
1.5 Thesis Aims 37
1.5.1 Understanding the functions of SETD2 37
1.5.2 Targeting SETD2 loss by synthetic lethality 37
1.5.3 Expanding the synthetic lethal interaction to pathways . . 38

2 Materials and Methods 39

2.1 Tissue culture 39
2.1.1 Resuscitation of frozen cell lines 39
2.1.2 Maintenance of cell lines 39
2.1.3 Cryopreservation of cell lines 40
2.2 Cell lines 40
2.3 Generation of stable cell lines 42
2.3.1 Generation of stable cell lines by electroporation 42
2.3.2 Generation of stable cell lines by viral transduction 43
2.3.3 Generation of stable cell lines by 'Flip-In' 43
2.4 Site-directed mutagenesis and Gateway cloning 44
2.4.1 Site-directed mutagenesis 45
2.4.2 Gateway cloning 45
2.5 Bacterial transformation and plasmid purification 46
2.5.1 Bacterial transformation 46

2.5.2 Plasmid purification 47
2.6 Gene silencing 48
2.6.1 siRNA transfection 48
2.6.2 shRNA transduction 49
2.7 Protein detection by Western blotting 49
2.7.1 Detection of proteins by Enhanced Chemiluminescence . . 49
2.7.2 Detection of histone modifications by Infrared Fluorescence 51
2.8 Antibodies 52
2.9 Inhibitors 52
2.10 Cell survival assays 53
2.10.1 Clonogenic survival assay 53
2.10.2 Resazurin assay for cell viability 53
2.11 Assay for apoptosis 54
2.12 DNA fiber assay using CldU/IdU labelling 55
2.13 Cell cycle analysis by BrdU incorporation 56
2.14 Reporter assay for determining DNA repair pathways 56
2.15 Analysing repair foci by Incell 58
2.16 Microirradiation for studying the recruitment of repair proteins . 58
2.17 Co-Immunoprecipitation 59
2.18 iPOND (isolation of proteins on nascent DNA) 60
2.19 The comet assay 61
2.19.1 The alkaline comet assay 61

2.19.2 The neutral comet assay 62
2.20 Measurement of dNTP levels 62
2.21 qRT-PCR (Quantitative reverse transcription polymerase chain reaction) 63
2.22 ChIP (Chromatin Immunoprecipitation) 64
2.23 Xenograft studies 65

3 A new role for H3K36me3 in homologous recombination repair 66

3.1 SETD2 is required for the repair of DNA double-stranded breaks . 67
3.2 SETD2 is involved in homologous recombination 69
3.3 An early role for SETD2 in the HR process 73
3.4 The methyltransferase activity of SETD2 is required for HR . . . 80
3.5 Histone H3K36 trimethylation is required for HR 86
3.6 SETD2 promotes DSB end-resection 92
3.7 Discussion of Chapter 3 98
3.7.1 The SETD2 in HR model 98
3.7.2 Future directions 99

4 A new synthetic lethal interaction: SETD2 and WEE1 101

4.1 SETD2-deficient cancer cells are hypersensitive to WEE1 inhibition 102
4.2 WEE1 inhibition induces mitotic catastrophe in p53-deficient cells, but not in SETD2-deficient cells 107

4.3 WEE1 inhibition induces replication stalling in SETD2-deficient cells . . . 114
4.4 MK1775 inhibits replication fork progression and increases fork stalling in SETD2-deficient cells . . . 118
4.5 Replication stress is converted into lethal DNA damage by MUS81 125
4.6 SETD2 and WEE1 regulate RRM2 and the dNTP pool . . . 126
4.7 SETD2 in transcriptional activation . . . 138
4.8 The synthetic lethality model . . . 141
4.9 *In vivo* efficacy of the WEE1 inhibitor MK1775 on SETD2-deficient tumors . . . 143
4.10 Discussion of Chapter 4 . . . 145

5 From genes to pathways: a synthetic lethal interaction between H3K36me3 and CDK1 regulators 150

5.1 SETD2-deficient cells are hypersensitive to CHK1 and ATR inhibition . . . 151
5.2 H3K36me3-deficient cells are hypersensitive to WEE1, CHK1 and ATR inhibition . . . 156
5.2.1 H3.3K36M expression sensitises cells to WEE1, CHK1 and ATR inhibitors . . . 160
5.2.2 KDM4A over-expression sensitises cells to WEE1, CHK1 and ATR inhibitors . . . 162

5.3 WEE1, CHK1 and ATR all arrest SETD2-deficient cells in S-phase 163

5.4 H3K36me3 and CDK1 represent two redundant pathways that regulate RRM2 169

5.4.1 CDK1 hyper-activation due to WEE1, CHK1 and ATR inhibition degrades RRM2 169

5.4.2 H3K36me3 depletion reduces RRM2 and mildly affects DNA replication 170

5.4.3 CDK1 and H3K36me3 redundantly regulate RRM2 173

5.5 The synthetic lethal model 175

5.6 Discussion of Chapter 5 176

6 Discussion **180**

6.1 The current understanding of SETD2 in DNA repair 180

6.1.1 Human SETD2 is required for DSB repair by homologous recombination 181

6.1.2 Is SETD2 required for DNA damage sensing? 183

6.1.3 The relationship between H3K36 dimethylation and trimethylation in DNA repair 184

6.2 Potential interplay between SETD2's role in HR and DNA replication 188

6.2.1 Do the two functions originate from the same molecular mechanism? 189

6.2.2 Can the role of SETD2 in HR contribute to the synthetic lethality? . . . 190
6.2.3 Can the role of SETD2 in dNTP production contribute to its function in HR? . . . 194
6.3 Additional ways to make use of this synthetic lethal interaction . 196
6.3.1 Enhancing the efficacy by increasing DNA damage . . . 197
6.3.2 Enhancing the efficacy by inhibiting the DDR response . . 201
6.3.3 Enhancing the efficacy by increasing replication stress . . . 202
6.3.4 Treating ATR, CHK1 or WEE1-deficient cancers with SETD2 inhibitors . . . 205
6.4 Future directions . . . 206
6.4.1 How does H3K36me3 control transcriptional activation? . 206
6.4.2 Is RRM2 the entire story? . . . 209
6.4.3 Other combinational therapies . . . 217
6.4.4 Do the kinases work through the same mechanism? . . . 222
6.4.5 Which kinase has the best therapeutic potential? . . . 223
6.4.6 The resistance mechanism . . . 226
6.4.7 How can these discoveries serve patients? . . . 226
6.4.8 SETD2 and cancer stem cells . . . 228
6.5 Summary . . . 228

7 Appendix **230**

Chapter 1

Introduction

1.1 Cancer and genome instability

According to World Health Organization (WHO), in 2012 there were 14.1 million new cancer cases, 8.2 million cancer deaths and 32.6 million people living with cancer worldwide (Globocan 2012, IARC). According to Cancer Research UK (CRUK), more than 1 in 3 people in the UK will develop some form of cancer during their lifetime, and only 50% of the people diagnosed with cancer will survive for more than 10 years (CRUK 2014). As the rate of cancer incidence continue to rise (Globocan 2012, IARC), cancer has become the number one fear for the British public (CRUK 2014).

Owing to the advances in medicine, cancer survival rates in the UK have doubled in the last 40 years. Responding to the call to increase the survival rate to 75% within the next 20 years (CRUK 2014), we are urged to understand the

disease better and to discover new ways to prevent, diagnose and treat cancer.

1.1.1 Genome instability as a hallmark of cancer

In the revised Hallmarks of Cancer, genome instability is defined as an 'enabling characteristic' of cancer (Hanahan and Weinberg, 2011). The authors proposed that the genomic instability generates random mutations that occasionally introduce genetic changes that help cancer cells to acquire the other hallmarks, such as sustained proliferation signalling, angiogenesis, metastasis and resistance against cell death (Hanahan and Weinberg, 2011).

Genome instability (such as chromosomal rearrangement, copy number changes, and DNA sequence mutations) is observed in a large number of human cancer cells, and a wide range of genes in DNA damage response and repair are found to be mutated in cancers (Ciccia and Elledge, 2010; Jackson and Bartek, 2010). This suggest that genome instability is common and facilitates cancer progression and drug resistance.

While mutations in DNA repair genes can generate mutations that drive tumorigenesis, inhibiting DNA repair can also cause cell death through elevated DNA damage. This is a rationale for us to find new DNA repair genes, and target their defects in cancer for the purpose of therapy.

1.1.2 Synthetic lethality as a cancer therapy

One way of targeting genetic defects in cancer is the concept of synthetic lethality. Synthetic lethality describes a genetic interaction between two genes or two pathways, where loss of either one alone has little effect on cell viability, but the simultaneous loss in both results in cell death. Therefore synthetic lethal interactions can be exploited to selectively kill cancer cells that carry mutations in one of the genes in the interaction by chemically inhibiting the second gene (Chan and Giaccia, 2011).

The first clinically relevant synthetic lethal interaction described in human is between the PARP inhibitor and BRCA1/2 deficiency (Bryant et al., 2005; Farmer et al., 2005). To date, approximately 190 papers have been published reporting the underlying mechanisms of this synthetic lethal interaction, related drug combinations or clinical trial results. Many different hypotheses have been proposed for the mechanism of interaction, and PARP has been shown to be involved in a number of functions including base excision repair, replication fork restart, alternative-NHEJ etc. (Michels et al., 2013; Helleday, 2011). A unifying theme is that the simultaneous loss of PARP and BRCA1/2 leads to the accumulation of DNA double-stranded breaks that are lethal to the cells. Since BRCA1/2 are essential for the homologous recombination (HR) repair pathway, their interaction has been expanded from defining the relationship between two genes to defining the relationship between two pathways (Michels et al., 2013):

cancer cells with a wide range of mutations that abolish HR were reported to be sensitive to PARP inhibitors (Michels et al., 2013).

Encouraged by the 100-fold differential response between BRCA-negative and BRCA-positive cells reported in (Farmer et al., 2005), 108 clinical trials on PARP inhibitors are underway (ClinicalTrials.gov). Curiously, more negative results were received than positive. The PARP inhibitor Iniparib failed FDA approval as it did not significantly improve the survival of advanced triple-negative breast cancer patients (Mateo et al., 2013). However, the failure of Iniparib is not surprising as the trial did not select patients based on their BRCA status, probably because Iniparib is not a true PARP inhibitor (Liu et al., 2012b; Patel et al., 2012). A re-analysis of the clinical trials on the PARP inhibitor Olaparib showed that although it did not improve overall survival in patients with BRCA defects, it did improve progression-free survival (Ledermann et al., 2014). Encouraged by the re-analysis, Olaparib is currently in two Phase III clinical trials (Ledford, 2014).

In addition to PARP and BRCA, other clinically relevant synthetic lethal interactions have been reported, for example, between PTEN loss and the mTOR inhibitor (Neshat et al., 2001); VHL loss and CDK4/6 inhibitors (Bommi-Reddy et al., 2008); RAS gain and the CDK4 inhibitor (Puyol et al., 2010). However, 'although several years have passed since the initial reports on the PARP-BRCA synthetic lethality, we have so far not seen any other synthetic lethal approach reach the clinic', said one of the authors involved in the initial discovery (Helleday,

Types of DNA damage	Single-stranded breaks  Single base damage 	Bulky-adducts  Crosslinks 	Mismatch 	Double-stranded breaks 
Repair pathway	Base excision repair (BER)	Nucleotide excision repair (NER)	Mismatch repair (MMR)	HR, NHEJ alt-NHEJ, SSA
Key proteins	PARP1/2 XRCC1 Polβ LigIII	XP proteins ERCC1 Polδ LigI	MSH2/3/6, MLH1 EXO1 Polδ LigI	Pathway-dependent see below

Table 1.1: Different forms of DNA damage and their repair pathways.

2011). Perhaps it is time to provide more examples showing that this concept could indeed be used for patient benefit.

1.2 DNA Repair

1.2.1 Overview of DNA damage

Cellular DNA can be damaged by various external and internal factors. DNA damage is potentially lethal if left unrepaired, and their mis-repair can give rise to genome instability (Jeggo and Lavin, 2009). To survive and maintain genome stability, cells employ several pathways to repair DNA damage. There are multiple forms of DNA damage, each repaired by one or more pathways as described below and summarised in Table 1.1.

DNA single-stranded breaks (SSBs) and single base damage can be generated

by ionising radiation (IR) or oxidising agents. They are repaired predominantly by base-excision repair (BER) (David et al., 2007).

DNA helix-distorting base lesions, such as bulky-adducts and cross-links, can be generated by chemicals or UV light. They are repaired mainly by nucleotide-excision repair (NER). In addition, some of these lesions are bypassed by translesion synthesis, catalysed by special DNA polymerases such as Polη (Loeb and Monnat, 2008).

DNA mismatches usually originate from DNA synthesis, when the microstallite sequences re-anneal incorrectly, or when errors caused by DNA polymerases are not proofread properly (Jiricny, 2006). These partnerless nucleotides are removed by the mismatch repair machinery (Jiricny, 2006).

DNA double-stranded breaks (DSBs) can be caused by ionising radiation (IR), chemotherapeutical agents, replication across a SSB, colocalisation of two SSBs, enzymatic activity, or through the collapse of replication forks (Jackson and Bartek, 2010). DNA double-stranded breaks (DSBs) are probably the most lethal DNA lesions, and a single unrepaired DSB can kill the cell. The pathways that repair DSBs are described in detail below.

1.2.2 Repair of DNA double-stranded breaks

DNA double-stranded breaks (DSBs) can be repaired through multiple pathways. There have been various views on how many independent pathways there are in

DSB repair. The most common view is two: homologous recombination (HR) and non-homologous end-joining (NHEJ). However, recent literature suggests that there may be more, based on the requirement of resection and the key proteins involved.

According to (Ciccia and Elledge, 2010), there are four independent DSB pathways: HR, NHEJ, micro-homology mediated end-joining (MMEJ) (which the authors refer to as alternative-NHEJ), and single-strand annealing (SSA) (Fig 1.1). After DSB, classical NHEJ is initiated by KU binding without needing DNA end resection, but the other three pathways (MMEJ, HR, and SSA) all require resection (Ciccia and Elledge, 2010). The resection length is shorter in MMEJ (5 – 25 nt) than in HR and SSA (Hartlerode and Scully, 2009). Each pathway utilises a range of repair proteins. While some proteins overlap, others are unique, and thus may help to distinguish the pathways: for example, LIG4 (NHEJ); LIG3 (MMEJ); RAD51 (HR) and ERCC1/XPF (SSA). The key steps in each pathway are described below.

Homologous recombination

Homologous recombination (HR) usually occurs in S and G2 phases of the cell cycle due to the presence of sister chromatids, which can serve as the template for homology-directed synthesis. DSBs are recognised by the MRE11-RAD50-NBS1 (MRN) complex, which activates ATM (Williams et al., 2007). ATM in turn activates CtIP, which initiates HR by $5'$ end resection, and generates a $3'$

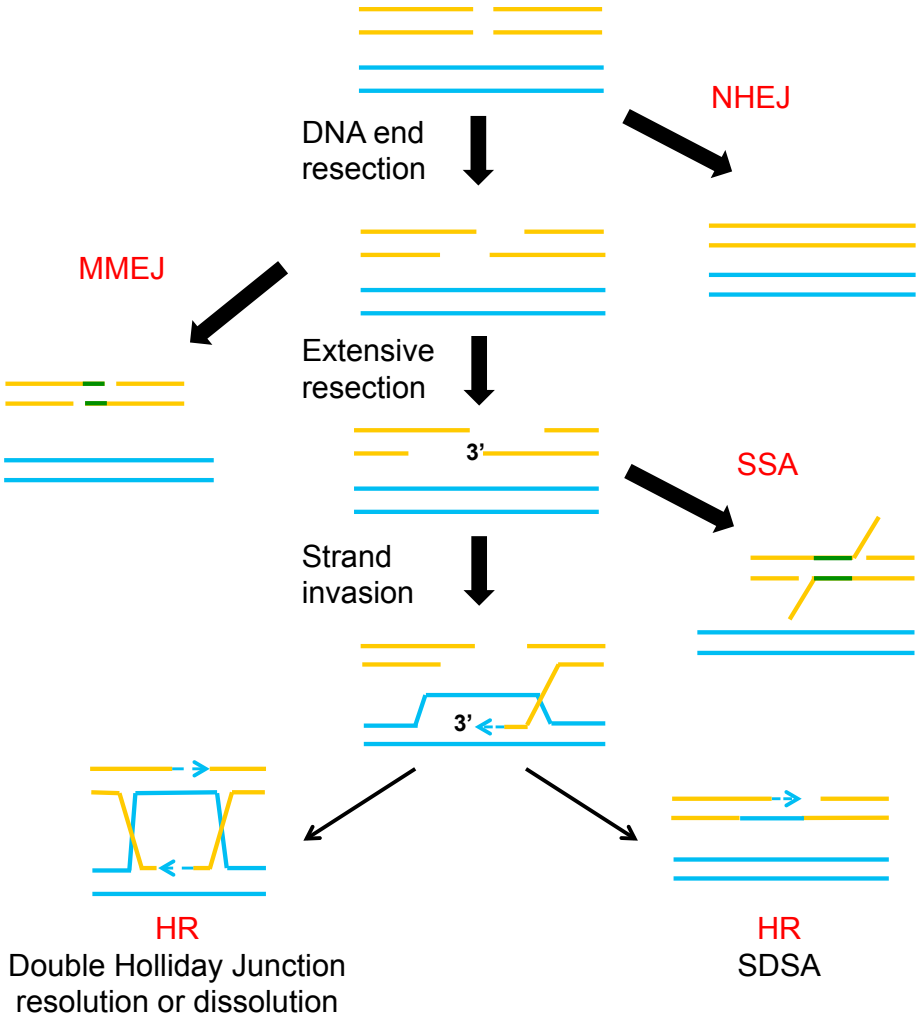


Figure 1.1: Overview of the four key pathways that repair DNA double-stranded breaks. Non-homologous end-joining (NHEJ) does not require resection; micro-homology mediated end-joining (MMEJ) requires minimal resection; single-stranded annealing (SSA) requires extensive resection; and homologous recombination (HR) requires extensive resection followed by strand invasion.

single-stranded DNA (ssDNA) overhang (You and Bailis, 2010).

Following initial resection by CtIP, extensive resection is performed by EXO1 together with DNA2-BLM. The ssDNA generated by resection is bound by replication Protein A (RPA) (Wold, 1997), which stabilises the ssDNA and recruits RAD51. BRCA2, regulated by ATM/ATR (Matsuoka et al., 2007) and CDK (Esashi et al., 2005), binds to RAD51 and loads RAD51 onto RPA-coated DNA. The RAD51 nucleofilament promotes strand invasion of the sister chromatid, which is used as a template for homology-directed synthesis.

After homology-directed synthesis, the invading strand can directly reanneal to the other end, in a process called synthesis-dependent strand annealing (SDSA), mediated by RTEL1 helicase (Barber et al., 2008). Alternatively, holliday junctions are formed if the invading strand is ligated with the other end inside the D-loop, and the holliday junctions can be resolved by GEN1, MUS81/EME1 or SLX1/SLX4 (Ciccia and Elledge, 2010). The key steps of the HR process are summaried in a schematic diagram (Fig 1.2).

Non-homologous end-joining

Non-homologous end-joining (NHEJ) can occur in all phases of the cell cycle. During classical NHEJ the broken ends are rapidly bound and protected by the KU70/KU80 heterodimer, which recruits and activates the catalytic subunit of DNA-PK (DNA-PKcs) (Mahaney et al., 2009). DNA ends can be processed by ARTEMIS prior to ligation, but excessive processing is prevented by DNA-PKcs

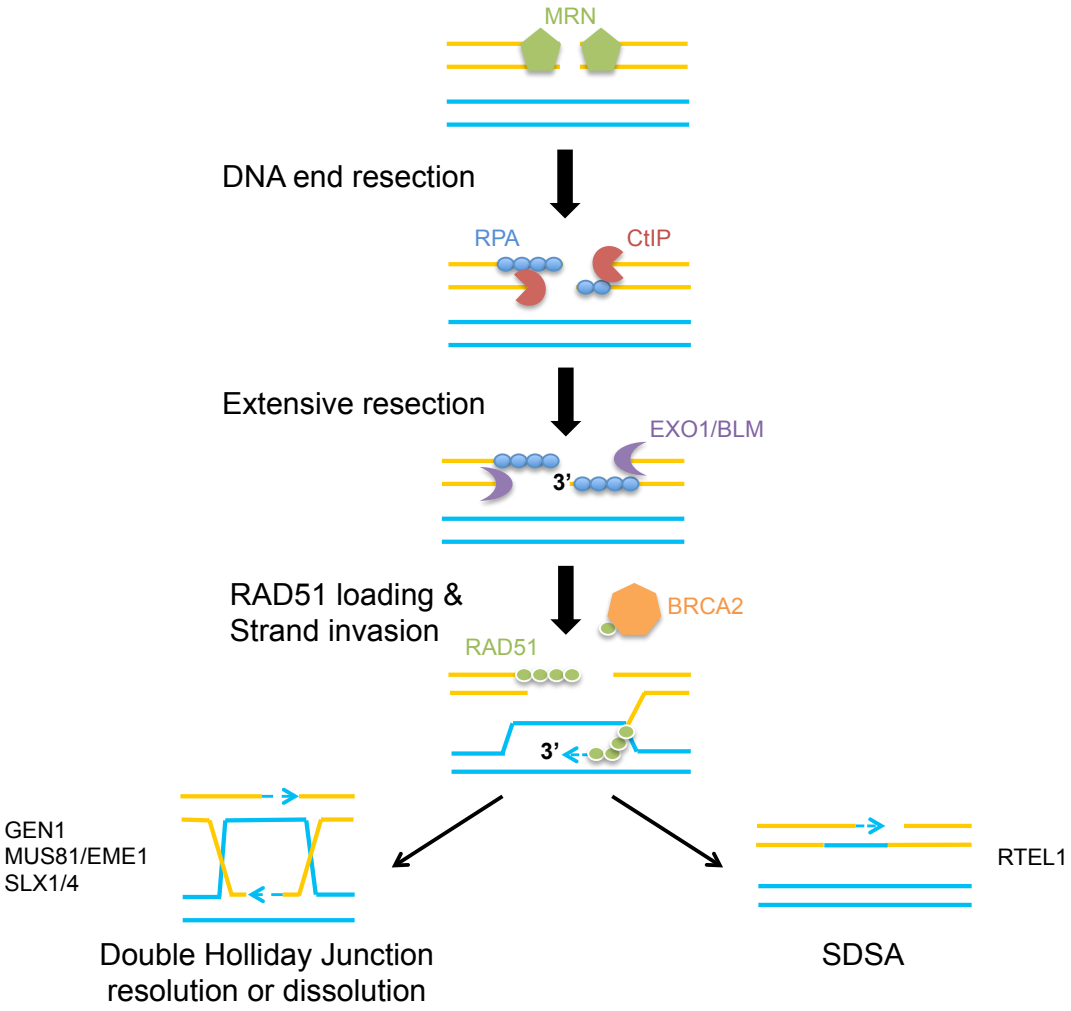


Figure 1.2: The key steps and key proteins involved in homologous recombination repair.

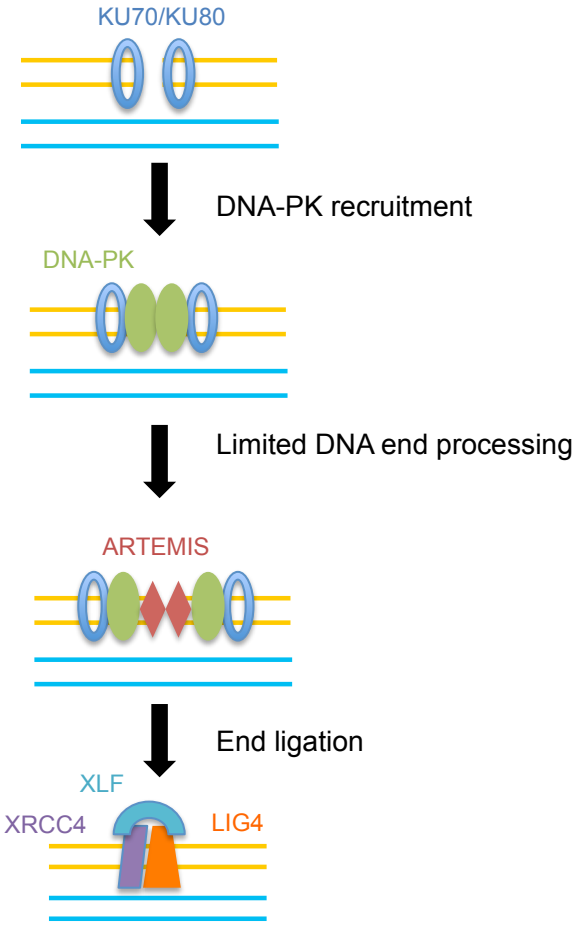


Figure 1.3: The key steps and key proteins involved in non-homologous end-joining repair.

(Meek et al., 2008). XRCC4/LIG4 and XLF are subsequently recruited and promote the religation of the broken ends in a template-independent manner, which can lead to inaccurate repair (Lieber, 2010). The key steps of NHEJ are summarised in a schematic diagram (Fig 1.3).

Microhomology-mediated end-joining

Current literature suggests that there are at least two alternative end-joining pathways: one requires microhomology and LIG3 (presumably the Microhomology-

mediated end-joining (MMEJ) pathway); the other pathway does not depend on microhomology and requires LIG1 (Simsek et al., 2011).

The switch from classical NHEJ to MMEJ is probably by PARP1 (Wang et al., 2006), which competes with KU and also functions to protect HR from NHEJ (Hochegger et al., 2006). MMEJ is initiated by limited resection. The end-joining process is mediated through annealing of short direct repeats of microhomology, and is catalysed by LIG3. MMEJ leads to deletions as well as chromosomal rearrangements (McVey and Lee, 2008).

Curiously, the resection step for both MMEJ and HR is carried out by CtIP. However, the regulation of CtIP in G1 and S/G2 are different: in S/G2, CtIP is phosphorylated at S327 (Yun and Hiom, 2009) and associates with BRCA1, which ubiquitinates CtIP and facilitates its association with damage sites (Huen et al., 2010). In G1, CtIP is phosphorylated by Polo-like kinase 3 (PLK3) at T847, which activates CtIP specifically in G1, promotes MMEJ and increases the incidence of chromosome translocations (Barton et al., 2014).

Single-strand annealing

Single-strand annealing (SSA) is initiated by resection mediated by CtIP and EXO1/BLM (Ciccia and Elledge, 2010). Following resection, RAD52 catalyses direct annealing of $3'$ ssDNA ends with homologous sequences, and the $3'$ flap (the stretch of ssDNA which cannot pair with the homology sequence) is removed by the ERCC1/XPF endonuclease (Motycka et al., 2004). SSA does not occur fre-

quently in G1 (Al-minawi et al., 2008), and can lead to gene conversion, deletions and translocations.

1.3 Cell cycle checkpoints

1.3.1 DNA damage checkpoints

Cells have evolved a complex DNA damage response (DDR), which functions to maintain genome stability under conditions of genotoxic stress. The DDR responses – DNA repair, DNA replication, cell cycle arrest, transcription and apoptosis – are coordinated by the DNA damage checkpoint protein kinases ATM (Ataxia telangiectasia mutated) and ATR (ATM and Rad3-related), which have a wide range of overlapping substrate specificities (Jackson and Bartek, 2010; Sø rensen and Syljuå sen, 2012).

ATM is activated by DSBs and is primarily responsible for the activation of the CHK2 kinase (Ahn et al., 2004). In contrast, ATR (activated by RPA-ATRIP) responds to single-stranded DNA (ssDNA) arising at stalled replication forks or at resected DNA double-strand breaks (Zou and Elledge, 2003), and primarily phosphorylates and activates the CHK1 kinase (Mordes and Cortez, 2008). After activation, CHK2 and CHK1 can arrest the cell cycle at G1, S or G2/M checkpoints by inhibiting CDC25A, CDC25B and CDC25C to allow DNA repair (Bouwman and Jonkers, 2012) (Fig 1.4).

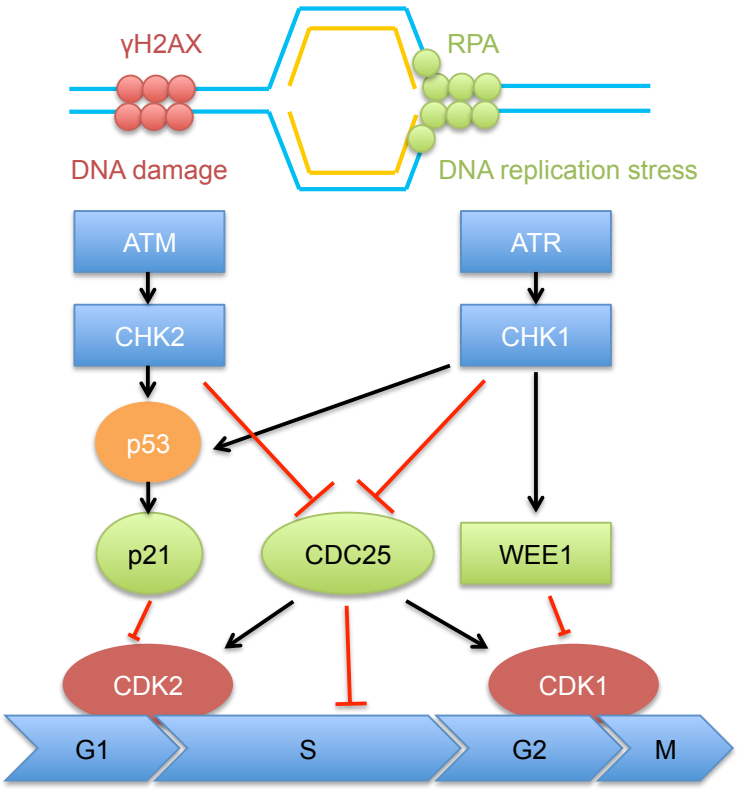


Figure 1.4: The DNA damage checkpoints. In response to DNA damage or replication fork stalling, two signalling cascades mediated by ATM and ATR arrest the cells in G1/S, S or G2/M by modulating the activity of cyclin-dependent kinases (CDK1 and CDK2).

Two CDC25-independent mechanisms for arresting the cell cycle are through p53 or WEE1. ATM and CHK2 can activate p53 (and its target p21), which inhibits CDK2 and arrests cells in the G1/S checkpoint. The WEE1 kinase delays entry into mitosis by adding inhibitory phosphorylation on CDKs in both stressed and unperturbed cell cycles (Parker and Piwnica-Worms, 1992; McGowan and Russell, 1995) (Fig 1.4).

1.3.2 The intra-S checkpoint

The intra-S-phase checkpoint has two functions in response to replication stress or DNA damage during S-phase: inhibiting unfired origins, and/or stabilising stalled replication forks to allow fork restart.

Following disruption of replication, the ATR/CHK1 pathway functions to prevent the firing of late replication origins, to inhibit further unwinding of MCM2, to stabilise the stalled fork, and to arrest the cell cycle (Cimprich and Cortez, 2008) (Fig 1.5).

In response to genotoxic insults such as ionising radiation, UV light or mitomycin C in S-phase, the intra-S checkpoint can be activated through two mechanisms. (1) The ATM/ATR–CHK2/CHK1 signalling cascade inhibits CDK2 activity and blocks the loading of CDC45 onto the chromatin. Since CDC45 is required for the recruitment of DNA polymerase alpha onto pre-replication complexes (pre-RC), the lack of CDC45 prevents the firing of new origins (Bartek et al., 2004). (2) ATM activates NBS1, SMC1 (cohesin protein) and FANCD2 (Fanconi anaemia complementation group D2), which function to inhibit DNA synthesis until the damage is repaired (Nakanishi et al., 2002) (Fig 1.5).

In addition to restraining CDK activity in response to exogenous DNA damage or collapsed replication forks, recent evidence has highlighted the importance of restraining CDK activity during the normal S-phase. During DNA replication, ATR, CHK1 and WEE1 control CDK activity to prevent aberrant origin firing

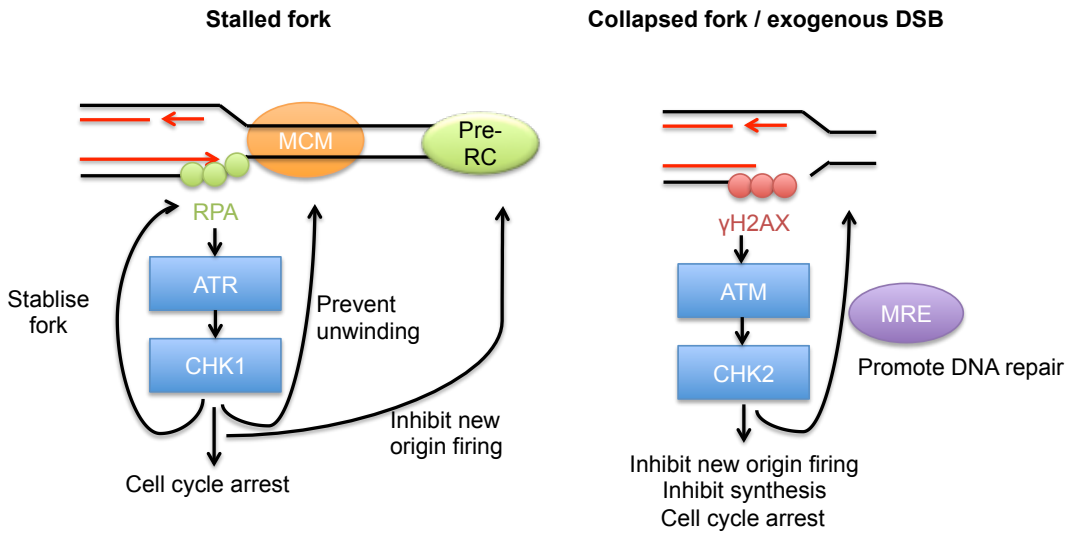


Figure 1.5: The intra-S checkpoint. ATR/CHK1 is primarily responsible for signalling stalled replication forks, while ATM/CHK2 respond to DNA double-stranded breaks during S-phase.

(which can lead to nucleotide depletion) (Beck et al., 2012), and promote replication fork stability and restart. Depletion or inhibition of these kinases leads to DNA double-stranded breaks arising from MUS81-EME1 mediated cleavage of stalled replication forks (Martín et al., 2011). WEE1 also directly regulates the MUS81-EME1 endonuclease activity (Martín et al., 2011).

1.3.3 Checkpoint kinase inhibitors as a cancer therapy

A number of small molecule inhibitors for ATR, CHK1 and WEE1 have been developed, and primarily used to sensitise cancers to DNA damaging reagents through abrogation of DNA damage response. For example, the ATR inhibitor VE821 selectively sensitises pancreatic cancer cells and hypoxic cancer cells to radiation (Prevo et al., 2012; Pires et al., 2012). One of the CHK1 inhibitors

LY2603618 has been tested in combination with Pemetrexed in Phase I trials (Weiss et al., 2013; Calvo et al., 2014). The WEE1 inhibitor MK1775 in combination with gemcitabine, cisplatin or carboplatin, has shown promising activity in patients with advanced solid tumours in Phase I trials (Do et al., 2013).

However, combining the inhibitors with DNA damage is inevitably toxic for normal tissue as non-cancer cells also rely on ATR/CHK1/WEE1 for repairing DNA damage. The recent discovery of the synthetic lethal interaction between p53-deficiency and ATR, CHK1 or WEE1 inhibition sheds light on the targeted use of these inhibitors (Aarts et al., 2012; Kohn et al., 2003; Reaper et al., 2011). However, other publications argue that these inhibitors may also chemosensitise cancer cells independent of their p53 status (Van Linden et al., 2013). In addition, some p53 negative cells may not be hypersensitive to these inhibitors due to additional genetic changes that compensate for the loss of p53, such as the basal (p53-independent) pools of p21 (Origanti et al., 2012).

1.4 SETD2 and histone H3K36 trimethylation

Identifying and exploiting driver mutations in cancers is central to personalised cancer medicine. Mutations in the human SETD2 (SET domain-containing 2) gene have been recently identified in several cancer types, including breast (Al Sarakbi et al., 2009; Newbold and Mokbel, 2010), lung (Gerlinger et al., 2012), renal carcinomas (ccRCC) (Duns et al., 2010; Dalgliesh et al., 2010; Hakimi et al.,

2013), high-grade gliomas (HGG) (Fontebasso et al., 2013) and acute lymphoblastic leukemia (ALL) (Zhang et al., 2012), leading to its classification as a novel tumour suppressor. SETD2 is also identified as one of the most frequently mutated genes (Lawrence et al., 2014), justifying it as an important target for therapeutic intervention.

The SETD2 gene and protein

The SETD2 gene (also known as Huntingtin-interacting protein B, HYPB) is located on the short arm of chromosome 3 (3p21.31), spanning 147.57 kb across 21 exons and encodes a protein of 2564 amino acids. The SETD2 protein contains a SET domain (flanked by the AWS and Post-SET domain), which is responsible for the catalytic activity of SETD2. The WW domain regulates the interaction between SETD2 and the huntingtin protein, contributing to the pathology of Huntington's disease (Gao et al., 2014). The SRI domain mediates the binding of SETD2 to RNA polymerase II (Li et al., 2005), which is required for the transcriptional-associated trimethylation of H3K36 (Fig 1.6).

There are various processes in cancer that contribute to the loss of SETD2. Sequence analysis indicates that loss of function could be caused by various types of mutations, including missense, substitution nonsense and frameshift mutations (Sanger Insititute). Large deletions on chromosome 3p (frequently observed in renal cancers) can also lead to deletion of the SETD2 gene. Down-regulation of SETD2 transcription by aberrant promoter hypermethylation was found to be

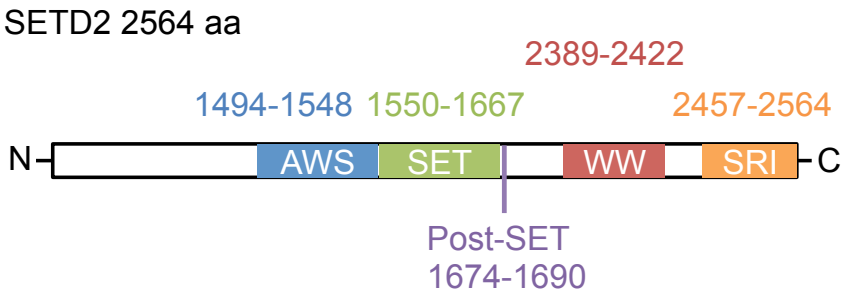


Figure 1.6: The SETD2 protein consists of a AWS-SET-postSET domain (for catalytic activity), a WW domain (for binding Proline-rich sequences such as huntingtin) and an SRI domain (for interaction with RNA polymerase II).

rare, at least in renal cancer (Ibragimova et al., 2013).

The histone H3K36 methylation

In humans, H3K36 methylation is catalysed through the activities of eight distinct enzymes. Out of these, seven (NSD1, NSD2, NSD3, SETMAR, ASH1L, and SETD3) are responsible for H3K36 mono- and/or di-methylation, while the eighth (SETD2) uniquely catalyses the di- to tri-methylation of H3K36 (Sun et al., 2005; Edmunds et al., 2008) (Fig 1.7).

In addition to the methyltransferases that set the mark, various other genes or mutations can also affect the levels of H3K36me3 in the cell. Here are some examples:

The KDM4/JMJD2 family of histone demethylases removes the tri- and di-methylation of H3K36 and H3K9 (Berry and Janknecht, 2013; Klose et al., 2006; Whetstine et al., 2006). Various studies have shown that KDM4A, KDM4B, and/or KDM4C are overexpressed in breast, colorectal, lung and prostate cancers,

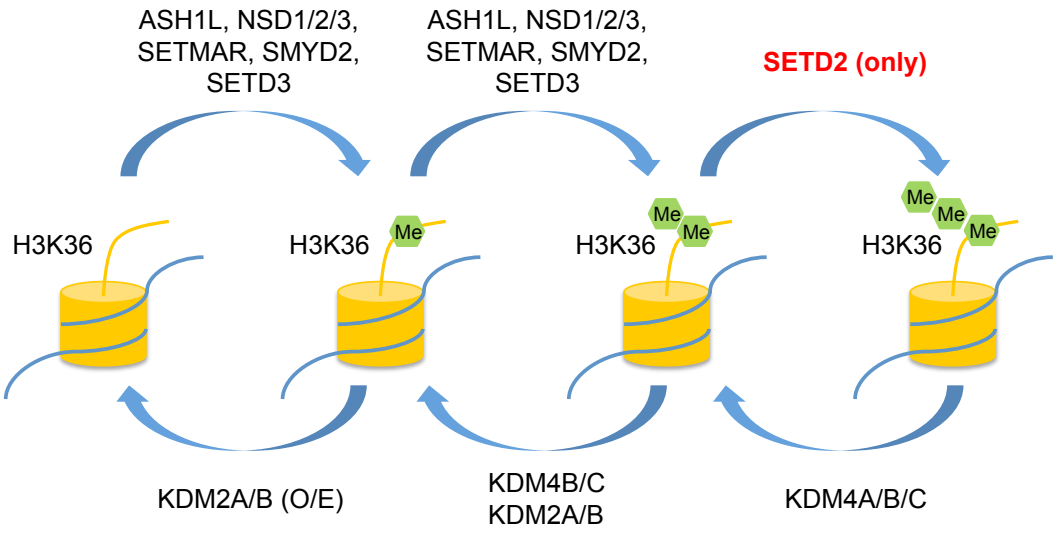


Figure 1.7: The methyltransferases and demethylases that regulate H3K36 methylation states. O/E, the activity is only seen when the demethylases are over-expressed.

and are required for efficient cancer cell growth (Berry and Janknecht, 2013).

NSD1 methylates H3K36me and H3K36me2 (Fig 1.7) and the loss of NSD1 can reduce the levels of all three forms of H3K36 methylation (Lucio-Eterovic et al., 2010). Therefore mutations in other H3K36 methyltransferases can also reduce H3K36me3 by failing to provide the histone substrate for SETD2.

Histone H3.3 mutation (G34R/V) identified in paediatric high-grade glioma (HGG) reduces H3K36me3/me2 (Fontebasso et al., 2013; Lewis et al., 2013). In addition, exogenous expression of the transgene H3.3K36M reduces global levels of H3K36me3/me2, probably through inhibition of SET domain-containing proteins that catalyses H3K36me2 and H3K36me3 (Lewis et al., 2013).

Global levels of H3K36me3 can also be affected by the tumorigenic mutations in the Isocitrate dehydrogenase 1 (IDH1) gene, which leads to hyperactive IDH1,

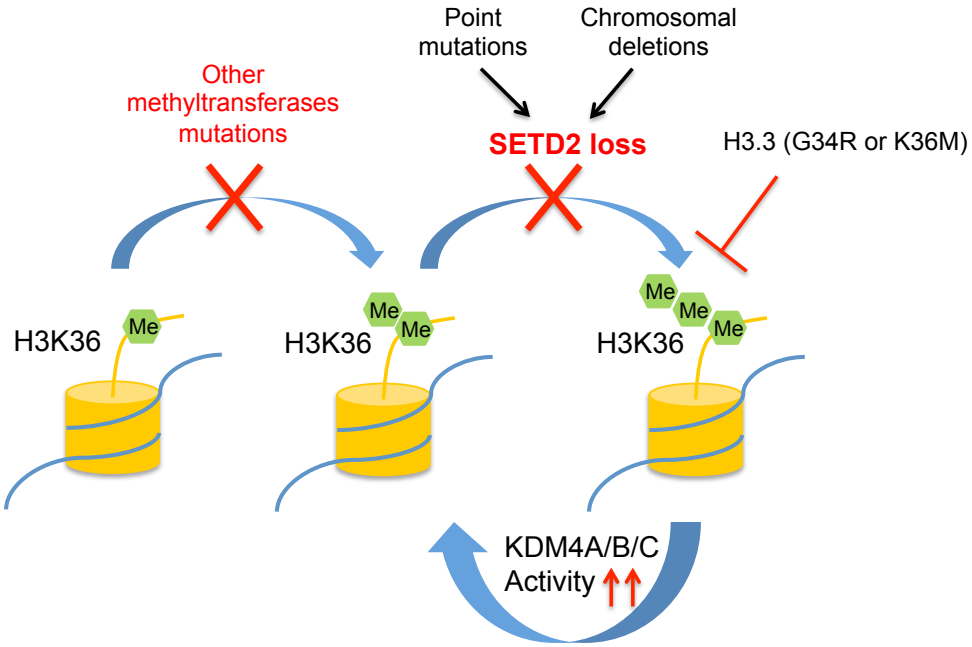


Figure 1.8: The mechanisms of histone H3K36me3 loss.

whose product (2HG) inhibits KDM4 proteins, leading to increased levels of H3K36me3 (Yang et al., 2012).

In fact, SETD2 mutation or histone H3.3 mutation together results in H3K36me3 deficiency in 43% of paediatric HGG (Fontebasso et al., 2013), as frequently as p53 defects are observed in some cancers. This suggest that cancer cells have evolved several methods for reducing the levels of H3K36me3, and therapeutic targeting of H3K36me3 deficiency would benefit a broader patient population than targeting SETD2 deficiency alone (Fig 1.8).

1.4.1 Histone H3K36 modifications in DNA repair

DNA repair can be facilitated through chromatin modification by chromatin remodelling complexes, by incorporation of histone variants, and by histone modification (Smeenk and van Attikum, 2013).

Roles for H3K36 modification have been identified in DNA repair. For example, H3K36me2 increases at DSB sites and enhances DNA repair by non-homologous end joining (NHEJ) through recruiting NBS1 and KU70 repair factors (Fnu et al., 2011).

Furthermore, H3K36me3 has also been shown to regulate DNA mismatch repair by recruiting the mismatch repair protein MSH6 to the chromatin, bringing it closer to the DNA replication machinery (where mismatch lesions first occur) (Li et al., 2013). However, SETD2-deficient cancers exhibit a wide range of mutations, including insertions, deletions, and chromosomal aberrations (Sato et al., 2013; Zhu et al., 2014), which usually stem from mis-repair of DSBs. This suggests an additional role for SETD2 in genome stability, likely through accurate repair of DSBs.

This accurate repair of DSBs is carried out by the homologous recombination (HR) pathway. To associate H3K36me3 with HR, the protein LEDGF provides a viable link. LEDGF is constitutively associated with the chromatin through its PWWP domain that binds preferentially to H3K36me2/me3, and it was found to promote DNA-end resection and HR through recruiting the resection protein

CtIP to DSBs (Daugaard et al., 2012).

1.4.2 Histone H3K36 modifications in DNA replication

The role of human SETD2 in normal or stressed DNA replication has not yet been described, despite the observation that H3K36me3 levels peak at G1 and S-phase (Li et al., 2013).

The H3K36me2 methyltransferase Metnase is reported to be required for the restart of stalled replication forks without affecting replication fork progression (de Haro et al., 2010). For a NHEJ protein to be involved in replication fork restart, the authors argued that Metnase is involved in TopoIIα-mediated relaxation of positively supercoiled DNA (de Haro et al., 2010). However, since Metnase is both a histone methylase and endonuclease, the restart function may be due to its endonuclease activity (Shaheen et al., 2010).

The evidence for H3K36 in replication initiation comes from studies in yeast. Set2 regulates replication origin firing, and the deletion of Set2 causes a delay in the loading of Cdc45 (human CDC45, required for origin firing) at replication origins (Pryde et al., 2009).

1.4.3 Histone H3K36 modifications in transcription

Suppression of intragenic transcription

Various studies have suggested that human SETD2 prevents intragenic or cryptic transcription of active genes. One study showed that H3K36me3 recruits histone H3K4me2/3 demethylase KDM5B, which represses cryptic transcription by removing intragenic H3K4me3 (which usually marks promoters) (Xie et al., 2011). Another study showed that SETD2 promotes loading of FACT (Facilitates Chromatin Transcription), which maintains nucleosome occupancy after transcription (Carvalho et al., 2013). H3K36me/me2 are also shown to enforce a repressive chromatin state in actively transcribed genes, e.g. through interacting with KDM1B (H3K4 demethylase).

Despite the above-mentioned mechanisms in mammalian cells, a study in yeast showed that H3K36me2 is sufficient to target the histone deacetylase complex Rpd3S to prevent spurious (cryptic) transcription (Li et al., 2009). This suggests that the mechanisms of suppressing cryptic transcription are different in yeast and mammalian cells, and different methyl states are required.

Transcription initiation

There have not been any reports on human SETD2 on transcription initiation. However, recently murine Setd2 was shown to initiate transcription of the Fgfr3 gene by binding and catalysing H3K36me3 at the distal promoter of Fgfr3 (Zhang

et al., 2014). H3K36me/me2 also regulates transcription initiation. For example, NSD1 binds upstream of the promoter and recruits RNAPII to the promoter (Lucio-Eterovic et al., 2010).

Transcription inhibition

However, for some genes, occupancy of NSD1 or NSD2 at the promoters leads to transcription repression (Wagner and Carpenter, 2012). Therefore, whether H3K36 methylation acts as an activating or inhibitory signal may depend on the surrounding marks and their corresponding readers (Wagner and Carpenter, 2012).

Splicing

SETD2 also affects splicing of the gene transcript by marking the alternatively spliced exons with H3K36me3, which recruits MRG15 and PTB to the marked exons. PTB then regulates the splicing as the transcript emerges from the RNAPII complex (Wagner and Carpenter, 2012).

Summary

Fig 1.9 shows a graphical summary of the above-mentioned functions that H3K36 methylation is involved in. Given the fact that H3K36 methylation are involved in various cellular processes, it may be able to coordinate the cross-talk between transcription and replication; replication and repair; and repair and transcription.

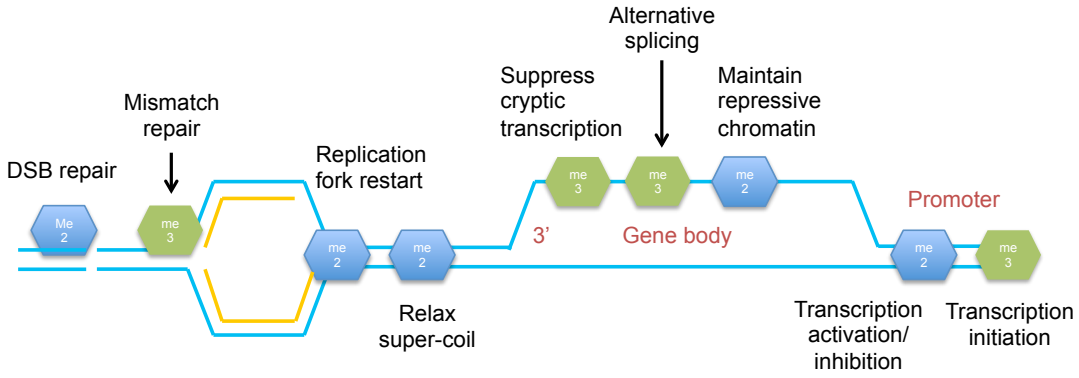


Figure 1.9: The functions of histone H3K36 methylation in DNA repair, DNA replication and gene transcription.

1.4.4 Other functions of SETD2

Numerous other functions have been ascribed to human SETD2, including regulating the telomere function (Newbold and Mokbel, 2010); regulating the transcription factor activity of p53 (Xie et al., 2008) and promoting the self-renewal potential of leukemia stem cells (Zhu et al., 2014).

Murine Setd2 was involved in embryonic vascular remodeling and angiogenesis in embryonic development (Hu et al., 2010) as well as in the differentiation of murine embryonic stem cells (Zhang et al., 2014).

1.4.5 The evolution of SETD2

As described in Figure 1.7, human cells have eight methyltransferases for histone H3K36, but yeast cells have only one H3K36 methyltransferase, Set2. Yeast Set2 sets all three methyl forms of H3K36 (H3K36me, H3K36me2 and H3K36me3), while human SETD2 only sets H3K36me3. This suggests that during evolution,

different methyl states start to acquire different functions, and different H3K36 methyltransferases were evolved to allow these states to be independently regulated. This view is also supported by Workman and colleagues (Venkatesh and Workman, 2013).

1.5 Thesis Aims

The following three key questions will be addressed in the three results chapters.

1.5.1 Understanding the functions of SETD2

Sequencing of the cancer genome has identified SETD2 as a tumour suppressor, but it is still not clear how it contributes to tumour suppression. Chapter 3 will explore the cause of genome instability (insertions, deletions, and chromosomal aberrations) observed in SETD2-deficient cancers, and investigate why multiple mutations target H3K36me3.

1.5.2 Targeting SETD2 loss by synthetic lethality

Can the loss of SETD2 be exploited for cancer therapy based on the concept of synthetic lethality? If so, what is the mechanism of the synthetic lethality? Chapter 4 will investigate these questions.

1.5.3 Expanding the synthetic lethal interaction to pathways

The power of synthetic lethality is in that it describes the interaction between two pathways (A and B). Once the mechanism is revealed, cancer cells carrying any gene mutations in pathway A can be targeted by inhibitors for any proteins in pathway B. Chapter 5 outlines how the synthetic lethal interaction is expanded from defining the relationship between two genes to defining the relationship between two pathways.

Chapter 2

Materials and Methods

2.1 Tissue culture

2.1.1 Resuscitation of frozen cell lines

Cells stored in liquid nitrogen were rapidly thawed at 37°C for 2 minutes. The cells were washed once with 10ml complete media to remove DMSO from the freezing media and pelleted by centrifugation at 1300 rpm for 3 minutes. The supernatant was aspirated and the cell pellet was resuspended in 5ml complete media and transferred to a T25 tissue culture flask.

2.1.2 Maintenance of cell lines

All cell lines except LB996 were maintained in complete media consisting of Dulbeccos modified minimal essential media (DMEM) (Invitrogen) supplemented

with 10% foetal bovine serum (FBS) (Invitrogen), 100U penicillin and 0.1mg/ml streptomycin (Sigma). LB996 was maintained in Iscove's Modified Dulbecco's Medium (IMDM) (Invitrogen) supplemented with 10% FBS, 100U penicillin, 0.1mg/ml streptomycin (Sigma) and G5 supplement (Invitrogen). All cells were grown at 37°C in a humidified incubator with 5% carbon dioxide. Cells were sub-cultured every 3 days, where cells were washed with phosphate buffered saline (PBS) and then incubated with Trypsin-EDTA for 5 minutes at 37°C. Trypsinised cells were re-suspended in complete media and re-plated at 1:5 dilution. All cell lines were routinely tested for mycoplasma and found to be negative.

2.1.3 Cryopreservation of cell lines

Log-phase growing cells were trypsinised as described above. 1×10^6 cells were spun down at 1300 rpm for 3 minutes and re-suspended in 1ml freezing media (FBS containing 10% (v/v) tissue culture ready DMSO (Sigma)). The suspension was transferred to a cyrotube and frozen at -80°C overnight before being transferred into liquid nitrogen for long-term storage.

2.2 Cell lines

The cell lines used in this study are described below:

The U2OS cell line was derived from human osteosarcoma and obtained from ATCC (ATCC number HTB-96).

The UGFP cell line was derived from U2OS by stably integrating a DR-GFP (HR) reporter construct. It was obtained from the lab of Professor Thomas Helleday.

The H1299 cell line was derived from human non-small cell lung carcinoma and obtained from the lab of Dr Andy Ryan.

The H1299-NHEJ cell line was derived from H1299 by stably integrating a NHEJ reporter construct. It was obtained from Dr Atsushi Shibata and Dr Hideaki Ogiwara.

A498, RCC4 and LB996 cell lines were derived from human clear cell renal cell carcinoma (ccRCC). A498 was obtained from the lab of Dr Ester Hammond; RCC4 was obtained from the lab of Dr Valentine Macaulay; and LB996 was obtained from the lab of Dr Benoît Van den Eynde.

The FLIPIN T-REx cell line was derived from U2OS by stably integrating a single FRT site in the genome and stably integrating a separate plasmid encoding the Tet-repressor gene. The FLIPIN T-REx DR-GFP cell line was derived from FLIPIN T-REx U2OS cells by stably integrating a DR-GFP (HR) reporter. Both cell lines were obtained from Dr Csanád Bachrati.

HCT116 was derived from human colorectal carcinoma and contained wild type p53. HCT116 p53-/- was derived from HCT116 and was p53-defective. Both isogenic cell lines were obtained from the lab of Dr Grigory Dianov.

DLD-1 was derived from human colorectal adenocarcinoma and contained mutant p53. DLD-1 p53+/+ was derived from DLD-1 where the p53 gene was

corrected. Both isogenic cell lines were obtained from the lab of Dr Ricky Sharma.

The VC8 cell line was derived from the V79 Chinese hamster lung fibroblast cell line and is defective in BRCA2. VC8-B2 was derived from VC8 where the BRCA2 gene was corrected. Both isogenic cell lines were obtained from the lab of Professor Thomas Helleday.

2.3 Generation of stable cell lines

2.3.1 Generation of stable cell lines by electroporation

Linearised plasmids were introduced to A498 cells by electroporation as suggested by 'Molecular Cloning: A Laboratory Manual'. Briefly 1×10^6 log-phase cells were resuspended in 400μl PBS and mixed with 10μg linearised plasmids in a 4mm cuvette. Electroporation was performed using the Gene Pulser Xcell System (Bio-Rad) set up with the following parameters: 800V, infinite resistance and 1.3ms time constant. After electroporation, cells were left to recover in fresh media for 48 hours, then split at 1/5 dilutions in media with appropriate selection. About 20 days after selection, single-cell colonies were isolated and expanded in individual flasks with selection media.

2.3.2 Generation of stable cell lines by viral transduction

The H3.3 and H3.3K36M lentiviral plasmids were obtained from the lab of Dr David Allis. Lentiviral particles were generated by co-transfecting the lentiviral plasmids and the viral packaging mix (System Biosciences) into 293T cells using lipofectamine transfection reagent (Invitrogen). Viral particles produced from 293T cells were collected, filtered and used to infect U2OS cells. Five days after viral infection, U2OS cells were selected for stable integration of the gene using Puromycin (5μg/ml). Stable cell lines were tested for levels of H3K36me3 by Western blotting and subsequently subjected to further experiments.

2.3.3 Generation of stable cell lines by 'Flip-In'

The FLIPIN receptor cell lines

The U2OS/FLIPIN/T-REx cell line was originally generated in the lab of Jeffrey Parvin (Ohio State University) and was a kind gift of Catherine Millar (University of Manchester). These cells express the tet repressor and contain a single integrated copy of the pFRT/lacZeo plasmid (Invitrogen).

U2OS/FLIPIN/T-REx/DRGFP cells were generated by transfecting the pDR-GFP (HR reporter) plasmid (Pierce et al., 1999) into the U2OS/FLIPIN/T-REx cells. Stable integrants were selected with 1μg/ml puromycin (Invivogen), 15μg/ml Blasticidin S (Invivogen) and 100μg/ml Zeocin (Invitrogen). Clones with best inducible GFP expression were chosen for further studies.

Flip-In reaction

The cDNA of the gene of interest (e.g., KDM4A or SETD2) was cloned into the pDESTfrtto destination vector by a Gateway LR reaction (Life Technologies). U2OS/FLIPIN/T-REx cells or U2OS/FLIPIN/T-REx/DRGFP cells were co-transfected with the resulting destination plasmid and a plasmid encoding the Flp recombinase pOG44 (Invitrogen) in a ratio of 1:9 using the Fugene transfection reagent (Promega). Once inside the cell, the FRT site on the destination plasmid recombines with the FRT site in the genome, resulting in the integration of the gene of interest into the genome. 48 hours after transfection, stable integrants were selected using 100μg/ml Hygromycin (Invivogen) and 15μg/ml Blasticidin S (Invivogen). About 20 days after selection, single-cell colonies were isolated and expanded in individual flasks with selection media (100μg/ml Hygromycin and 15μg/ml Blasticidin S). Individual colonies were tested for expression of the gene of interest in response to Doxycycline by Western blotting. Cells expressing the gene of interest under the control of Doxycycline were subsequently subjected to treatments.

2.4 Site-directed mutagenesis and Gateway cloning

Site-directed mutagenesis was performed to generate a SETD2 cDNA that is refractory to SETD2 siRNA#3. Then based on the siRNA-refractory wild type cDNA, a methyltransferase-dead mutant was generated by mutating two evolu-

tionarily conserved amino-acids at the SET domain of SETD2.

2.4.1 Site-directed mutagenesis

The wild type SETD2 cDNA was mutated from the original sequence (AGAAAC-CGTCTCCAGTCTGTT) to the new sequence (AGGAATCGGCTGCAATC-CGTG) without changing any amino acid. The new cDNA is refractory to SETD2 siRNA#3 because the siRNA can no longer hybridise to the new sequence.

The siRNA-refractory cDNA was then mutated to abolish the methyltransferase activity at amino acid 1625 (R to G) and 1631 (C to A) by a two-step mutagenesis. Primers for site-directed mutagenesis are listed below: SS1/SS2 for R1625G, and SS3/SS4 for C1631A.

SS1: CTCAAAAAGGAAATTGCTCTGGTTTCATGAATCACAGCTGT

SS2: ACAGCTGTGATTCATGAAACCAGAGCAATTTCCTTTTTGAG

SS3: CTCGTTTCATGAATCACAGCGCTGAACCAAATTGTGAAAC

SS4: GTTTCACAATTTGGTTCAGCGCTGATTCATGAAACGAG

2.4.2 Gateway cloning

The tetracycline inducible Flp-In Gateway destination vector pDESTfrtto was generated by replacing the CMV promoter of the pcDNA5/FRT plasmid backbone (Invitrogen) with the CMV/TO promoter of pcDNA4/TO/myc-His A (Invitrogen) on an MluI/HindIII fragment. The Gateway conversion cassette RfA

was then inserted into the EcoRV site of the resulting plasmid construct. The generation of the destination vector pDESTfrtto was done by Dr Csanád Bachrati.

A Gateway LR reaction enables the transfer of the gene of interest from the entry vector (pDONR221) to the destination vector (pDESTfrtto). The LR reaction was performed according to the manufacturer's instructions. In summary, the entry clone and the destination vector was mixed 1:1 (150ng each) in the TE buffer (pH 8.0) containing 2μl of the LR Clonase II enzyme mix (Invitrogen) and incubated for 1 hour at 25°C. The reaction was terminated by adding 1μl of the Proteinase K solution to the mix and incubating at 37°C for 10 minutes.

To obtain the LR reaction product (the gene of interest in the destination vector), 1μl of the reaction mix was used to transform DH5α bacteria cells (according to the standard protocol of bacteria transformation as described below). 100μl of transformed bacteria was plated onto LB agar plates containing 100μg/ml ampicillin and was incubated overnight at 37°C.

2.5 Bacterial transformation and plasmid purification

2.5.1 Bacterial transformation

Chemically competent *E. coli* DH5α cells (produced in-house by Carol Walker) were used for plasmid amplification. 1–5μl of plasmid DNA (1pg–100ng) was

added to 50μl of the bacteria cells. The mixture was incubated on ice for 30 minutes, heat-shocked at 42°C for 30 seconds, left on ice for 5 minutes and allowed to recover in 1ml S.O.C (super optimal broth) for 1 hour at 37°C with shaking. 50–100μl of the mixture was plated onto a selection plate and incubated overnight at 37°C. Depending on the plasmid backbone, selection of the plasmid-carrying bacteria clones was achieved by adding either 100μg/ml ampicillin or 50μg/ml kanamycin to the LB agar plates.

2.5.2 Plasmid purification

Plasmid purification from bacterial cultures was performed using QIAprep spin miniprep kits (Qiagen) according to the manufacturer's instructions. The QIAprep columns contain a silica membrane that binds DNA in the presence of a high concentration of chaotropic salt, and allows DNA elution in low-salt buffer or water.

In summary, following overnight growth in 5ml of selective LB in a 50ml tube, bacterial cells were harvested by centrifugation at 4000g for 20 minutes. The pellet was re-suspended in 250μl P1 buffer (containing RNase A) and cells were lysed by addition of 250μl P2 buffer and inverting. The lysis buffer was neutralised by adding 350μl of P3 buffer. Cell debris and genomic DNA were precipitated from the solution by centrifugation at 13,000rpm for 10 minutes at room temperature. The supernatant (containing plasmid DNA) was pipetted

into a QIAprep spin column and centrifuged for 1 minute at 13,000rpm, and the flow-through was discarded. The plasmid DNA bound to the silica membrane was washed with 0.75ml PE buffer to remove impurities. The plasmid DNA was eluted by incubating 50μl H_2O in the column for 1 minute before centrifugation into a collection tube.

2.6 Gene silencing

2.6.1 siRNA transfection

All siRNAs (10nM final concentration) were delivered to the cells by Lipofectamine RNAiMAX (Invitrogen) according to the manufacturer's instructions. Cells were incubated with siRNA-lipofectamine mix in suspension (reverse transfection). The medium was replaced 24 hours after transfection. Cells were analysed or further treated at various time points after transfection (usually between 48 and 120 hours). Western blotting was performed to determine knockdown efficiency.

The sequences of the siRNAs are listed below.

siSETD2#3 (si#3) (Dharmacon): GAAACCGUCUCCAGUCUGU

siSETD2#5 (si#5) (Dharmacon): UAAAGGAGGUAUAUCGAAU

siWEE1 (Dharmacon): AAUAGAACAUCUCGACUUA, AAUAUGAAGUCCCGGUAUA, GAUCAUAUGCUUAUACAGA, CGACAGACUCCUCAAGUGA

siCHK1 (Invitrogen): GGCUUGGCAACAGUAUUUCGGUAUA, CCCAGCCCACAUGUCCUGAUCAUAU, UGCCAGUGAAGAUUGUAGAUAUGAA,

siCHK2 (Dharmacon): GUAAGAAAGUAGCCAUAAA, GCAUAGGACUCAAGUGUCA, GUUGUGAACUCCGUGGUUU, CUCAGGAACUCUAUUCUAU

siATM (Invitrogen): GCGCAGUGUAGCUACUUCUUCUAUU

siATR (Invitrogen): GGGAAAUACUAGAACCUCAUCUAAA

siE2F1 (Santa Cruz): ACUGACCAUCAGUACCUGGUU, GAAGUCCAAGAACCACAUCUU.

2.6.2 shRNA transduction

Lentiviral particles containing shRNA for MUS81 was obtained from Dr Songmin Ying. 3μl of the lentiviral particle was added per well of a 6-well plate. MUS81 knockdown was analysed by Western blotting 72 hours after incubation.

2.7 Protein detection by Western blotting

2.7.1 Detection of proteins by Enhanced Chemiluminescence

Cells were lysed in the lysis buffer (50 mM Tris HCl pH7.5, 150 mM NaCl, 1% Triton X-100, supplemented with protease and phosphatase inhibitors) for 10 minutes on ice. Lysate was centrifuged for 10 minutes at 13,000 rpm to

pellet cellular debris. The supernatant was transferred to fresh tubes and protein concentrations were measured by the Bradford assay.

25μg of protein was mixed with the NuPAGE LDS loading buffer (Invitrogen) and the reducing agent Dithiothreitol (DTT), and denatured by boiling at 95°C for 5 minutes. Samples and molecular weight ladder (Invitrogen) were loaded onto pre-cast NuPAGE gels (Invitrogen) and electrophoresis was performed according to the manufacturer's instructions. Proteins were transferred onto a PVDF membrane (0.45μm pore size) in a transfer unit (Invitrogen) at 30V for 2 hours according to manufacturer's instructions.

The membrane was blocked in blocking buffer (PBS containing 5% skimmed milk and 0.2% Tween) for 1 hour at room temperature before incubating with the primary antibody diluted in the blocking buffer at 4°C overnight. After washing three times with PBS-T (PBS containing 0.2% Tween), the membrane was then incubated with a HRP-conjugated secondary antibody diluted 1:5000 in the blocking buffer for 1 hour at room temperature. After washing three times with PBS-T, the proteins on the membrane were visualised with the ECL chemiluminescence substrates (Thermo Scientific) according to the manufacturer's instructions.

2.7.2 Detection of histone modifications by Infrared Fluorescence

While most antibodies work well with enhanced chemiluminescence (ECL), antibodies against histones and histone modifications perform better in the Odyssey infrared fluorescence system. One additional advantage of this method over ECL is that the signal is directly proportional to the amount of target protein, allowing quantification of proteins according to signal intensity.

Cell lysates were prepared the same way as described above. 25μg of protein was mixed with the NuPAGE LDS loading buffer (Invitrogen) and the reducing agent Dithiothreitol (DTT), and denatured by boiling at 95°C for 5 minutes. Samples and molecular weight ladder (Invitrogen) were loaded onto pre-cast 4-12% Bis-Tris NuPAGE gels (Invitrogen) and electrophoresis was performed according to the manufacturer's instructions. Proteins were transferred onto a nitrocellulose membrane (0.2μm pore size) in a transfer unit (Invitrogen) at 30V for 2 hours (with 20% Methanol in the transfer buffer) according to manufacturer's instructions.

The membrane was blocked in the blocking buffer (Odyssey buffer containing 0.1% Tween) for 1 hour at room temperature before incubating with a primary antibody diluted in the blocking buffer at 4°C overnight. After washing three times with PBS-T (PBS containing 0.1% Tween), the membrane was then incubated with IRDye secondary antibodies diluted 1:1000 in the blocking buffer for

1 hour at room temperature. After washing three times with PBS-T, the proteins on the membrane were visualised by an Odyssey Imager (LI-COR) according to the manufacturer's instructions.

2.8 Antibodies

The antibodies used in this thesis are summarised below:

SETD2 (Abcam, 31358), H3K36me3 (Abcam, 9050), Histone H3 (Abcam, 10799), KDM4A (Cell Signaling, 5328), PCNA (Santa Cruz, PC-10), RRM2 (Santa Cruz), RRM1, E2F1 (Santa Cruz), E2F2 (Santa Cruz), E2F3 (Santa Cruz), E2F4 (Santa Cruz), RPA32 (Abcam, 2175), pRPA (S33) (Bethyl, A300-246A), γH2AX (Upstate, 05-636), RAD51 (Santa Cruz, sc-8349), p53 (Santa Cruz), pCHK1(S345) (Cell Signalling, 2341), pKAP1 (S824) (Bethyl, A300-767A), pATM (S1981) (Epitomics, 2152-1).

2.9 Inhibitors

All inhibitors (except Hydroxyurea) were dissolved in Dimethyl sulfoxide (DMSO) and stored at -80°C, and used according to the manufacturer's instructions.

WEE1 inhibitor: MK1775 (Axon Medchem)

CHK1 inhibitor: LY2603618 (IC-83) (Selleck Chemicals)

CHK1/CHK2 inhibitor: AZD7762 (Selleck Chemicals)

CHK1 inhibitor: Gö6976 (Sigma-Aldrich)

ATR inhibitor: VE821 (Axon Medchem)

ATM inhibitor: KU55933 (Tocris Bioscience)

DNA-PK inhibitor: NU7441 (Axon Medchem)

CDC25(A, B and C) inhibitor: NSC95397 (Calbiochem)

DNA polymerase alpha inhibitor: Aphidicolin (Sigma)

Ribonucleotide reductase inhibitor: Hydroxyurea (Sigma)

2.10 Cell survival assays

2.10.1 Clonogenic survival assay

48 hours after siRNA transfection, 400 cells were plated per well in 6-well plates. 4 hours after plating, cells were treated with desired inhibitors or DNA damaging reagents. Colonies were fixed and stained 12 days later. Plating efficiency (PE) and surviving fraction (SF) were calculated according to the equations in Nature Protocol (Franken et al., 2006).

2.10.2 Resazurin assay for cell viability

Equal numbers of cells were seeded in a 96-well plate 24 hours before inhibitor treatment. DMSO (solvent for the inhibitors) was used as a negative control. Three days after addition of inhibitors, the media were replaced by fresh media

without inhibitors. Five days after addition of inhibitors, the media were removed and fresh media containing Resazurin were added to each well. Resazurin is a nonfluorescent dye, which can be converted (by redox reaction) to a red fluorescent resorufin by living cells. The fluorescent signal is proportional to the number of living cells, and was measured by a fluorescence plate reader (BMG Labtech).

2.11 Assay for apoptosis

While the apoptotic population can be measured by FACS using a Caspase3 antibody plus a fixable viability dye (Ebioscience) or plus propidium iodide, a high-throughput method based on Hoechst was used here to enable simultaneous measurements of different cell lines under multiple treatment conditions.

Equal numbers of cells were seeded in a 96-well plate 24 hours prior to inhibitor treatment. 48 hours after inhibitor treatment, Hoechst was added to the media. Hoechst stains the DNA, and the nuclei of apoptotic cells appear condensed and very bright. For each well, 15 images were taken by Incell (GE Healthcare) and the number of apoptotic cells was counted using the Incell Analysis software (GE Healthcare), and presented as a percentage of total number of cells.

2.12 DNA fiber assay using CldU/IdU labelling

Cells were labelled for 20 minutes in media containing 25μM CldU, followed by 20 minutes in media containing 250μM IdU at 37°C. Cell were collected by trypsinisation and resuspended in ice-cold PBS at the concentration of 5×10^5 cells/ml. 2μl of the suspension was pipetted onto a microscope slide, and was let semi-dry before adding 7μl of the spreading buffer (200mM Tris-HCl pH7.4, 50mM EDTA, 0.5% SDS) and mixed. The DNA was allowed to run down the slide slowly, air-dried and fixed in methanol/acetic acid (3:1) for 10 minutes.

Before staining, the slides were washed with H_2O and denatured in 2.5M HCl for 1 hour 15 minutes. The slides were washed with PBS and incubated in the blocking buffer (PBS containing 1% BSA and 0.1% Tween) for 1 hour, and incubated in the blocking buffer containing the rat anti-BrdU antibody (1:1000 dilution) and the mouse anti-BrdU antibody (1:1000 dilution) overnight at 4°C. The slides were washed with PBS and fixed in 4% paraformaldehyde for 10 minutes. After rinsing, the slides were incubated in the blocking buffer containing the anti-rat AlexaFluor 555 antibody (1:500 dilution) and the anti-Mouse AlexaFluor 488 antibody (1:500 dilution) for 1.5 hours at room temperature. After washing, the slides were mounted in Vectashield and analysed using the Zeiss LSM780 confocal microscope. DNA fibre images were measured and counted using ImageJ.

2.13 Cell cycle analysis by BrdU incorporation

Cells were incubated in media containing 20μM BrdU for 20 minutes at 37°C and protected from light. Cells were collected by trypsinisation and fixed in ice-cold 70% ethanol for at least 30 minutes. Since the anti-BrdU antibody recognizes single-stranded DNA, cells were incubated for 20 minutes at room temperature in 2M HCl (which denatures double-stranded DNA) containing 0.1mg/ml pepsin (which digests nuclear proteins to expose DNA). Cells were washed once in PBS, followed by once in PBS containing 0.5% FBS and 0.5% Tween.

Cell were incubated in the blocking buffer (PBS with 2% FBS) containing the anti-BrdU monoclonal antibody (BD Biosciences) (1:100 dilution) for 90 minutes at room temperature. Cells were washed twice with PBS and incubated in the blocking buffer containing the Alexa Fluor 488 secondary antibody (Invitorgen) (1:200 dilution) for 60 min at room temperature in the dark. Cells were washed in PBS and resuspended in PBS containing 0.1mg/ml propidium iodide and analysed by FACS Scan (Becton Dickinson).

2.14 Reporter assay for determining DNA repair pathways

The reporter assays were used to determine the impact of a treatment (inhibitor or siRNA) on the efficiency of repair by either the HR or the NHEJ pathway.

Cells containing the HR and NHEJ reporter constructs will be described in detail in Chapter 3. I-SceI (intron-encoded endonuclease 1 from *Saccharomyces cerevisiae*) is a rare-cutting endonuclease that has no predicted recognition site in the mammalian genome. The HR and NHEJ reporters each contain an I-SceI recognition site that generates DNA-double-stranded breaks (DSBs) upon I-SceI expression. Successful repair by the pathway in question leads to the expression of the green fluorescent protein (GFP) which can be detected by FACS.

The reporter assay was performed in 96-well format and the procedure is described below:

2×10^4 reporter cells were seeded in 100μl antibiotics-free medium and reverse-transfected with a siRNA-RNAiMAX mixture according to the manufacturer's instructions. 24 hours after transfection, the medium was refreshed 100μl fresh antibiotic-free media. 48 hours after siRNA transfection, the I-SceI plasmid was delivered to the cells by Lipofectamine 2000 (Invitrogen) according to the manufacturer's instructions. 18 hours after plasmid transfection, the medium was refreshed with 100μl fresh antibiotic-free medium. Cells were allowed to repair the I-SceI induced DSBs for 48 hours before analysing the percentage of GFP-positive population by FACS.

2.15 Analysing repair foci by Incell

Cells were treated with inhibitors or DNA-damaging agents for the time indicated and fixed with 4% paraformaldehyde and permeablised with 0.5% Triton-X. After blocking in 3% BSA for 1 hour at room temperature, cells were incubated with appropriate primary antibodies diluted in the blocking buffer (3% BSA) overnight at 4°C. After washing three times with PBS, cells were incubated with secondary antibodies (Alexa Fluor dyes, Invitrogen) for 1 hour at room temperature, protected from light. After washing three times with PBS, the DNA was stained with DAPI to locate the nuclei. Fluorescence images were captured by Incell Analyzer (GE healthcare), with 15 images taken per well. The number of foci per nucleus was analysed using the Incell Analysis software (GE healthcare).

2.16 Microirradiation for studying the recruitment of repair proteins

In order to study the recruitment of proteins involved in DNA repair, DNA damage response, and chromatin remodeling to the site of DNA damage, localised DNA double-stranded breaks (DSBs) need to be generated. According to the Nature Protocol (Suzuki et al., 2011), localised DSBs can be generated by ultraviolet C (UVC) irradiation through porous membranes on cells labeled with BrdU. Depending on the choice of the micropore membrane, the method can gen-

erate 1–7 areas of DSBs per nucleus. In this thesis, a 5μm micropore membrane (Millipore) was used, which generated 1 or 2 areas of DSBs per nucleus.

In summary, 5×10^4 cells were plated on a 22mm×22mm cover slip in 6-well plates. After incubating in 10μM BrdU for 72 hours, cells were washed with PBS, covered with a 5μm micropore membrane and exposed to $30Jm^{-}2$ UVC light at a dose rate of $1Jm^{-}2s^{-}1$. Irradiated cells were fixed by 4% paraformaldehyde at various time points after UV irradiation. The cells were stained with desired antibodies (usually a γH2AX or a 53BP1 antibody was included to mark the DSB site). A Zeiss confocal microscope was used to capture the fluorescent images.

2.17 Co-Immunoprecipitation

5×10^6 cells were lysed in a 500μl lysis buffer (50 mM Tris HCl pH7.5, 150 mM NaCl, 1% Triton X-100, supplemented with protease/phosphatase inhibitors) for 10 minutes on ice. The cell lysate was centrifuged for 10 minutes at 13,000 rpm to pellet cellular debris. The supernatant was incubated with the primary antibody overnight at 4°C, followed by 20μl of protein G (or A) beads for 1 hour at 4°C. Bound proteins were eluted by boiling the beads in SDS loading buffer at 95°C for 5 minutes.

2.18 iPOND (isolation of proteins on nascent DNA)

The iPOND method allows a high-resolution spatiotemporal analysis of proteins (or chromatin modifications) at normal, stalled or collapsed replication forks.

The iPOND procedure was performed by Dr Enni Markkanen according to the Nature Protocol (Sirbu et al., 2012). In brief, 3×10^7 cells per condition were seeded, grown overnight, and treated with the WEE1 inhibitor MK1775 or DMSO for 24 hours. Subsequently, cells were pulsed with 10μM EdU for 10 minutes, after which they were either cross-linked (1% Formaldehyde in PBS), or washed and released into fresh chase medium containing 10μM thymidine and MK1775/DMSO for an additional 90 minutes before cross-linking. Washing of the cells, the click reaction and all other steps were performed according to the established procedures. Samples were boiled for 30 minutes to de-crosslink proteins before separation on 4-12% Bis-Tris gels (Invitrogen) and transfering to PVDF membranes according to established procedures. Immunoblotting was performed with the indicated antibodies, and was visualised using the Odyssey image analysis system (LI-COR Biosciences).

2.19 The comet assay

The comet assay measures the degree of DNA damage in individual cells (performed by Dr Enni Markkanen). The alkaline comet assay measures single-stranded and double-stranded DNA breaks while the neutral comet assay measures double-stranded DNA breaks.

2.19.1 The alkaline comet assay

As previously described (Parsons et al., 2009), cells were harvested by trypsinisation, diluted to a concentration of 2×10^5 cells/ml in media, and embedded on a microscope slide in 1% low-melting agarose in PBS (Bio-Rad). The slides were lysed in a buffer containing 2.5M NaCl, 100mM EDTA, 10mM Tris-HCl pH 10.5, 1% (v/v) DMSO and 1% (v/v) Triton X-100 for 1 hour at 4°C. Subsequently, the slides were then incubated in the dark for 30 minutes in cold electrophoresis buffer (300mM NaOH, 1mM EDTA, 1% (v/v) DMSO, pH $>$ 13) to allow DNA unwinding prior to electrophoresis at 25 V, 300 mA for 25 minutes. Neutralization of the slides was performed with 0.5M Tris-HCl (pH 8.0). The slides were stained with SYBR Gold (Invitrogen) and analysed using the Komet 5.5 image analysis software (Andor Technology).

2.19.2 The neutral comet assay

The comet assay was performed as recently described (Wojewódzka et al., 2002). Briefly, cells were harvested by trypsinization, diluted to a concentration of 2×10^5 cells/ml in medium, and embedded on a microscope slide in 1% low-melting agarose in PBS (Bio-Rad). The slides were lysed in buffer containing 2.5M NaCl, 100mM EDTA, 10mM Tris, 1% N-lauroylsarcosine, pH 9.5, with freshly added 10% (v/v) DMSO and 0.5% (v/v) Triton X-100 for 1 hour at 4°C in the dark. Subsequently, the slides were washed 3 times in electrophoresis buffer (300mM sodium acetate, 100mM Tris-HCl, pH 8.3), and incubated for 1 hour in fresh electrophoresis buffer. Electrophoresis was performed in fresh electrophoresis buffer for 1 hour at 25V, (ca. 120 mA). After electrophoresis, the slides were washed 3 times with Milli-Q water, stained with SYBR Gold (Invitrogen) and analysed using the Komet 5.5 image analysis software (Andor Technology).

2.20 Measurement of dNTP levels

This method of measuring dNTP levels is based on a DNA polymerase-catalysed incorporation of radioactive dNTP into the synthetic oligonucleotide template.

1×10^6 cells were treated and harvested by trypsin, which was neutralised with ice-cold 1% BSA in PBS. Cells were washed three more times in ice-cold PBS, and nucleotides were extracted by incubating cells in 1ml of 60% methanol for 1h at -20°C. Samples were boiled for 3 minutes in a water bath, followed by

centrifugation for 10 minutes at 13,000 rpm to remove cellular debris. The supernatant was dried under a vacuum, the pellet was dissolved in 100μl sterile water and stored at -20°C. Determining the dNTP pool size was done based on DNA polymerase-catalyzed incorporation of radioactive dNTP into synthetic oligonucleotide templates, as described (Sherman and Fyfe, 1989), and was performed by Dr Enni Markkanen.

2.21 qRT-PCR (Quantitative reverse transcription polymerase chain reaction)

qRT-PCR was performed to analyse the relative levels of a specific RNA sequence, in this case to measure the changes in mRNA levels.

Total RNA was purified using the RNeasy kit (Qiagen) and cDNA was prepared using the SuperScript RT-PCR system (Invitrogen). Quantitative RT-PCR was performed using Absolute Blue QPCR SYBR low ROX Mix (Thermo Scientific) according to the manufacturer's protocol. Reactions were carried out in duplicates for each target transcript using a 7500 Fast Real-Time PCR System (Applied Biosystems). The comparative CT method was applied for quantifying the gene expression, and values were normalised against GAPDH as a control. Results were expressed as fold changes compared to the control condition. The qRT-PCR was performed by Dr Enni Markkanen. The following primers were

used:

E2F1 frw (5′-GCCACTGACTCTGCCACCATAG-3′)

E2F1 rev (5′-CTGCCCATCCGGGACAAC-3′)

RRM2 frw (5′-TTTAAAGGCTGCTGGAGTGAGG-3′)

RRM2 rev (5′-GCAGCTGCTTTAGTTTTCGGCT-3′)

GAPDH frw (5′-AGCCACATCGCTCAGACAC-3′)

GAPDH rev (5′-GCCCAATACGACCAAATCC-3′)

2.22 ChIP (Chromatin Immunoprecipitation)

Chromatin immunoprecipitation was performed to study the levels of a protein of interest at specific regions of the genome.

ChIP experiments were performed by Lykourgos-Panagiotis Zalmas as described previously (Zalmas et al., 2013). Species-matched non-specific immunoglobulins (NS) or specific antibodies against H3K36me3 (Abcam), RNA polymerase 2 (Santa-Cruz), TAF6 (gift of Shona Murphy), and TAF4 (Santa-Cruz) were used for ChIP. The DNA was amplified with Paq5000 polymerase (Agilent) using primers pairs for the promoter region of E2F1. ChIP-qPCR data are presented as the fold change in the siSETD2 samples over the siNT samples. Fold changes were calculated from $2(-\Delta\Delta Ct)$ values; $\Delta\Delta Ct = \Delta CtSP - \Delta CtNS$, where SP stands for specific IPs, and NS stands for non-specific IPs (background). $\Delta Ct=$ CtIP − corrected Ct(input), where corrected Ct(input) = Ct(input) − $\log_2(10)$

to account for the 1/10 dilution factor of the input. IP = immunoprecipitation, and input = chromatin.

The following primers were used:

E2F1-ChIP frw (5′-GCTATACGTTGGCTGTTGGAG-3′)

E2F1-ChIP rev (5′-CAGAGCCCAAGCTGAAGAGC-3′)

2.23 Xenograft studies

Mouse xenograft studies for the efficacy of MK1775 were performed by Dr Yanyan Jiang. BALB/C nude mice (female, 6 – 8 weeks old, n = 14) were injected subcutaneously with A498 tumour cells (5×10^6 cells per mouse in 50% v/v matrigel). When the mean tumour size reached 110 mm^3, mice were divided into two groups. Group 1 (control, n = 7) received the vehicle alone (0.5% w/v methylcellulose, 0.1mL/10g body weight, twice daily by oral gavage) for 12 days. Group 2 (n = 7) received MK1775 (60mg/kg in 0.5% w/v methylcellulose, 0.1 mL/10g body weight, twice daily by oral gavage) for 12 days. The tumour size was determined by calliper measurements. The tumour volume was calculated according to the formula (width × length × height)/2. All mice in the control group were sacrificed on day 13, 24 hours after the last dose of vehicle. Three mice in the treatment group were sacrificed on day 13, 24 hours after the last dose of MK1775, and tumour re-growth in the remaining mice (n=4) was followed until day 33, when all remaining mice were sacrificed.

Chapter 3

A new role for H3K36me3 in homologous recombination repair

This chapter describes how SETD2 and its catalytic product H3K36me3 facilitate homologous recombination (HR) repair of DNA double-stranded breaks (DSBs). This new ascribed role for SETD2 helps to explain how it functions as a tumour suppressor: by favouring HR repair, it suppresses mutations arising from inaccurate repair of DNA damage and thus maintains genome stability.

3.1 SETD2 is required for the repair of DNA double-stranded breaks

To test whether SETD2 has a role in DNA repair, the sensitivity of SETD2-depleted cells to several DNA-damaging agents were tested, because cells deficient in DNA repair are usually more sensitive to DNA damage. In clonogenic survival assays, SETD2 knockdown by two independent siRNAs (si#3 and si#5) significantly reduced survival after treatment with Mitomycin C (MMC), Camptothecin (CPT) or ionising radiation (IR) in both U2OS and HeLa cell lines (Fig 3.1). IR generates DNA double-stranded breaks (DSBs), both MMC and CPT generate damage that are readily converted to DSBs, thus the increased sensitivity to these agents suggested that SETD2-depleted cells were less efficient in DSB repair.

SETD2 knockdown efficiency by the two siRNAs was validated by Western blotting. Western blots also showed that SETD2 knockdown significantly reduced global levels of H3K36me3, confirming SETD2 as the major H3K36me3 methyltransferase in human cells (Fig 3.2a).

DNA repair efficiency and repair pathway choices can be affected either directly or indirectly. A protein can indirectly affect repair by altering the expression of some repair genes, or altering the cell cycle distribution. Therefore whether SETD2 knockdown affected repair indirectly was tested. A recent siRNA screen paper indicated that RAD51 (a major HR protein) was much more likely

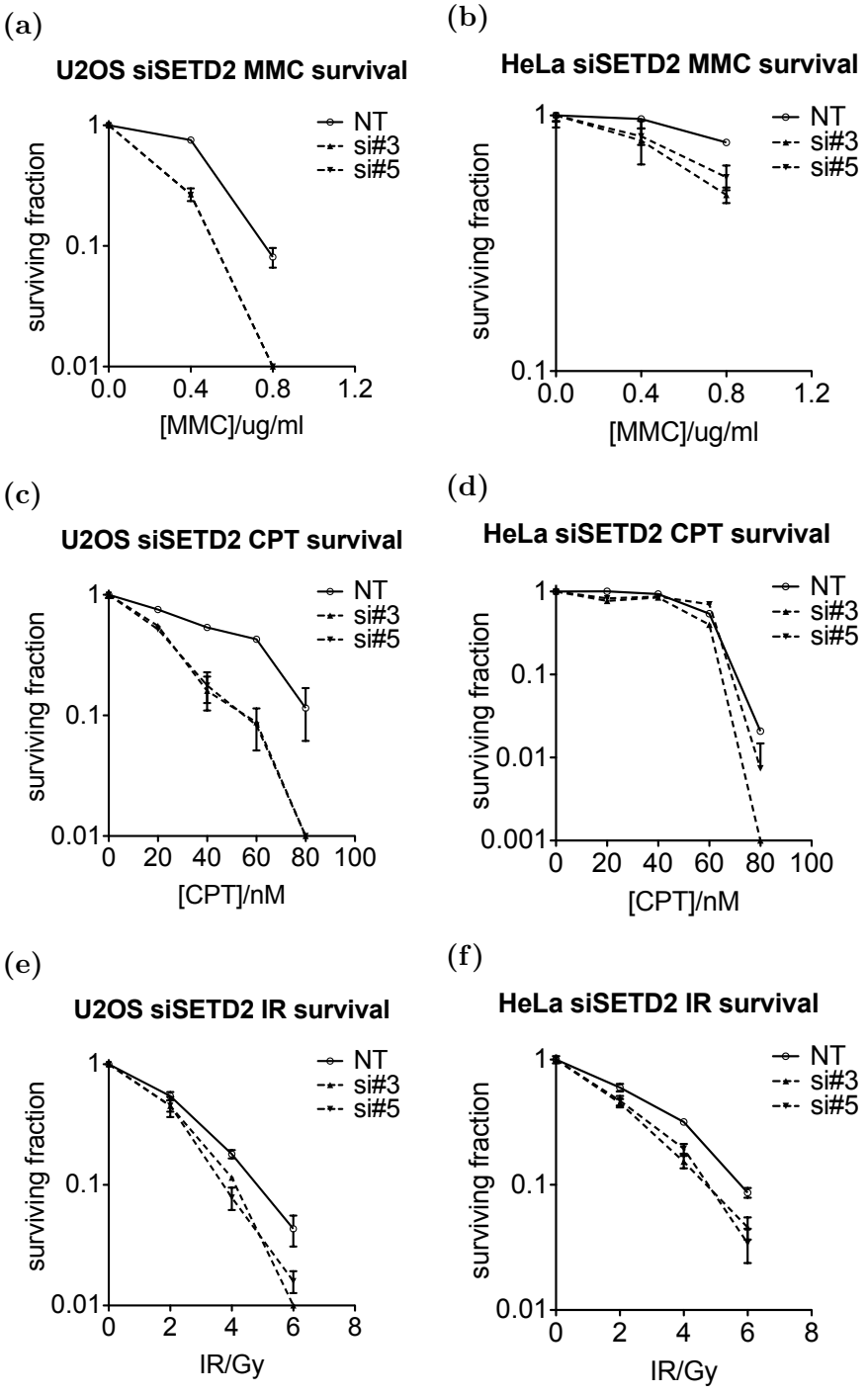


Figure 3.1: SETD2 knockdown reduces cell survival after DNA damage. Clonogenic survival of U2OS or HeLa cells transfected with non-targeting control siRNA (NT) or SETD2 siRNAs (si#3 and si#5) 48 hours prior to treatment with (a-b) MMC, (c-d) CPT and (e-f) IR. Data are presented as mean ± SEM, n=3 independent experiments independent experiments. The HeLa clonogenic survival experiments (b, d, f) were performed by Ms Sara Ahrabi.

to be affected amongst DNA repair genes by siRNA off-target effects (Adamson et al., 2012). Therefore Western blots were performed to confirm that SETD2 siRNA did not affect RAD51 expression (Fig 3.2a). Likewise, SETD2 knockdown had no effect on the expression of other major HR proteins (before and after DNA damage), including BRCA2, RAD50, CtIP, MRE11 and RPA; and the NHEJ protein KU80 (Fig 3.2b). FACS analysis of cell cycle also showed that SETD2 knockdown did not significantly alter cell cycle distribution (Fig 3.2c). Therefore SETD2 is more likely to be directly involved in DNA repair, instead of affecting the expression of repair proteins or cell cycle distribution.

3.2 SETD2 is involved in homologous recombination

DSBs can be repaired by two major pathways, homologous recombination (HR) and non-homologous end-joining (NHEJ). NHEJ branches into canonical NHEJ and alternative end-joining (which includes microhomology-mediated end-joining (MMEJ); alternative non-homologous end joining (A-NHEJ) and synthesis-dependent end joining (SDEJ)). For detailed description of the repair pathways, please refer to Introduction (Chapter 1.2).

Both MMC and CPT induce S phase-specific DSBs, which are predominantly repaired by HR (Arnaudeau et al., 2001; Moynahan et al., 2001), suggesting a role

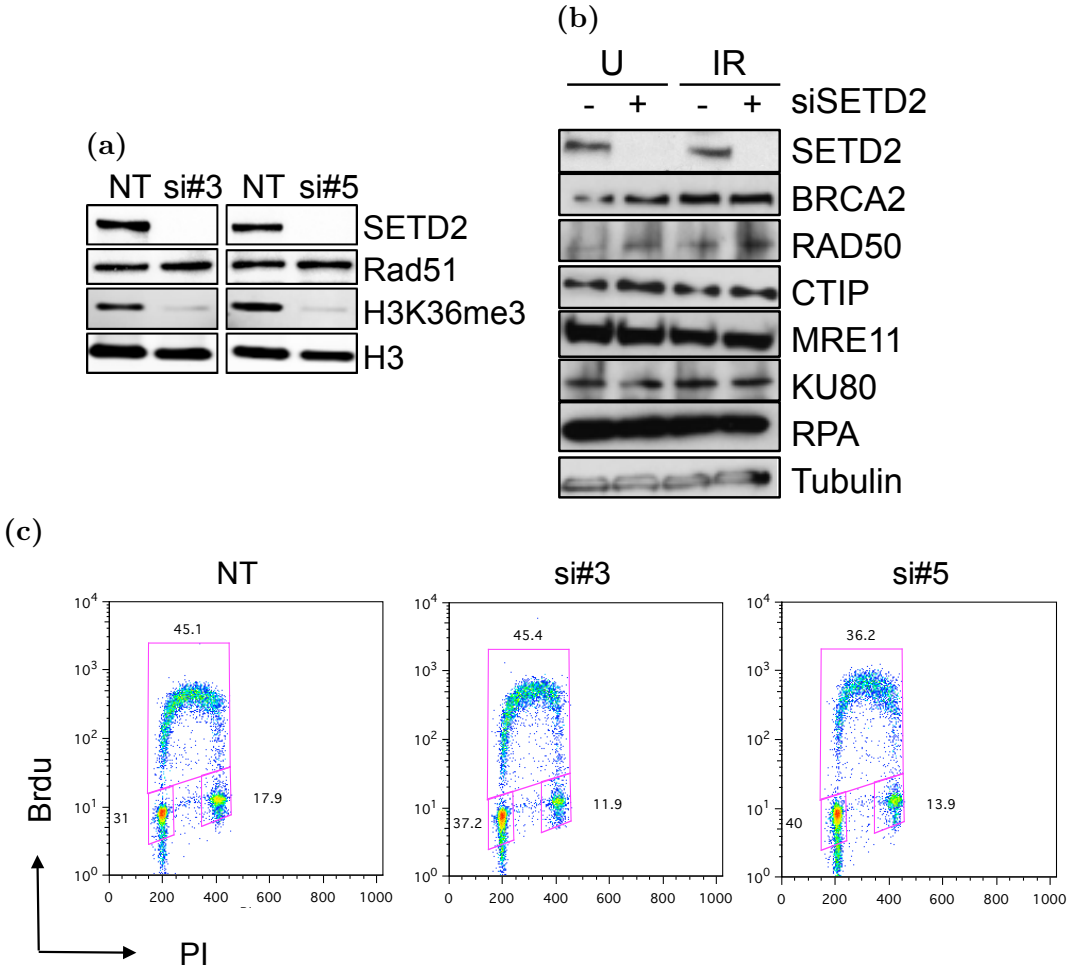


Figure 3.2: SETD2 siRNAs reduce the levels of SETD2 protein and H3K36 trimethylation, but do not affect the expression of other repair proteins. (a) Western blots showing levels of SETD2, RAD51 and H3K36me3 in U2OS cells transfected with non-targeting siRNA (NT) or SETD2 siRNA (si#3 and si#5) for 72 hours. (b) Western blot analysis of the protein levels of major HR and NHEJ factors before and after SETD2 si#3 knockdown, in the presence or absence of IR damage (5Gy following 2 hours of repair). The cells were transfected, treated and harvested by me, the Western blots in (b) were performed by Dr Sovan Sarkar. (c) Cell cycle analysis by FACS showing BrdU incorporation in U2OS cells transfected with control (NT) or SETD2 siRNA (si#3 and si#5) for 48 hours.

for SETD2 in HR. To test this, a well-characterised GFP-based reporter for HR (DR-GFP) was used. The HR reporter contains an I-SceI recognition sequence, which upon I-SceI expression is cleaved to generate a DSB. DSB repair by HR using a direct repeat within the reporter cassette as an HR repair template results in an intact GFP gene (Fig 3.3a) (Pierce et al., 1999). SETD2 knockdown by two independent siRNAs significantly reduced HR efficiency of the I-SceI induced DSB by 67-77% compared to non-targeting control cells ($p<0.0003$) (Fig 3.3b). As a control for the HR reporter, knockdown of RAD51 reduced HR activity by 97% ($p<0.0001$), while DNA-PKcs inhibitor NU7441 had no effect on HR (Fig 3.3b). These results identify a role for SETD2 in HR repair.

In contrast, SETD2 knockdown had no effect on NHEJ as measured by an NHEJ reporter (IRES-TK-EGFP). The NHEJ reporter is designed such that when two I-SceI sites separated by a thymidine kinase gene (TK) are joined by NHEJ, the GFP gene is expressed (Fig 3.3c) (Ogiwara et al., 2011). As a control, RAD51 knockdown had no effect on the same NHEJ reporter, while the DNA-PK inhibitor NU7441 reduced NHEJ activity by 98% ($p<0.0001$) (Fig 3.3d). It is interesting that SETD2 knockdown reduced HR but did not increase NHEJ frequency. Further experiments showed that repair is channeled through the alternative end-joining pathway – MMEJ, which joins two DNA ends that have been processed by partial resection. This work was performed independently and was described in (Pfister et al., 2014) (Appendix).

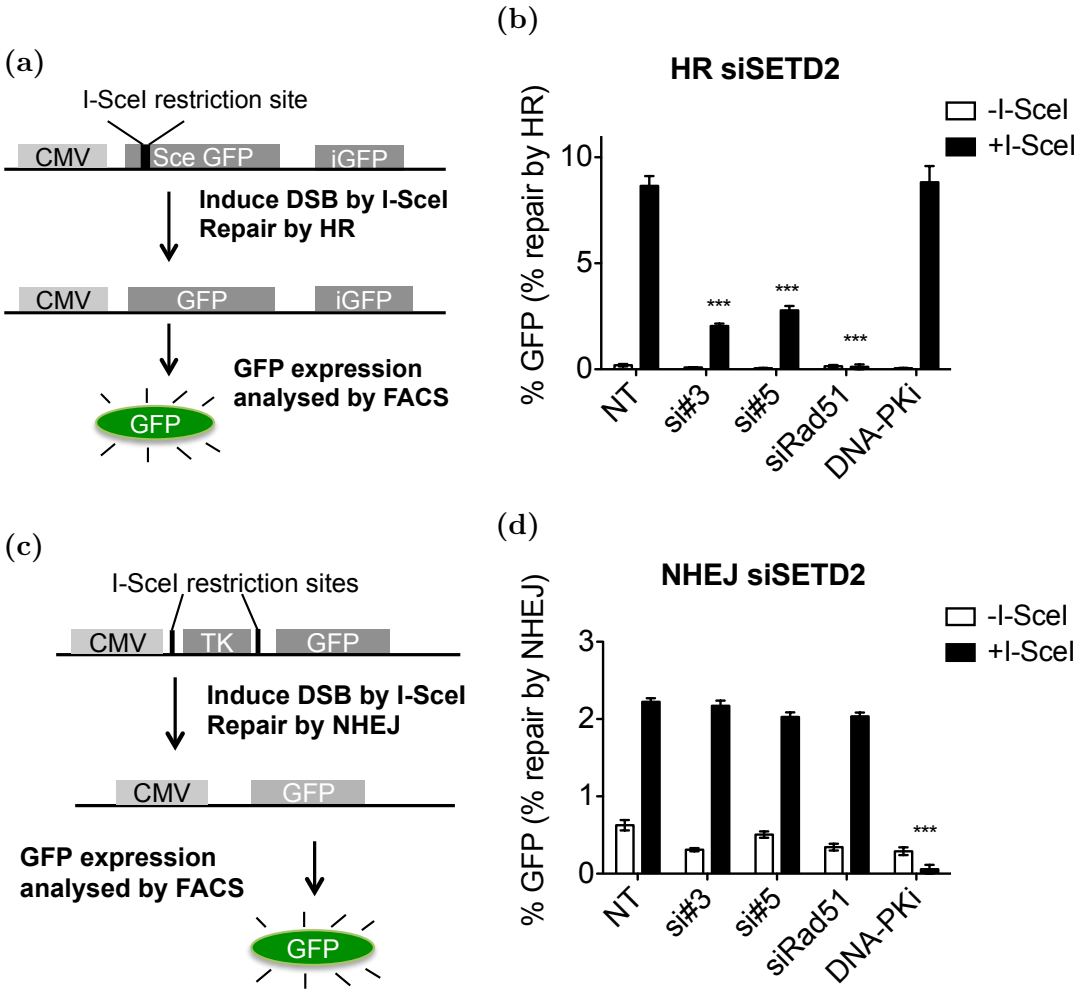


Figure 3.3: SETD2 knockdown reduces HR efficacy without affecting NHEJ efficacy. (a) Schematic map of the DR-GFP cassette for assessing HR efficacy. (b) HR repair efficacy of reporter cells treated with control siRNA (NT), SETD2 siRNAs (si#3 and si#5), RAD51 siRNA (siRad51) or DNA-PK inhibitor NU7441 (Axon), indicated by the percentage of GFP-positive cells. Data are presented as mean ± SEM, n=3 independent experiments independent experiments. ***P<0.001. (c) Schematic map of the NHEJ cassette for assessing NHEJ efficacy. (d) NHEJ repair efficacy of reporter cells treated with control siRNA (NT) or SETD2 siRNAs (si#3 and si#5), RAD51 siRNA (siRAD51) or DNA-PK inhibitor NU7441, indicated by the percentage of GFP-positive cells. Data are presented as mean ± SEM, n=3 independent experiments independent experiments. ***P<0.001.

3.3 An early role for SETD2 in the HR process

During the HR process, HR proteins are recruited sequentially to the break site, in the (simplified) order of MRN/CtIP, RPA, RAD51 and BRCA2. To investigate which step of the HR repair process SETD2 is involved in, foci formation assays were conducted to assess its impact on DNA damage signalling (γH2AX) and on the recruitment of major HR proteins (RPA and RAD51).

Following DSB induction, γH2AX foci form rapidly at the break site to signal DNA damage; and as DSBs are repaired, γH2AX foci disappear over time. Following ioniing radiation (IR, 5Gy), SETD2-depleted cells showed similar rate of γH2AX foci formation compared to non-targeting controls (4 and 8 hours post-IR). However, the removal of γH2AX foci was but significantly delayed in SETD2-depleted cells (48 hours post-IR). This observation supports a role for SETD2 in efficient DSB repair, but not in damage signalling.

Next, the effect of SETD2 depletion on the recruitment of HR proteins following DSB was examined. SETD2 knockdown significantly reduced RAD51 foci formation (4 and 8 hours post-IR) (Fig 3.5a, b). To exclude the possibility that this observation was specific to IR damage, cells were also exposed to CPT, which generates DSBs in S-phase. SETD2 knockdown also significantly reduced RAD51 foci formation after exposure to CPT (1, 2 and 4 hours post-CPT) (Fig 3.5c).

Finally, the effect of SETD2 depletion on the recruitment of an early acting HR protein RPA (Replication factor A) was examined. DSBs was induced in

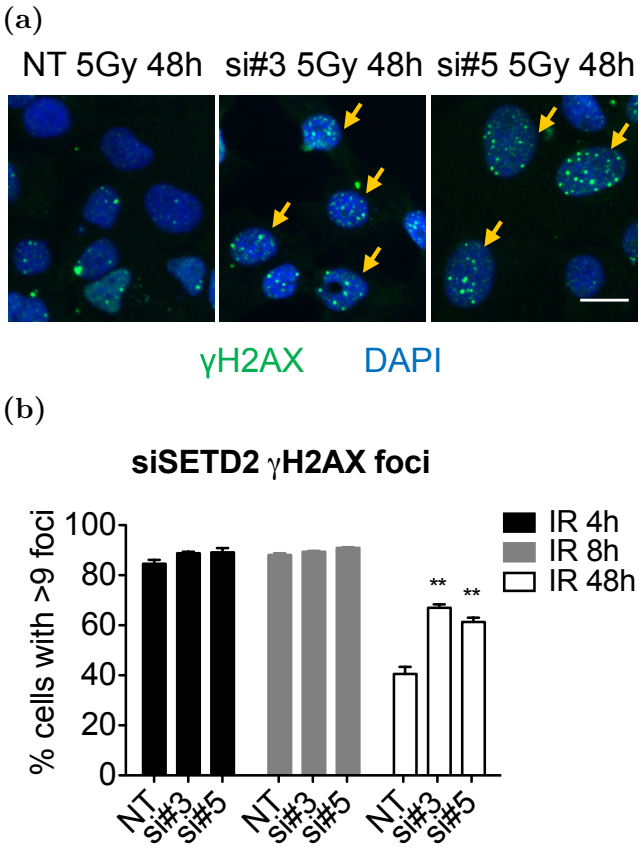


Figure 3.4: SETD2 knockdown delays removed of γH2AX. γH2AX foci formation at indicated times after IR (5Gy) in U2OS cells transfected with non-targeting siRNA (NT) or SETD2 siRNAs (si#3 and si#5). (a) Representative fluorescent images taken at 48 hours after 5Gy, arrows indicate more than 9 foci per nucleus. Scale bar = 20μm. (b) Quantification of the percentage of cells containing more than 9 γH2AX foci in their nuclei after IR (5Gy). For each condition, 45 fields and at least 500 cells were examined by Incell (GE healthcare). Data are presented as mean $\pm$ SEM, n=3 independent experiments independent experiments. **P<0.01.

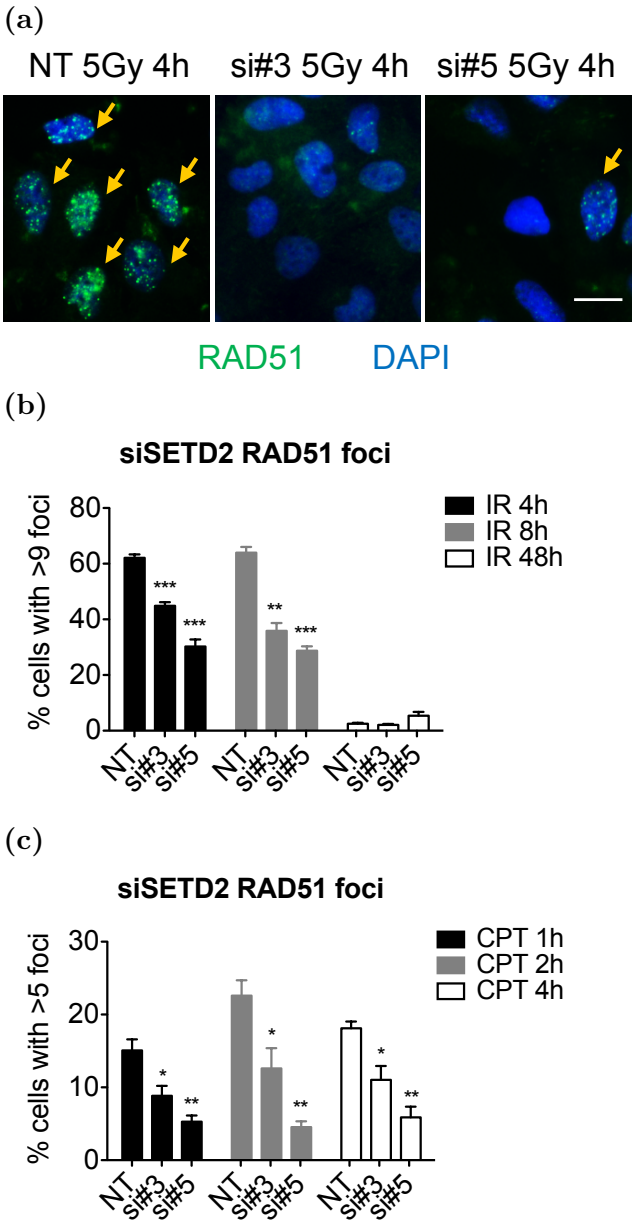


Figure 3.5: SETD2 knockdown reduces RAD51 foci formation. RAD51 foci formation at indicated times after DNA damage in U2OS cells transfected with non-targeting siRNA (NT) or SETD2 siRNAs (si#3 and si#5). (a) Representative fluorescent images taken at 4 hours after IR (5Gy), arrows indicate more than 9 foci per nucleus. Scale bar = 20μm. Quantification of the percentage of cells containing (b) more than 9 RAD51 foci after IR (5Gy), or (c) more than 5 RAD51 foci after CPT (10μM) treatment. For each condition, 45 fields and at least 500 cells were examined by Incell (GE healthcare). Data are presented as mean ± SEM, n=3 independent experiments independent experiments. ***P<0.001,**P<0.01, *P<0.05.

S-phase cells using CPT or MMC. SETD2 knockdown significantly reduced RPA foci formation after CPT (1, 4, and 24 hours post-CPT) (Fig 3.6a, b) and after MMC (24 and 48 hours post-MMC) (Fig 3.6c). IR was not used as the numbers of RPA foci induced per nucleus were too low to be quantified accurately.

Immunofluorescence experiments also helped to visualise the loss of H3K36me3 staining in the nucleus following SETD2 knockdown (Fig 3.7). This means that in the future, one could determine the H3K36me3 status of a patient sample or a cell line using either western blotting or immuno-staining (by immunofluorescence or immunohistochemistry).

Together these immunofluorescence experiments support a role for SETD2 in HR through facilitating recruitment of RPA and RAD51 to DSB sites.

In addition to repair foci, another way to assess the recruitment of HR proteins to the site of DSBs is by chromatin immunoprecipitation (ChIP). A ChIP experiment was designed to monitor three regions near the I-SceI site in the DR-GFP cassette (Fig 3.8a). The I-SceI site is located within the DR-GFP cassette under the control of the highly active CMV promoter, and thus H3K36me3, which is associated with active transcription, is predicted to be present throughout the cassette, allowing comparison between non-targeting control and SETD2/H3K36me3-depleted conditions.

The recruitment of RPA and RAD51 to the DSB site was monitored before and after DSB induction by I-SceI. In control cells, RPA and RAD51 were recruited to the DSB site, resulting in increased binding to the 'up' site 18 hours

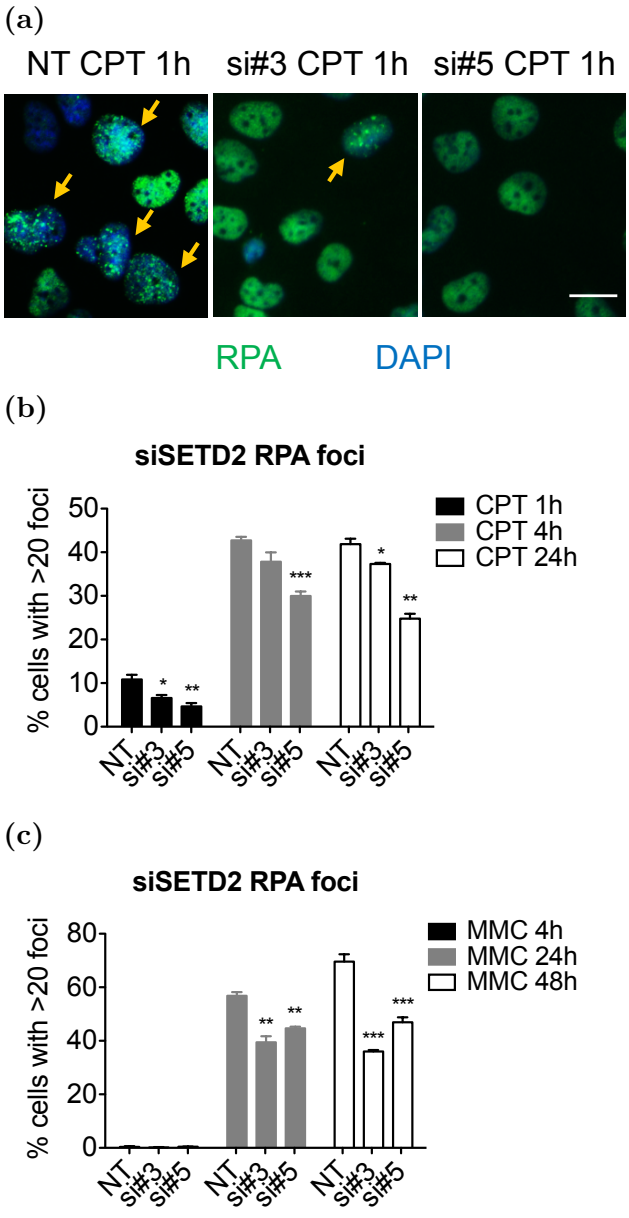


Figure 3.6: SETD2 knockdown reduces RPA foci formation. RPA foci formation after DNA damage in U2OS cells transfected with non-targeting siRNA (NT) or SETD2 siRNAs (si#3 and si#5). (a) Representative fluorescent images taken at 1 hour after CPT (10μM) treatment, arrows indicate more than 20 foci per nucleus. Scale bar = 20μm. Quantification of the percentage of cells containing more than 20 RPA foci in their nuclei at indicated times after (b) CPT (10μM) treatment, or (c) a 2-hour MMC (2μM) treatment. For each condition, 45 fields and at least 500 cells were examined by Incell (GE healthcare). Data are presented as mean $\pm$ SEM, n=3 independent experiments independent experiments. ***P<0.001,**P<0.01, *P<0.05.

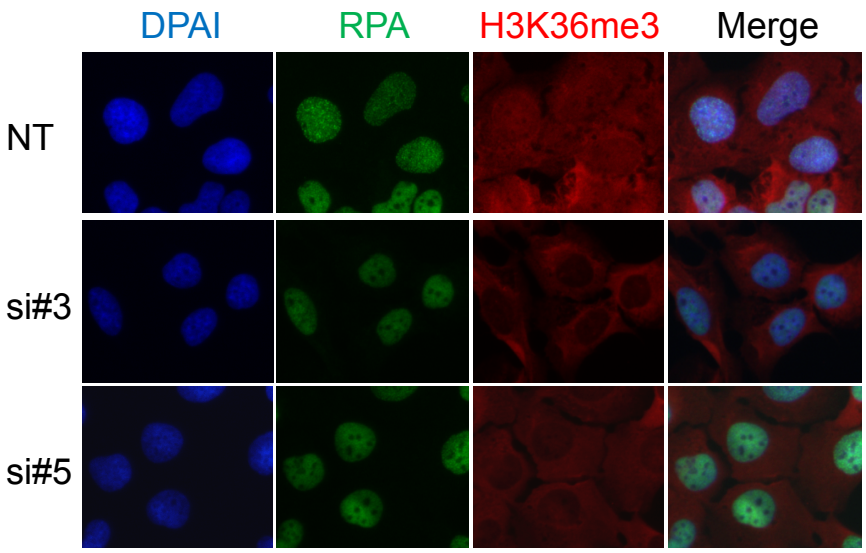


Figure 3.7: SETD2 knockdown reduced the level of H3K36me3 in the nuclei. Immunofluorescence images acquired by double staining with antibodies against RPA32 (mouse, Abcam) and H3K36me3 (rabbit, Abcam) in U2OS cells transfected with non-targeting siRNA (NT) or SETD2 siRNAs (si#3 and si#5) 48 hours prior to CPT (10μM) treatment for 1 hour.

after I-SceI transfection. In SETD2 depleted cells, RPA and RAD51 were absent from the 'up' site after the I-SceI transfection (Fig 3.8b). SETD2 depletion at protein level was validated by western blotting (Fig 3.8c), and was further confirmed by the absence of SETD2 or H3K36me3 at the break site after knockdown (Fig 3.8b). These findings are consistent with the RPA and RAD51 foci results, indicating that SETD2 is required to recruit RPA and RAD51 to DSB sites. Together, these findings confirm a presynaptic role (i.e. before RAD51 presynaptic filament formation) for SETD2 in facilitating HR repair of DSBs.

This raised the question whether SETD2 is recruited to the damage site to catalyse the trimethylation of H3K36 in response to DSBs. Therefore a ChIP

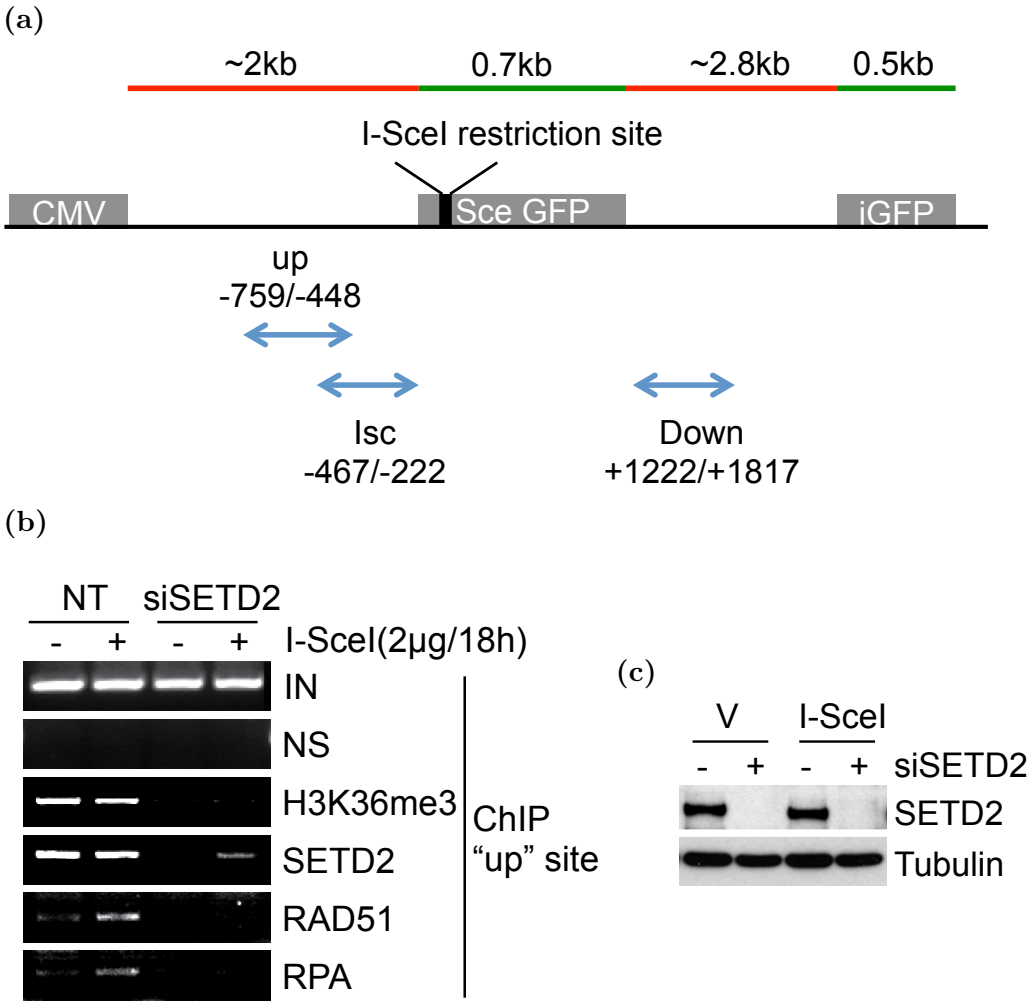


Figure 3.8: SETD2 knockdown reduced recruitment of RAD51 and RPA to the DSB site. (a) Schematic map of the DR-GFP cassette, where arrows indicate the three pairs of PCR primers ('up', 'Isc', 'down') used to amplify genomic DNA after ChIP, the numbers indicate the position relative to the I-SceI site. (b) ChIP analysis on DR-GFP U2OS cells transfected with control (NT) or SETD2 siRNA for 72 hours, followed by transfection of either vector or I-SceI plasmid for a further 18 hours, as indicated. ChIP on the 'up' site of the DR-GFP cassette was performed on the lysate using antibodies against non-specific Ig (NS), H3K36me3 (Abcam), SETD2 (Abcam), RAD51 (Santa Cruz) or RPA (Millipore); inputs (IN) are also indicated. The cells were transfected and treated by me, the ChIP experiments were performed by Dr Lykourgos-Panagiotis Zalmas. (c) Western blot confirming SETD2 knockdown in the cells used for ChIP. Samples were taken from the ChIP experiment shown in (b).

experiment was performed using the same DR-GFP cassette to detect any changes in SETD2 or H3K36me3 levels at the DSB site over time. However, no changes in SETD2 levels was detected proximal or distal to the break-site at 8, 24 or 48 hours following I-SceI transfection (Fig 3.9).

Similarly, no changes in H3K36me3 levels were observed under the same conditions post DSB induction (Fig 3.10). While other groups also observed no changes to H3K36me3 level after DSB, either globally (Fnu et al., 2011) or locally at the break site (Pei et al., 2011; Aymard et al., 2014), this lack of reduction in H3K36me3 or SETD2 was a surprising finding. Because regional transcriptional silencing has been observed at sites of DSBs (Shanbhag et al., 2010), this unexpected maintenance of H3K36me3 at the DSB site by SETD2 may serve as an anchor to recruit other HR proteins.

3.4 The methyltransferase activity of SETD2 is required for HR

To investigate if the methyltransferase function of SETD2 is required for its role in HR, one needs to find out whether the catalytic activity is dispensable or not, i.e. if a methyltransferase-dead mutant of SETD2 could also carry out the HR function.

To enable this genetic engineering, a FLIPIN T-REx system was utilised.

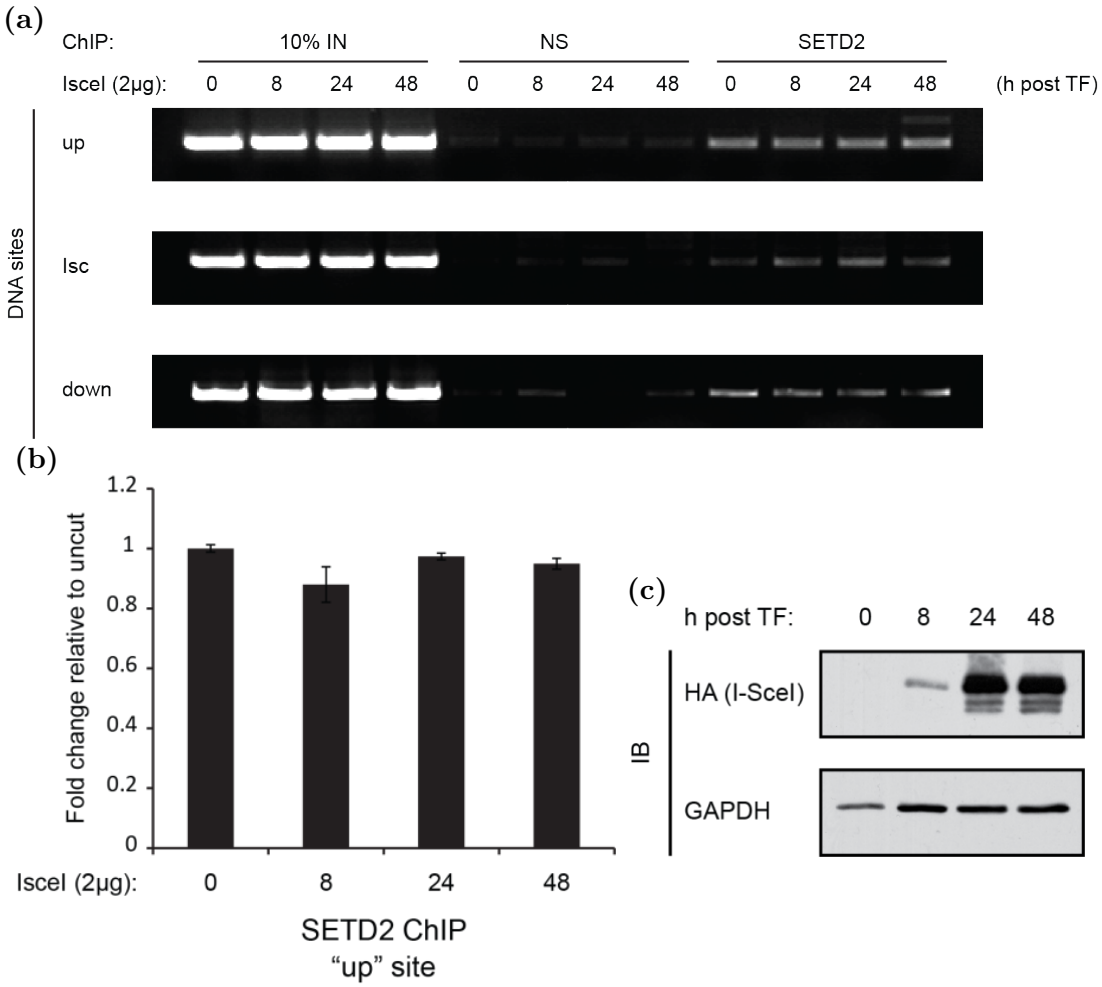


Figure 3.9: SETD2 levels were unchanged at the DSB site. (a) ChIP-PCR analysis on DR-GFP U2OS cells transfected with I-SceI plasmid and harvested at the indicated time post-transfection. ChIP was performed on the lysate using antibodies against SETD2 (Abcam, rabbit) or non-specific normal rabbit IgG (NS); chromatin inputs (IN) are also indicated. The three PCR primer pairs (covering 'up', 'Isc', and 'down' sites) are as shown in Fig 3.8a. (b) ChIP-qPCR analysis of enrichment of SETD2 at the 'up' site. Data are presented as fold change over the uncut condition, mean ± SD, n=3 independent experiments independent experiments. (c) Western blot showing HA-tagged I-SceI expression levels over the time course, GAPDH serves as a loading control. The cells were transfected and treated by me, the ChIP experiments were performed by Dr Lykourgos-Panagiotis Zalmas.

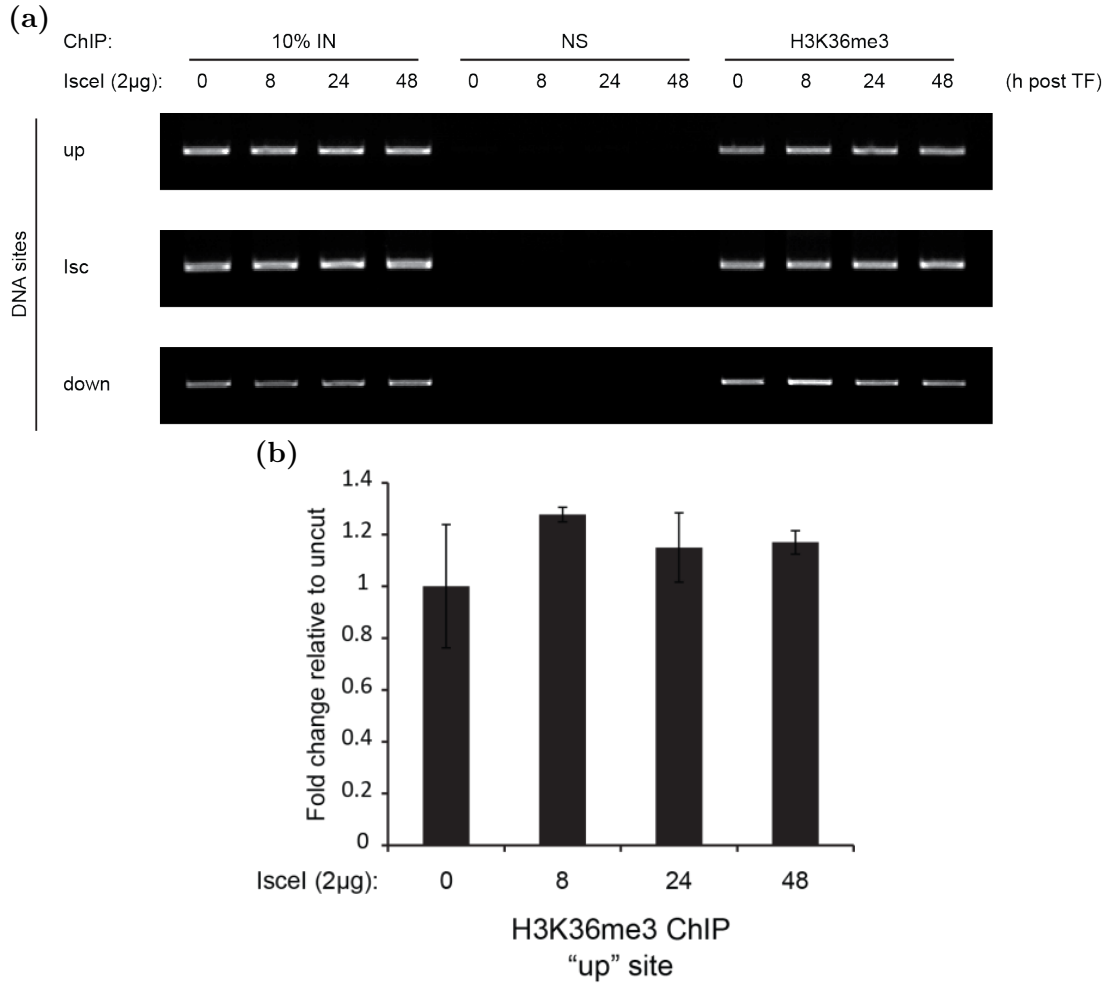


Figure 3.10: H3K36me3 levels were unchanged at the DSB site. (a) ChIP-PCR analysis on DR-GFP U2OS cells transfected with I-SceI plasmid and harvested at the indicated times post-transfection. ChIP was performed on the lysate using antibodies against H3K36me3 (Abcam, rabbit) or non-specific normal rabbit IgG (NS); chromatin inputs (IN) are also indicated. The three PCR primer pairs (covering 'up', 'Isc', and 'down' sites) are as shown in Fig 3.8a. (b) ChIP-qPCR analysis of enrichment of H3K36me3 at the 'up' site. Data are presented as fold change over the uncut condition, mean ± SD, n=3 independent experiments independent experiments. These experiments were performed together with Dr Lykourgos-Panagiotis Zalmas.

The system allows the integration of a gene of interest into a single FLIP-IN site in the genome. The expression of the gene of interest is under the control of a Tet-operator: upon addition of Doxycycline to the cell culture medium, the Tet-operator becomes de-repressed and the gene is expressed (Fig 3.11).

Two Doxycycline-inducible U2OS cell lines were generated using the system, where either a wild-type SETD2 cDNA or a methyltransferase-dead SETD2 cDNA was inserted behind a Tet-operator in the genome of the U2OS FLIPIN T-REx cells. Similarly, two Doxycycline-inducible U2OS FLIPIN T-REx DR-GFP cell lines were generated, where the parental cells also have a HR reporter integrated in the genome, to allow GFP-based assessment of HR efficiency.

The wild-type and methyltransferase-dead SETD2 cDNAs were generated as the following: firstly the wild-type SETD2 cDNA was mutated so that it is refractory to SETD2 siRNA#3 without changing the amino acid sequence (Fig 3.12a). Secondly, two amino acid residues (R1625G and C1631A) located within the evolutionarily conserved catalytic site of the SET domain were mutated, to generate the methyltransferase-dead SETD2 (Fig 3.12b). The corresponding mutations in yeast Set2 were shown to abolish the methyltransferase activity (Rea et al., 2000; Strahl et al., 2002).

Western blot analysis confirmed that Doxycycline-induced expression of wild-type SETD2 (WT) could restore the level of H3K36me3 after SETD2 siRNA#3 knockdown, while expression of methyltransferase-dead SETD2 (MD) did not restore the level of H3K36me3 (Fig 3.12c).

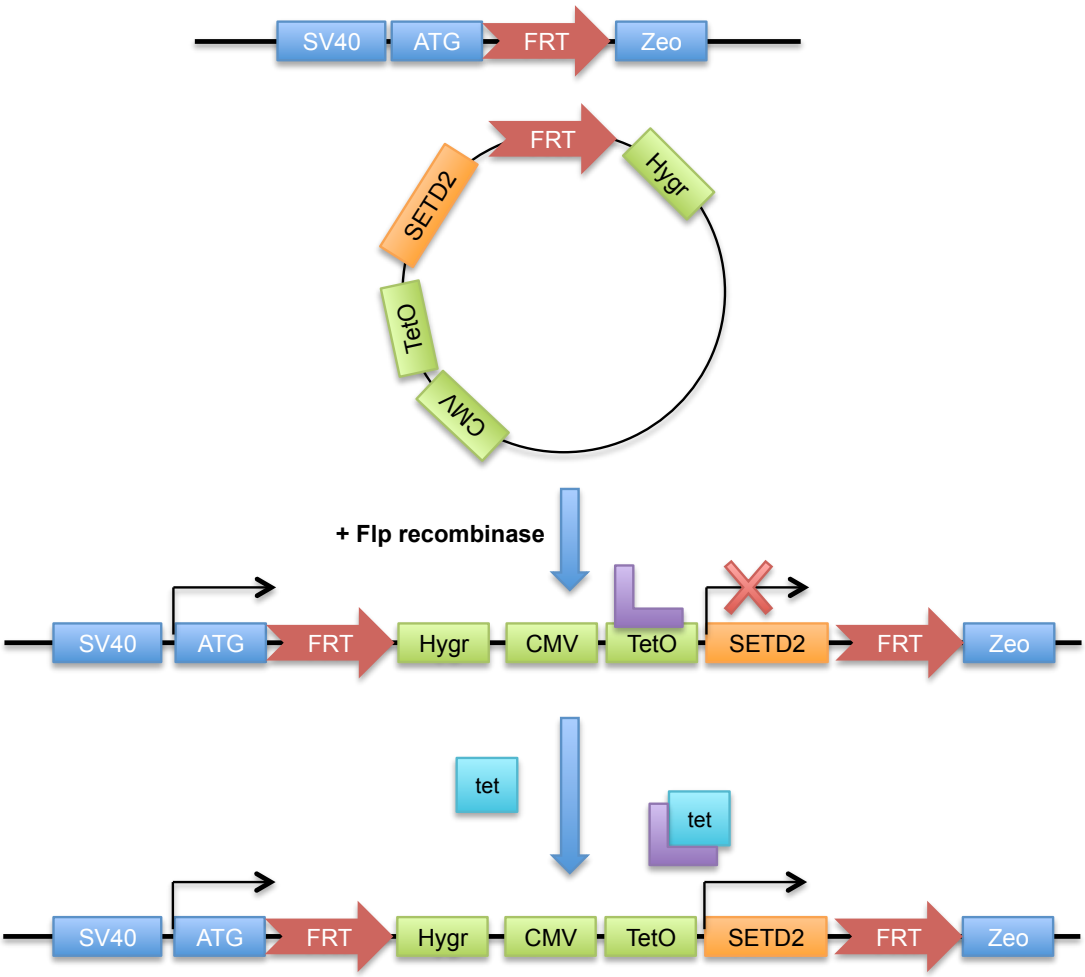


Figure 3.11: Schematic map of the FLIPIN T-REx system. A FRT site was stably integrated into the genome of U2OS cells (using Zeocin for selection). Upon transfection of a plasmid containing the gene of interest and a plasmid encoding the Flp recombinase, the FRT site in the genome recombined with the FRT site on the plasmid, resulted in the integration of gene of interest into the genome (using Hygromycin for selection). The expression of the gene of interest is under the control of a Tet operator, which is normally bound by the Tet repressor (expressed from a separate stably integrated plasmid, selected by Blasticidin). Upon treatment of Tetracycline (or Doxycycline), the Tet-operator becomes de-repressed and the gene of interest is expressed.



Figure 3.12: Generation of the U2OS cells expressing exogenous wild-type or methyltransferase-dead SETD2 that are refractory to siRNA#3. (a) Schematic map showing site-directed mutagenesis to generate a SETD2 cDNA refractory to SETD2 siRNA#3. Base substitutions at the 'wobble' bases are marked red, and the target sequence of siRNA#3 is underlined. This mutagenesis experiment was performed by the commercial company GeneCopoeia. (b) Schematic map showing site-directed mutagenesis to abolish the methyltransferase activity of SETD2, with both R and C residues mutated simultaneously. Sequence alignment of human SETD2 and *Saccharomyces cerevisiae* Set2 and *Schizosaccharomyces pombe* Set2 amino acid sequences reveals evolutionarily conserved residues that reside in the SET domain. This mutagenesis experiment was performed by Dr Sovan Sarkar. (c) Western blots showing the induction of SETD2 protein expression by Doxycycline (5μg/ml) in T-REx DR-GFP SETD2 clones 48 hours after NT or SETD2 siRNA treatment. The clone expressing wild-type (WT) SETD2 cDNA showed restored levels of H3K36me3 after siSETD2. The clone expressing methyltransferase-dead (MD) SETD2 cDNA showed no restoration of H3K36me3 levels after siSETD2.

To allow the HR function of the two cDNA constructs to be assessed, the endogenous SETD2 was depleted with siRNA#3, and expression from the cDNA constructs was induced by Doxycycline (DOX). The HR efficiency was measured by repair foci formation (RPA and RAD51) and HR reporter assay, both of which were reduced by SETD2 knockdown as shown previously (section 3.3).

Expression of the wild-type SETD2 cDNA (WT+DOX) increased foci formation of RPA and RAD51 after DNA damage in SETD2 siRNA#3 knockdown cells, but expression of the methyltransferase-dead mutant (MD+DOX) did not (Fig 3.13).

This is consistent with the observation that the wild-type SETD2 construct (WT) partially restored HR efficacy while the methyltransferase-dead (MD) mutant did not (Fig 3.14a). In fact, five to six U2OS FLIPIN T-REx DR-GFP clones containing each construct were independently isolated and tested. Five out of six WT clones were able to restore HR efficacy (Fig 3.14b), but none of the five MD clones showed any rescue (Fig 3.14c).

3.5 Histone H3K36 trimethylation is required for HR

The observation that the methyltransferase-dead SETD2 was defective in HR suggested that histone H3K36me3 (the catalytic product of SETD2) is required

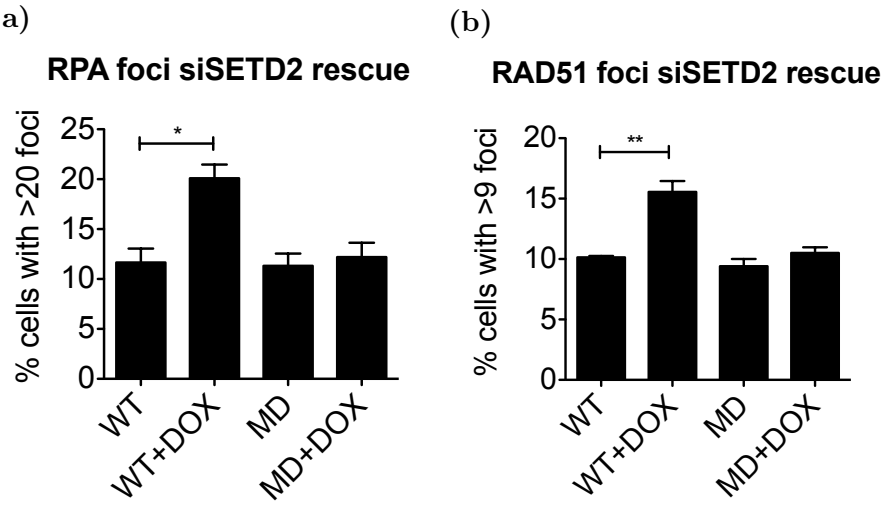


Figure 3.13: Rescue of the RPA and RAD51 foci formation by wild-type but not by methyltransferase-dead SETD2. (a) RPA32 foci formation at 2 hours after treatment with CPT (10μM) in cells transfected with SETD2 siRNA#3. WT: T-REx U2OS clone with wild-type SETD2 cDNA integrated but not expressing exogenous SETD2. WT+DOX: the same WT clone expressing exogenous wild-type SETD2. MD: T-Rex U2OS clone with methyltransferase-dead mutant SETD2 cDNA integrated but not expressing exogenous SETD2. MD+DOX: the same MD clone expressing exogenous mutant SETD2. Data are presented as mean ± SEM, n=3 independent experiments independent experiments *$p<0.05$. (b) RAD51 foci formation at 4 hours after IR (5Gy) in cells transfected with SETD2 siRNA#3. The clones used are the same as in (a). Data are presented as mean ± SEM, n=3 independent experiments independent experiments, **$p<0.01$.

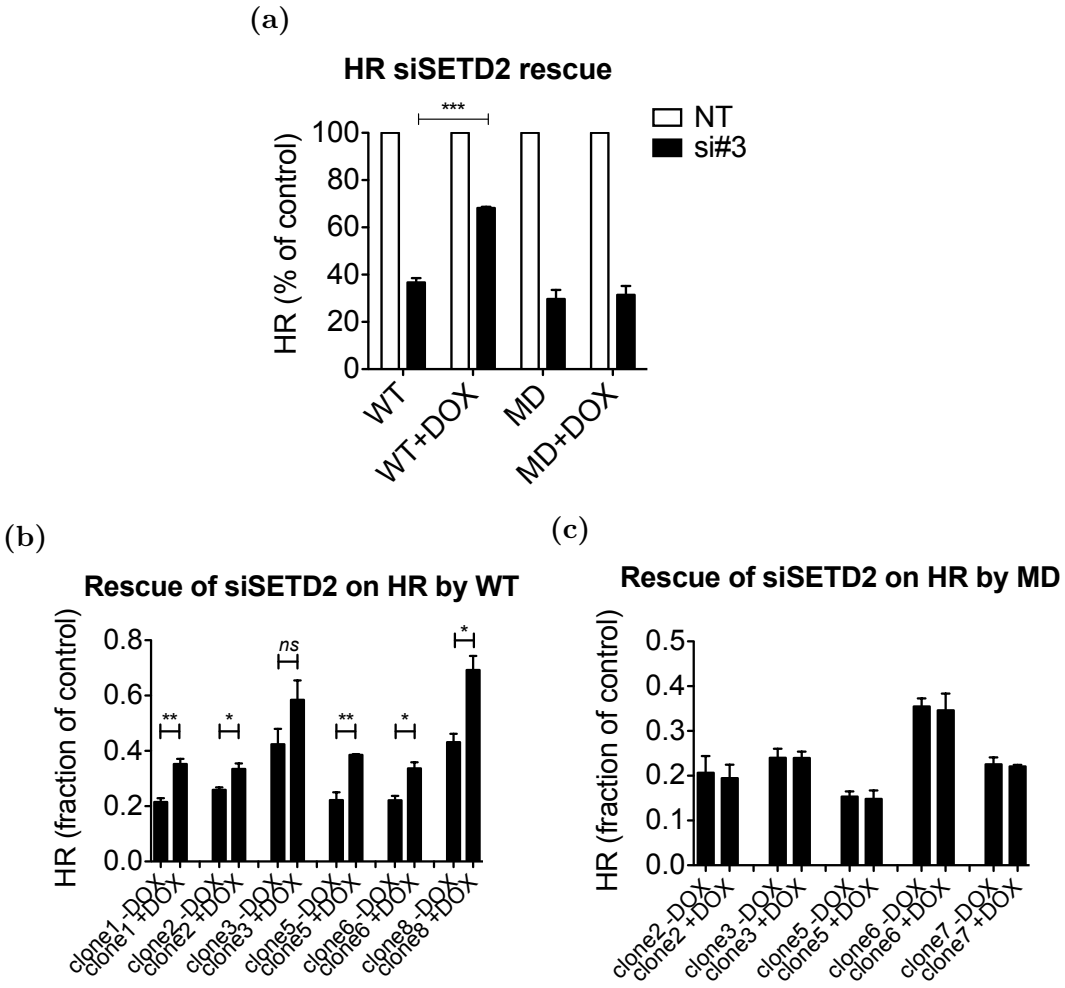


Figure 3.14: Rescue of the HR efficacy by wild-type but not by methyltransferase-dead SETD2. (a) HR efficacy in U2OS FLIPIN T-REx DR-GFP cells transfected with NT or SETD2 siRNA (si#3). WT: A T-REx DR-GFP clone with wild-type SETD2 cDNA integrated but not expressing exogenous SETD2. WT+DOX: the same WT clone expressing exogenous wild-type SETD2. MD: A T-REx DR-GFP clone with methyltransferase-dead mutant SETD2 cDNA integrated but not expressing exogenous SETD2. MD+DOX: the same MD clone expressing exogenous mutant SETD2. Data are presented as mean ± SEM, n=3 independent experiments independent experiments, ***p<0.001. (b) Rescue of HR efficacy after SETD2 siRNA knockdown (si#3) in five out of six independent wild-type (WT) T-REx DR-GFP clones. Data are presented as mean ± SEM, n=3 independent experiments independent experiments, **p<0.01, *p<0.05. (c) Lack of rescue of HR efficacy after SETD2 siRNA knockdown (si#3) in five independent methyltransferase-dead (MD) T-REx DR-GFP clones. Data are presented as mean ± SEM, n=3 independent experiments independent experiments.

for efficient HR. To test this, two approaches were taken to reduced H3K36me3 levels without affecting SETD2 protein levels.

The first approach involved KDM4A, a demethylase specific for trimethylated histone H3K36 and H3K9. If H3K36me3 is required for HR, then over-expression of KDM4A is expected to impair HR as it reduces the levels of H3K36me3. To test this, a Doxycycline-inducible KDM4A-expression U2OS cell line was generated using the FLIPIN T-REx system. Upon addition of Doxycycline, KDM4A was over-expressed, which led to a global reduction in H3K36me3 levels (Fig 3.15a). In agreement with this hypothesis, KDM4A over-expression reduced formation of RPA and RAD51 foci after DNA damage (Fig 3.15b, c).

Accordingly, KDM4A over-expression also reduced HR efficacy as assessed by the HR reporter (Fig 3.16a). As a control, the parental FLIPIN T-REx DR-GFP cell line (without KDM4A cDNA integration) showed that Doxycycline itself had no effect on HR efficacy (Fig 3.16b). Also, cell cycle progression was not affected by KDM4A over-expression (Fig 3.16c). These findings indicated that one important cellular impact of the oncogene KDM4A over-expression was reduced DSB repair by HR.

The second approach involved expressing a dominant-negative mutant in histone H3.3 gene (H3.3K36M) that was recently shown to reduce H3K36me3 specifically without affecting other histone methylations (Lewis et al., 2013). As expected, cells expressing the mutant H3.3K36M transgene had lower levels of H3K36me3 compared to the wild-type H3.3 control (Fig 3.17a). Cells express-

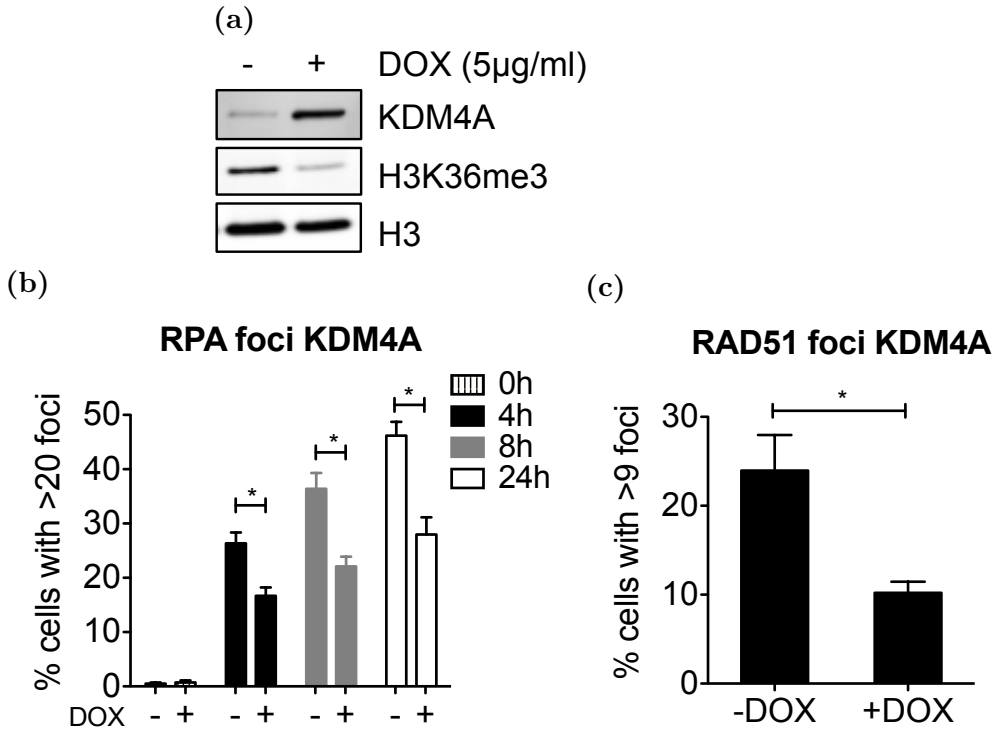


Figure 3.15: KDM4A over-expression reduced H3K36me3 levels and inhibited repair foci formation. (a) Western blot showing levels of KDM4A, H3K36me3 and H3 following KDM4A induction with 5μg/ml Doxycycline (DOX) for 72 hours in the KDM4A T-REx U2OS cells (see Experimental Procedures). (b) RPA32 foci formation at indicated time after 2- hour CPT (10μM) treatment in KDM4A T-REx cells treated with or without 5μg/ml Doxycycline (DOX). Data are presented as mean $\pm$ SEM, n=3 independent experiments independent experiments, *P$<$0.05. (c) RAD51 foci formation 8 hours after IR (5Gy) in KDM4A T-REx cells treated with or without 5μg/ml Doxycycline (DOX). Data are presented as mean $\pm$ SEM, n=3 independent experiments independent experiments, *P$<$0.05.

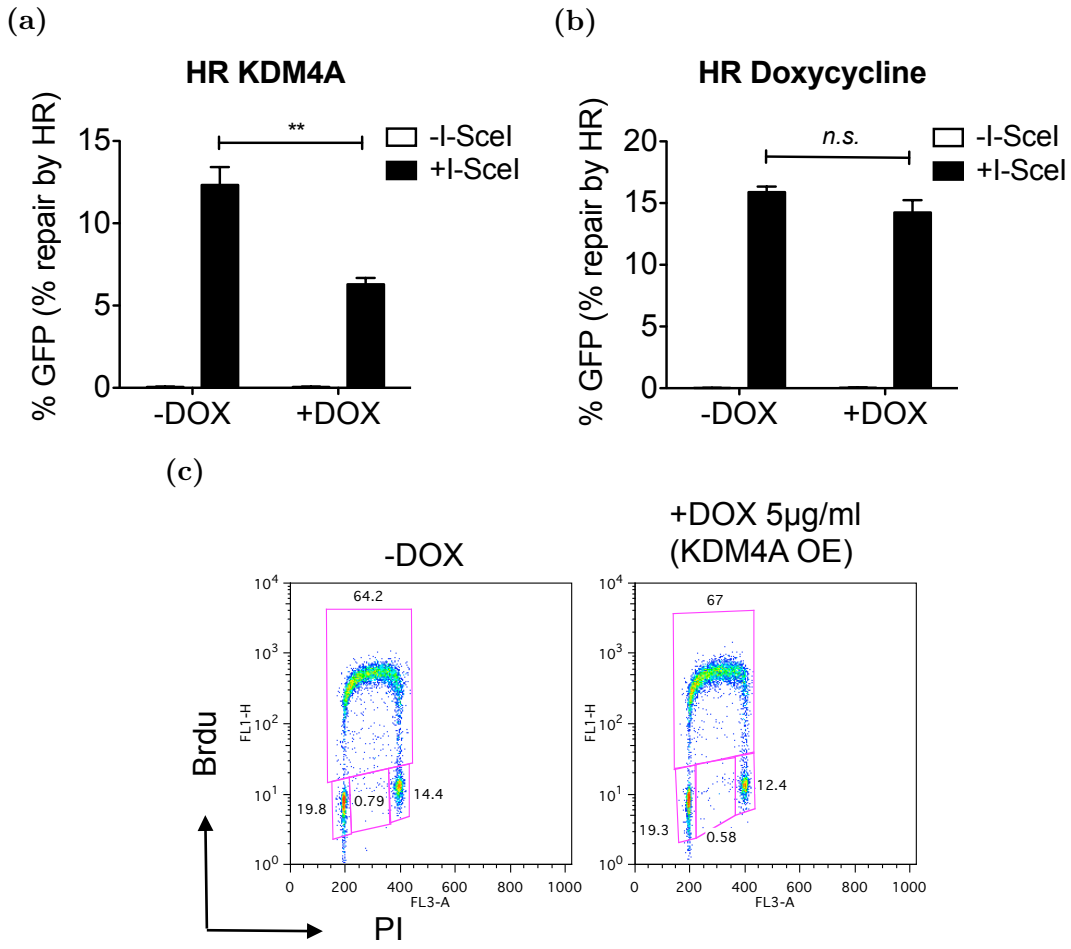


Figure 3.16: KDM4A over-expression reduced HR efficacy without affecting cell cycle distribution. (a) HR efficacy in KDM4A T-REx DR-GFP U2OS cells treated with or without 5μg/ml Doxycycline (DOX). Data are presented as mean ± SEM, n=3 independent experiments independent experiments, **P<0.01. (b) The HR efficacy in parental T-REx DR-GFP U2OS cells (without any cDNA integration) with or without Doxycycline (5μg/ml) treatment. Data are presented as mean ± SEM, n=3 independent experiments, *n.s.* not significant. (c) FACS analysis of cell cycle distribution of KDM4A T-REx U2OS cells with or without induction of KDM4A by Doxycycline (5μg/ml).

ing H3.3K36M also exhibited reduced RPA and RAD51 foci formation following DNA damage (Fig 3.17b, c), similar to those seen in KDM4A over-expressing cells or SETD2-depleted cells. Cell cycle was not significantly affected by H3.3K36M expression (Fig 3.17d), thus excluding the possibility that the reduction in RPA and RAD51 foci formation was due to cell cycle effects.

The common feature of all three different systems (SETD2 methyltransferase-dead mutant, KDM4A over-expression and H3.3K36M expression) was that reduced HR efficiency was associated with reduced H3K36me3 levels. Together these findings suggested a novel role for H3K36me3 in HR repair of DSBs.

3.6 SETD2 promotes DSB end-resection

Lens Epithelial Growth Factor p75 (LEDGF) binds preferentially to H3K36me3 constitutively through its PWWP domain. Upon DNA damage, LEDGF recruits CtIP, which facilitates the resection step during HR repair (Daugaard et al., 2012). Therefore a model was proposed to link H3K36me3 with resection: in the absence of H3K36me3, LEDGF binding to the chromatin would be reduced, leading to reduced recruitment of CtIP to the DSB site and reduced resection.

Accordingly, LEDGF and H3K36me3 were co-immunoprecipitated (co-IP), independently of DNA damage in U2OS cells (Fig 3.18a). In addition, LEDGF binding to chromatin was reduced upon SETD2 depletion, also independent of DNA damage (Fig 3.18b), consistent with preferential binding of LEDGF to

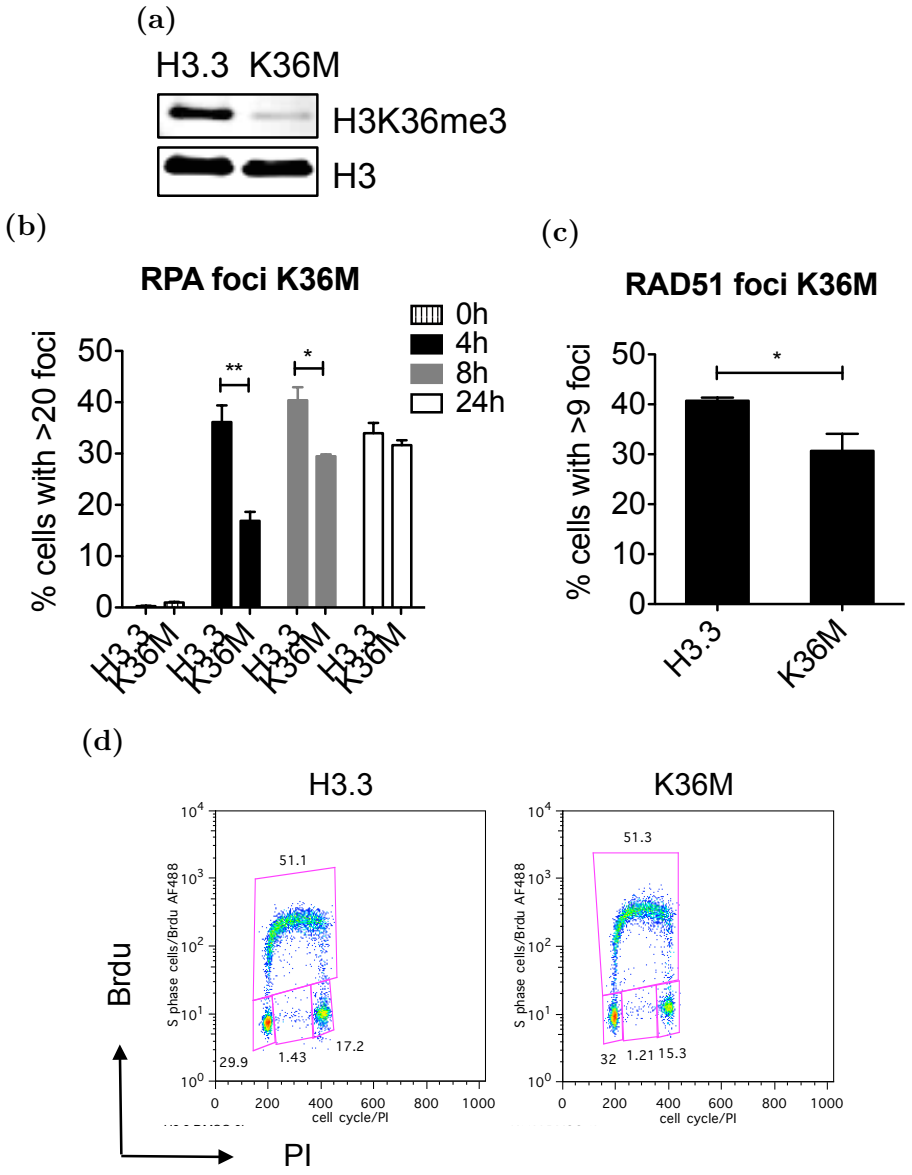


Figure 3.17: H3.3K36M expression reduced H3K36me3 levels and inhibited repair foci formation without affecting cell cycle distribution. (a) Western blot analysis of the levels of H3K36me3 in U2OS cells with stably integrated H3.3 (control) or H3.3K36M lentiviral construct. Histone H3 was used as a loading control. (b) RPA32 foci formation at indicated time after 2-hour CPT (10μM) treatment in H3.3 or H3.3K36M stable expression cells. Data are presented as mean ± SEM, n=3 independent experiments, **P<0.01, *P<0.05. (c) RAD51 foci formation 8 hours after IR (5Gy) in H3.3 or H3.3K36M stable expression cells. Data are presented as mean ± SEM, n=3 independent experiments, *P<0.05. (d) FACS analysis of cell cycle distribution of U2OS cells stably expressing H3.3 or H3.3K36M transgene.

H3K36me3 (Eidahl et al., 2013).

If the model is correct, this reduced LEDGF binding following SETD2 depletion would lead to reduced recruitment of CtIP to the DSB sites. To study the recruitment of CtIP to DSBs, micro-irradiation (Suzuki et al., 2011) was used to induce localised DSBs in a U2OS cell line expressing a GFP-tagged CtIP (Sartori et al., 2007). In control cells transfected with non-targeting siRNA, CtIP was found to localise to the sites of DSBs marked by γH2AX (Fig 3.19). In contrast, SETD2 knockdown resulted in reduced recruitment of CtIP to the DSB sites (Fig 3.19).

If SETD2 facilitates HR through CtIP recruitment, it is expected that SETD2 would be epistatic with CtIP (i.e. depleting SETD2 and CtIP simultaneously would result in the same phenotype as depleting CtIP alone). Indeed, co-depletion of SETD2 and CtIP (siCtIP+siSETD2) showed the same level of reduction in HR as CtIP depletion alone (Fig 3.20). CtIP depletion also increased NHEJ, to the same level as co-depletion of SETD2 and CtIP. These findings were consistent with the hypothesis that SETD2-dependent H3K36me3 promotes recruitment of CtIP by anchoring LEDGF to the DSB sites.

Reduced CtIP recruitment, together with the reduced RPA foci formation following SETD2 depletion suggested that SETD2 was required for DNA end-resection at DSB sites. DNA end-resection initiates HR by creating single-stranded DNA which becomes the substrate for homology-directed strand invasion. To directly measure DNA resection, a new *in vivo* resection assay (Zhou

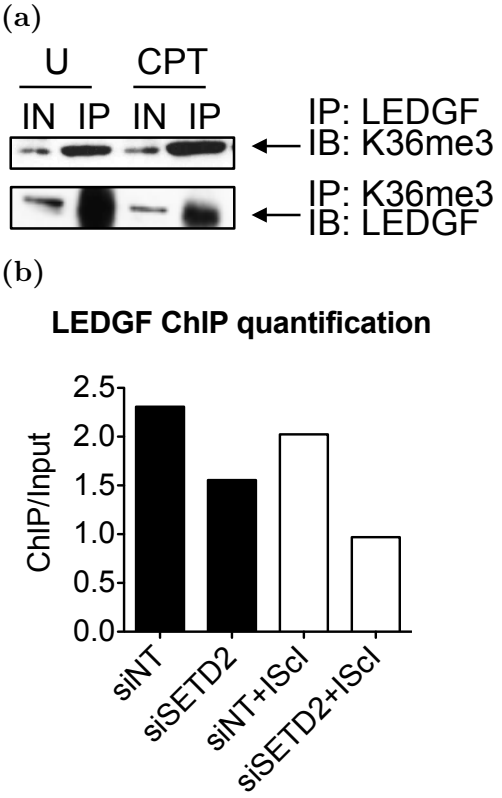


Figure 3.18: SETD2 knockdown reduced binding of LEDGF to the chromatin independent of DSBs. (a) Co-immunoprecipitation of LEDGF and H3K36me3 in the presence or absence of DNA damage. U2OS cells were left untreated (U) or treated with CPT (15μM for 4 hours). Reciprocal co-IPs are shown. This experiment is performed together with Dr Sovan Sarkar. (b) ChIP analysis of LEDGF binding to the DSB site before and after I-SceI induction in NT or SETD2 knockdown DR-GFP cells. siNT: control siRNA treated cells before cut; siS: SETD2 siRNA treated cells before cut; siNT+IScI: control siRNA treated cells after cut; siS+IScI: SETD2 siRNA treated cells after cut. Numbers quantified from one ChIP-PCR experiment and show LEDGF-ChIP over input. The cells were transfected and treated by me, and the ChIP experiments were performed by Dr Lykourgos-Panagiotis Zalmas.

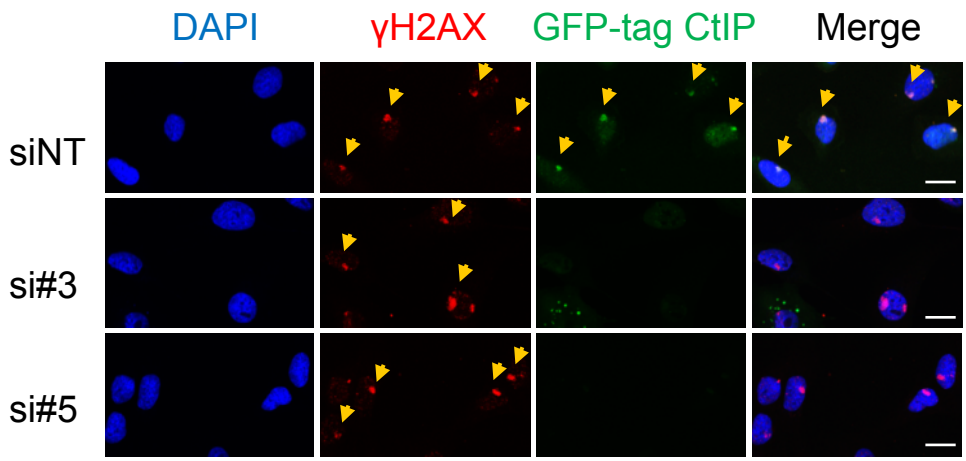
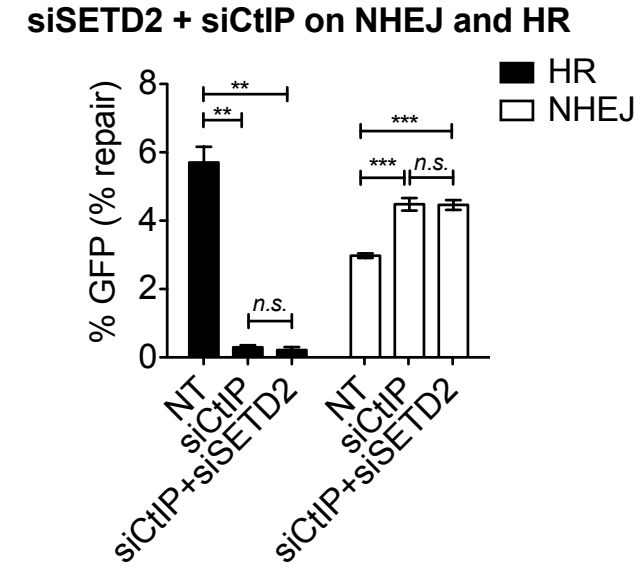


Figure 3.19: SETD2 knockdown reduced recruitment of CtIP to the sites of DSBs. Microirradiation showing CtIP recruitment to damage site in U2OS cells treated with non-targeting control siRNA (siNT) or SETD2 siRNAs (si#3 and si#5). Sites of DNA damage were marked by γH2AX. Fluorescent images were acquired using a confocal microscope (Zeiss), scale bars represent 20μm.

et al., 2014) was used to measure the amount of single-stranded DNA at increasing distances from a specific DSB site (induced by the AsiSI restriction enzyme), which was found to recruit RAD51 (Iacovoni et al., 2010; Aymard et al., 2014).

Through collaboration with the lab of Gaëlle Legube (where the resection assay was first developed), the impact of SETD2 knockdown on resection was assessed. Following DSB induction, single-stranded DNA (ssDNA) was readily detected 231bp from the break-site and at reduced levels further away (918bp). SETD2 depletion significantly reduced ssDNA at 231bp and 918bp from the break-site, similarly to CtIP depletion. SETD2 depletion did not affect cutting efficiency or the recruitment of NHEJ proteins to these sites as measured by XRCC4 (see (Pfister et al., 2014) in the Appendix). The resection assay

(a)



(b)

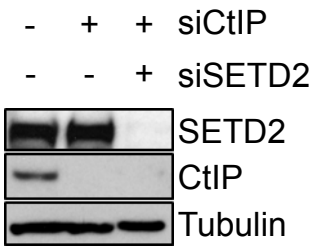


Figure 3.20: SETD2 was epistatic with CtIP. (a) HR and NHEJ efficacy (as measured by the reporter assays described earlier) in cells transfected with control siRNA (NT), CtIP siRNA (siCtIP) or both CtIP and SETD2 siRNAs (siCtIP+siSETD2). Data are presented as mean ± SEM, n=3 independent experiments, ***p<0.001, **p<0.01, *n.s.* not significant. (b) Western blots showing the siRNA knockdown of CtIP or both CtIP and SETD2.

confirmed that SETD2 was required for DNA end-resection following DSBs.

3.7 Discussion of Chapter 3

3.7.1 The SETD2 in HR model

The tumour suppressor SETD2 gene encoding the H3K36 trimethyltransferase was found to be among the most mutated in human cancers (Lawrence et al., 2014). Yet it was unclear how SETD2-deficient cancer cells had accumulated large amounts of genomic mutations (Sato et al., 2013; Zhu et al., 2014).

This project has assigned a new role to SETD2 and its catalytic product H3K36me3 in facilitating error-free repair of DNA double-stranded breaks (DSB) and maintaing genome stability through homologous recombination (HR). The data supports a model in which LEDGF is constitutively anchored to H3K36me3-decorated chromatin (through its PWWP domain). It is speculated that upon sensing of DNA damage, CtIP is activated (phosphorylated) by the DDR proteins such as ATM, ATR or BRCA2. Activated CtIP is tethered to its nearby chromatin by the chromatin-bound LEDGF (since LEDGF binds CtIP in a DNA damage-dependent manner (Daugaard et al., 2012)). This tethering of activated CtIP to the damage site promotes resection – an essential step in HR repair (Fig 3.21a). In the absence of SETD2 and/or H3K36me3, LEDGF binding to the chromatin is compromised, and CtIP recruitment is impaired after DSBs,

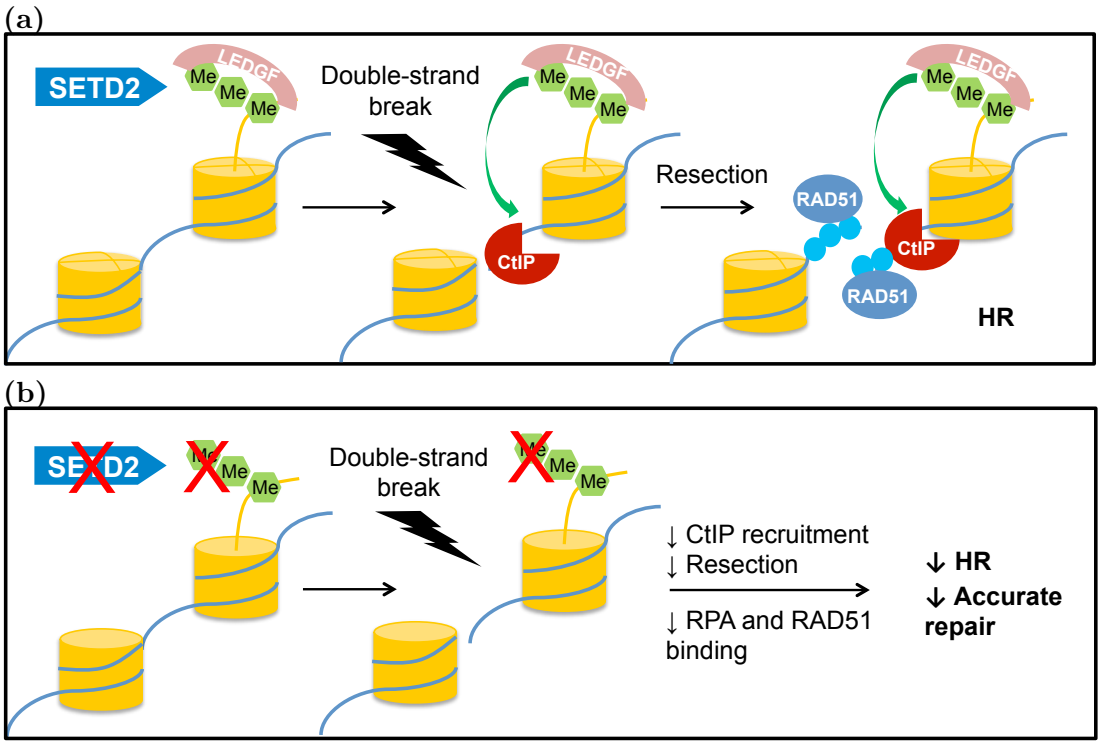


Figure 3.21: Model for the role of SETD2 and H3K36me3 in HR and genome stability. (a) SETD2-dependent H3K36me3 constitutively recruits LEDGF to chromatin. Following DNA double-stranded breaks, LEDGF recruits CtIP and thereby promoting resection, facilitating RPA and RAD51 recruitment. (b) In the absence of H3K36me3, the lack of LEDGF chromatin association results in reduced recruitment of CtIP after DSBs, impairing resection and error-free HR repair, leading to inaccurate DSB repair and genome instability.

leading to reduced resection and reduced HR (Fig 3.21b). The model does not, however, exclude the possibility that other H3K36me3 binding factors may also contribute to efficient HR.

3.7.2 Future directions

A mild G1 arrest was observed in cells treated with SETD2 siRNAs compared to non-targeting siRNAs (Fig 3.2c). This may be consistent with the role of SETD2

in E2F1 expression and S-phase entry (see Chapter 4). To confirm such a mild effect, more repeats of the cell cycle analysis need to be performed and a bar chat can be used to quantify the statistical significance.

It is speculated that H3K36me3 is required for the accurate repair (HR) of the actively transcribed genes. To test this, the effect of H3K36me3 on HR efficacy in transcribed vs. untranscribed genes can be measured by modifying the DR-GFP reporter (Fig 3.3a), such that the CMV promoter is replaced by a promoter (e.g. a Tet-operator) that can switch the transcription on and off. If the hypothesis is correct, HR efficiency will not be affected by SETD2 depletion if the promoter is switched off.

The DR-GFP reporter assay is perhaps not the best way to test the epistasis between CtIP and SETD2 in HR (Fig 3.20a). Since the percentage of GPF-positive cells is very close to zero after CtIP knockdown, any additional effect caused by SETD2 knockdown would not be visible. Alternative methods such as RPA or RAD51 foci may be used where there is still room for further reduction, should CtIP and SETD2 co-depletion have a synergistic effect on HR.

Chapter 4

A new synthetic lethal interaction: SETD2 and WEE1

This chapter describes a new synthetic lethal interaction between loss of SETD2 and inhibition of WEE1 (a negative regulator of CDK1), which could enable therapeutic development of WEE1 inhibitors against SETD2-deficient cancers. It also provides insights into the underlying mechanism of this synthetic lethality, which reveals a new function of SETD2 in deoxyribonucleotide (dNTP) production and thus in DNA replication.

4.1 SETD2-deficient cancer cells are hypersensitive to WEE1 inhibition

Synthetic lethal interactions between cellular pathways can be exploited to selectively kill cancer cells that carry a mutation in a gene of one pathway by chemically inhibiting the function of a gene in a second pathway. *SETD2*, which encodes the histone H3K36me3 methyltransferase, was recently found to be among the most frequently mutated genes in cancer (Lawrence et al., 2014). It was also found to be mutated in multiple major cancer types, summarised in (Table 4.1), which indicates the percentage of *SETD2* mutations in different cancers according to the COSMIC project by the Sanger Institute. The COSMIC sequencing results are also supported by independent studies on renal cancer, lung cancer, glioma, leukaemia and breast cancer (Duns et al., 2010; Dalgliesh et al., 2010; Gerlinger et al., 2012; Fontebasso et al., 2013; Zhang et al., 2012; Al Sarakbi et al., 2009). The high frequency of SETD2 loss in a wide range of cancers identifies SETD2 loss-of-function mutation as a potential target for cancer therapy.

In order to selectively kill cancer cells that are deficient in SETD2 without harming normal tissues, one must find a synthetic lethal partner for SETD2. Instead of performing an siRNA or chemical compound screen, this project took a different approach where an unexpected discovery in yeast was investigated in human cancer cell lines. In fission yeast, loss of Set2 and Wee1 (orthologues of human SETD2 and WEE1) were found to be synthetically lethal (unpublished

Tissue	SETD2 point mutation (%)	SETD2 copy number loss (%)	SETD2 under expression (%)
Large Intestine	9.19	0.16	4.43
Kidney	8.74	1.05	1.63
Endometrium	4.75	0.22	2.58
Lung	2.77	0.35	3.05
Breast	1.78	0.21	7.25
Central nervous system	1.24	0.13	4.10
Ovary	0.92	-	6.79
Hematopoietic and lymphoid	0.85	-	2.31

Table 4.1: Summary of the frequency of SETD2 mutation, copy number loss and under-expression in different cancer types. Numbers acquired from http://cancer.sanger.ac.uk/cancergenome/projects/cosmic/. The frequency of under-expression is generally higher than copy number loss because SETD2 expression can also be epigenetically regulated, such as promoter silencing.

data from Dr Rachel Deegan). If this synthetic lethal interaction holds true in human, then SETD2-deficient cancers can be potentially eliminated by inhibiting WEE1, a cell cycle kinase that negatively regulates cyclin-dependent kinase 1 (CDK1).

The WEE1 inhibitor MK1775 (AZD1775) was chosen for this study because it is the most clinically advanced chemical inhibitor for WEE1. According to ClinicalTrials.gov, 19 trials have been conducted on MK1775, 12 of which are in Phase II. Therefore any useful scientific findings could be converted into patient benefits more readily.

The effect of MK1775 was examined on four human cancer cell lines: two SETD2-deficient lines (A498 and LB996) (Dalgliesh et al., 2010) and two SETD2-



Figure 4.1: Schematic map showing SETD2 mutations in LB996 and A498 cell lines. The locations of SET domain and SRI domain were mapped according to Uniprot.org. The amino acid changes were quoted from (Dalgliesh et al., 2010) but adjusted to the updated sequence of SETD2 (in the new version, 503 amino acids were added to the N-terminus of the protein).

wildtype lines (RCC4 and U2OS). A498 and LB996 each harbours an interesting homozygous mutation in the *SETD2* gene: A498 has a truncation mutation in the SRI domain of SETD2, which is required for its interaction with RNA polymerase II (Pol II) (Fig 4.1). As a result, A498 cells expressed near full-length SETD2 protein, but had reduced levels of H3K36me3 (Fig 4.2). This observation agreed with the literature where SETD2 binds to Pol II and catalyses the trimethylation of H3K36 in the wake of Pol II transcription. LB996 has a homozygous nonsense mutation in the SET domain (Fig 4.1). As a result, LB996 cells did not express SETD2 protein due to the premature stop codon and nonsense-mediated decay, and had reduced levels of H3K36me3 (Fig 4.2).

Cell viability experiments show that SETD2-deficient cells were hypersensitive to MK1775. IC50 (half maximal inhibitory concentration) of MK1775 for each cell lines are: A498 IC50=83nM, LB996 IC50=48nM vs. U2OS IC50=377nM, RCC4 IC50>400nM ($p<0.0001$) (Fig 4.3a). Increased cell death by apoptosis was also observed in SETD2-deficient cells after MK1775 treatment (Fig 4.3b). Cell

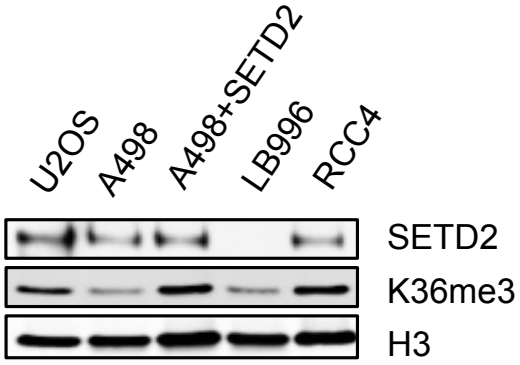


Figure 4.2: Western blotting analysis of the levels of SETD2 and H3K36me3 in the cell lines indicated. H3 was used as a loading control. A498+SETD2 represented A498 cells stably expressing an exogenous wild-type SETD2.

death and growth arrest is also visible under bright-field microscope (Fig 4.3c).

To confirm that the loss of SETD2 is the primary cause of sensitivity to MK1775, a wild-type SETD2 cDNA was stably integrated into SETD2-deficient A498 cells, which restored the level of H3K36me3 (Fig 4.2) and reduced sensitivity to MK1775 (Fig 4.4). To confirm that it is the methyltransferase activity that is causing the sensitivity, an additional rescue experiment needs to be performed with the methyltransferase-dead SETD2 cDNA.

A498, LB996 and RCC4 are human clear cell Renal Cell Carcinoma (ccRCC) cell lines, and U2OS is a human osteosarcoma cell line, but only SETD2-deficient A498 and LB996 were sensitive to MK1775. Therefore the effect of MK1775 is unlikely to be dependent on cancer tissue type, but dependent on SETD2 status. To prove this, the sensitivity to MK1775 was compared between SETD2 siRNA knockdown cells and control siRNA treated cells. Indeed, U2OS cells treated

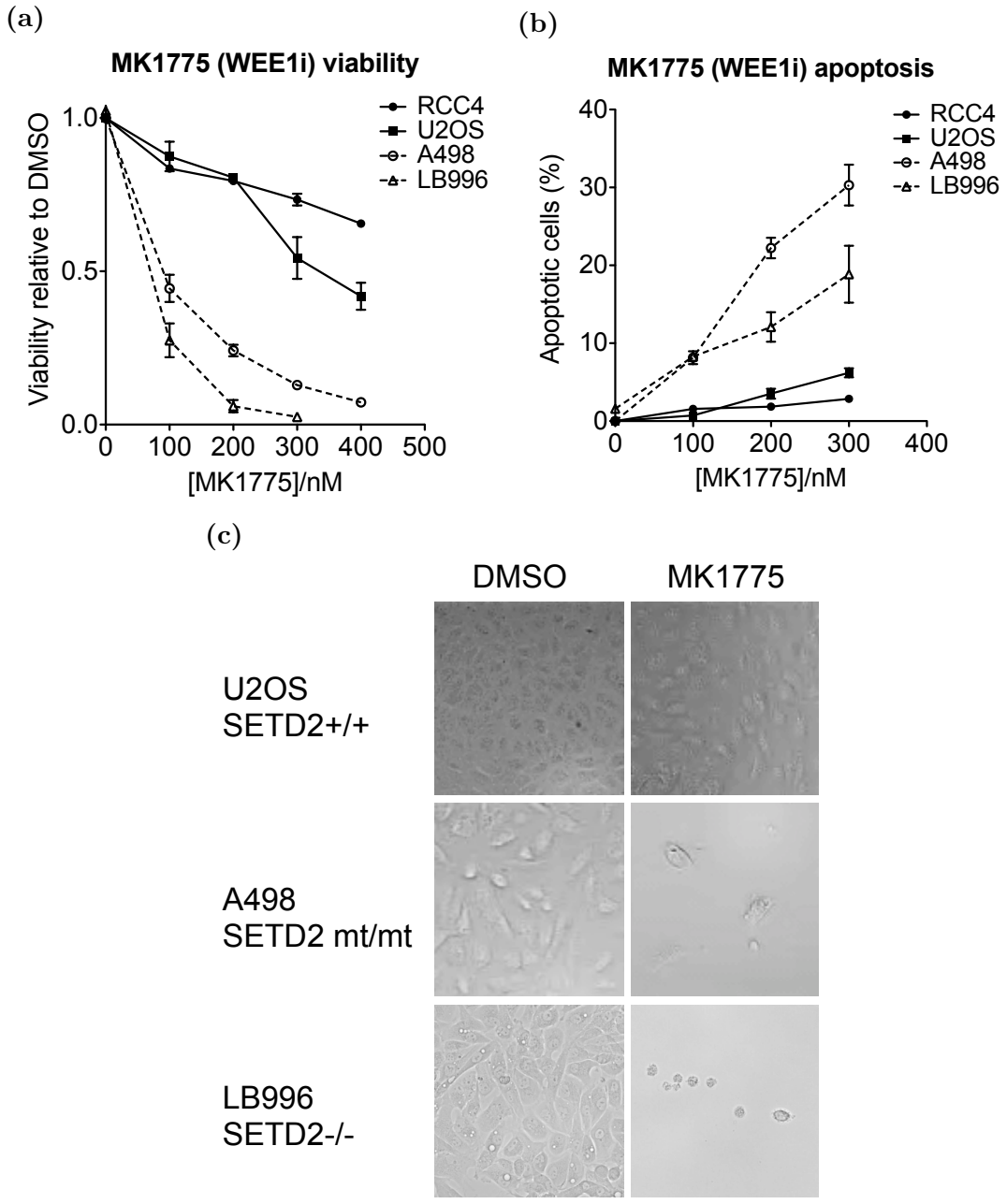


Figure 4.3: SETD2-deficient cancer cells are more sensitive to WEE1 inhibitor MK1775. (a) Viability of human cancer cell lines RCC4 (SETD2+/+), U2OS (SETD2+/+), A498 (SETD2 homozygous mutation) and LB996 (SETD2-/-) were measured by Resazurin five days after a single treatment with WEE1 inhibitor MK1775 at the indicated concentrations. (b) Percentage of cells undergoing apoptosis as determined by Hoechst nuclear staining 48 hours after MK1775 treatment. Data are presented as mean ± SEM, n=3 independent experiments. (c) Representative bright-field microscope images of the cells after DMSO or MK1775 (200nM) treatment for five days.

with two independent SETD2 siRNAs showed reduced viability and increased apoptosis following exposure to MK1775 (Fig 4.5). To exclude the possibility of siRNA off-target effects, SETD2-deficient A498 cells were also treated with SETD2 siRNAs, and no further reduction in viability was observed following exposure to MK1775 (Fig 4.6).

To exclude any possible side-effect of the WEE1 inhibitor, WEE1 siRNAs were used to deplete the protein. In agreement with the results obtained from MK1775, WEE1 siRNA knockdown was more toxic to SETD2-deficient cells than to SETD2-proficient cells (as measured by viability and apoptosis) (Fig 4.7). Taken together, these results suggest that loss of SETD2 renders cancer cells hypersensitive to WEE1 inhibition.

4.2 WEE1 inhibition induces mitotic catastrophe in p53-deficient cells, but not in SETD2-deficient cells

WEE1 inhibitors have been used to kill TP53 mutant cells, predominantly through mitotic catastrophe (Aarts et al., 2012). Therefore whether p53 inactivation or premature mitosis is contributing to the death of SETD2-deficient cells was investigated.

FACS analysis revealed that p53-deficient cells entered mitosis prematurely

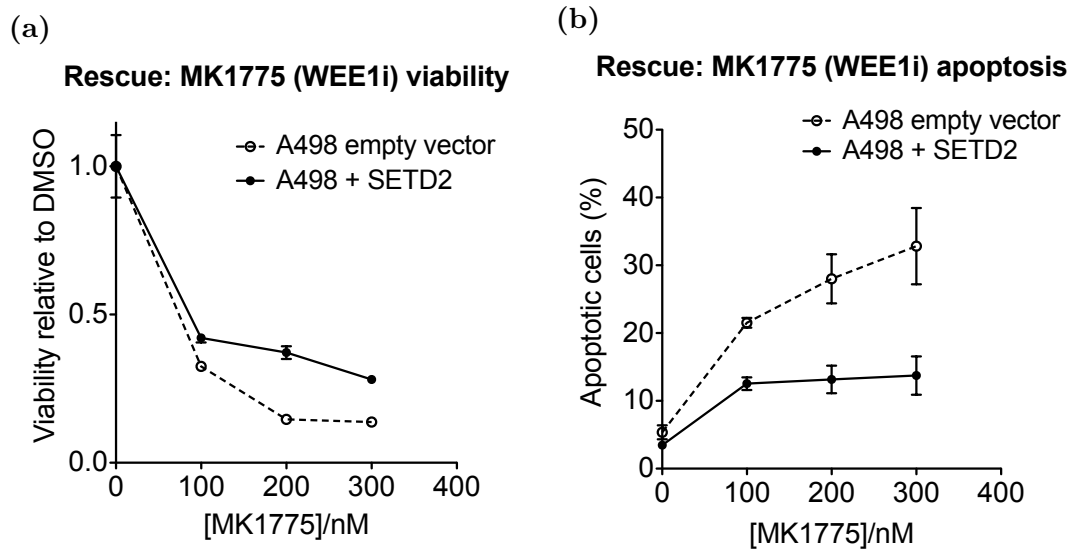


Figure 4.4: The sensitivity to MK1775 can be suppressed by expressing exogenous wild-type SETD2. (a) Viability of A498 cells expressing an empty vector or SETD2 cDNA 72 hours after MK1775 treatment, measured by a Resazurin assay. (b) Percentage of cells undergoing apoptosis, determined by Hoechst nuclear staining 48 hours after MK1775 treatment. Data are presented as mean ± SEM, n=3 independent experiments

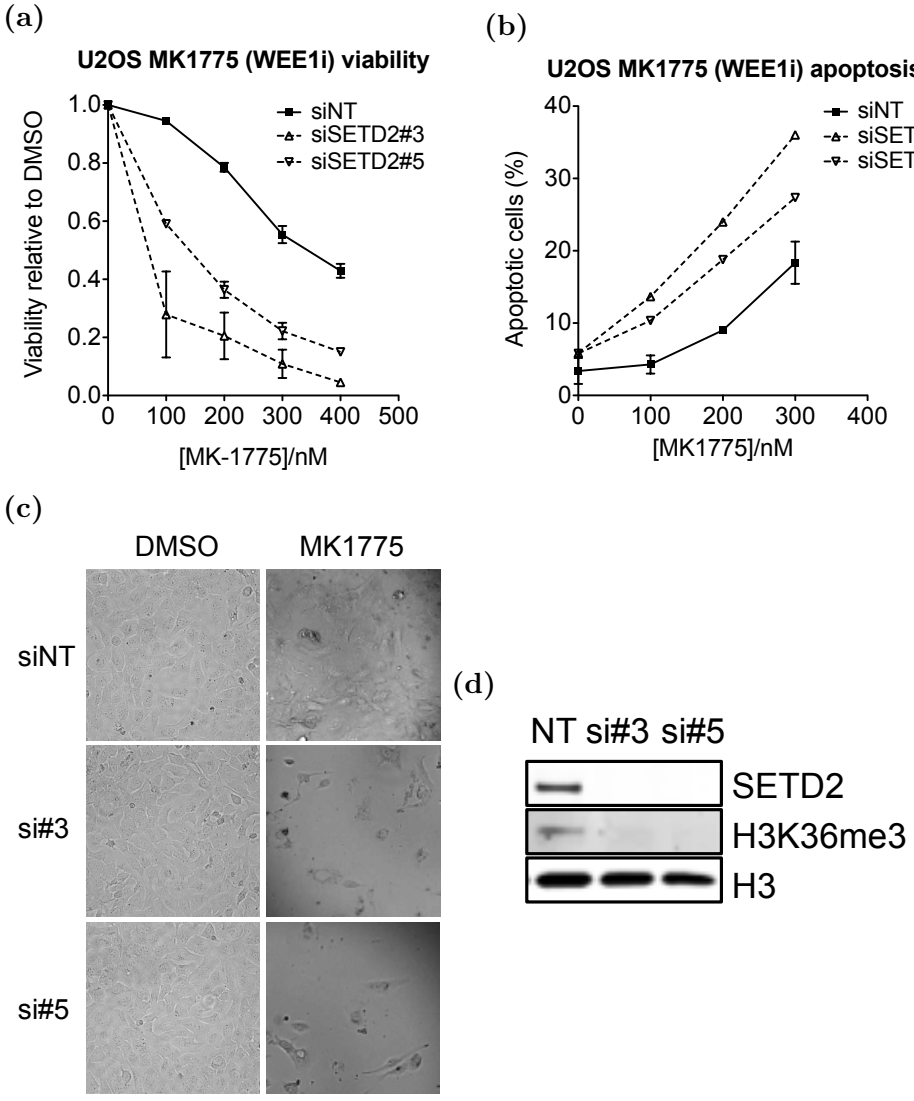


Figure 4.5: SETD2 knockdown sensitises cells to WEE1 inhibitor MK1775. (a) Viability as measured by Resazurin of U2OS cells transfected with non-targeting siRNA (siNT) or two independent SETD2 siRNAs (si#3 and si#5) 48 hours prior to treatment with indicated concentrations of MK1775 for five days. Results were normalised to the same siRNA-transfected cells treated with DMSO for five days. For each knockdown condition, viability was normalised to the viability of cells transfected with the same siRNA but treated with DMSO instead of the inhibitors (thus siRNA toxicity was accounted for). (b) Percentage of cells undergoing apoptosis, determined by Hoechst nuclear staining 48 hours after MK1775 treatment. Data are presented as mean ± SEM, n=3 independent experiments. (c) Representative bright-field microscope images of knockdown U2OS cells five days after treatment with either DMSO or MK1775 (300nM). (d) Western blots confirming the depletion of SETD2 and H3K36me3 by the siRNAs.

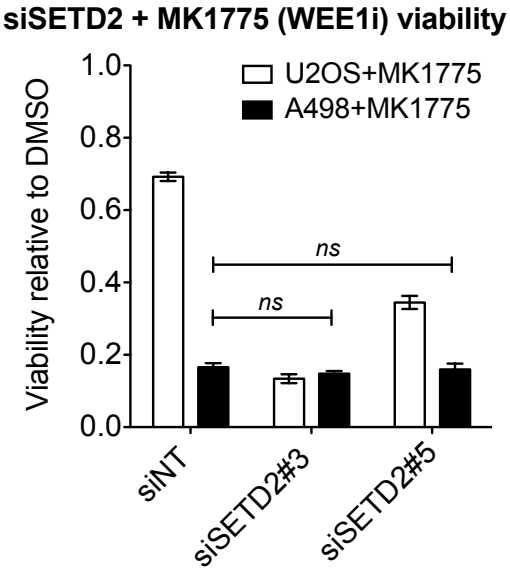


Figure 4.6: SETD2 siRNAs do not further sensitise SETD2-deficient cells. Viability as measured by Resazurin of U2OS or A498 treated with control non-targeting siRNA (siNT) or SETD2 siRNAs (si#3 and si#5) 48 hours prior to incubation with MK1775 (200nM) for five days. Results were normalised to the same siRNA-transfected cells incubated with DMSO for five days. Data are presented as mean ± SEM, n=3 independent experiments.

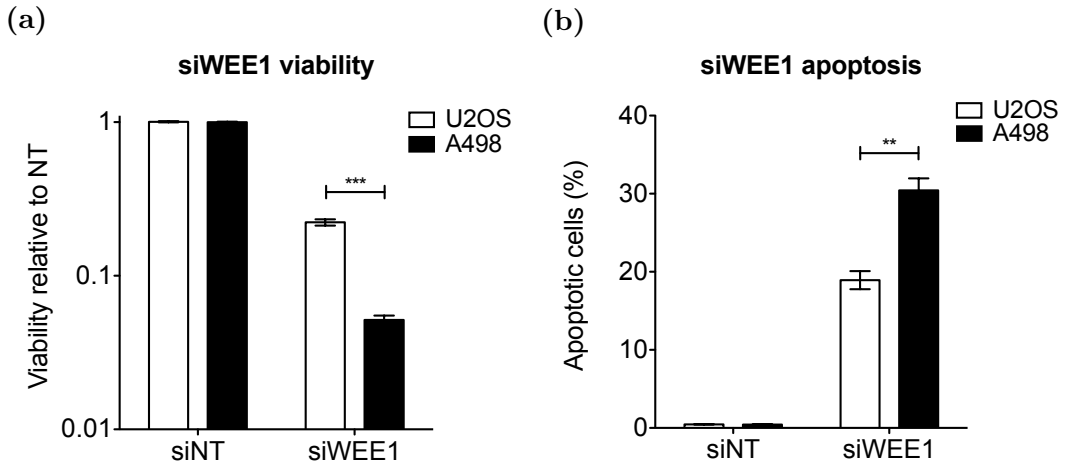


Figure 4.7: SETD2-deficient cells are more sensitive to WEE1 siRNA knockdown. (a) Viability as measured by Resazurin of U2OS or A498 cells transfected with either control non-targeting siRNA (siNT) or WEE1 siRNAs (siWEE1) for five days. (b) Percentage of cells undergoing apoptosis, determined by Hoechst nuclear staining 48 hours after WEE1 siRNA treatment. Data are presented as mean ± SEM, n=3 independent experiments. ***P<0.001, **P<0.01.

upon MK1775 treatment, as S-phase cells stained positive for the mitotic marker H3 phosphorylation at Serine 28 (pH3 S28) and Serine 10 (pH3 S10). Unlike p53-deficient cells, SETD2-deficient cells did not show any increase in the mitotic population, nor any pH3 S28 staining in S-phase cells (Fig 4.8).

The activation of p53 after MK1775 treatment was tested in SETD2-deficient cells, as two publications suggested that SETD2 may affect the activity of p53 (Xie et al., 2008; Carvalho et al., 2014). However, western blots showed that p53 was activated (stabilised) by MK1775 in both SETD2-proficient and SETD2-deficient cell lines (Fig 4.9a). Furthermore, SETD2 knockdown in U2OS cells did not affect the activation of p53 after MK1775 treatment, as demonstrated by the stabilisation of the protein and its transcriptional activation of p21 (Fig 4.9b).

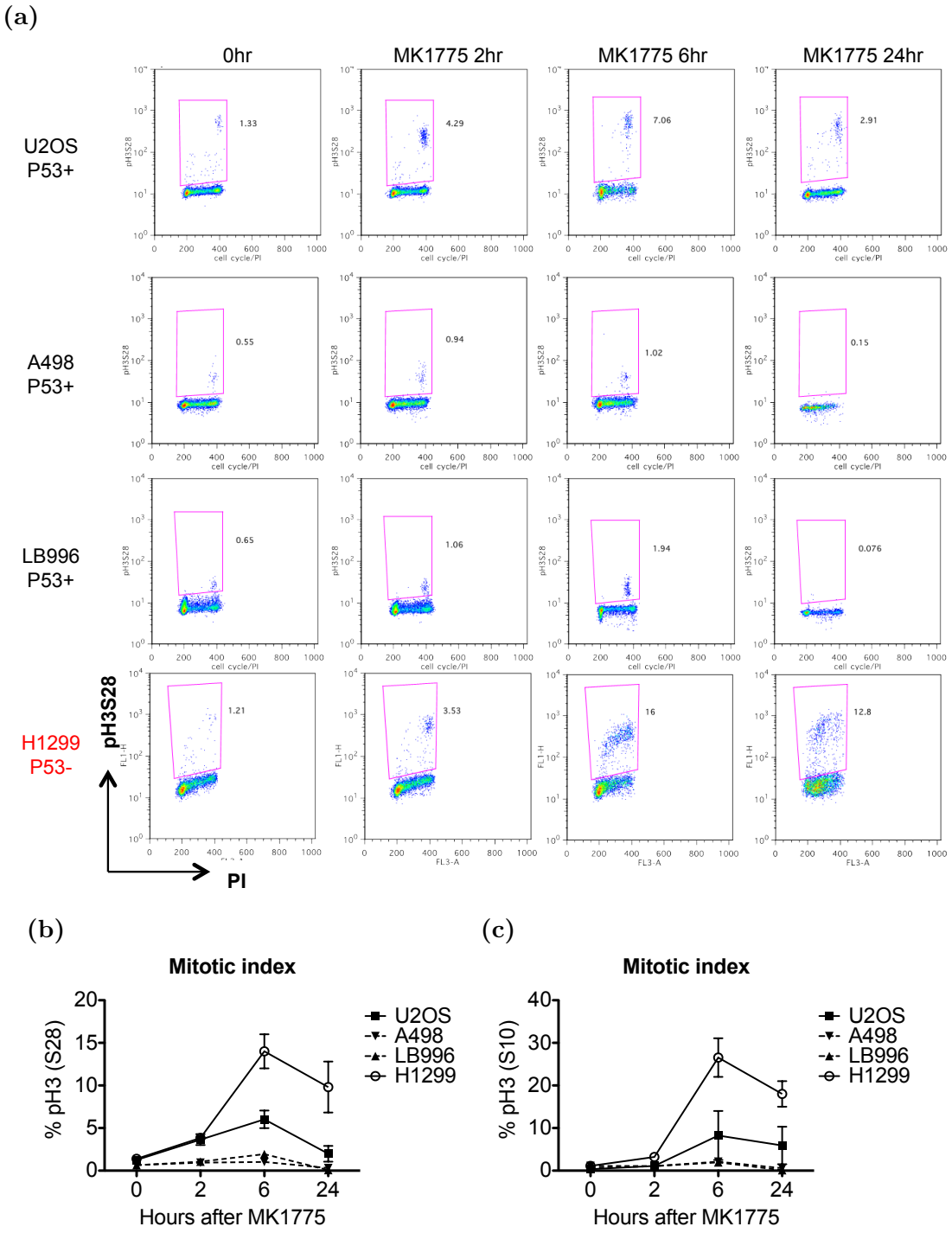


Figure 4.8: p53-deficient cells enter mitosis prematurely upon MK1775 treatment, but SETD2-deficient cells do not. (a) FACS analysis of histone H3 phosphorylation at S28 (mitosis marker) at indicated hours after MK1775 (200nM) treatment. Quantification of H3 phosphorylation at (b) Serine 28 or (c) Serine 10 in U2OS, A498, LB996 and H1299 cells at indicated hours after MK1775 (200nM) treatment.

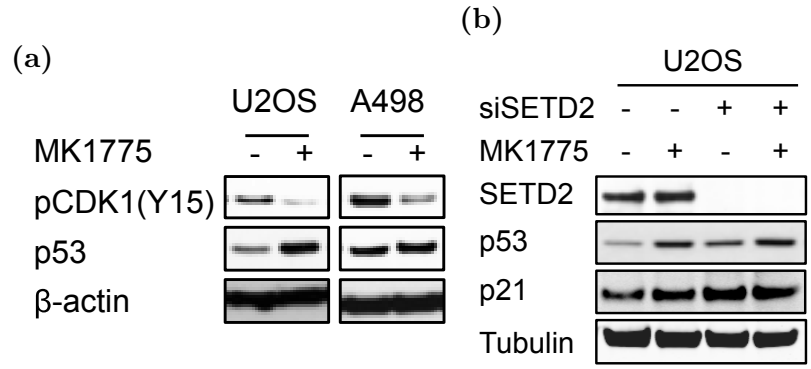


Figure 4.9: SETD2 deficiency does not affect p53 activation by MK1775. (a) Western blots showing the levels of CDK1 inhibitory phosphorylation at Tyrosine 15 (Y15), and p53 stabilisation in U2OS and A498 cells after treatment with the WEE1 inhibitor MK1775 (200nM) for 48 hours. (b) Western blots showing the stabilisation of p53 and the activation of p21 in U2OS cells transfected with non-targeting siRNA or SETD2 siRNA, 48 hours prior to MK1775 treatment, for 24 hours.

The western blot also confirmed that the concentration of the WEE1 inhibitor MK1775 used in the experiments (200nM) effectively inhibited the kinase activity of WEE1 in both U2OS and A498 cells. This was demonstrated by the reduced inhibitory phosphorylation of CDK1 on tyrosine 15 (pCDK1 Y15), a target of WEE1 (Fig 4.9a).

These data suggest that the WEE1 inhibitor kills SETD2-deficient cells through a different mechanism from p53-deficient cells, and that inhibiting WEE1 targets an additional group of cancers which are p53-wildtype and SETD2-deficient.

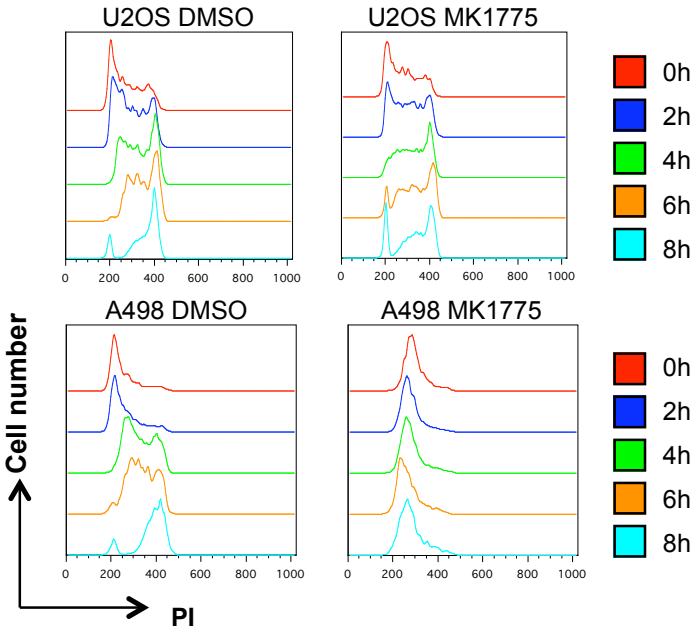
4.3 WEE1 inhibition induces replication stalling in SETD2-deficient cells

To investigate the mechanism of this synthetic lethality, the cell cycle progression of MK1775-treated cells was analysed because WEE1 is a cell cycle regulatory kinase. Surprisingly, MK1775 inhibited DNA replication of SETD2-deficient cells, as S-phase (BrdU-labeled) A498 cells failed to increase their DNA contents (from 2n to 4n) in the presence of MK1775 (Fig 4.10a). Consistently, these cells exhibited an extremely long S-phase, calculated from a BrdU-pulse time course experiment according to a published protocol (Begg et al., 1985) (Fig 4.10b).

The inhibition of DNA replication led to 40% of A498 cells becoming accumulated in a non-replicating S-phase state after MK1775 treatment (Fig 4.11). The non-replicating S-phase population consisted of cells having partially-replicated DNA (between 2n and 4n) but could not incorporate BrdU. On the other hand, MK1775 had little effect on the S-phase of SETD2-proficient cells (Fig 4.10 and Fig 4.11). Therefore, the dramatic effect of MK1775 on S-phase is dependent on the cell's SETD2 status, similarly to its effect on viability and apoptosis.

On the other hand, p53-deficient cells did not encounter replication inhibition, i.e. no non-replicating S-phase population and or S-phase delay (Fig 4.12). These data further suggest WEE1 inhibitor kills SETD2-deficient cells through a different mechanism from p53-deficient cells.

(a)



(b)

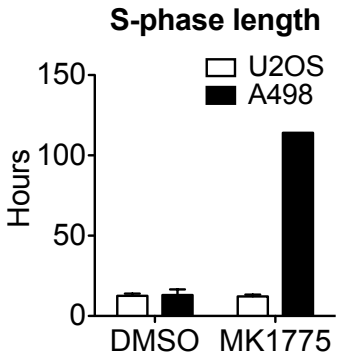
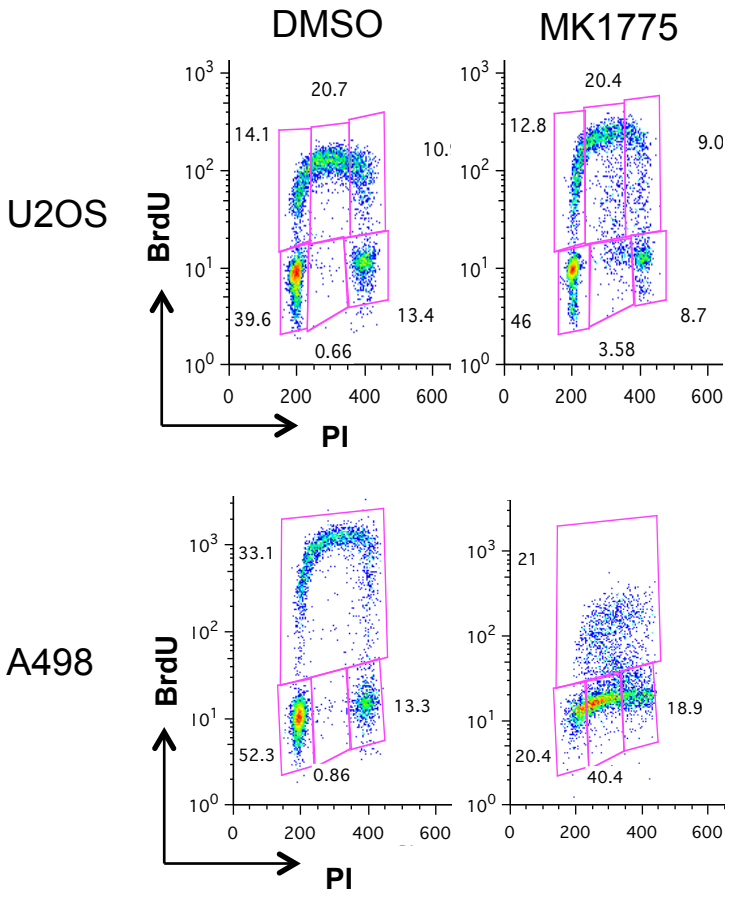


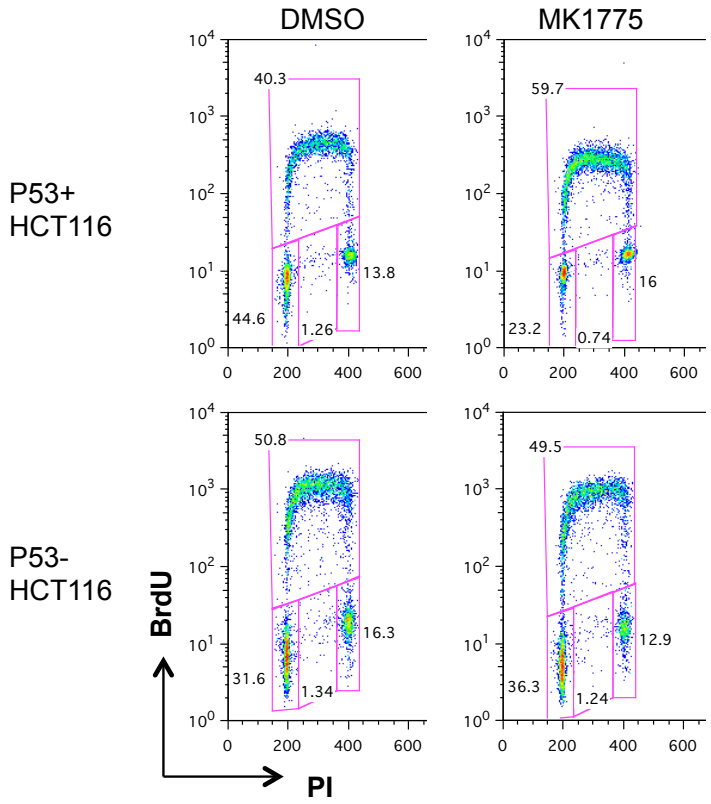
Figure 4.10: MK1775 inhibits S-phase progression specifically in SETD2-deficient cells. A498 and U2OS cells were treated with DMSO or MK1775 for 48 hours and pulse-labeled with BrdU for 20 minutes. Samples were taken every 2 hours after BrdU labelling, and were stained with anti-BrdU antibody and analysed by FACS. (a) Increase in DNA contents of BrdU-labeled (S-phase) cells over 8 hours. (b) Estimated time taken to complete the S-phase (based on samples harvested at 0 hour and 8 hours post BrdU labelling). These experiments were performed together with Mr Mick Woodcock.



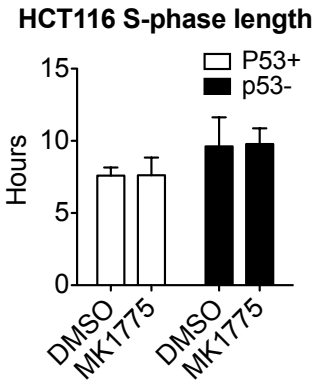
Non-replicating S	DMSO	MK1775
U2OS	0.7%	3.6%
A498	0.9%	40.4%

Figure 4.11: MK1775 induced non-replicating S-phase population specifically in SETD2-deficient cells. FACS analysis of BrdU incorporation by U2OS and A498 cells after treatment with DMSO or MK1775 (200nM) for 48 hours. The table shows the percentage of the S-phase population that is non-replicating (cells which have DNA content between 2n and 4n, but not incorporating BrdU).

(a)



(b)



Non-replicating S	DMSO	MK1775
p53+	1.3%	0.7%
p53-	1.3%	1.2%

Figure 4.12: MK1775 did not induce non-replicating S-phase population nor S-phase arrest in p53-deficient cells. (a) FACS analysis of BrdU incorporation by P53-positive or negative HCT116 cells after treatment with DMSO or MK1775 (200nM) for 48 hours. (b) Estimated time taken to complete the S-phase based on samples harvested at 0 hour and 8 hours post BrdU labelling.

4.4 MK1775 inhibits replication fork progression and increases fork stalling in SETD2-deficient cells

In order to find the cause of S-phase arrest, a DNA fibre assay was conducted to visualise the progression of individual replication forks. The fork velocity was mildly reduced by SETD2 siRNA knockdown or MK1775 treatment (from an average of 0.6-0.8kb/min to 0.4-0.6kb/min in both cases) (Fig 4.13). This suggested that both SETD2 and WEE1 are required for efficient DNA replication. Remarkably, combining SETD2 knockdown with MK1775 abolished fork progression (average <0.2kb/min) (Fig 4.13).

WEE1 inhibition is known to increase origin firing, which reduces fork velocity through a feedback mechanism which prevents extensive fork stalling (Sø rensen and Syljuå sen, 2012). However, in this case, the extremely slow fork progression is accompanied by significantly increased fork stalling (Fig 4.14), suggesting that the combination disrupts DNA replication to a much greater extent than WEE1 inhibition alone.

To investigate the molecular changes induced by MK1775 at the replication fork, a recently published technique called iPOND (isolation of proteins on nascent DNA) (Sirbu et al., 2011, 2012) was used. This technique in summary, pulls down proteins bound to the newly replicated (nascent) DNA by labeling

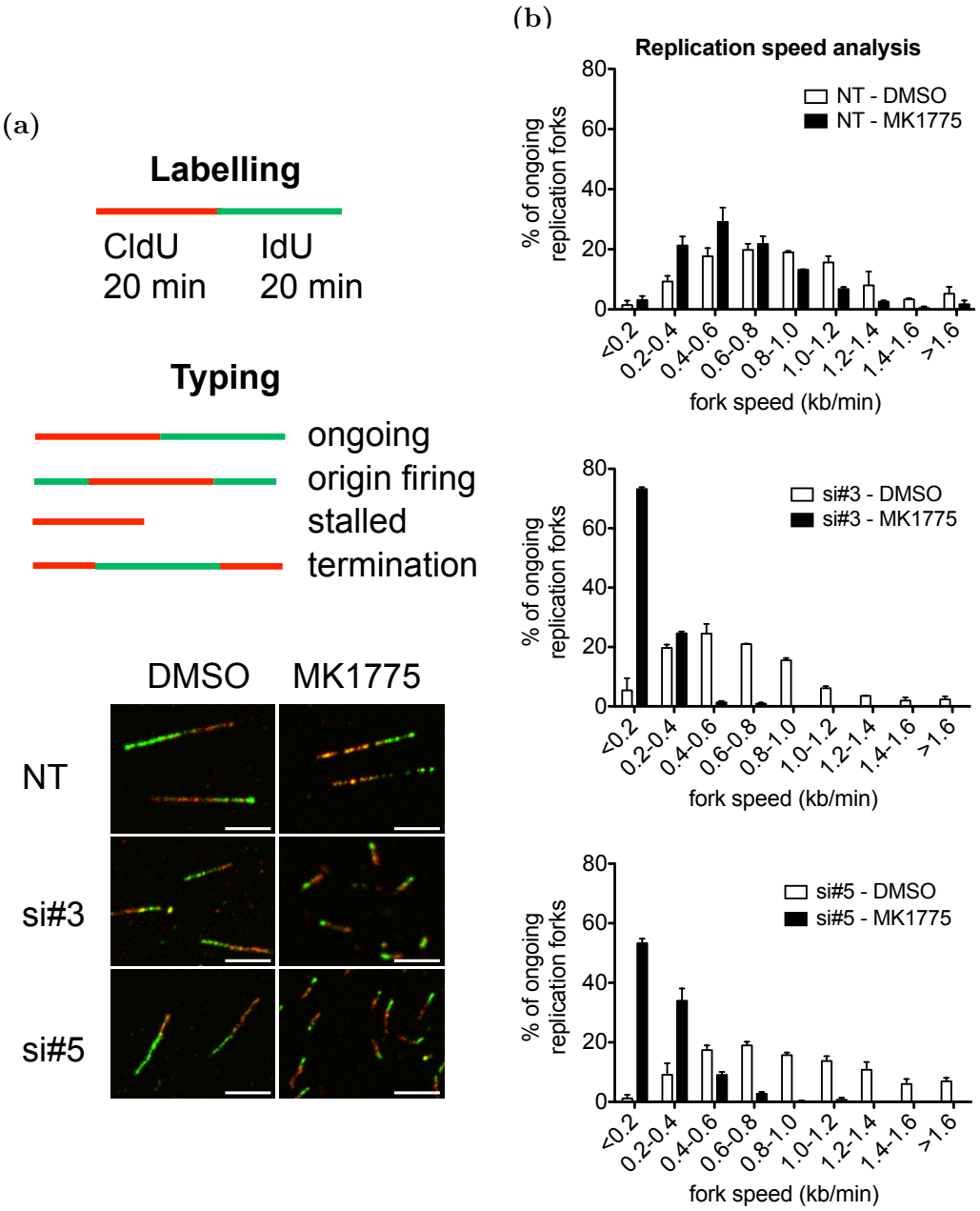


Figure 4.13: MK1775 reduces fork velocity specifically in SETD2-depleted cells. DNA fibre analysis of replication fork velocity in U2OS cells transfected with non-targeting siRNA (NT) or SETD2 siRNAs (si#3 and si#5) 48 hours prior to treatment with DMSO or MK1775 (200nM) for 48 hours. (a) Schematic diagram illustrating the labelling and typing of the fibres, with representative images of the fork length after treatments. Scale bar is 5 μm. (b) Analysis of the distribution of fork velocity. A minimum of 100 ongoing replication forks were analysed for each condition. Data are presented as mean ± SEM, n=3 independent experiments.

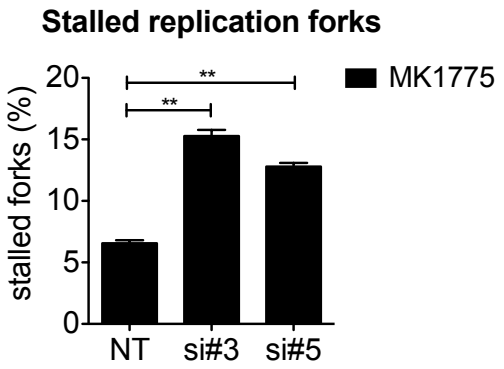


Figure 4.14: MK1775 increases fork stalling specifically in SETD2-depleted cells. DNA fibre analysis of stalled replication forks in U2OS cells transfected with non-targeting siRNA (NT) or SETD2 siRNAs (si#3 and si#5) 48 hours prior to treatment with DMSO or MK1775 (200nM) for 48 hours. Data are presented as mean ± SEM, n=3 independent experiments. **P<0.01.

nascent DNA with EdU (a nucleoside analog), which is then covalently tagged with biotin in a 'click reaction' catalysed by copper. Biotin conjugated DNA (and proteins bound to it) is then pulled down by streptavidin, and analysed by western blotting. A 'thymidine chase' can also be included to monitor the proteins bound behind the replication fork, or the protein recruited to the stalled or collapsed forks.

MK1775 treatment of SETD2-proficient cells (U2OS) resulted in a transient recruitment of RPA to replication forks, which dissociated after 90 minutes. No γH2AX was detected, suggesting that MK1775-induced replication stalling was efficiently resolved. In contrast, SETD2-deficient cells (A498) showed RPA accumulation at forks even without MK1775 treatment, suggesting that SETD2 loss generated replication stress. Upon MK1775 treatment, γH2AX accumulated at

forks, which indicated that stalled fork had collapsed, leading to DNA double-stand breaks. Further, γH2AX and RPA binding at forks persisted after 90 minutes, indicating that the fork stalling and double-strand breaks were not resolved (Fig 4.15). Although 53BP1 can be a more robust indicator than ?H2AX for DNA double-stranded breaks, the current iPOND technique is unable to keep such large proteins intact during the treatment with copper.

The replication stress and DNA damage generated by the stalled and collapsed replication fork is also visible at the cellular level. MK1775 dramatically increased whole-cell staining for phospho-RPA at Serine 33 (pRPA S33) and γH2AX in SETD2-deficient cells (Fig 4.16). Serine 33 of RPA is primarily phosphorylated by ATR in response to replication stress (Liu et al., 2012a).

After analysing the immunofluorescence images, γH2AX staining was found to be both pan-nuclear and punctate (foci) (Fig 4.17). Pan-nuclear γH2AX staining indicates replication stress, and is dependent on ATR (Toledo et al., 2011). Punctate (foci) staining of γH2AX is usually a sign of DNA double-stranded breaks, and is dependent on ATM, ATR and DNA-PK. Therefore these data supported that the elevated and prolonged replication stress leads to DNA damage.

Apart from γH2AX staining, another way to measure DNA damage is by comet assay, which combines DNA gel electrophoresis with a fluorescence microscope to measure DNA damage in individual cells (Olive and Banáth, 2006). An alkaline comet assay (which measures both single-stranded and double-stranded DNA damage) showed that MK1775 dramatically increases DNA damage in

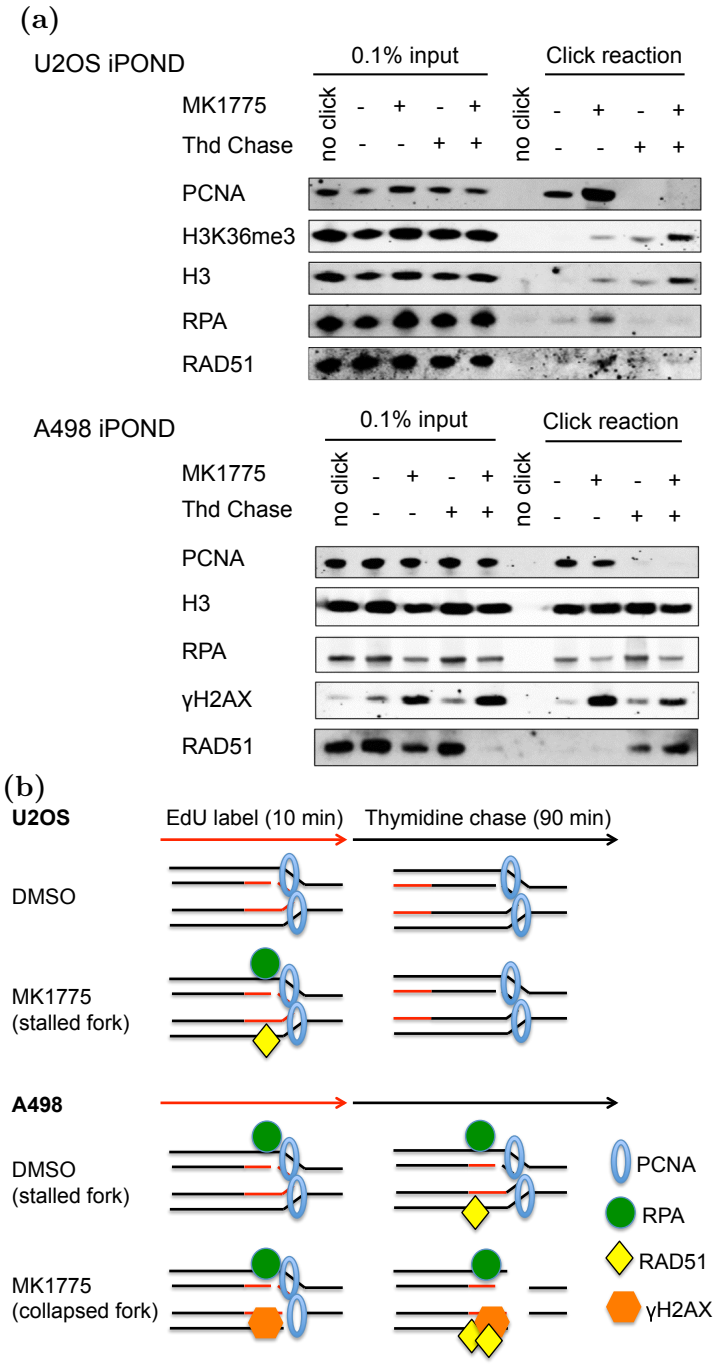


Figure 4.15: MK1775 collapses replication forks specifically in SETD2-deficient cells. iPOND analysis of proteins bound to normal, stalled or collapsed replication forks. U2OS and A498 cells were treated with DMSO or MK1775 (200nM) for 24 hours, pulsed with EdU for 10 minutes, and harvested either immediately or 90 minutes after thymidine chase (Thd Chase). These experiments were performed together with Dr Enni Markkanen. (a) Western blot analysis of proteins bound to the nascent DNA. (b) Graphical interpretation of the iPOND data.

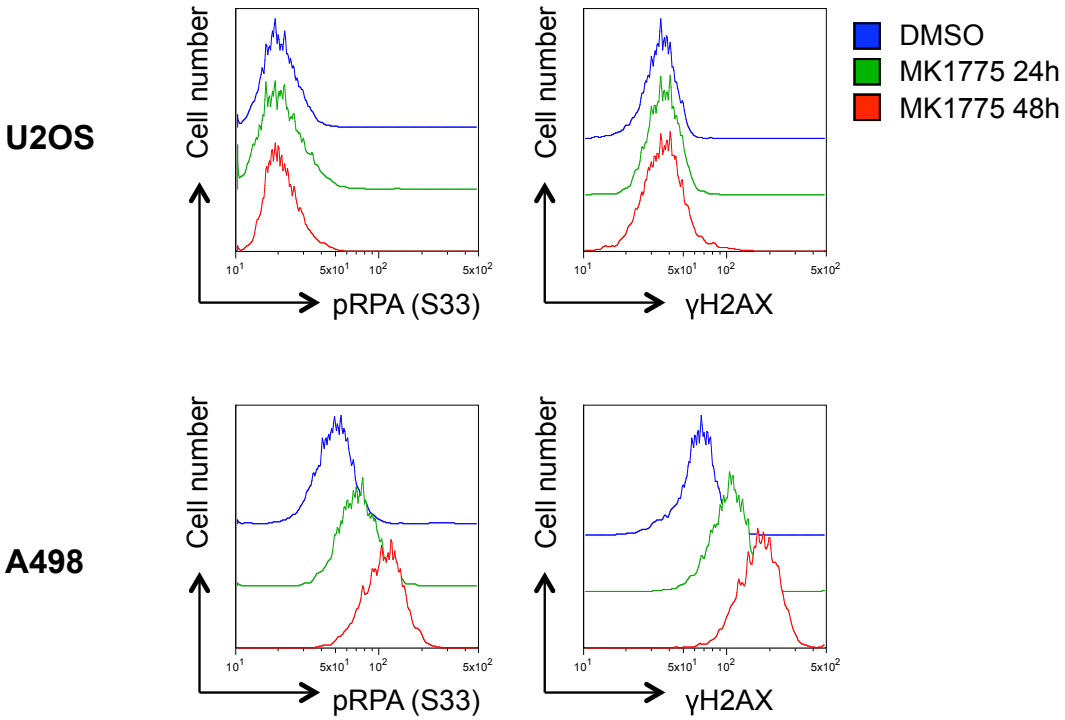


Figure 4.16: MK1775 increases phospho-RPA and γH2AX staining specifically in SETD2-deficient cells. FACS analysis of RPA phosphorylation at Serine 33 (pRPA S33), and γH2AX levels in U2OS and A498 cells treated with DMSO or MK1775 (200nM) for 24 or 48 hours. These experiments were performed together with Mr Mick Woodcock.

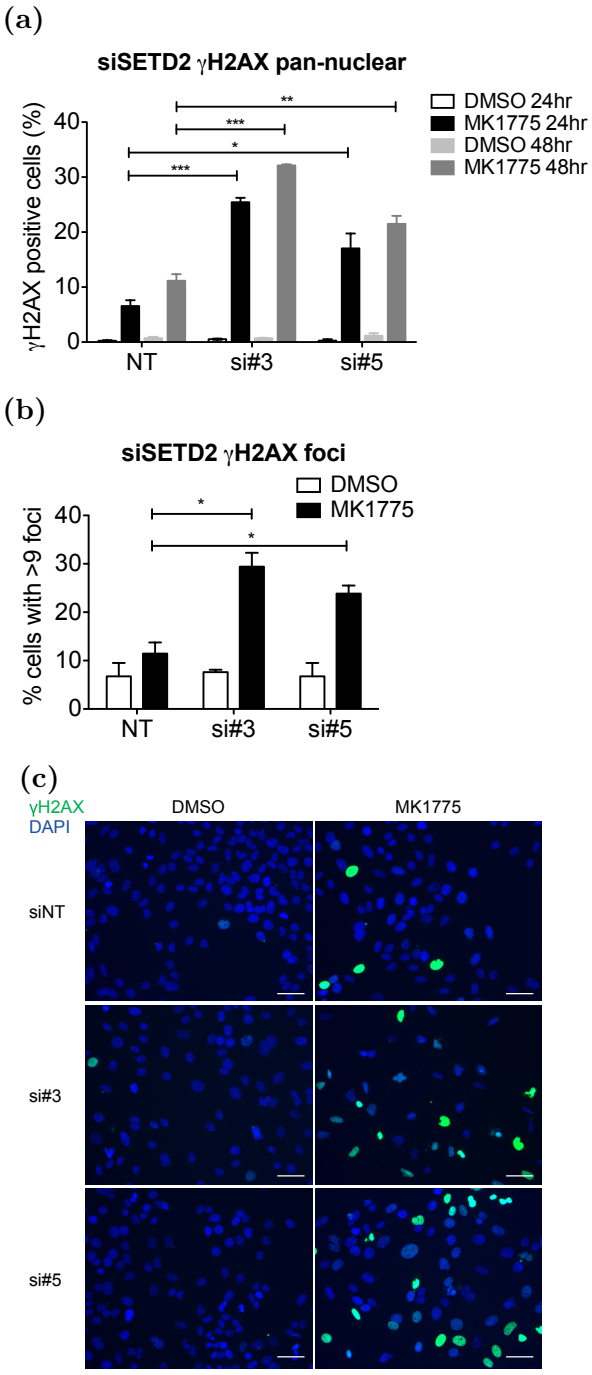


Figure 4.17: MK1775 significantly increases both pan-nuclear and punctate staining of γH2AX in SETD2-depleted cells. U2OS cells were transfected with non-targeting siRNA (NT) or SETD2 siRNA (si#3 and si#5) 48 hours prior to DMSO or MK1775 (200nM) treatment for 48 hours. Immunofluorescence analysis of (a) pan-nuclear γH2AX staining and (b) γH2AX foci staining. (c) Representative microscope images of γH2AX staining. Both pan-nuclear and punctate staining are visible. Scale bar = 50μm.

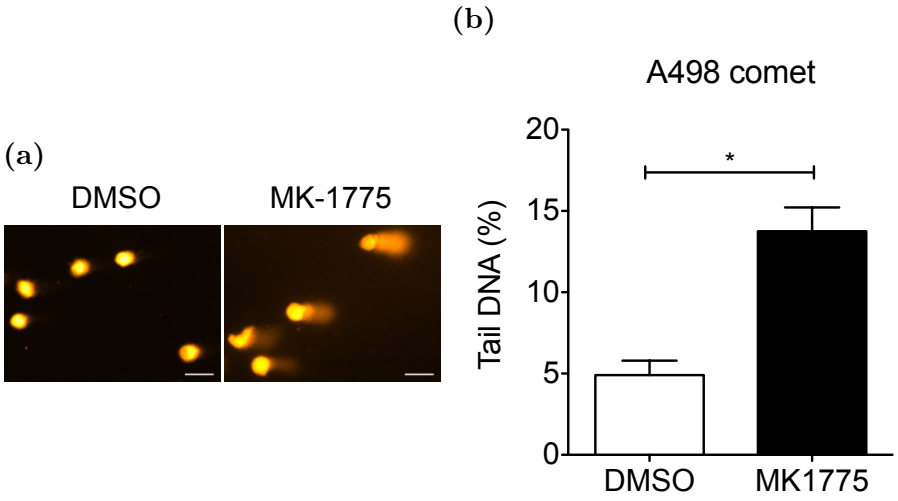


Figure 4.18: MK1775 increases DNA damage in SETD2-deficient A498 cells. An alkaline comet assay of A498 cells treated with DMSO or MK1775 (200nM) for 48 hours. (a) Representative images of nuclear DNA after electrophoresis. Scale bar is 50μm. (b) Quantification of the levels of DNA damage from the comet assay. Presented as the percentage of DNA in the tail over total DNA. Data are presented as mean $\pm$ SEM, n=3 independent experiments. *P<0.05. Cells were treated and harvested by me and the alkaline comet assay was performed by Dr Enni Markkanen.

SETD2-deficient A498 cells (Fig 4.18), but not in SETD2-proficient U2OS cells (Fig 4.19).

4.5 Replication stress is converted into lethal DNA damage by MUS81

To understand how the replication stress is converted into DNA damage, the contribution from the endonuclease MUS81 was investigated. MUS81 is known to cleave stalled replication forks, resulting in DNA double-stranded breaks (Hanada

et al., 2007), which become substrates for fork restart by homologous recombination (Shimura et al., 2008; Regairaz et al., 2011) (Fig 4.19a). If this is the case, depletion of MUS81 should reduce MK1775-induced DNA damage. Indeed, MUS81 shRNA knockdown significantly reduced DNA damage arising from combined depletion of SETD2 and WEE1 in U2OS cells (measured by the alkaline comet assay) (Fig 4.19b, c).

MUS81 knockdown experiments also showed that DSBs are the major contributors to cell death, as MUS81 shRNA significantly reduced apoptosis induced by MK1775 in SETD2-deficient cells (Fig 4.20c). However, MUS81 shRNA only mildly suppressed viability loss (Fig 4.20b), thus reducing DSBs is unable to overcome growth arrest. In addition, MUS81 knockdown could not reverse S-phase arrest (Fig 4.20d), which indicated that the synthetic lethal combination affected the process before MUS81 cleavage, i.e. it directly inhibited DNA replication.

4.6 SETD2 and WEE1 regulate RRM2 and the dNTP pool

DNA replication is rate-limited by deoxyribonucleotides (dNTP) production, which is catalysed by ribonucleotide-reductase (RNR). Active RNR is a hetrotetramer composed of RRM1 and RRM2 dimers that catalyses the reduction of ribonucleotide diphosphate (ADP, GDP, CDP and UDP) to their corresponding

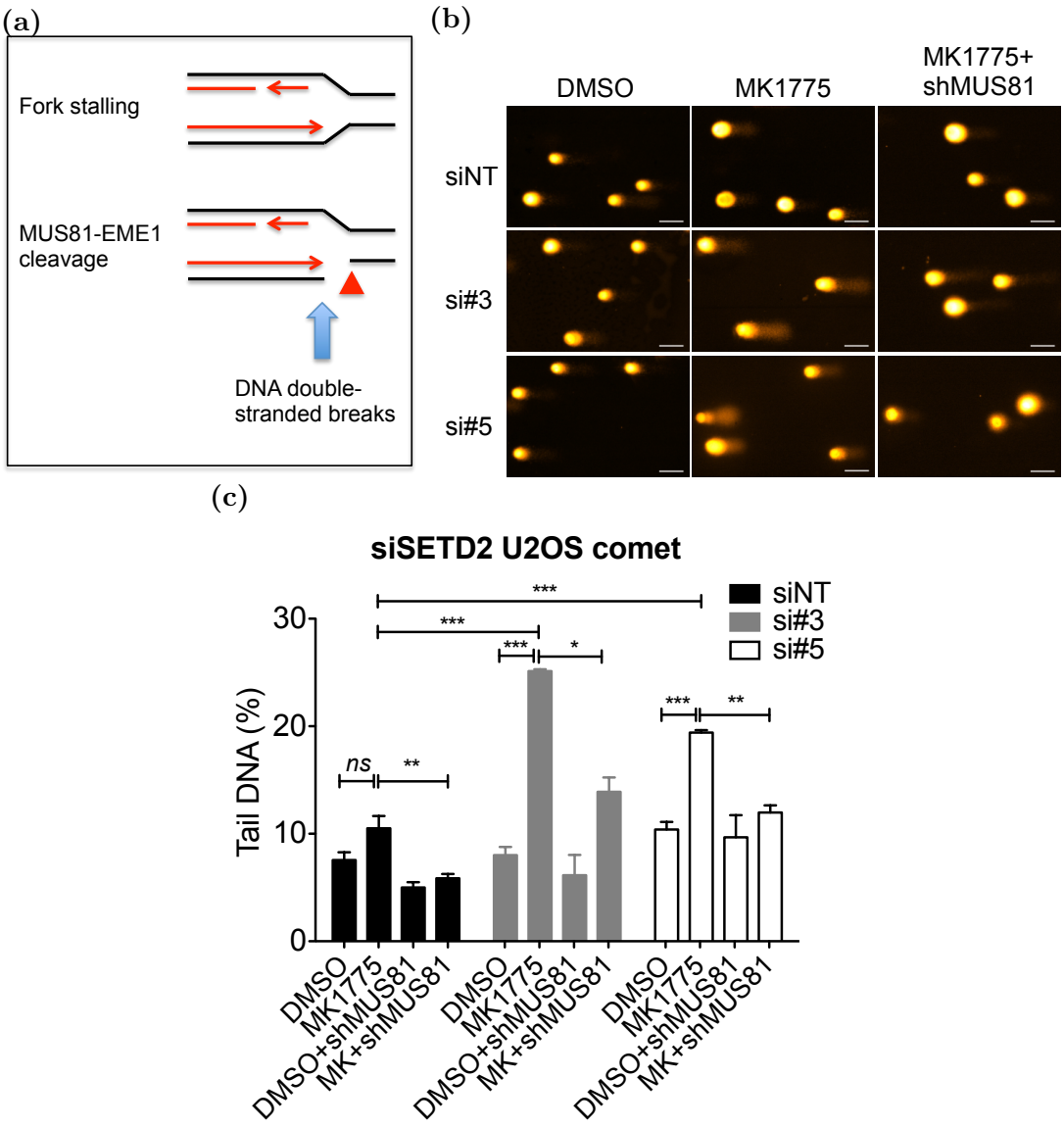


Figure 4.19: MK1775-induced DNA damage in SETD2-knockdown cells can be suppressed by MUS81 knockdown. An alkaline comet assay of U2OS cells transfected with non-targeting siRNA (siNT) or SETD2 siRNA (si#3 and si#5) and MUS81 shRNA lentiviral particles 48 hours prior to treatment with DMSO or MK1775 (200nM) for 48 hours. (a) Schematic map showing MUS81 cleavage of stalled replication forks. (b) Representative images of nuclear DNA after electrophoresis. Scale bar is 50μm. (c) Quantification of the levels of DNA damage from the comet assay. Presented as the percentage of DNA in the tail over total DNA. Data are presented as mean ± SEM, n=3 independent experiments. ***P<0.001, **P<0.01, *P<0.05. The experiments were designed, cells were treated and harvested by me and the alkaline comet assay was performed by Dr Enni Markkanen.

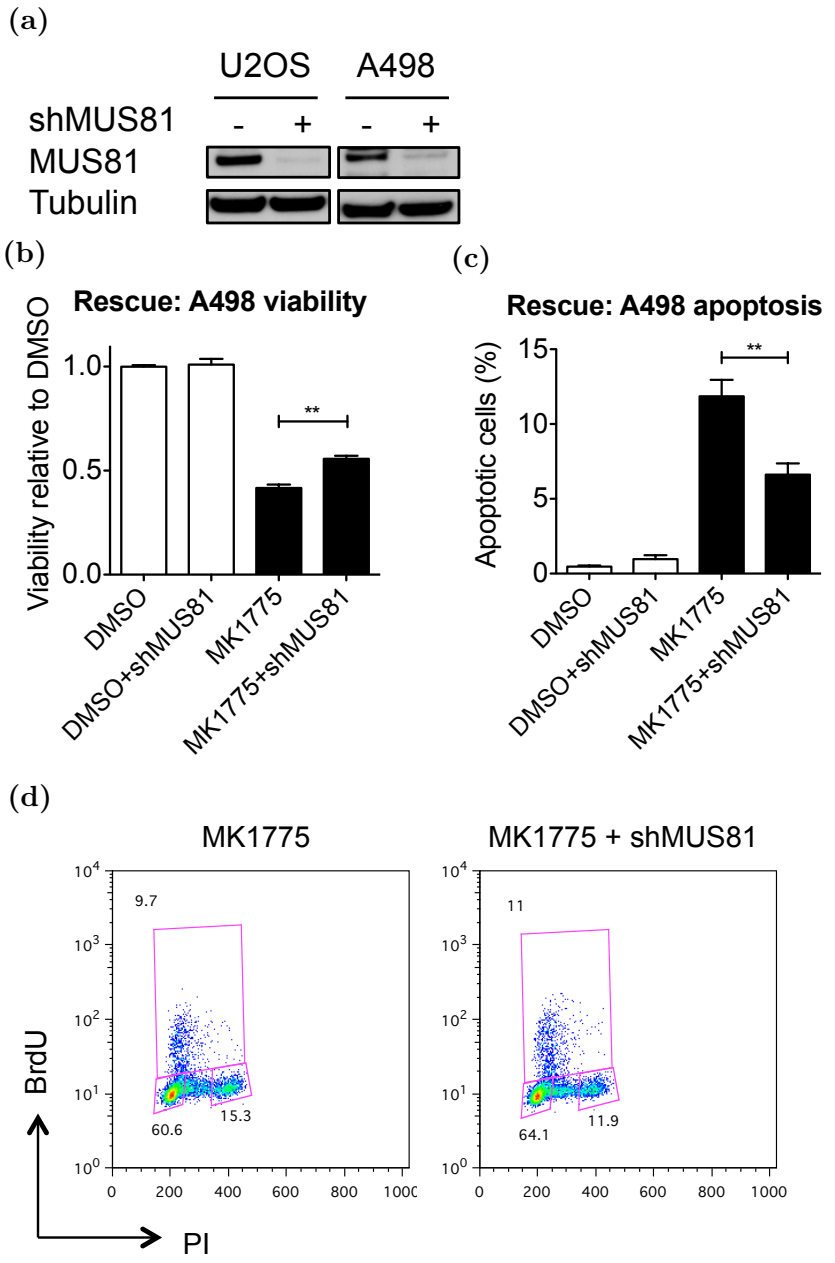


Figure 4.20: MUS81 knockdown suppresses MK1775-induced apoptosis, but does not suppress MK1775-induced S-phase arrest. (a) Western blot confirming that the MUS81 protein depletes at 72 hours after MUS81 shRNA (shMUS81) lentiviral infection. (b) Viability and (c) apoptosis of A498 cells infected with shMUS81 lentiviral particles 48 hours prior to MK1775 treatment for 72 hours. Data are presented as mean ± SEM, n=3 independent experiments. **P<0.01. (d) FACS analysis of BrdU incorporation by A498 cells infected with shMUS81 lentiviral particles 48 hours prior to MK1775 treatment for 24 hours.

deoxyribonucleotide diphosphate (dNDP) (Nordlund and Reichard, 2006). While RRM1 levels remain constant, RRM2 levels are cell cycle regulated (Chabes and Thelander, 2000): E2F1 drives RRM2 transcription in G1/S (Chabes et al., 2004), whereas APC/C^{Cdh1} and CDK1/$SCF^{CyclinF}$ promote the ubiquitin-mediated proteolysis of RRM2 during G1 and G2 respectively (D'Angiolella et al., 2012).

Given that WEE1 and SETD2 co-depletion leads to DNA replication arrest, the role of WEE1 and SETD2 on dNTP synthesis was examined. Western blot analysis showed that RRM2 protein levels were reduced by either MK1775 treatment or SETD2 siRNA knockdown, and were further depleted after combining the two (Fig 4.21). This is unlikely to be a consequence of S-phase arrest induced by MK1775 in SETD2-deficient cells because RRM2 level normally peaks at S-phase. This pattern resembled the classic synthetic lethal model: two genes (WEE1 and SETD2) independently regulate an essential cellular function (RRM2), and simultaneous depletion of both genes abolishes that function.

Interestingly, SETD2 knockdown also reduced E2F1 protein levels without affecting RRM1 and other E2Fs (including E2F2, E2F3 and E2F4) (Fig 4.21), suggesting that the effect is specific to E2F1 and RRM2.

To understand if the reduction in E2F1 and RRM2 protein levels are due to reduction in the transcription of the two genes, quantitative reverse transcription polymerase chain reaction (qRT-PCR) was performed to measure the mRNA levels of *E2F1* and *RRM2*. SETD2 siRNA knockdown reduced both *E2F1* and *RRM2* mRNA (Fig 4.22). Consistent with published literature, E2F1 siRNA

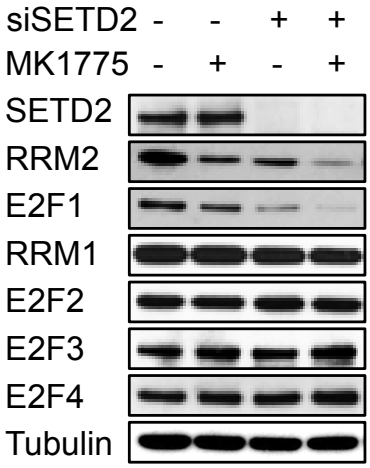


Figure 4.21: SETD2 knockdown or MK1775 reduced the protein levels of RRM2 and E2F1. Western blotting analysis of protein levels in U2OS cells transfected with non-targeting or SETD2 siRNA 48 hours prior to treatment with DMSO or MK1775 (200nM) for 24 hours.

knockdown reduced *RRM2* mRNA, but co-knockdown of SETD2 and E2F1 did not further reduce *RRM2* transcription (Fig 4.22b), suggesting that SETD2 affects *RRM2* transcription through regulating *E2F1* transcription. SETD2 knockdown did not reduce the transcription of other E2Fs (including E2F2, E2F3, E2F4, E2F6 and E2F7) (Fig 4.23), suggesting that the transcriptional regulation is specific to E2F1, and it is not due to cell cycle disturbance (other E2F genes are also cell-cycle regulated).

Given the reduction in RRM2 protein, one would expect a reduction in the cellular dNTP pool levels, especially in the purines dATP and dGTP (likely due to a more efficient nucleotide salvage pathway for the pyrimidines). Indeed, dATP levels were reduced to 50% of non-targeting controls following either SETD2 knockdown or MK1775 treatment, and to 30% of non-targeting controls when

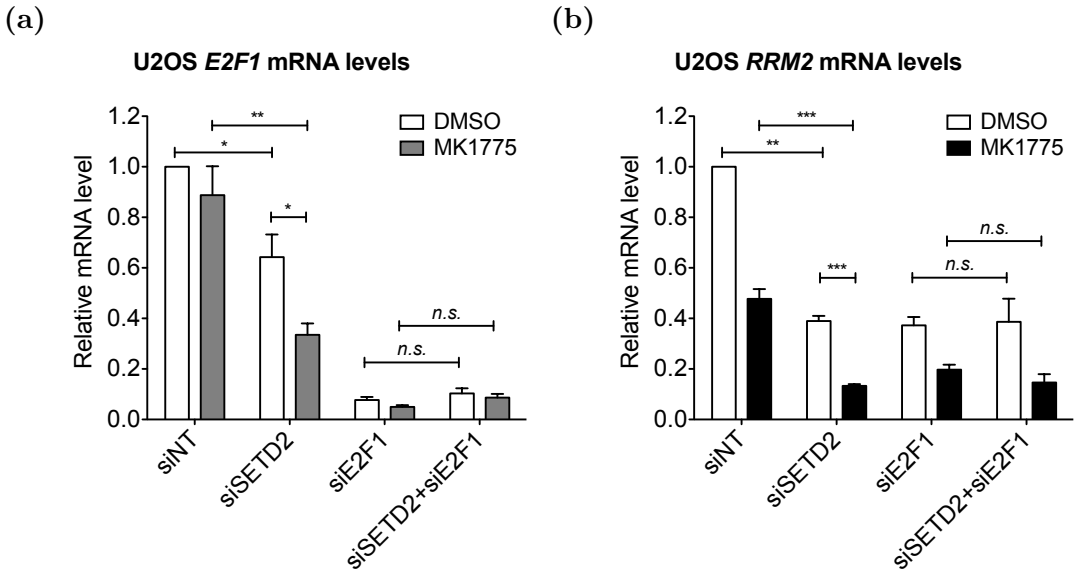


Figure 4.22: SETD2 knockdown or MK1775 reduced the transcription of *RRM2* and *E2F1*. qRT-PCR analysis of (a) *E2F1* and (b) *RRM2* mRNA levels normalised to *GAPDH* in U2OS cells transfected with indicated siRNAs 48 hours prior to DMSO or MK1775 (200nM) treatment for 24 hours. Data are presented as mean ± SEM, n=3 independent experiments. ***P<0.001, **P<0.01, *P<0.05, *n.s.*, not significant. These experiments were performed together with Dr Enni Markkanen.

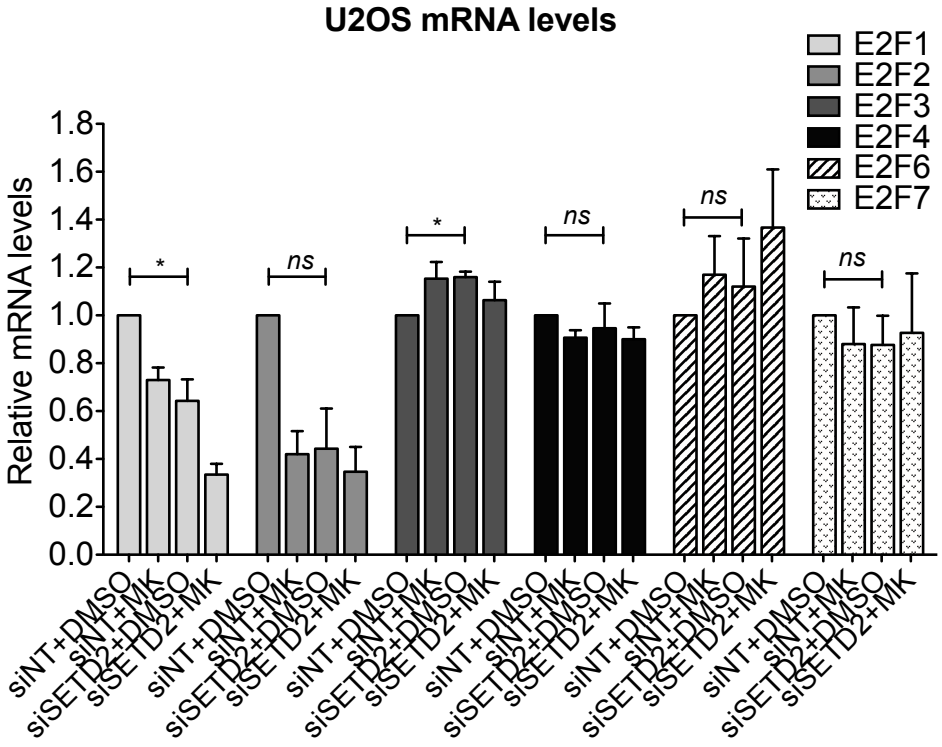


Figure 4.23: SETD2 knockdown or MK1775 did not reduce the transcription of other *E2F* genes. qRT-PCR analysis of mRNA levels of the indicated *E2F* genes normalised to *GAPDH* in U2OS cells transfected with non-targeting siRNA (siNT) or SETD2 siRNA (siSETD2) 48 hours prior to DMSO or MK1775 (200nM) treatment for 24 hours. Data are presented as mean ± SEM, n=3 independent experiments. *P<0.05, *ns*, not significant. These experiments were performed together with Dr Enni Markkanen.

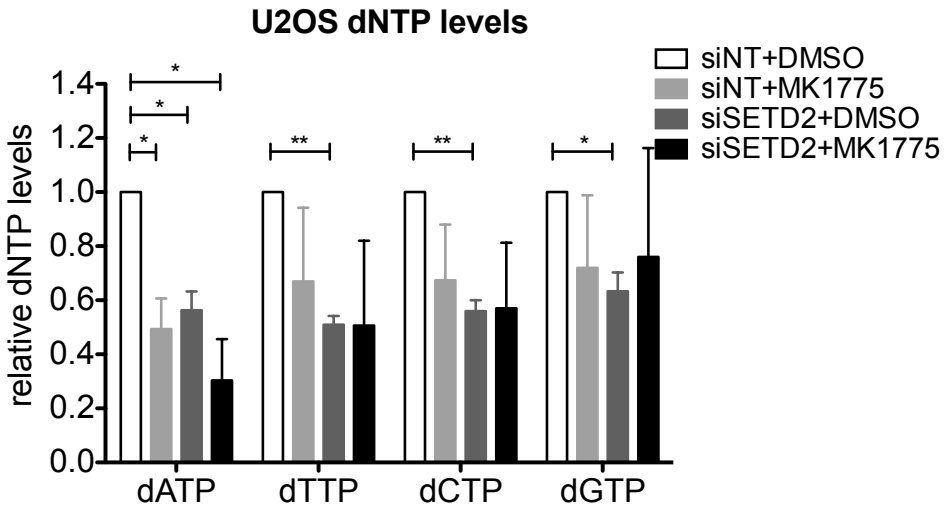


Figure 4.24: SETD2 knockdown reduced dNTP pool. Measurement of dNTP levels in U2OS cells transfected with non-targeting siRNA (siNT) or SETD2 siRNA (siSETD2) 48 hours prior to DMSO or MK1775 (200nM) treatment for 24 hours. Data are normalised to siNT+DMSO condition and presented as mean ± SEM, n=3 independent experiments. **P<0.01, *P<0.05. These experiments were performed together with Dr Enni Markkanen.

treatments were combined (Fig 4.24).

To show that RRM2 depletion was the real cause of the synthetic lethality between SETD2 loss and WEE1 inhibition, a U2OS cell line (T33A) that expresses exogenous RRM2 was tested for its ability to rescue the synthetic lethal phenotype. T33A cells stably express (under a CMV promoter) a mutant RRM2 (Threonine 33 to Alanine) that cannot be phosphorylated by CDK1, and is thus unable to be bound and degraded by CyclinF (D'Angiolella et al., 2012). After SETD2 knockdown and/or MK1775 treatment, T33A cells had higher levels of RRM2 protein (Fig 4.25a) and was more resistant to the reduction in dNTP pool (Fig 4.25b). The increase in dNTP (dATP) levels in turn suppressed the viability

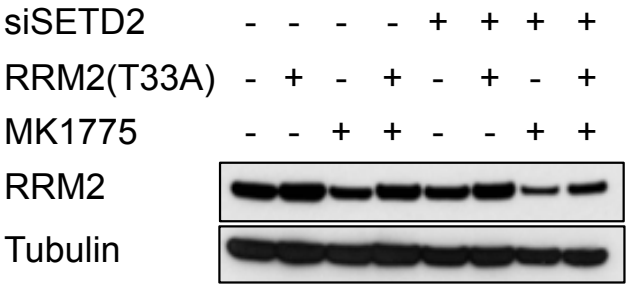
loss caused by siSETD2 and siSETD2+MK1775 (Fig 4.26).

Interestingly, in addition to T33A, the viability loss after co-depletion of SETD2 and WEE1 can also be suppressed by another mutant variant of RRM2: RxI/AxA (Fig 4.27). The RxI/AxA mutation locates at residue 49-51 of RRM2, and abolishes its interaction with Cyclin F, thus preventing its degradation (D'Angiolella et al., 2012).

It is noteworthy that expressing wild-type RRM2 suppressed the viability loss due to siSETD2 but not the viability loss following siSETD2+MK1775 (Fig 4.27). This observation suggests that SETD2 and WEE1 regulates RRM2 by two different mechanisms: SETD2 knockdown reduces *RRM2* transcription, thus its toxicity can be suppressed by expressing wild-type *RRM2* under a CMV promoter (instead of endogenous promoter). WEE1 inhibition increases RRM2 degradation, thus its toxicity cannot be suppressed by expressing wild-type *RRM2*, but only by RRM2 mutants which are resistant to cyclin F-mediated degradation (T33A or RxI/AxA).

To test the hypothesis that WEE1 inhibition promotes RRM2 degradation, two chemical inhibitors were used to prevent the degradation of RRM2. The Nedd8-Activating Enzyme (NAE) inhibitor MLN4924 (which inhibits the Neddylation of RRM2), and the CDK1 inhibitor RO3306 (which blocks CDK1-mediated RRM2 phosphorylation) both stablished RRM2 protein and suppressed the synthetic lethality between SETD2 knockdown and MK1775 (Fig 4.28). In contrast, supplying nucleosides did not reduce the MK1775 sensitivity (Fig 4.28) as they

(a)



(b)

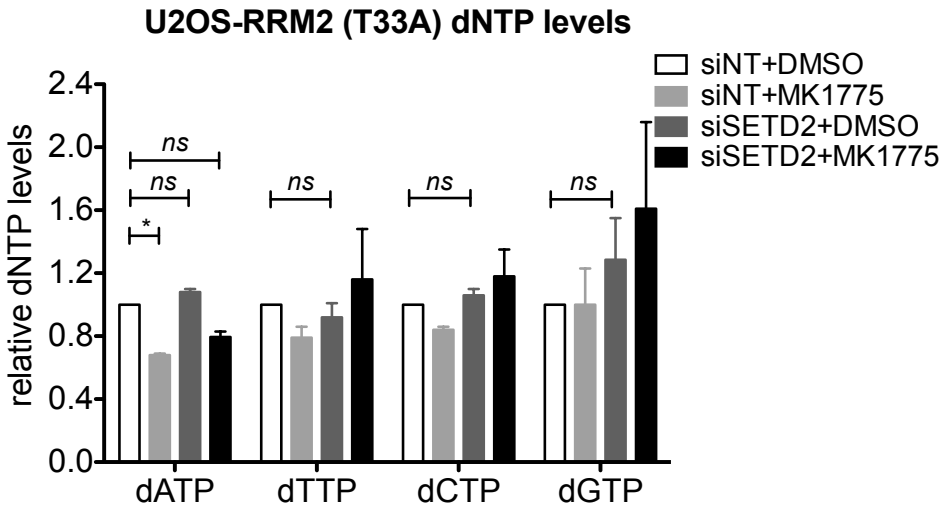
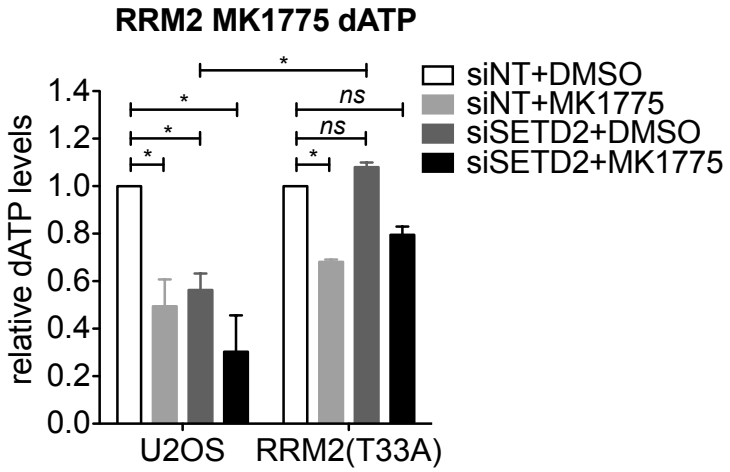


Figure 4.25: Expression of exogenous RRM2 rescues the dNTP pool. (a) Western blot analysis of RRM2 protein levels in U2OS cells expressing either an empty vector or a RRM-T33A plasmid. (b) Measurement of dNTP levels in U2OS-T33A cells transfected with non-targeting siRNA (siNT) or SETD2 siRNA (siSETD2) 48 hours prior to DMSO or MK1775 (200nM) treatment for 24 hours. Data are normalised to siNT+DMSO condition and presented as mean ± SEM, n=3 independent experiments. *P<0.05, *ns*, not significant. The cells were treated and harvested by me and dNTP pool measurements were performed by Dr Enni Markkanen.

(a)



(b)

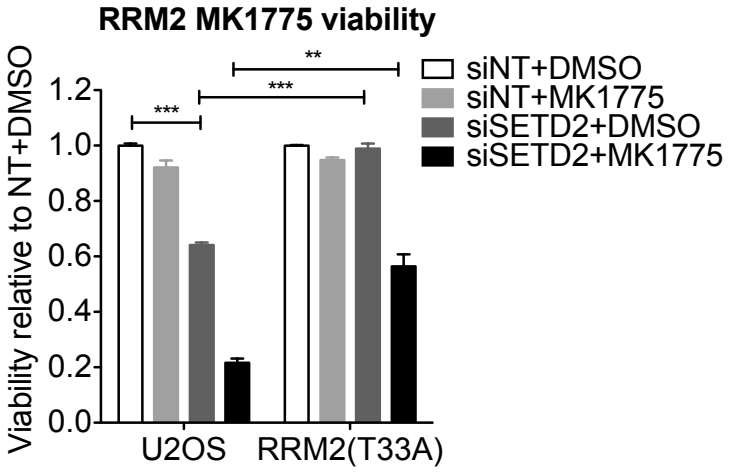


Figure 4.26: Expression of exogenous RRM2 rescues the dNTP pool and increased survival after MK1775 treatment. U2OS or U2OS-T33A cells were transfected with non-targeting siRNA (siNT) or SETD2 siRNA (siSETD2) 48 hours prior to DMSO or MK1775 (200nM) treatment for 24 hours. Data are normalised to siNT+DMSO condition and presented as mean ± SEM, n=3 independent experiments. ***P<0.001, **P<0.01, *P<0.05, *ns*, not significant. (a) Measurement of dATP levels in U2OS cells or U2OS cells expressing mutant RRM2 (T33A). This graph summarised the data from Fig 4.24 and 4.25. (b) Viability of U2OS expressing empty vector or mutant RRM2 (T33A) four days after DMSO or MK1775 (200nM) treatment.

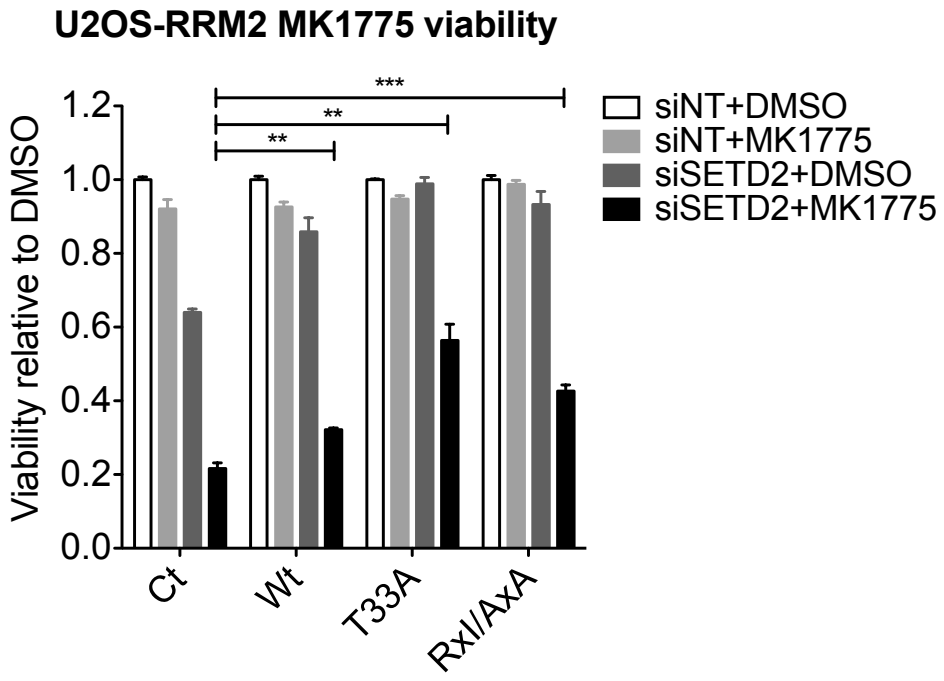


Figure 4.27: Expression of exogenous wild-type RRM2 suppresses the viability loss due to siSETD2 but not the viability loss following siSETD2+MK1775. U2OS cells stably expressing empty vector (Ct), wild-type RRM2 (Wt), RRM2-T33A mutant (T33A) orRRM2-RxI/AxA mutant (RxI/AxA) were transfected with non-targeting siRNA (siNT) or SETD2 siRNA (siSETD2) 48 hours prior to DMSO or MK1775 (200nM) treatment for 4 days. Data are normalised to siNT+DMSO condition and presented as mean ± SEM, n=3 independent experiments. ***P<0.001, **P<0.01.

require RRM2 for conversion into deoxyribonucleotides. These data support the hypothesis that WEE1 inhibition promotes RRM2 degradation through CDK1 hyperactivity.

Consistent with suppression of viability loss and apoptosis, MLN4924 and RO3306 also suppressed the MK1775-induced replication stress and DNA damage in SETD2-deficient cells. The non-replicating S-phase population was dramatically reduced by MLN4924 and RO3306, indicating a release from S-phase arrest (Fig 4.29a). Nuclear staining of phospho-RPA Serine 33 was reduced, indicating a reduction in replication stress (from fork stalling); nuclear staining of γH2AX was also reduced, indicating a reduction in DNA damage (Fig 4.29b).

4.7 SETD2 in transcriptional activation

The next question to be addressed was how does SETD2, the methyltransferase that catalyses histone H3K36me3, regulate *E2F1* transcription (or transcription in general).

Although H3K36me3 was commonly seen at the gene body of actively transcribed genes, an *in-silico* search on the UCSC Genome Browser database (URL: genome.ucsc.edu) showed that H3K36me3 is also present at the promoter of some genes, covering the promoter sequence and overlapping with H3K27ace (a marker for active transcription) as well as H3K4me3 (a marker for the active promoter) (Fig 4.30).

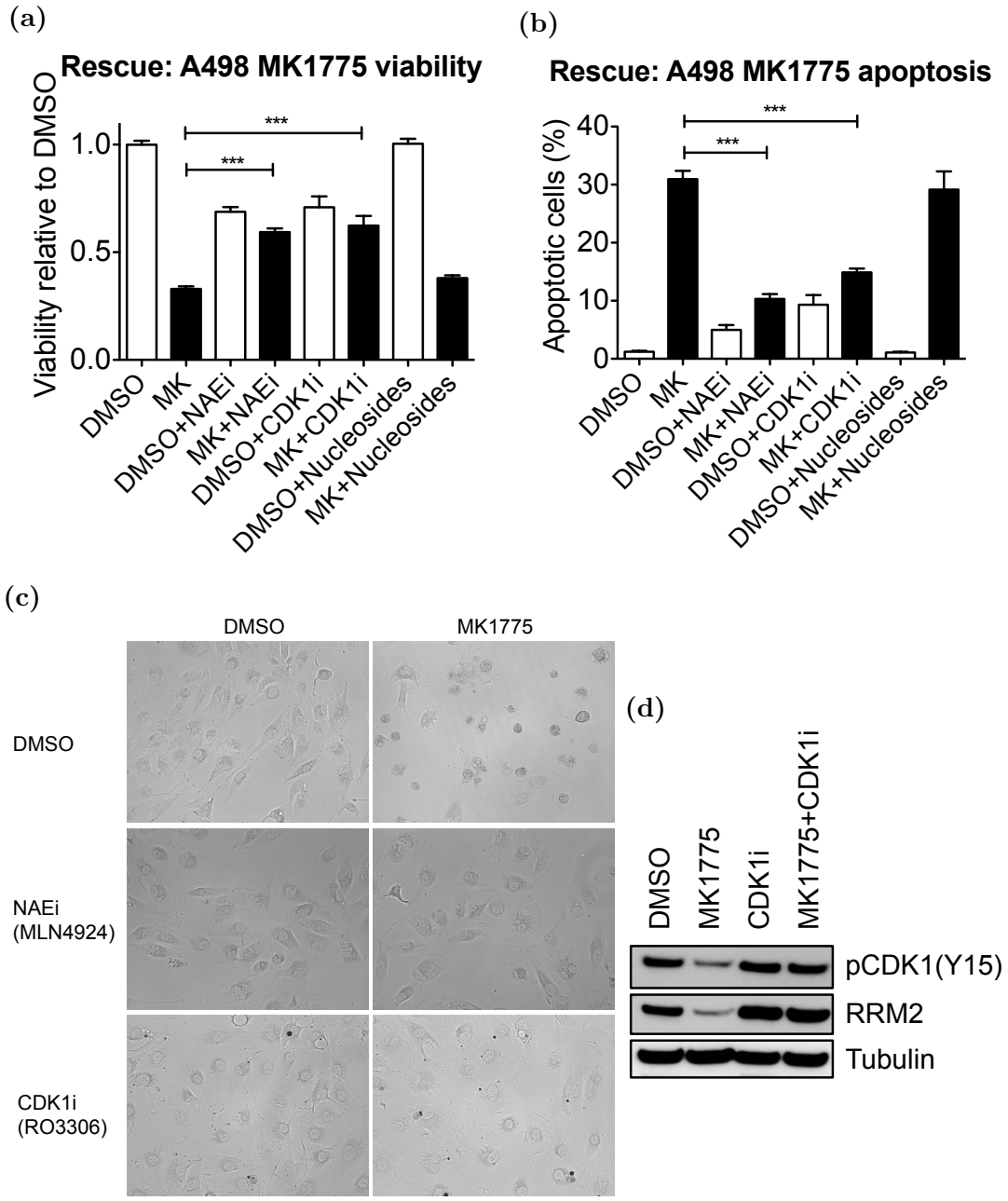
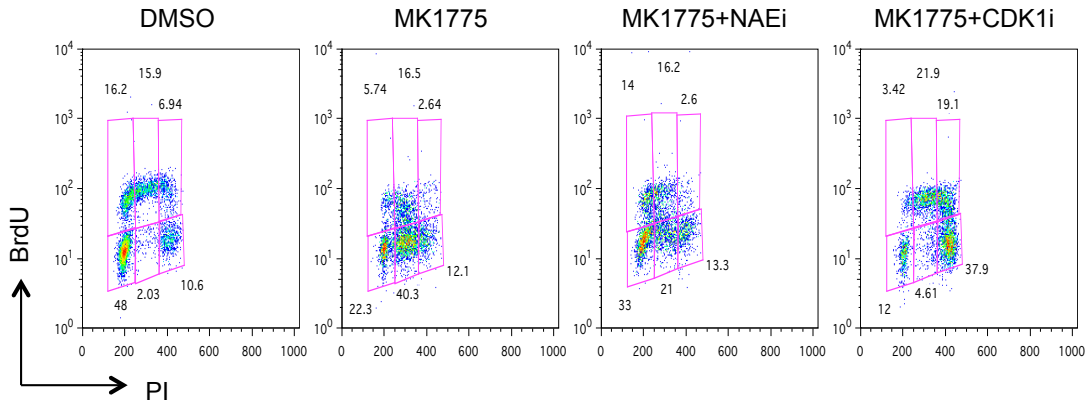


Figure 4.28: NAE and CDK1 inhibitors prevented the loss of RRM2 and rescued the survival of SETD2-deficient cells after MK1775 treatment. (a) Viability and (b) apoptosis of A498 cells treated with DMSO or MK1775 (200nM) combined with either Neddylation inhibitor MLN4924 (NAEi) (0.1mmol/L) or CDK1 inhibitor RO3306 (CDK1i) (10μM) or nucleosides (20μM of each A, G, C, U) for 48 hours. Data are presented as mean ± SEM, n=3 independent experiments. ***P<0.001. (c) Bright-field images of A498 cells after inhibitors treatment for 48 hours. (d) Western blots showing restoration of RRM2 levels by CDK1 inhibitor or NAE inhibitor in A498 cells.

(a)



	DMSO	MK1775	MK1775+NAEi	MK1775+CDK1i
Non-replicating S	2%	40%	21%	5%

(b)

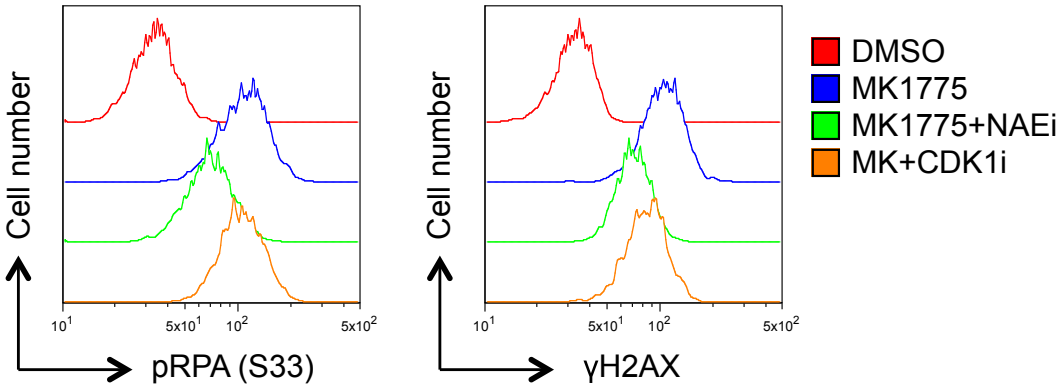


Figure 4.29: NAE and CDK1 inhibitors resolved S-phase arrest and reduced replication stress in SETD2-deficient cells after MK1775 treatment. (a) FACS analysis of BrdU incorporation by A498 cells after treatment with the indicated inhibitors for 48 hours. (b) FACS analysis of RPA phosphorylation (S33) and γH2AX levels in A498 cells after treatment with the indicated inhibitors for 48 hours. These experiments were performed together with Mr Mick Woodcock.

Furthermore, genome-wide ChIP mass-spectrometry shows that 9 out of 16 TAFs (TBP-associated factors, required for initiation of transcription by RNA polymerase II) are enriched at the histone mark H3K36me3, including TAF6 and TAF4 (Vermeulen et al., 2010). If such an observation made by ChIP-mass-spec could be validated by ChIP with relevant antibodies, one could hypothesize that H3K36me3 was present at the E2F1 promoter, thus facilitating TAF binding, and enhancing assembly of the transcription machinery (consisting of TBP, TAFs and Pol II), ultimately promotes *E2F1* transcription (Fig 4.31).

Indeed, using ChIP-qPCR analysis, H3K36me3 was detected at the *E2F1* promoter, which was reduced upon SETD2 knockdown, as was binding of TAF6, TAF4 and RNA PolII to the E2F1 promoter (Fig 4.32). Consistent with this observation, H3K36me3 levels are cell cycle regulated: high in G1/S and low in G2/M (Li et al., 2013), coincides with the highest level of E2F1 at G1/S (Grant et al., 2013).

4.8 The synthetic lethality model

Together, these data support a model for synthetic lethality in which RRM2 levels are regulated by two independent pathways. Disrupting the first through SETD2/H3K36me3 depletion reduces *E2F1* transcription, RRM2 expression and dNTP production. Disrupting the second through WEE1 inhibition leads to aberrant CDK1 activity in S-phase, resulting in untimely RRM2 degradation and

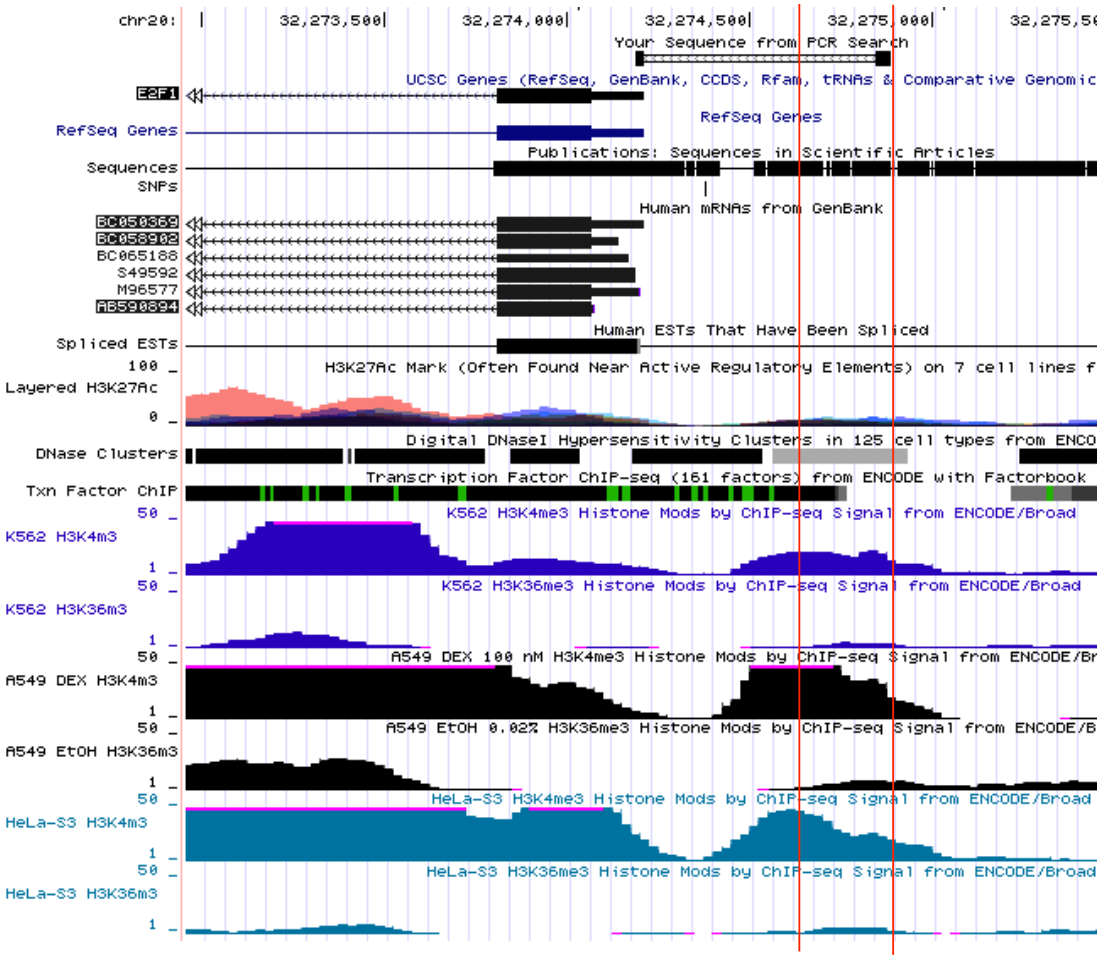


Figure 4.30: H3K36me3 colocalises with H3K4me3 and H3K27ace at the promoter of the E2F1 gene. UCSC database analysis of the distribution of histone marks across the promoter of E2F1 gene. The bar at the top indicates the promoter region of E2F1. ChIP-seq data from three cell lines (K562, A549 and HeLa) is presented. The red lines mark the region that H3K36me3 colocalises with the promoter sequence, H3K4me3 and H3K27ace. The absence of H3K36me3 outside the promoter region suggests that its presence at the promoter is unlikely to be by chance.

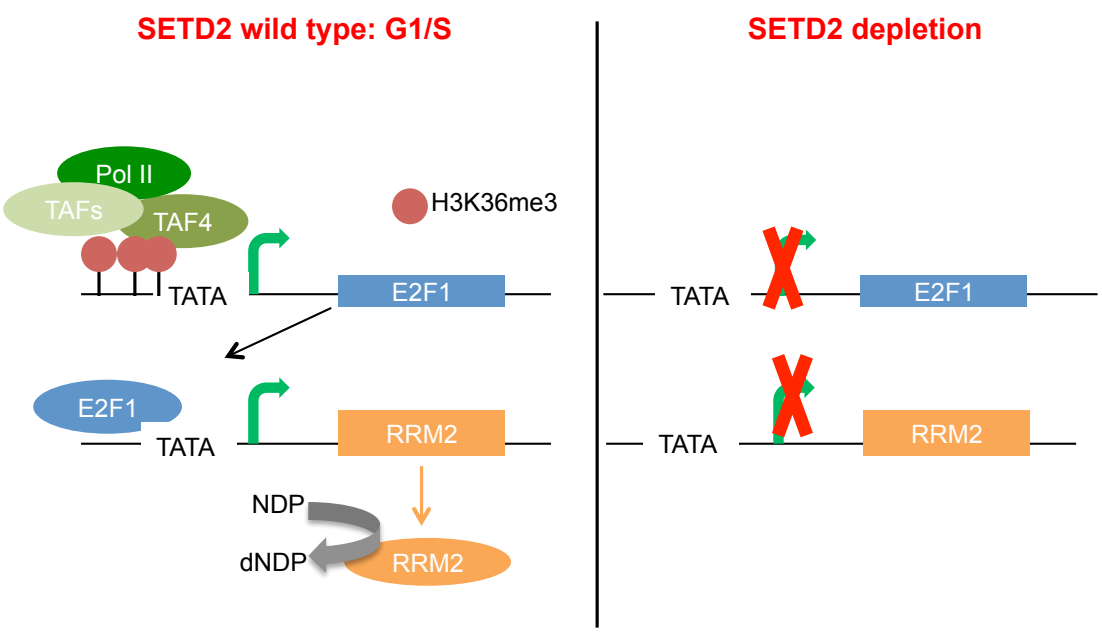


Figure 4.31: Schematic overview of how H3K36me3 regulates *E2F1* and *RRM2* transcription.

reduced dNTP production. Simultaneous disruption of both causes viability loss due to critically low dNTP levels, resulting in permanent S-phase arrest, MUS81-induced DNA double-stranded breaks at stalled forks and cell death (Fig 4.33).

4.9 *In vivo* efficacy of the WEE1 inhibitor MK1775 on SETD2-deficient tumors

The selective and potent killing of SETD2-deficient cells by MK1775 raised the possibility that MK1775 could be used to treat SETD2-deficient cancers. To test the *in vivo* efficacy of MK1775, SETD2-deficient A498 xenografts was established in nude mice. All seven tumours regressed from day three of MK1775

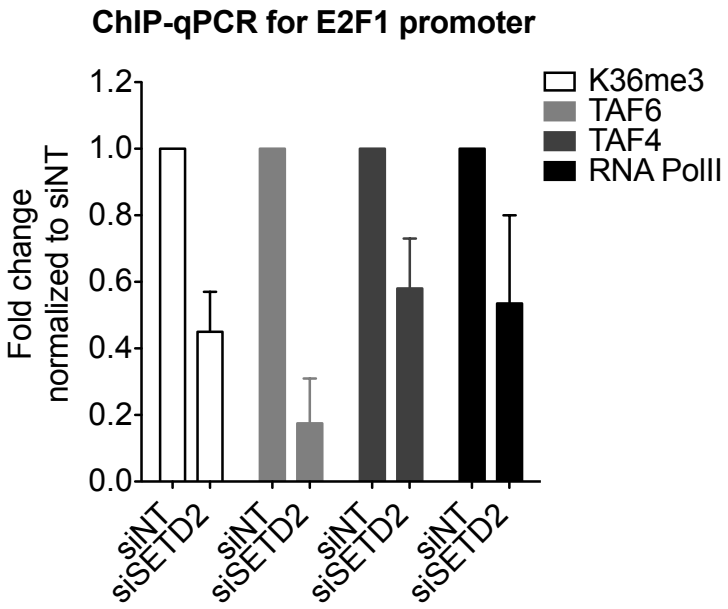


Figure 4.32: SETD2 knockdown reduced the recruitment of TAF6, TAF4 and PolII to the promoter of *E2F1* gene. ChIP-qPCR analysis of H3K36me3, TAF6, TAF4 and RNA Polymerase II levels at the *E2F1* promoter. Data are presented as mean ± SEM, n=2. This experiment was performed together with Dr Lykourgos-Panagiotis Zalmas and Dr Enni Markkanen.

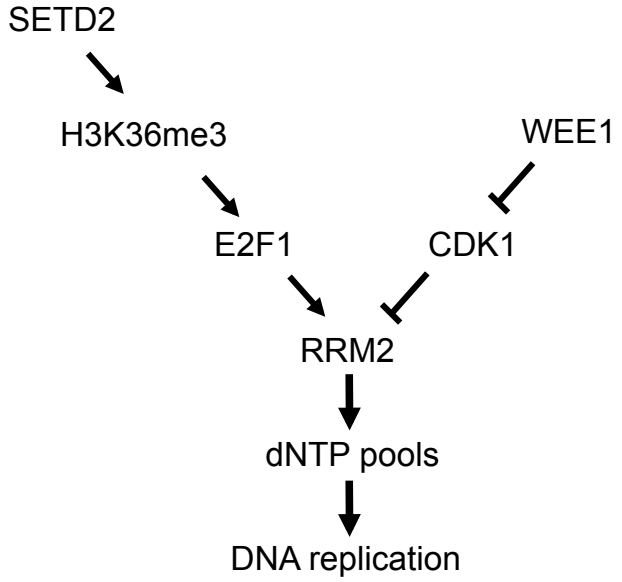


Figure 4.33: Schematic overview of the two pathways regulating RRM2 and dNTP synthesis.

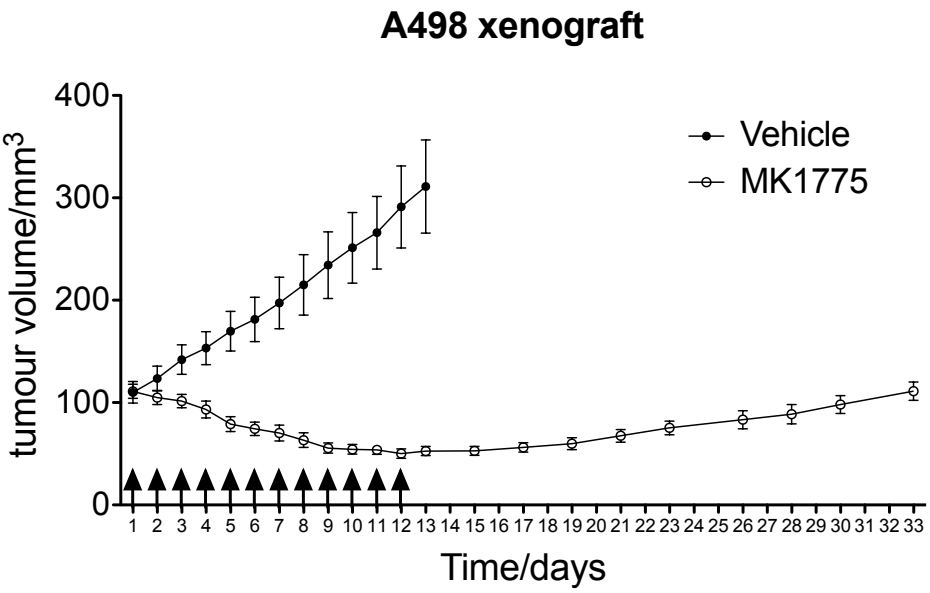
treatment, resulting in a 5.8-fold reduction in tumour size compared to vehicle-treated control animals (tumour size at day 13 = 50.2 ± 4.7 mm^3 vs 291.2 ± 40.0 mm^3, $p<0.0001$) (Fig 4.34). No difference in body weight was observed between MK1775-treated mice and vehicle-treated control (Fig 4.34), suggesting that MK1775 was well tolerated.

Consistent with the *in vitro* data, immunohistochemistry (IHC) staining showed that MK1777-treated tumours had significantly greater levels of replication stress and DNA damage as measured by γH2AX pan-nuclear staining and γH2AX foci (Fig 4.35a, b). Cleaved Caspase-3 (apoptotic marker) staining was also significantly higher in MK1775-treated tumours, in agreement with increased apoptosis observed *in vitro* (Fig 4.35c, d). These *in vivo* findings indicate that targeted inhibition of WEE1 could provide a more effective and less toxic treatment for SETD2-deficient cancers.

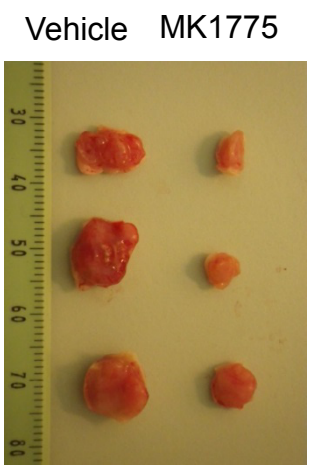
4.10 Discussion of Chapter 4

One consideration of the current model is how specific is the effect of E2F1 on replication. E2F family proteins regulate the transcription of a wide range of genes that also affect DNA synthesis, such as DHFR and thymidine kinase (TK) (Johnson et al., 1993), Cyclin A and Cyclin E (DeGregori et al., 1995). However, recent investigations of E2F1 knockout mouse cells suggest that the loss of E2F1 affects much fewer genes than previously believed: the common E2F targets

(a)



(b)



(c)

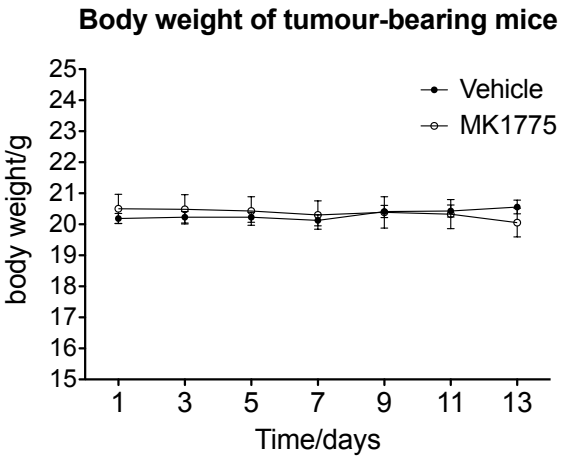


Figure 4.34: MK1775 regressed SETD2-deficient tumours *in vivo*. BALB/c nude mice were subcutaneously injected with A498 cells. When tumors reached a mean volume of 110 mm3, mice were divided into two groups (n=7 per group), receiving either vehicle or MK1775 (60mg/kg), twice daily by oral gavage for 12 days (arrows). (a) Tumor volumes for each treatment group. Data are presented as mean ± SEM, n=7. (b) Representative tumors in mice treated with either vehicle or MK1775 (day 13). (c) Mean body weight of tumour-bearing mice treated with either vehicle or MK1775. Data are presented as mean ± SEM, n=7. This experiment was designed by me together with Dr Yanyan Jiang. Since doing the *in vivo* experiment required a licence, this experiment was performed by Dr Yanyan Jiang.

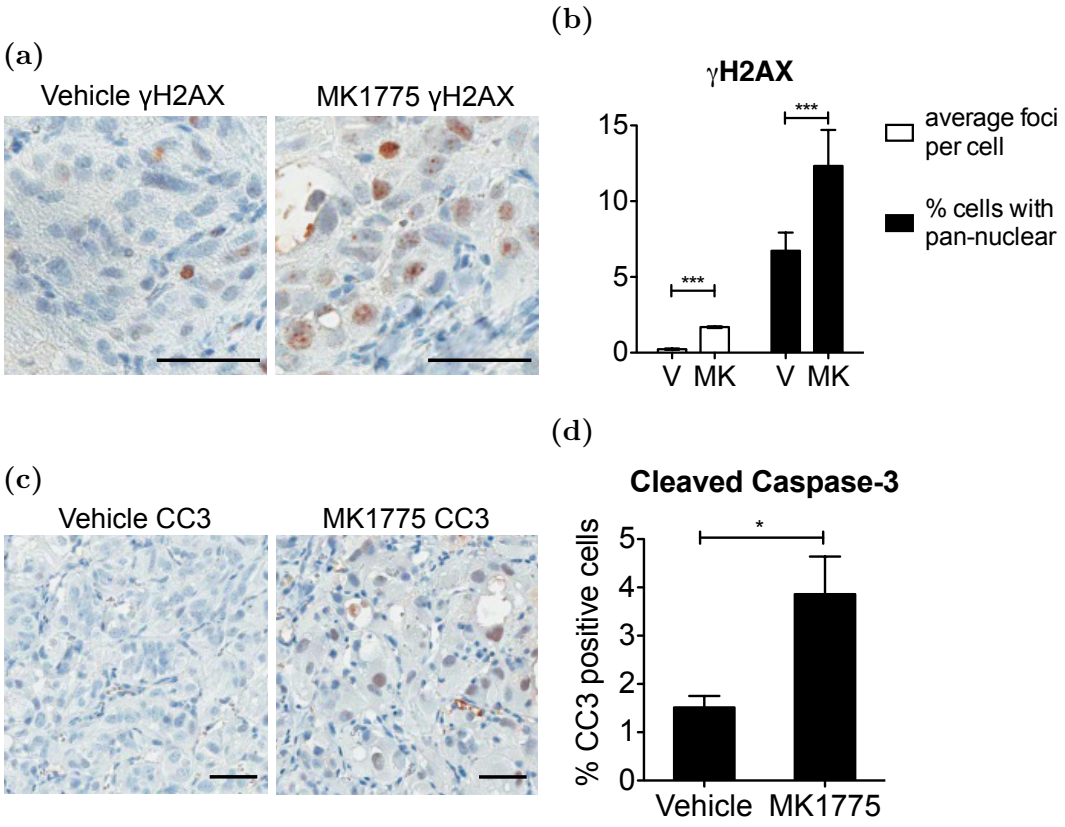


Figure 4.35: MK1775 induced DNA damage and apoptosis in SETD2-deficient tumours *in vivo*. A498 tumours were recovered on day 13, 24 hours after the last dose of vehicle or MK1775. (a, b) Immunohistochemistry analysis of γH2AX levels and (c, d) cleaved-Caspase3 (CC3) levels in A498 tumours. Scale bar = 50μm. These experiments were performed by Dr Yanyan Jiang.

(thymidine kinase, RB and Cyclin E) were unaffected due to the redundancy of E2F family members (Wells et al., 2002). This indicates the possibility that the effect of E2F1 on DNA replication may be more specific than previously believed (i.e. E2F1 affects replication through RRM2 rather than through other genes).

To show that RRM2 is the true and only target for the synthetic lethal interaction, one approach would be to explore whether RRM2 depletion pheno-copies siSETD2+MK1775. In addition, a partial reduction or inhibition of RRM2 should pheno-copy SETD2 loss. This could be investigated for example through viability, apoptosis and DNA fibre assays. In addition, one could explore whether the synthetic lethality can be rescued by supplying deoxyribonucleosides in the medium, which could compensate for the shortage in dNTPs independent of RRM2-deficiency. Alternatively, one could try rescuing the synthetic lethality by supplying deoxyribonucleotides in horse serum (where the horse serum prevents the degradation of deoxyribonucleotides), which would help confirm whether RRM2 is the true target of this synthetic lethality.

To confirm whether it is SETD2 (particularly its methyltransferase activity) that is causing the sensitivity, an additional rescue experiment needs to be performed with the methyltransferase-dead SETD2 cDNA. When this experiment was performed, however, neither the wild-type or the methyltransferase-dead SETD2 cDNA rescued the viability, probably due to the low levels of expression of SETD2 protein (see western blots for SETD2 induction in Fig 3.12c).

To strengthen the evidence for the synthetic lethality model (given the chal-

lenges in rescuing the phenotype with SETD2 cDNA), a CRISPR SETD2 knockout U2OS (and A549) cell line was successfully generated. With this SETD2 knockout cell line, some of the siSETD2 experiments (e.g. the viability assay, the DNA fibre assay and the comet assay) could be repeated with the knockout cell line to avoid the off-target effect of siRNA. In addition, the in vivo efficacy could be further strengthened by using the SETD2-/- and SETD2+/+ isogenic cell lines. To study the function of SETD2 in normal cells (instead of cancer cells), or SETD2's role in transforming normal cells to cancer cells, another interesting future experiment would be to generate SETD2 knockout in primary cell lines.

Chapter 5

From genes to pathways: a synthetic lethal interaction between H3K36me3 and CDK1 regulators

Chapter 4 showed that SETD2-deficient cells are hypersensitive to WEE1 inhibition. Given that WEE1 is a checkpoint kinase that negatively regulates CDK1/2 activity, other checkpoint kinases that negatively regulate CDK1/2 are also hypothesised to be synthetically lethal with SETD2-deficiency. In addition, given that SETD2 is the only methyltransferase for H3K36me3, it is hypothesised that other genetic modifications that abolish the H3K36me3 mark would also sensitise

cells to WEE1 inhibition.

This chapter describes the expansion of the synthetic lethal interaction from defining the relationship between two genes (SETD2 and WEE1) to defining the relationship between two pathways based on the current understanding of the mechanism. The main finding supports the hypothesis hat CDK1 regulators (WEE1, CHK1 and ATR) and H3K36me3 regulators (SETD2, KDM4A and H3.3K36M) together control deoxyribonucleotide (dNTP) synthesis; therefore simultaneous depletion of both pathways leads to cell death.

5.1 SETD2-deficient cells are hypersensitive to CHK1 and ATR inhibition

Chapter 4 showed that SETD2-deficient cells were hypersensitive to WEE1 inhibition. Given that WEE1 is a cell cycle checkpoint kinase, the sensitivity of SETD2-deficient cells to the inhibition of other checkpoint kinases (CHK1, CHK2, ATR, ATM) was tested to understand the spectrum of the synthetic lethal interactions.

SETD2-proficient U2OS cells and SETD2-deficient A498 cells were treated with siRNAs against the individual checkpoint kinases, and cell viability was measured using a Resazurin assay five days after siRNA transfection. Cell death by apoptosis was also measured by Hoechst staining 48 hours after siRNA trans-

fection. It was found that SETD2-deficient A498 cells were significantly more sensitive to the knockdown of WEE1, CHK1 or ATR than U2OS cells, but not to the knockdown of CHK2 or ATM (Fig 5.1).

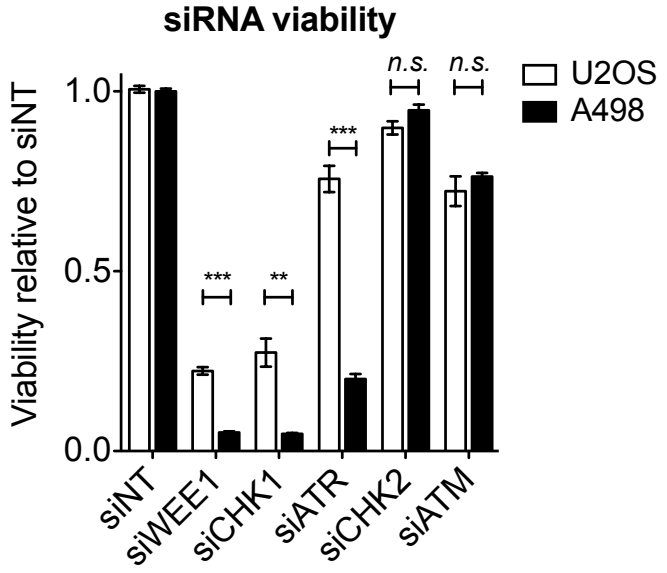
To complement the siRNA results, the sensitivity of U2OS and A498 cells to the small molecule inhibitors of these kinases was also tested. Three CHK1 inhibitors (Gö6976, LY2603618 and AZD7762) and two ATR inhibitors (VE821 and VE822) were chosen as they were in clinical development. In addition, an ATM inhibitor (KU55933) was included as a control, since ATM knockdown did not sensitise SETD2-deficient cells.

Cell viability and apoptosis measurements showed that SETD2-deficient A498 cells, compared to SETD2-proficient U2OS cells, were hypersensitive to the inhibitors of CHK1 (Fig 5.3) and ATR (Fig 5.5), but not to the inhibitor of ATM (Fig 5.6). Cell death and growth arrest after treatment with CHK1 and ATR inhibitors were also observed under a bright-field microscope (Fig 5.2, 5.4).

The results obtained from siRNA and inhibitor studies suggested that this synthetic lethal interaction is specific to checkpoint kinases involved in DNA replication (WEE1, ATR and CHK1) but not to those involved in DNA double-strand break signalling (ATM and CHK2).

To show that SETD2-deficiency is a primary cause of sensitivity to CHK1 and ATR inhibitors, the A498 cell line complimented with the SETD2 cDNA was challenged by the inhibitors. Similar to the WEE1 inhibitor, the sensitivity of A498 cells to the CHK1 and ATR inhibitors can be partially suppressed by the

(a)



(b)

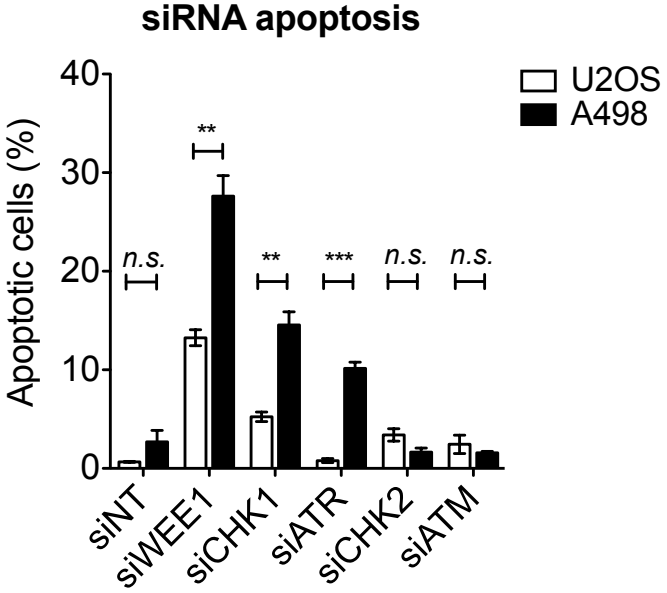


Figure 5.1: SETD2-deficient cells are hypersensitive to the depletion of WEE1, CHK1 and ATR. (a) Viability measured by Resazurin on U2OS or A498 cells five days after siRNA transfection. (b) Percentage of cells undergoing apoptosis, determined by Hoechst nuclear staining 48 hours after siRNA transfection. Data are presented as mean ± SEM, n=3 independent experiments. ***P<0.001, **P<0.01, *n.s.* not significant.

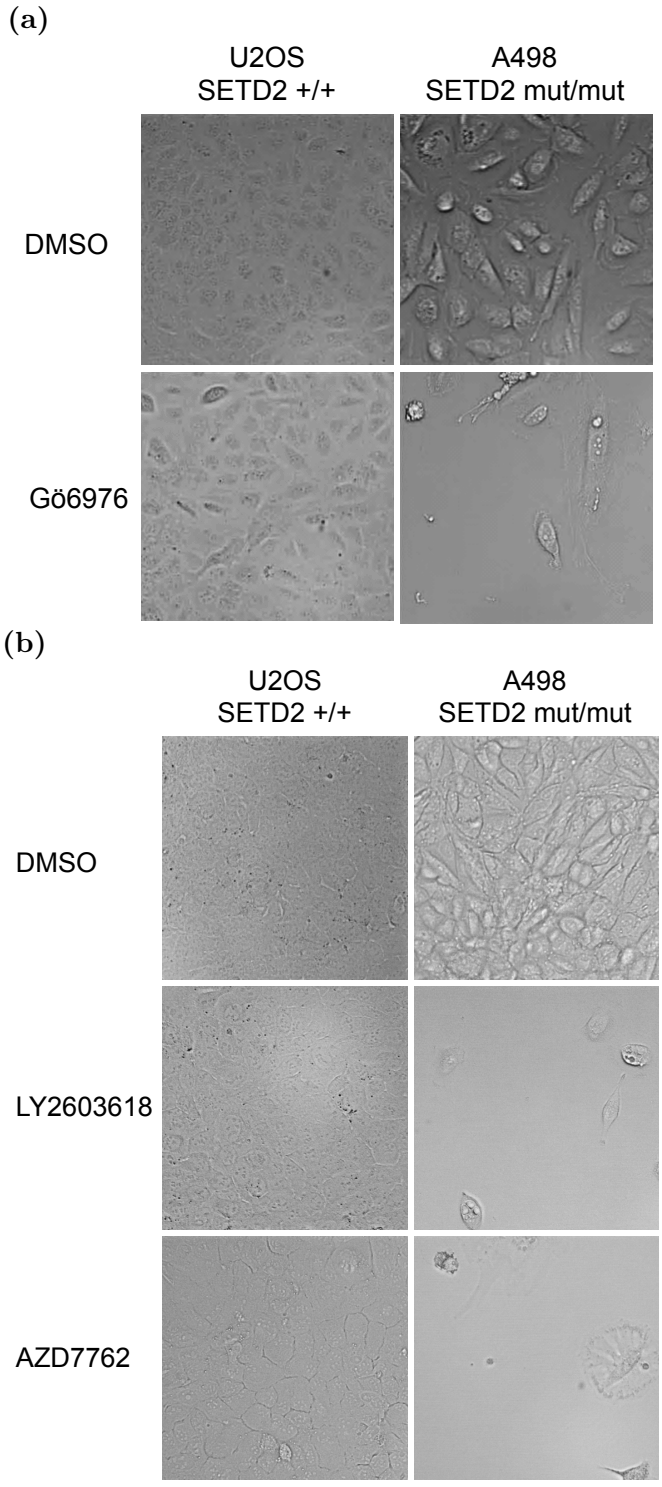


Figure 5.2: SETD2-deficient cells exhibit increased sensitivity to the CHK1 inhibitors. Representative bright-field microscope images showing U2OS and A498 cells five days after treatment with DMSO or (a) CHK1 inhibitors Gö6976 (100nM), (b) CHK1 inhibitor LY2603618 (500nM) and CHK1 inhibitor AZD7762 (100nM).

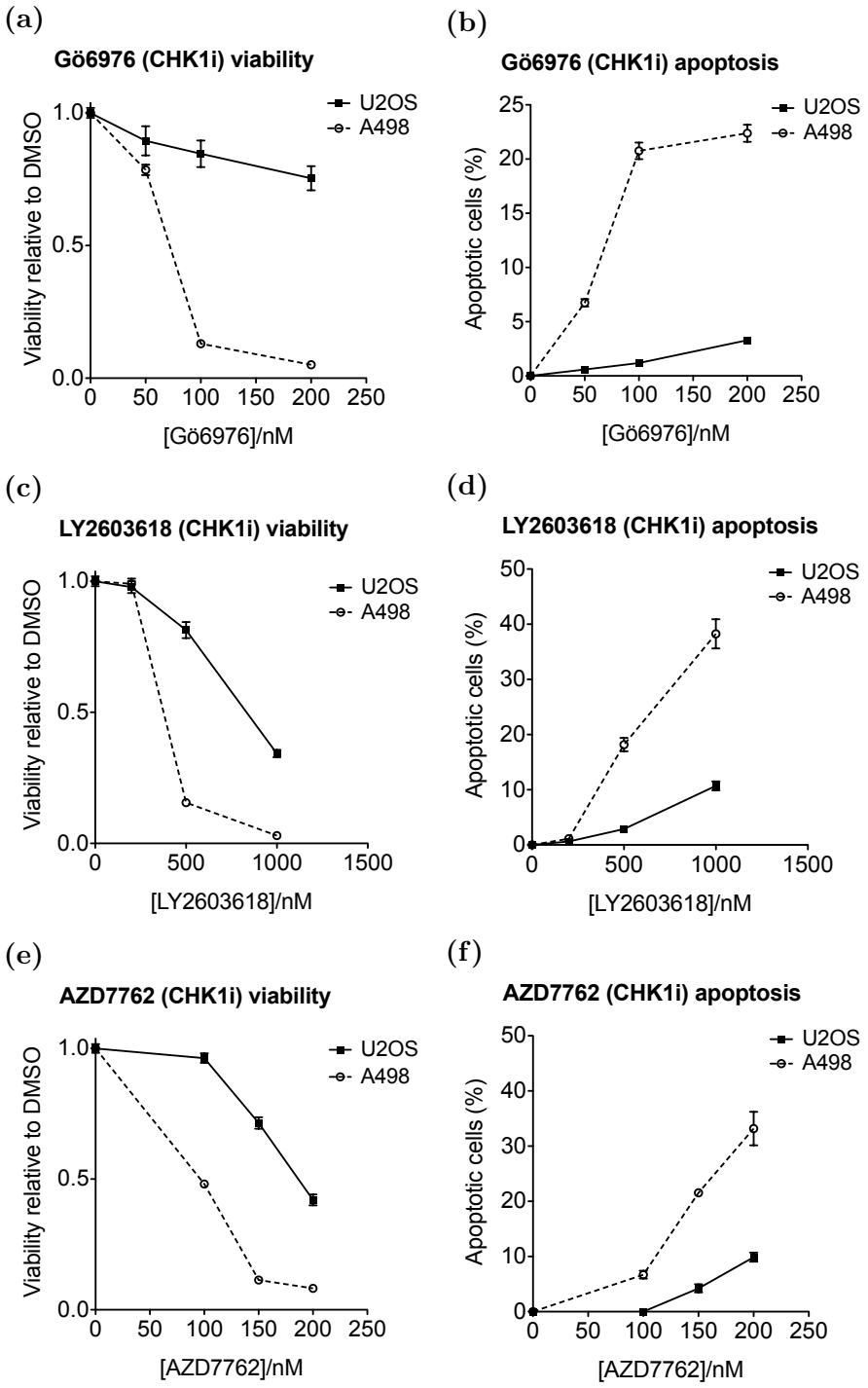


Figure 5.3: SETD2-deficient cells exhibit increased sensitivity to the CHK1 inhibitors. Viability of U2OS and A498 cells five days after CHK1 inhibitors (a) Gö6976 (c) LY2603618 or (e) AZD7762 treatment at indicated concentrations. (b, d, f) Percentage of U2OS and A498 cells undergoing apoptosis 48 hours after CHK1 inhibitors treatment. Data are presented as mean ± SEM, n=3 independent experiments.

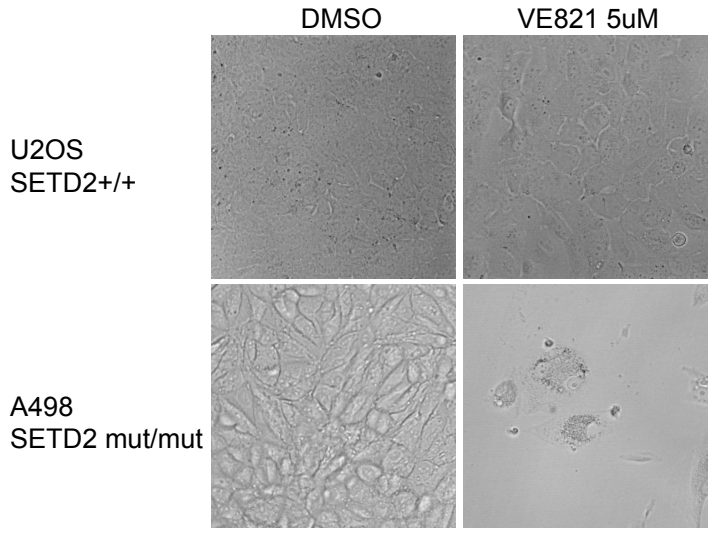


Figure 5.4: SETD2-deficient cells exhibit increased sensitivity to the ATR inhibitor. Representative bright-field microscope images showing U2OS and A498 cells five days after treatment with DMSO or ATR inhibitor VE821 (5μM).

exogenous expression of a wild-type *SETD2* cDNA (Fig 5.7), suggesting that the loss of SETD2 was the primary cause of the sensitivity to the CHK1 and ATR inhibitors. However, the levels of rescue were not very satisfactory, partially due to the growth inhibitory effect of re-expressing the tumour suppressor SETD2 in a cancer cell line that has inactivated SETD2 during the development.

5.2 H3K36me3-deficient cells are hypersensitive to WEE1, CHK1 and ATR inhibition

SETD2 non-redundantly catalyses histone H3K36 trimethylation (H3K36me3), and SETD2-deficient cells were more sensitive to the inhibitors WEE1, CHK1 and ATR. Therefore it was hypothesised that loss of the histone mark H3K36me3

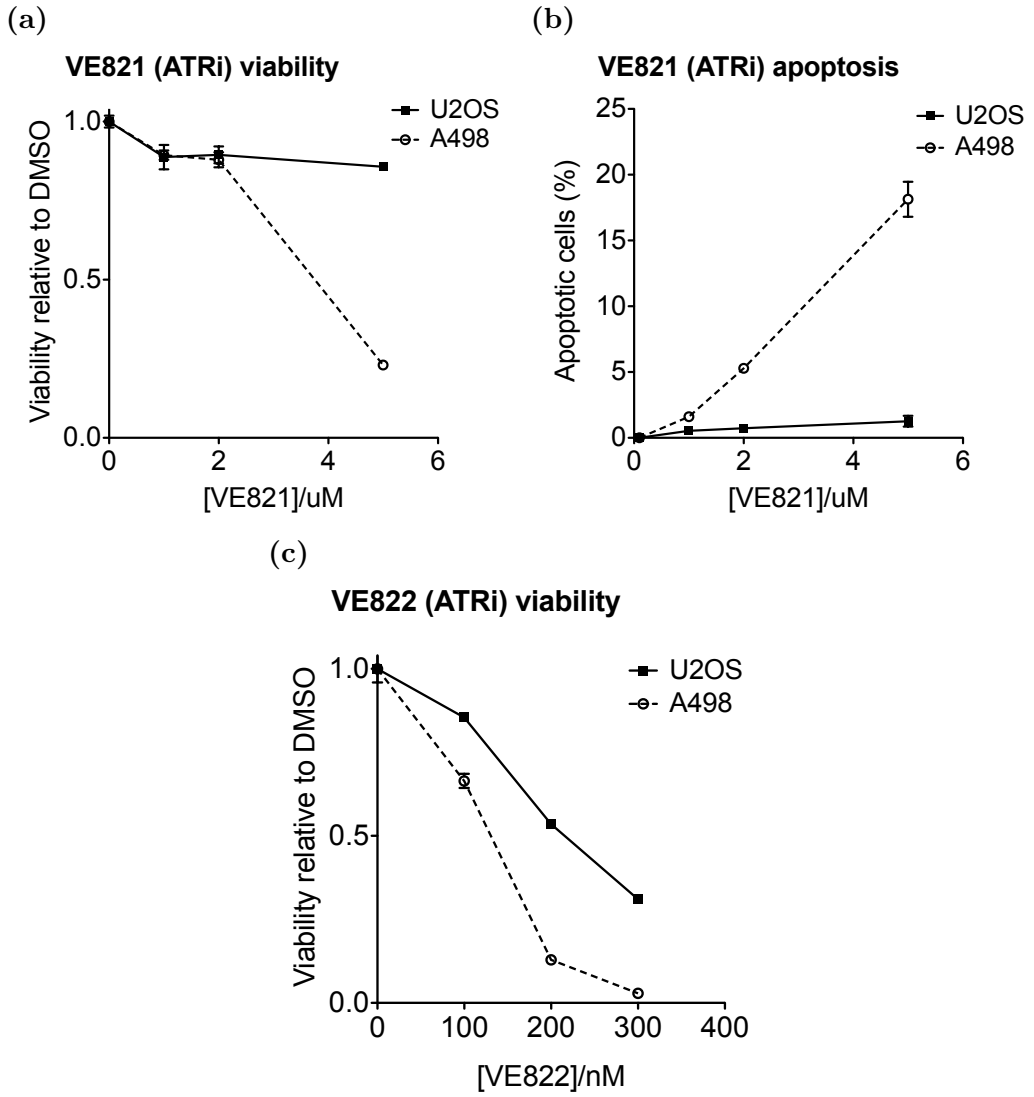


Figure 5.5: SETD2-deficient cells exhibit increased sensitivity to the ATR inhibitors. (a) Viability of U2OS and A498 cells five days after ATR inhibitor (VE821) treatment at indicated concentrations. (b) Percentage of U2OS and A498 cells undergoing apoptosis 48 hours after ATR inhibitor (VE821) treatment. (c) Viability of U2OS and A498 cells five days after ATR inhibitor (VE822) treatment at indicated concentrations. Data are presented as mean ± SEM, n=3 independent experiments.

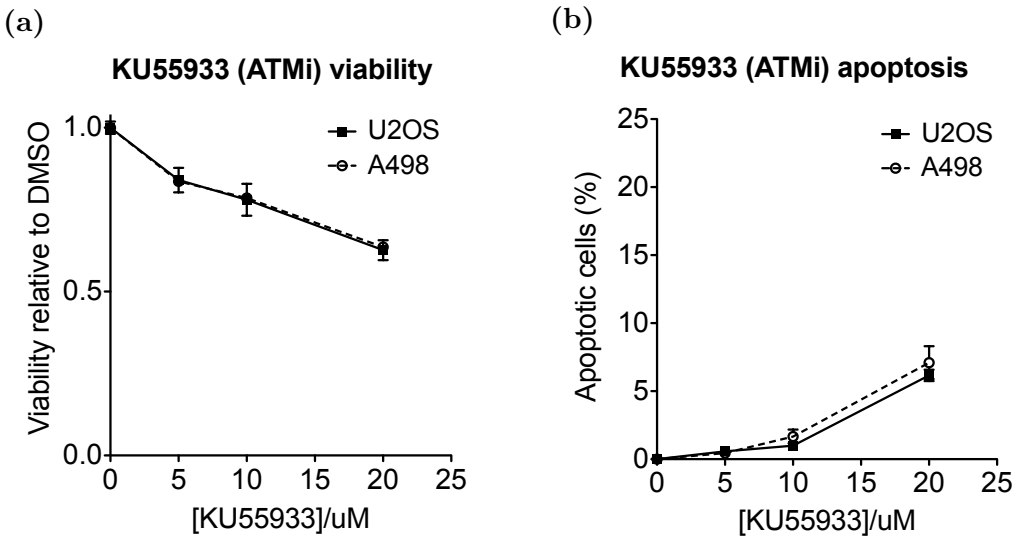


Figure 5.6: SETD2-deficient cells do not exhibit increased sensitivity to the ATM inhibitor. (a) Viability of U2OS and A498 cells five days after ATM inhibitor (KU55933) treatment at indicated concentrations. (b) Percentage of U2OS and A498 cells undergoing apoptosis 48 hours after ATM inhibitor (KU55933) treatment. Data are presented as mean ± SEM, n=3 independent experiments.

would also sensitise cells to these three inhibitors. Two approaches were taken to reduce H3K36me3 levels in U2OS cells without affecting SETD2 levels: expressing the dominant-negative mutant of histone H3.3 (H3.3K36M) (Lewis et al., 2013) and over-expressing KDM4A, a histone demethylase that removes methyl groups from H3K36me3 and H3K9me3 (these two methods were also used in Chapter 3). The sensitivity of these H3K36me3-depleted cells to the inhibitors of WEE1, CHK1 and ATR was tested.

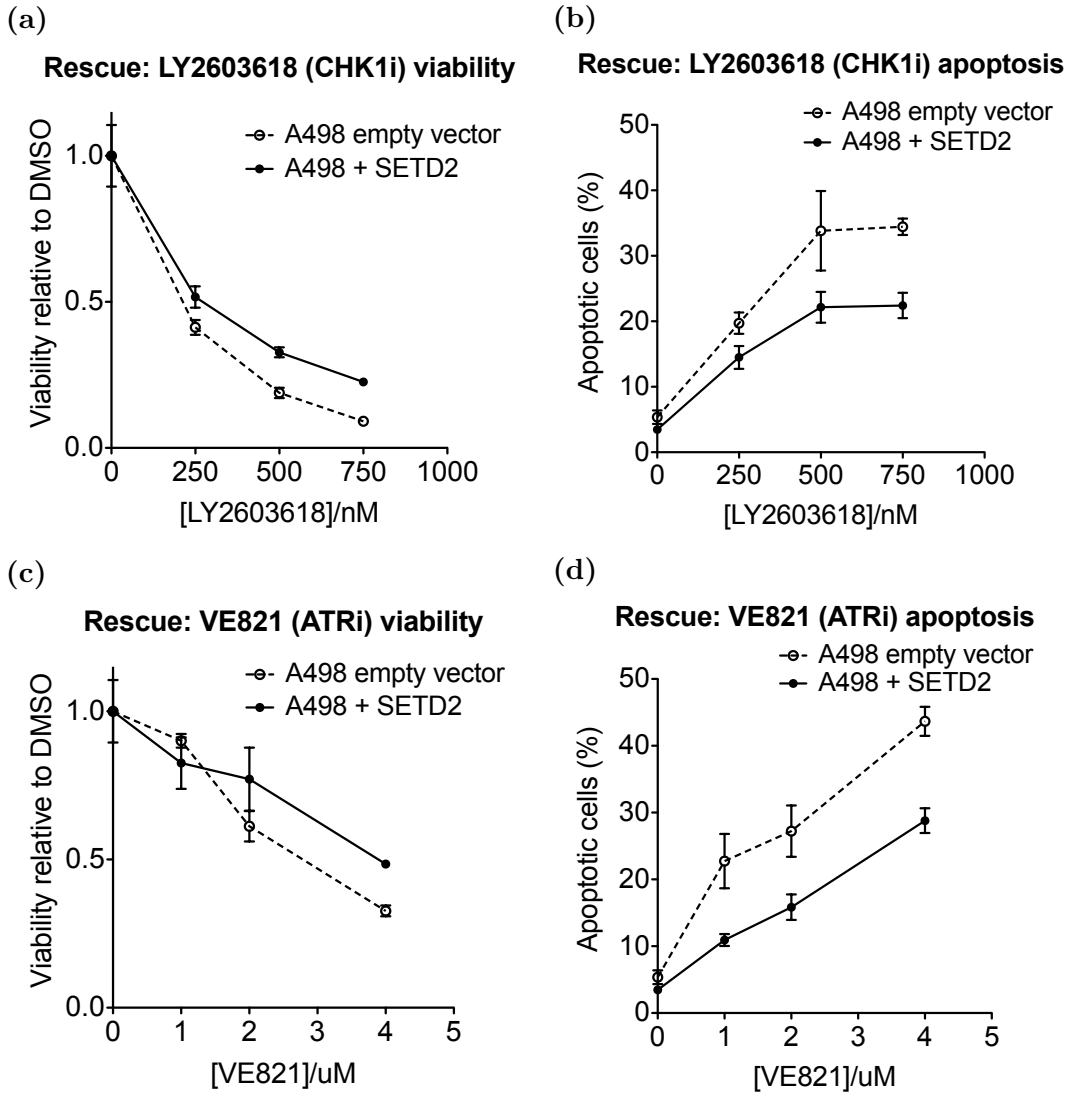


Figure 5.7: The sensitivity of A498 to the CHK1 and ATR inhibitors can be suppressed by the exogenous expression of a wild-type SETD2. (a) Viability and (b) apoptosis of A498 cells expressing an empty vector or *SETD2* cDNA after CHK1 inhibitor (LY2603618) treatment for 72 hours. (c) Viability and (d) apoptosis of A498 cells expressing an empty vector or *SETD2* cDNA after ATR inhibitor (VE821) treatment for 72 hours. Data are presented as mean ± SEM, n=3 independent experiments.

5.2.1 H3.3K36M expression sensitises cells to WEE1, CHK1 and ATR inhibitors

To test if H3K36me3-deficient cells are more sensitive to WEE1, CHK1 or ATR inhibitors than its counter part, the dominant-negative mutant of histone H3.3 (H3.3K36M) was expressed to reduce the global levels of H3K36me3. As described in Chapter 3, Lentiviral plasmids encoding either the wild-type histone H3.3 or the mutant histone H3.3K36M (Lysine 36 to Methionine) were packaged into lentiviral particles in 293T cells. U2OS cells were infected with these Lentiviral particles containing either gene. After selection for stable integrants, the levels of H3K36me3 were analysed by Western blotting. Western blots (different blots from the ones in Chapter 3, done with the cells used for inhibitor treatment) confirmed that expression of H3.3K36M reduced the levels of H3K36me3 without affecting SETD2 levels (Fig 5.8).

U2OS cells expressing either H3.3 or H3.3K36M were challenged with the inhibitors of WEE1, CHK1 and ATR, and cell viability and apoptosis were measured. Compared with H3.3-expressing cells, H3.3K36M-expressing cells were more sensitive to the WEE1 inhibitor MK1775 (Fig 5.9), CHK1 inhibitor LY2603618 (Fig 5.10) and ATR inhibitor VE821 (Fig 5.11). Cell death and growth arrest induced by these inhibitors were also observed under the microscope (Fig 5.12).

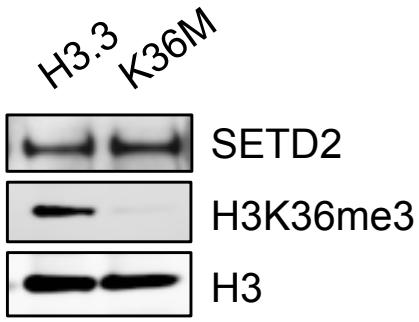


Figure 5.8: Expression of the dominant negative H3.3K36M mutant reduces the levels of H3K36me3 without affecting the levels of SETD2. Western blot analysis of the levels of SETD2 and H3K36me3 in U2OS cells with stably integrated H3.3 (control) or H3.3K36M lentiviral construct. Histone H3 was used as a loading control.

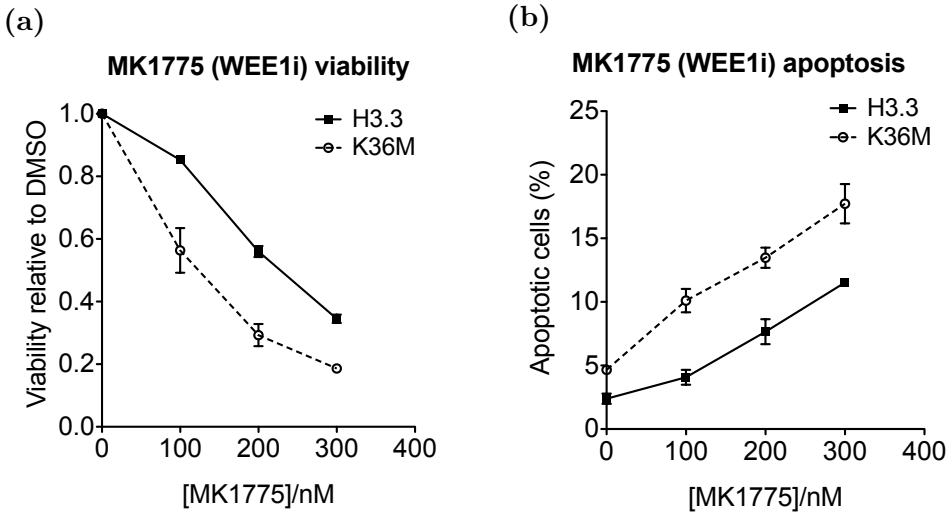


Figure 5.9: H3K36me3 depletion by H3.3K36M sensitises cells to WEE1 inhibitor. (a) Viability of U2OS cells stably expressing the dominant-negative H3.3K36M gene or the control H3.3 gene after treatment with WEE1 inhibitor MK1775 for five days. (b) Percentage of cells undergoing apoptosis as determined by Hoechst nuclear staining after MK1775 treatment for 48 hours. Data are presented as mean ± SEM, n=3 independent experiments.

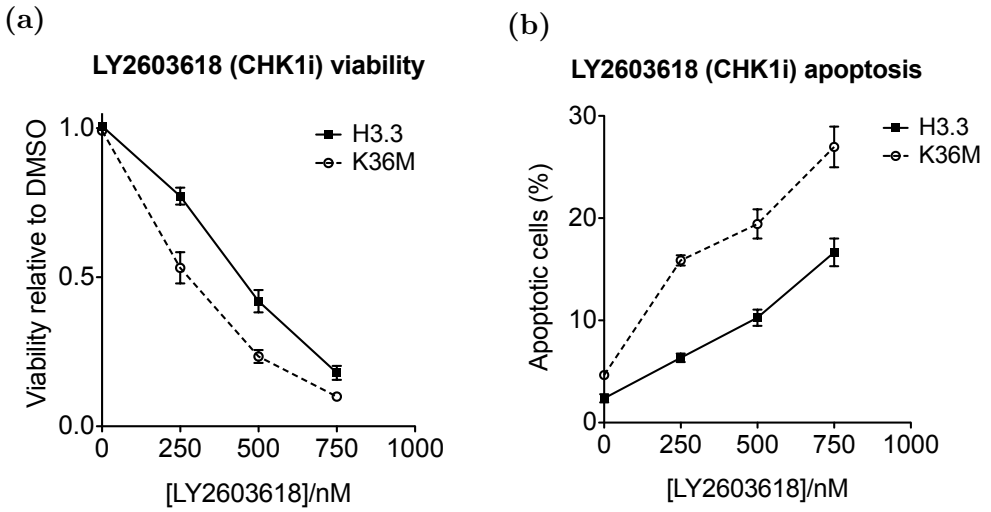


Figure 5.10: H3K36me3 depletion by H3.3K36M sensitises cells to the CHK1 inhibitor. (a) Viability of U2OS cells stably expressing the dominant-negative H3.3K36M gene or the control H3.3 gene after treatment with CHK1 inhibitor LY2603618 for five days. (b) Percentage of cells undergoing apoptosis as determined by Hoechst nuclear staining after LY2603618 treatment for 48 hours. Data are presented as mean ± SEM, n=3 independent experiments.

5.2.2 KDM4A over-expression sensitises cells to WEE1, CHK1 and ATR inhibitors

The *KDM4A* cDNA, which encodes the histone demethylase for H3K36me3 and H3K9me3, was stably integrated into the FRT site in the genome of the U2OS T-REx parental cell line (as described in Chapter 3). In the clones with stably integrated *KDM4A* cDNA, the over-expression of KDM4A could be induced by addition of Doxycycline to the cell culture medium. Western blots (different blots from the ones in Chapter 3, done with the cells used for inhibitor treatment) showed that KDM4A over-expression reduced the level of H3K36me3 without affecting the level of SETD2 (Fig 5.13).

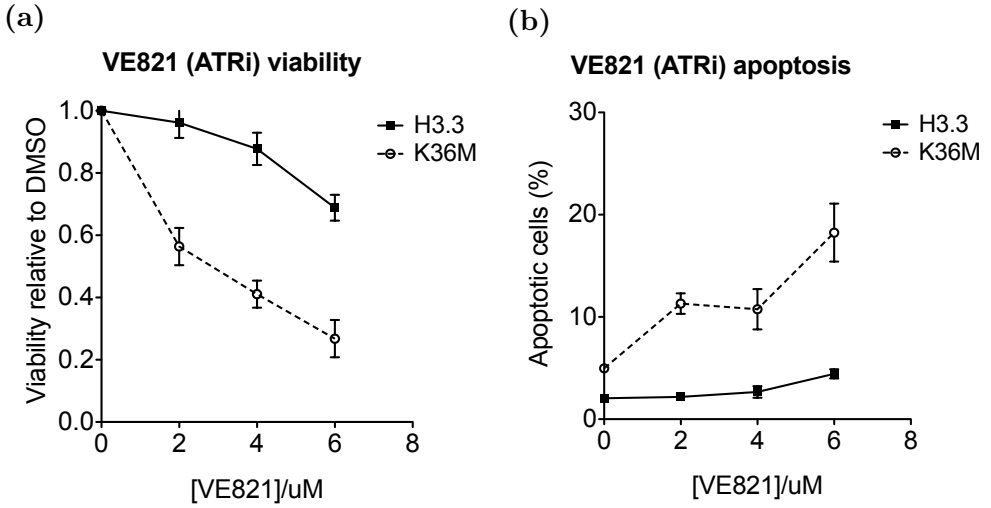


Figure 5.11: H3K36me3 depletion by H3.3K36M sensitises cells to the ATR inhibitor. (a) Viability of U2OS cells stably expressing the dominant-negative H3.3K36M gene or the control H3.3 gene after treatment with ATR inhibitor VE821 for five days. (b) Percentage of cells undergoing apoptosis as determined by Hoechst nuclear staining after VE821 treatment for 48 hours. Data are presented as mean ± SEM, n=3 independent experiments.

Cell viability measurements by Resazurin and apoptosis measurements by Hoechst staining showed that depletion of H3K36me3 by over-expressing KDM4A sensitised cells to the WEE1 inhibitor MK1775 (Fig 5.14), CHK1 inhibitor LY2603618 (Fig 5.15) and ATR inhibitor VE821 (Fig 5.16).

5.3 WEE1, CHK1 and ATR all arrest SETD2-deficient cells in S-phase

To understand whether CHK1 and ATR inhibition kills SETD2-deficient cells through the same mechanism as WEE1 inhibition, the impact of CHK1 and

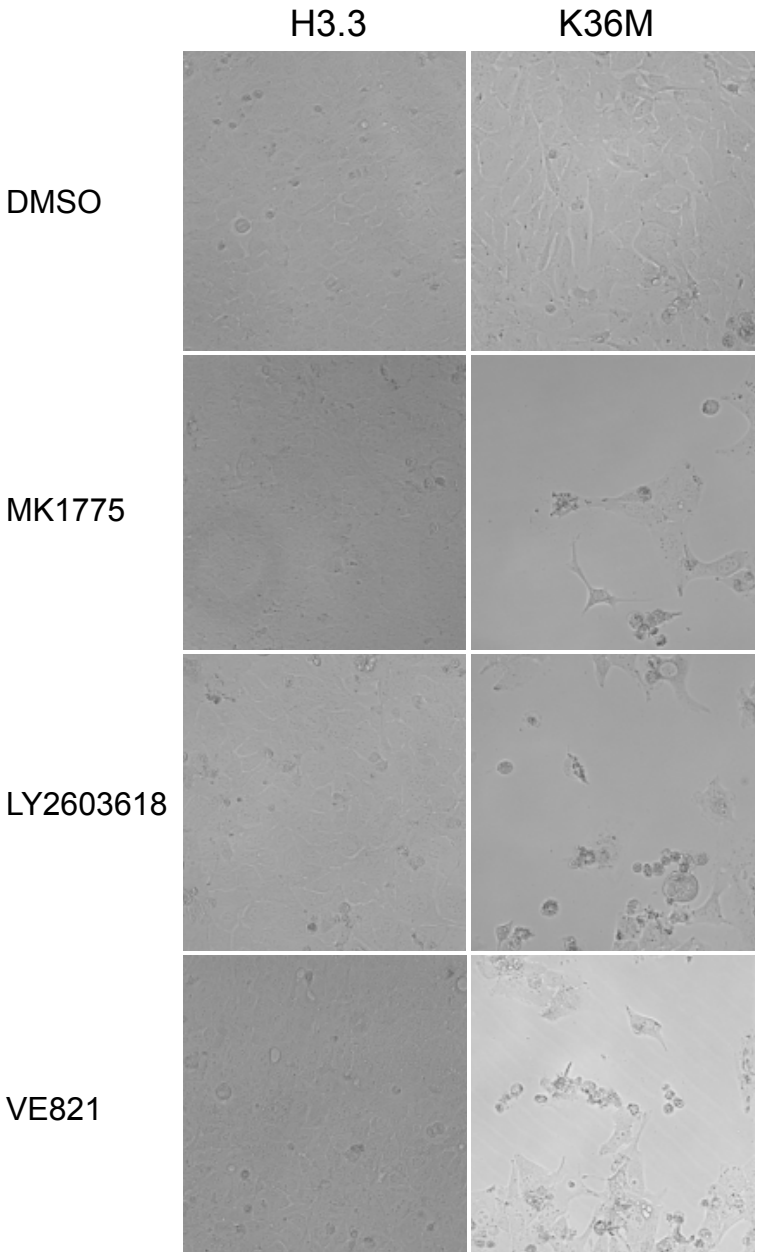


Figure 5.12: H3K36me3 depletion by H3.3K36M sensitises cells to the inhibitors of WEE1, CHK1 and ATR. Representative bright field microscope images of U2OS cells stably expressing either H3.3 control or H3.3K36M dominant-negative mutant and treated with DMSO, WEE1 inhibitor MK1775 (100nM), CHK1 inhibitor LY2603618 (250nM) or ATR inhibitor VE821 (2μM) for five days.

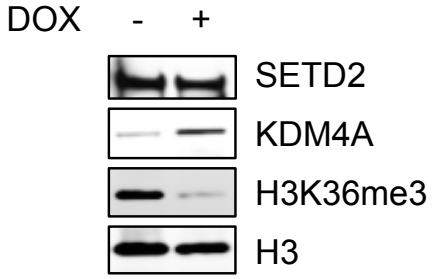


Figure 5.13: Over-expression of the demethylase KDM4A reduces the level of H3K36me3 without affecting the level of SETD2. Western blots showing the protein levels of SETD2, KDM4A, H3K36me3 following KDM4A induction with 5μg/ml Doxycycline (DOX) for 72 hours in the KDM4A T-REx U2OS cells. Histone H3 was used as a loading control.

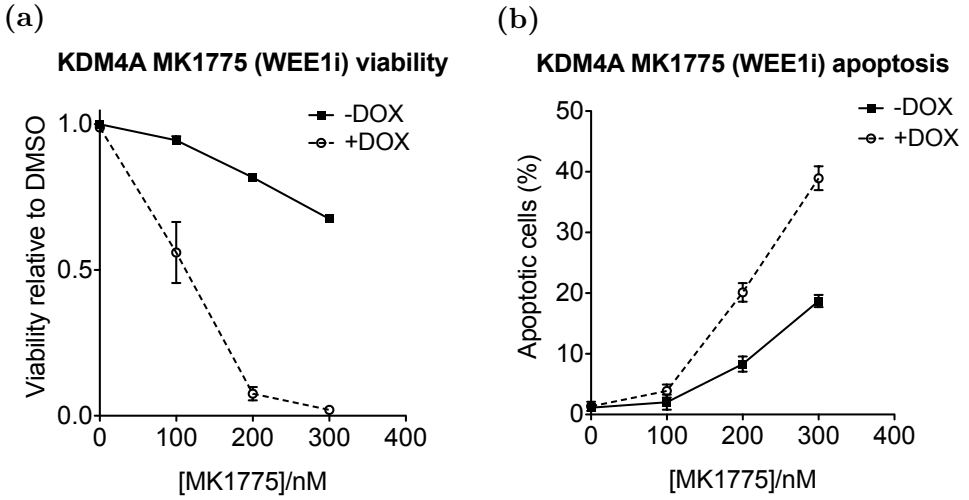


Figure 5.14: H3K36me3 depletion by over-expression of the demethylase KDM4A sensitises cells to WEE1 inhibitor. (a) Viability of KDM4A T-REx U2OS cells with or without Doxycycline-induced KDM4A over-expression after treatment with WEE1 inhibitor MK1775 for five days. (b) Percentage of cells undergoing apoptosis as determined by Hoechst nuclear staining after MK1775 treatment for 48 hours. Data are presented as mean ± SEM, n=3 independent experiments.

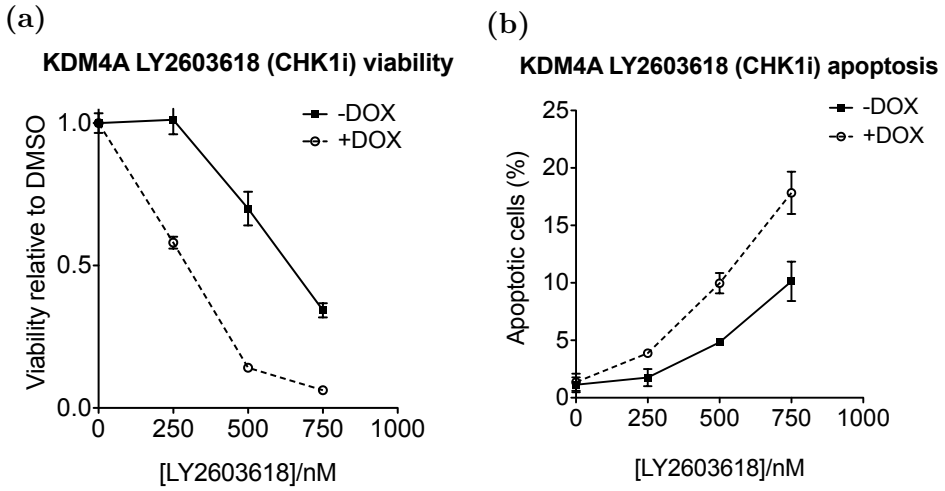


Figure 5.15: H3K36me3 depletion by over-expression of the demethylase KDM4A sensitises cells to the CHK1 inhibitor. (a) Viability of KDM4A T-REx U2OS cells with or without Doxycycline-induced KDM4A over-expression after treatment with CHK1 inhibitor LY2602618 for five days. (b) Percentage of cells undergoing apoptosis as determined by Hoechst nuclear staining after LY2602618 treatment for 48 hours. Data are presented as mean ± SEM, n=3 independent experiments.

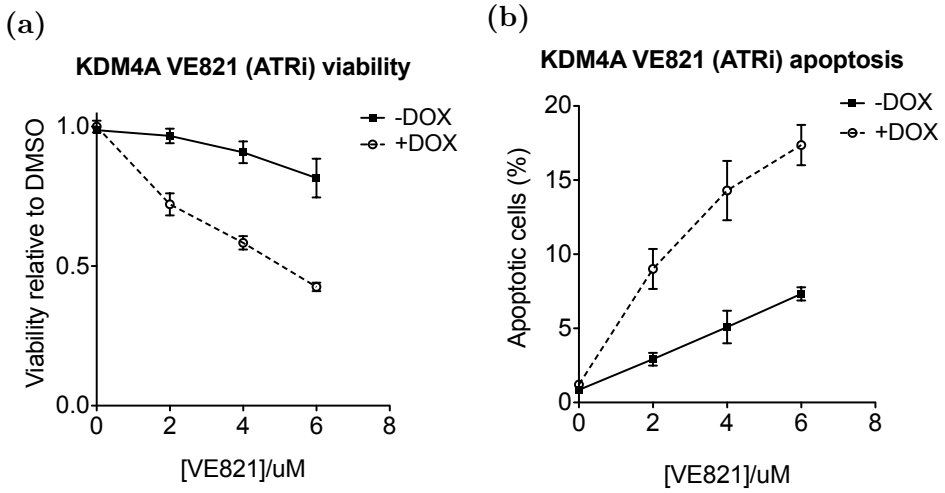


Figure 5.16: H3K36me3 depletion by over-expression of the demethylase KDM4A sensitises cells to the ATR inhibitor. (a) Viability of KDM4A T-REx U2OS cells with or without Doxycycline-induced KDM4A over-expression after treatment with ATR inhibitor VE821 for five days. (b) Percentage of cells undergoing apoptosis as determined by Hoechst nuclear staining after VE821 treatment for 48 hours. Data are presented as mean ± SEM, n=3 independent experiments.

ATR inhibitors on DNA replication was assessed. In Chapter 4, WEE1 inhibitor MK1775 was found to arrest SETD2-deficient cells in the S-phase, which resulted in a phenomenon called 'non-replicating S-phase population' – having half-replicated DNA but unable to incorporate BrdU. Therefore an experiment was conducted to test whether CHK1 and ATR inhibitors also induce S-phase arrest in SETD2-deficient cells.

Cell cycle distribution and DNA synthesis efficiency were assessed by the ability of cells to incorporate BrdU (5-bromo-2-deoxyuridine, a thymidine analog). FACS analysis of BrdU staining showed that, similar to the WEE1 inhibitor, ATR and CHK1 inhibitors also arrested SETD2-deficient A498 cells in 'non-replicating S-phase', while they had no effect on SETD2-proficient U2OS cells (Fig 5.17a). All three inhibitors (at their lowest working concentration) induced similar degrees of S-phase arrest: under each condition, between 33 and 41% of the A498 cells had became the non-replicating S-phase population (Fig 5.17b). This suggests that WEE1, CHK1 and ATR all modulate a same target (e.g. CDK1), which is responsible for S-phase progression.

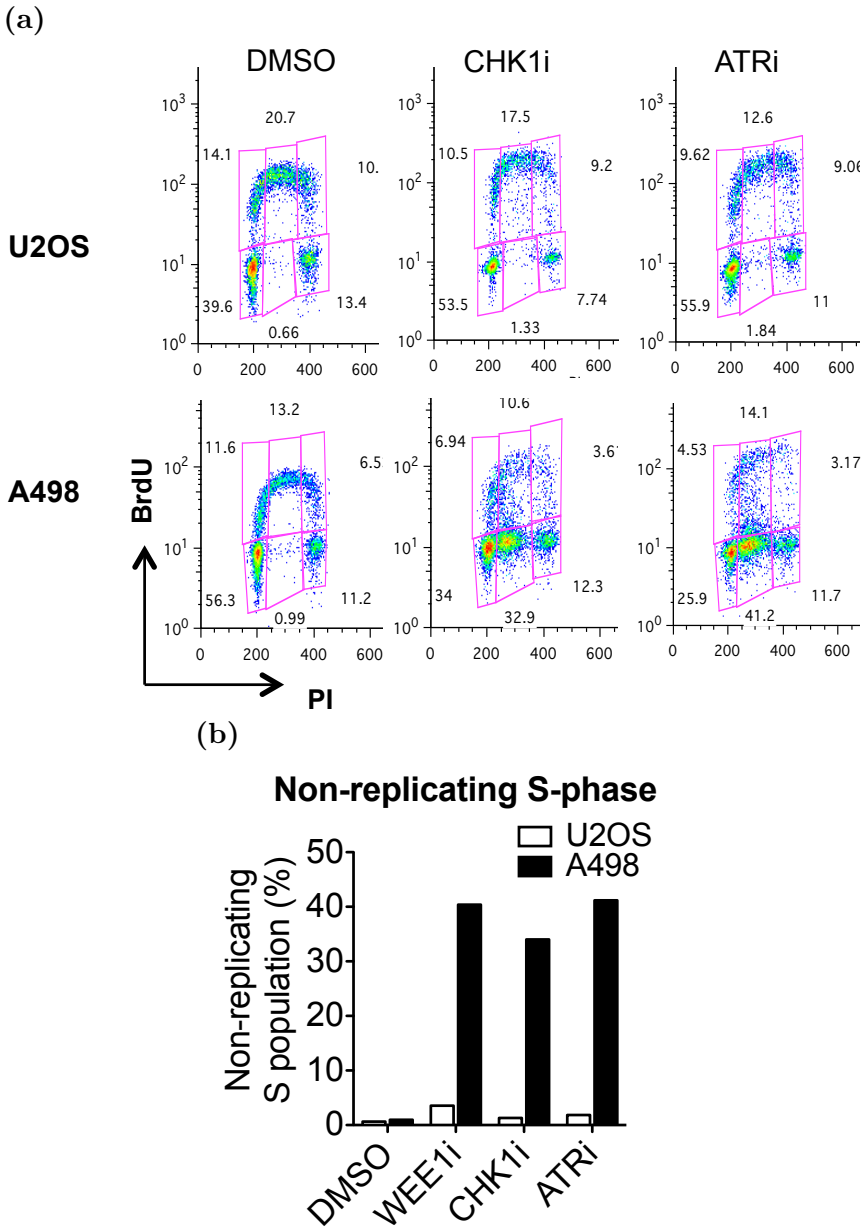


Figure 5.17: WEE1, CHK1 and ATR inhibitors induce non-replicating S-phase population specifically in SETD2-deficient A498 cells. (a) FACS analysis of BrdU incorporation by U2OS or A498 cells after treatment with DMSO, CHK1 inhibitor LY2603618 (250nM) or ATR inhibitor VE821 (2μM) for 48 hours. (b) Quantification of the non-replicating S-phase population based on (a).

5.4 H3K36me3 and CDK1 represent two redundant pathways that regulate RRM2

The induction of the non-replicating S-phase population suggested that the effect of the WEE1, CHK1 and ATR inhibitors converged at DNA replication in SETD2-deficient cells. In Chapter 4, the WEE1 inhibitor MK1775 promoted the degradation of RRM2 through untimely activation of CDK1. Given that both CHK1 and ATR inhibit CDK1, it was hypothesised that their inhibition, like WEE1 inhibition, would lead to untimely activation of CDK1 during the S-phase, resulting in CDK1-dependent RRM2 degradation in the S-phase.

5.4.1 CDK1 hyper-activation due to WEE1, CHK1 and ATR inhibition degrades RRM2

To test the hypothesis that CHK1 and ATR inhibition leads to CDK1-dependent RRM2 degradation, the activity of CDK1 and levels of RRM2 after inhibitor treatment were assessed by Western blotting. Western blots showed that both CHK1 and ATR inhibitors reduced the inhibitory phosphorylation of CDK1 at Tyrosine 15 (i.e. increased CDK1 activity), and reduced the levels of RRM2 in A498 cells (Fig 5.18).

To show that CHK1 and ATR inhibitors contribute to the synthetic lethality by activating CDK1 (instead of by activating their other targets), a CDK1-specific

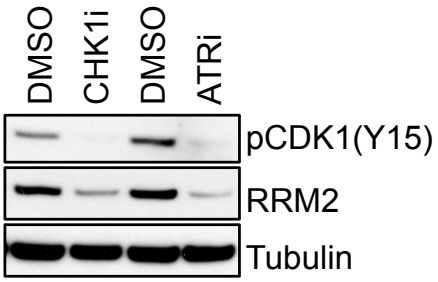


Figure 5.18: ATR and CHK1 inhibitors activate CDK1 and reduce the level of RRM2. Western blots showing the levels of CDK1 inhibitory phosphorylation at Y15 and RRM2 in A498 cells after CHK1 inhibitor LY2603618 (500nM) or ATR inhibitor VE821 (4μM) treatment for 24 hours.

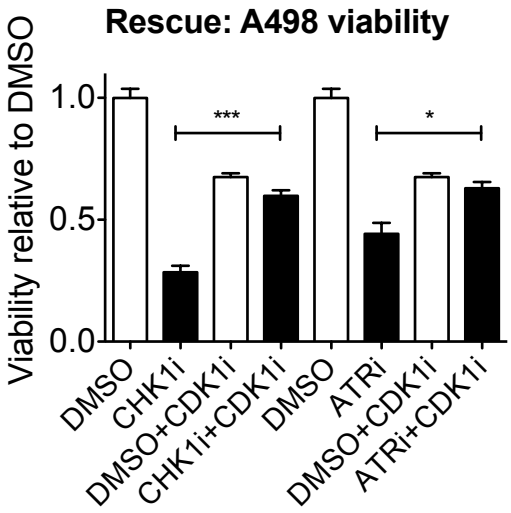
inhibitor RO3306 was used to rescue the phenotypes caused by CHK1 and ATR inhibitors. Cell viability and apoptosis experiments showed that, like for the WEE1 inhibitor, the toxicity of ATR and CHK1 inhibitors to SETD2-deficient cells was suppressed by the CDK1 inhibitor RO3306 (Fig 5.19).

The above Western blots and rescue experiments suggested that WEE1, CHK1 and ATR inhibitors all contribute to the synthetic lethality by de-repressing the CDK1 activity. As a result of CDK1 hyper-activation, RRM2 was degraded inappropriately in the S-phase.

5.4.2 H3K36me3 depletion reduces RRM2 and mildly affects DNA replication

It was shown in Chapter 4 that the histone mark H3K36me3 promotes E2F1-dependent RRM2 transcription by recruiting transcription initiation factors (such as TAF6 and TAF4) and RNA PolII to the promoter of E2F1. To further in-

(a)



(b)

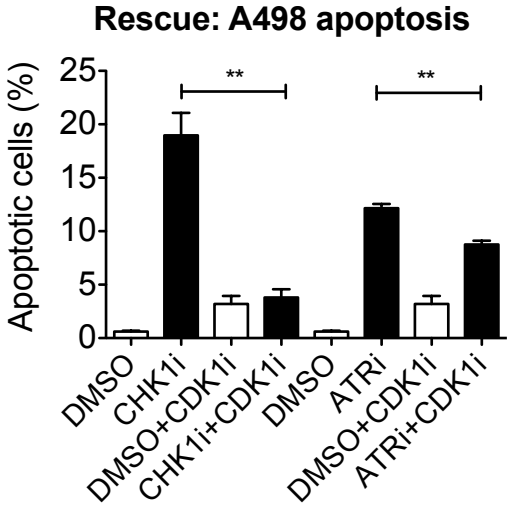


Figure 5.19: The CDK1 inhibitor suppressed the toxicity of CHK1 and ATR inhibitors to SETD2-deficient A498 cells. (a) Viability and (b) apoptosis of A498 cells 48 hours after treatment with either CHK1 inhibitor LY2603618 (500nM) or ATR inhibitor VE821 (4μM) combined with CDK1 inhibitor RO3306 (10μM).

vestigate the role of H3K36me3 in regulating the expression of E2F1, H3.3K36M was expressed to deplete H3K36me3 in U2OS cells, and the levels of E2F1 and RRM2 were assessed by Western blotting. Western blots showed that, like in SETD2 siRNA knockdown, H3.3K36M expression also reduced the protein levels of E2F1 and RRM2 (Fig 5.20).

Cells with reduced levels of RRM2 are expected to encounter difficulties in DNA replication. Thus H3K36me-depleted cells should exhibit a prolonged S-phase. However, when the cell cycle distribution of the H3K36me3-depleted cells was assessed, none of the H3K36me3-depleted cell lines exhibited significant alterations to the cell cycle, whether through SETD2 knockdown, KDM4A overexpression or H3.3K36M expression (see Chapter 3).

To investigate this further, a different approach was taken. Here, cells were synchronised in G1 by serum starvation and released into the cell cycle by serum stimulation. Under such conditions, H3.3K36M-expressing cells started to accumulate DNA contents slightly later than H3.3-expressing cells (Fig 5.21a), suggesting a delay in G1/S transition. Also, compared to H3.3-expressing cells, H3.3K36M-expressing cells had less cells in mid-S-phase at 23 hours after release and less cells in late-S-phase at 28 hours after release (Fig 5.21b), suggesting a slight delay in progression through S-phase. However, the difference was so small (31% v.s. 24% population in mid-S-phase when 66% cells are in S-phase) that in an unsynchronised population it would appear insignificant.

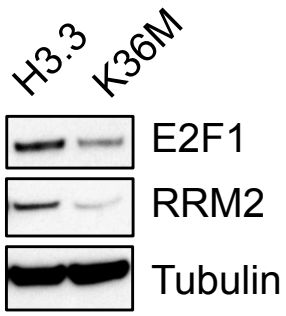


Figure 5.20: H3K36me3 depletion by H3.3K36M reduces the protein levels of E2F1 and RRM2. Western blot analysis of the levels of E2F1 and RRM2 in U2OS cells with stably integrated H3.3 (control) or H3.3K36M (dominant-negative mutant) lentiviral construct. Tubulin was used as a loading control.

5.4.3 CDK1 and H3K36me3 redundantly regulate RRM2

The cellular data above suggest that although either CDK1 aberrant activation or H3K36me3 loss alone reduces RRM2, the cells can still carry out DNA replication as the RRM2 and dNTP pool depletion have not reached a critical level. When both pathways are disturbed, cells can no longer cope with the further reduction in the RRM2 level.

To determine whether there is a synergistic effect on RRM2 levels after CDK1 activation and H3K36me3 loss, Western blotting was performed. SETD2-proficient U2OS cells were transfected with either control siRNA or SETD2 siRNA prior to the treatment with CHK1 or ATR inhibitors. Consistent with the Western blots shown in Chapter 4, SETD2 knockdown reduced the protein levels of E2F1 and RRM2. In addition, like the WEE1 inhibitor, CHK1 and ATR inhibitors also reduced the levels of RRM2. When SETD2 knockdown was combined with

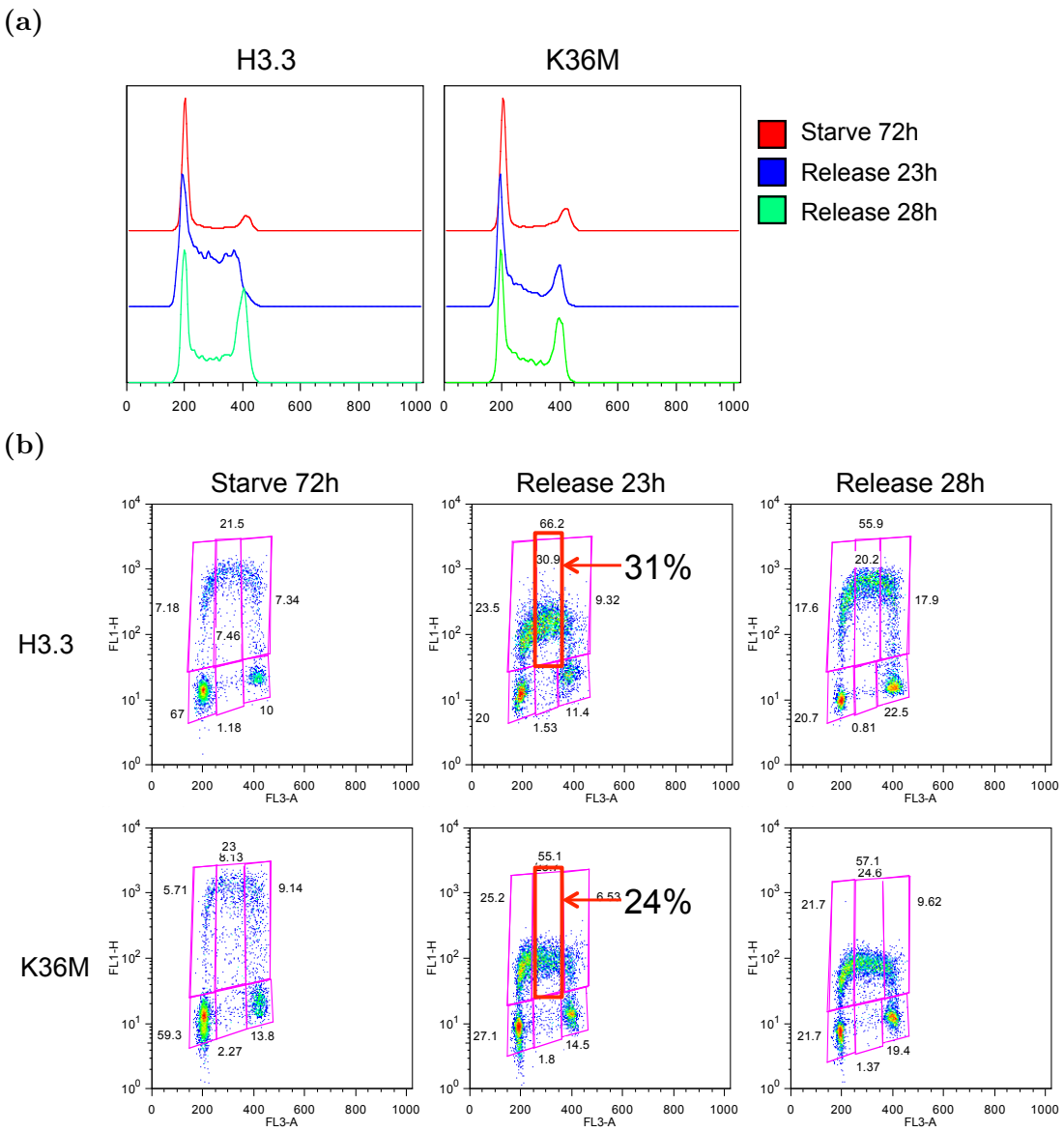


Figure 5.21: H3K36me3 depletion by H3.3K36M very mildly inhibits S-phase entry and DNA replication following G1 synchronisation and release. U2OS cells expressing either control H3.3 or H3.3K36M were synchronised in G1 by serum starvation (72 hours) and the cell cycle progression was analysed after serum stimulation. FACS analysis showing (a) PI staining of DNA contents and (b) BrdU incorporation. The arrows indicate mid-S population.

CHK1 or ATR inhibitors, the reduction in RRM2 was more dramatic than either treatment alone (Fig 5.22).

Both E2F1 and RRM2 protein levels are cell cycle regulated: E2F1 peaks at the G1-phase while RRM2 peaks at the S-phase. Therefore it is possible that the reduction in E2F1 by the combination may be a result of S-phase arrest. However the reduction in RRM2 is unlikely to be due to cell cycle alteration, as higher levels of RRM2 are expected if a larger proportion of cells are in S-phase.

These results again supported the synthetic lethal model: in the absence of either H3K36me3 or CDK1 suppressors, cells can survive since the remaining pathway is able to maintain the cellular function (in this case RRM2 levels and dNTP synthesis). Only when both pathways are inhibited simultaneously, the cellular stress reaches the threshold: in this case, a critical reduction in RRM2 and dNTP pool was observed, thus rendering cells unable to complete the DNA synthesis.

5.5 The synthetic lethal model

In this chapter, the relationship between H3K36me3 loss and the ATR or CHK1 inhibition was investigated. Similar to the findings with WEE1 inhibition (Chapter 4), ATR or CHK1 inhibition in H3K36me3-deficient cells leads to reduced viability, non-replicating S-phase population and reduced RRM2 levels. Together the data support a model for synthetic lethality in which RRM2 levels are reg-

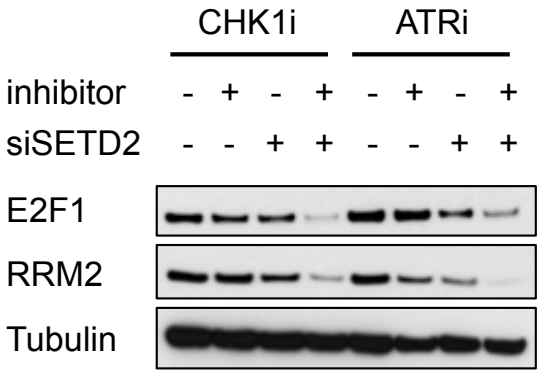


Figure 5.22: SETD2 knockdown or CHK1/ATR inhibition reduces the protein levels of RRM2 and E2F1. Western blotting analysis of protein levels in U2OS cells transfected with non-targeting or SETD2 siRNA 48 hours prior to treatment with DMSO or CHK1 inhibitor LY2602618 (500nM) or ATR inhibitor VE821 (4μM) for 24 hours. Tubulin was used as a loading control. Samples were treated and harvested by me and the Western blotting was performed by Ms Giulia Orlando.

ulated by two independent pathways. Disrupting the first through H3K36me3 depletion (e.g. by SETD2 knockdown, KDM4A over-expression or H3.3K36M expression) reduces E2F1 transcription, RRM2 expression and dNTP production. Disrupting the second through WEE1, CHK1 or ATR inhibition leads to aberrant CDK1 activity in S-phase, resulting in untimely RRM2 degradation and reduced dNTP production. Simultaneous disruption of both causes cell death due to critically low dNTP levels, resulting in permanent S-phase arrest, MUS81-induced DNA damage at stalled forks and cell death (Fig 5.23).

5.6 Discussion of Chapter 5

One challenge for this project is to provide strong enough evidence to demonstrate the role of H3K36me3 in transcription initiation. Chapter 4 and 5 have demon-

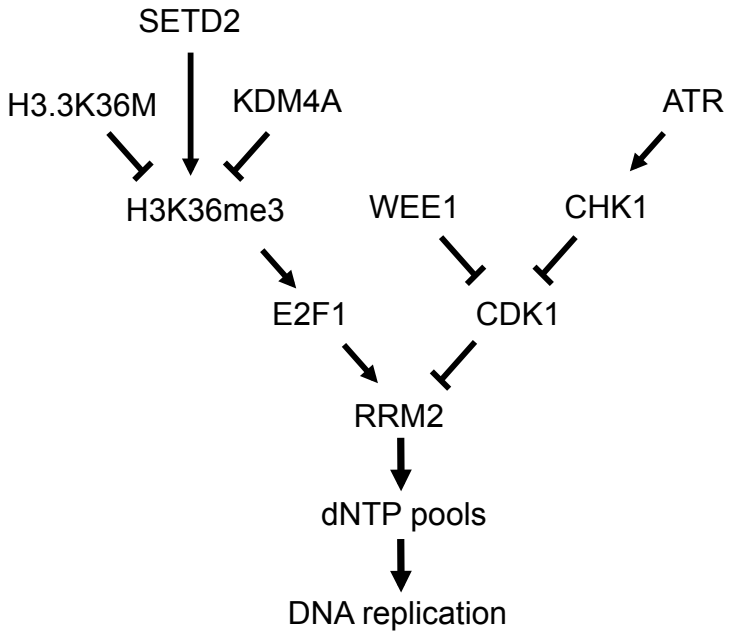


Figure 5.23: Schematic overview of the two redundant pathways regulating RRM2. In the pathway on the left, H3K36me3 (regulated by SETD2, KDM4A or H3.3K36M) transcriptionally activates E2F1, which in turn promotes transcription of RRM2. In the pathway on the right, ATR, CHK1 and WEE1 suppress the activity of CDK1 in S-phase, which is required to maintain the levels of RRM2 during DNA replication. Simultaneous inhibition of both pathways lead to critical reduction in RRM2 levels, pushing dNTP below threshold, thus abolishing DNA replication.

strated that the expression levels of E2F1 and RRM2 were reduced by SETD2 knockdown or knockout (by qRT-PCR and Western blotting), and this reduction is unlikely to be due to the cell cycle effect. However, more evidence is needed to narrow down the role of SETD2 in gene expression, since gene expression can be affected by several factors such as transcription initiation, elongation, splicing or the stability of mRNAs. To tackle this issue, the following experiments are planned: (1) the luciferase assay to measure the promoter activity; (2) phospho-Pol2 ChIP along the gene body to assess the processivity of the RNA polymerases; (3) qRT-PCR with primers to different introns to assess the efficiency of splicing; (4) block the degradation of mRNA and then perform qRT-PCR; (5) genome-wide analysis of H3K36me3 levels at the promoter regions, and see whether the genes with H3K36me3 at the promoter overlap with the genes affected by SETD2 knockout. With the additional experiments, one can strengthen the evidence for the novel role of promoter-located H3K36me3 in transcription initiation.

Chapter 4 and 5 have shown that the overexpression of KDM4A reduced the global levels of H3K36me3, sensitising cells to the inhibitors of WEE1, CHK1 and ATR. A negative control can be introduced, where a demethylase-dead KDM4A is overexpressed. Since the demthylase-dead KDM4A cannot drive down the levels of H3K36me3, one would expect it to be insensitive to the inhibitors.

The synthetic lethal model suggests that, like WEE1 inhibition, CHK1 inhibition leads to RRM2 degradation through CDK1 hyperactivity (Fig 5.23). Previous literature also reports that CHK1 depletion in MEFs reduces CDK1

transcription due to the loss of histone H3-T11 phosphorylation (Shimada et al., 2008). In the cancer cell lines used in this project however, CDK1 inhibitor rescued the loss of viability after CHK1 inhibitor treatment. Thus the mechanism may be mainly through the hyperactive CDK1-driven degradation of RRM2. One could test this by combining the CHK1 inhibitor and CDK1 inhibitor, and check whether the CDK1 inhibitor rescues the reduction in the RRM2 levels in a Western blot.

It appears that U2OS is hypersensitive to CHK1 and ATR inhibitors even though it is SETD2-positive (Fig 5.3, 5.5, 5.10, 5.15). Therefore it is important to test other cell lines to eliminate the possibility of a cell-line specific effect. Also, since the CRISPR SETD2-knockout A549 cells were generated, they can be used as an alternative to the SETD2-knockout U2OS cells in the experiment involving CHK1 and ATR inhibitors.

Chapter 6

Discussion

This chapter compares and contrasts the findings described in this thesis with the current literature. It also investigates the potential connections between the findings within this thesis. The discussion will focus on the following four topics: (1) The view on SETD2's role in DNA repair from other publications. (2) The potential interplay between SETD2's role in homologous recombination and in DNA replication. (3) Additional ways to clinically exploit the synthetic lethal interaction. (4) Future work.

6.1 The current understanding of SETD2 in DNA repair

This section consists of three parts:

Subsection 6.1.1 will draw three papers on human SETD2 together, which

independently but largely consistently described the role of SETD2 in homologous recombination (HR) repair.

Subsection 6.1.2 will discuss the differences between the three papers.

Subsection 6.1.3 will attempt to provide insights into why yeast Set2 and human SETD2 are involved in different DNA repair pathways.

6.1.1 Human SETD2 is required for DSB repair by homologous recombination

Almost the same time as we published the role of SETD2 in homologous recombination (HR) (Pfister et al., 2014), two other groups also showed that SETD2 promotes DNA double-strand break repair by HR (Aymard et al., 2014; Carvalho et al., 2014). All three groups used a well-established GFP reporter system in which repair of an I-SceI endonuclease-induced DSB by HR generates an intact GFP gene, and showed that SETD2 knockdown by siRNA resulted in reduced HR. Loss of SETD2 also reduced formation of RPA foci (Pfister et al., 2014), RAD51 foci (Carvalho et al., 2014; Pfister et al., 2014) and recruitment of RAD51 to DSBs, as measured by ChIP (Aymard et al., 2014; Pfister et al., 2014).

Moreover, SETD2 depletion reduces DSB end-resection, as shown by an *in vivo* assay that measures single-stranded DNA generated by the resection machinery in the vicinity of a DSB (Pfister et al., 2014). Two studies (Aymard et al., 2014; Pfister et al., 2014) agreed on a model in which SETD2-dependent

H3K36me3 anchors Lens Epithelium-derived Growth Factor p75 (LEDGF) to chromatin through its PWWP domain. Following DSB induction, chromatin-bound LEDGF recruits the resection enzyme CtIP, which promotes resection and recruitment of RAD51. However, the third group showed that RAD51 recruitment was reduced without defects in resection (Carvalho et al., 2014).

All three studies also agreed that there was no recruitment of SETD2 or H3K36me3 to the DSB sites, suggesting that H3K36me3 levels are pre-set, presumably by prior transcription, and may be sufficient for downstream functions in DSB repair. Indeed, (Aymard et al., 2014) showed that, in human cells, HR preferentially repairs transcriptionally active regions. A rare-cutting endonuclease (AsiSI) was used to generate around 150 DSBs across the genome, which were then sub-divided into RAD51- or XRCC1-enriched DSBs by chromatin immunoprecipitation-sequencing (ChIP-seq). RAD51 enrichment implied the use of HR while XRCC1 enrichment suggested that the DSB was being repaired by NHEJ. RAD51-enriched DSBs tended to occur in transcriptionally active regions and this preference was lost when transcription was abolished by addition of the transcriptional inhibitor DRB. Conversely, reactivating a repressed gene directed DSB repair towards HR. These findings indicate that HR preferentially repairs DSBs in transcriptionally active regions of the genome.

6.1.2 Is SETD2 required for DNA damage sensing?

One out of the three groups showed that the activation of DNA damage response (DDR) is defective in SETD2-deficient or -depleted cells, as measured by reduced ATM activation, reduced γH2AX and delayed 53BP1 recruitment to DNA damage sites (Carvalho et al., 2014). In addition, they observed reduced p53 stabilisation and downstream activation of p21, the major cyclin-dependent kinase inhibitor that is required for DNA damage dependent cell-cycle arrest. Another paper also suggested that SETD2 facilities p53 transactivation of p21 (Xie et al., 2008).

Based on the two publications, the hypothesis that SETD2 is required for DNA damage response (DDR) was tested here, as it would suggest an alternative mechanism on SETD2's role in HR as well as the sensitivity to checkpoint inhibitors (WEE1, CHK1 and ATR). However, so far no defects in DDR were observed in SETD2 knockdown cells.

Three independent siRNAs were used to knockdown SETD2 in U2OS cells. The depletion of the SETD2 protein by the three siRNAs was confirmed by Western blotting (Fig 6.1a). Ionising radiation (IR) was used to induce double-stranded breaks in those cells, and the formation of repair foci was assessed by immunofluorescence (IF). IF analysis showed that SETD2 knockdown did not reduce the formation of phospho-ATM foci, 53BP1 foci or γH2AX foci (Fig 6.1). The data suggested that SETD2 knockdown cells are unlikely to be defective in

response to IR-induced DNA double-strand breaks. The differences between our results and Carvalho et al may also be due to the use of different DNA damaging reagents (IR vs. etoposide/neocarzinostatin).

Since the WEE1 inhibitor also induces DNA damage (Chapter 4), the impact of SETD2 knockdown on the DDR after WEE1 inhibition was tested here. Western blots showed that upon treatment with the WEE1 inhibitor MK1775, ATM activation could be detected by ATM phosphorylation at Serine 1981, and KAP1 phosphorylation at Serine 824. ATR activation could be detected by CHK1 phosphorylation at Serine 345. P53 activation could be detected by the stabilisation (increase in the protein levels) of p53 and p21. Western blots showed that SETD2 knockdown has no effect on the degree of activation of any of the DDR effectors mentioned above (Fig 6.2). The data suggested that SETD2 knockdown cells are unlikely to be defective in response to MK1775-induced DNA damage (both double-stranded and single-stranded DNA damage).

6.1.3 The relationship between H3K36 dimethylation and trimethylation in DNA repair

A recent review article (Jha et al., 2014) pointed out that while all three human cell studies were in agreement that SETD2 is required for HR, two yeast studies show that set2 (yeast orthologue of SETD2) inhibits HR (Pai et al., 2014; Jha and Strahl, 2014). Pai et al. showed that loss of Set2 increases the frequency of gene

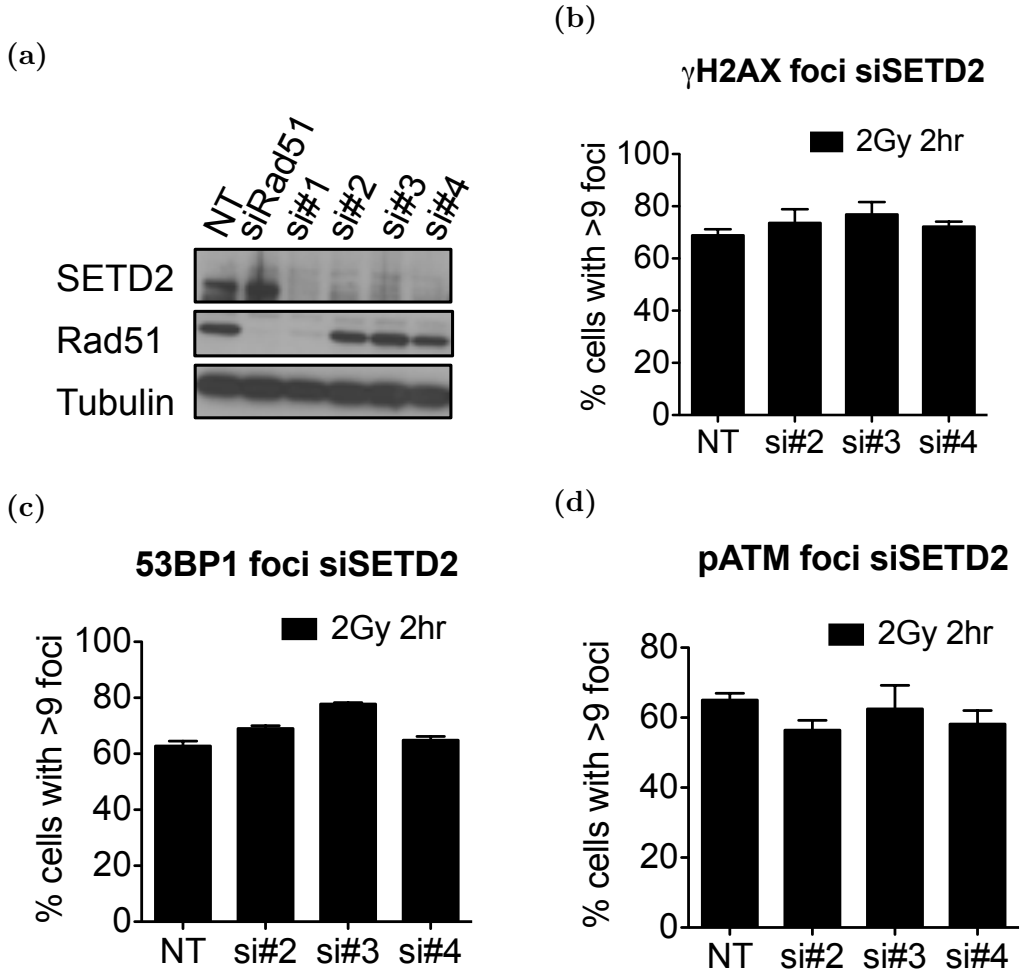


Figure 6.1: SETD2 depletion does not impede DNA damage response after ionising radiation. (a) Western blots showing the depletion of SETD2 protein by four independent siRNAs 48 hours after transfection. RAD51 was used as the control, for it is the common victim of the siRNA off-target effect, si#1 was no longer used since it also depleted RAD51. (b-d) U2OS cells were transfected with non-targeting siRNA (NT) or SETD2 siRNAs (si#2, si#3 and si#4) 48 hours prior to IR (2Gy) treatment and left to recover for 2 hours before fixing with 4% PFA. Quantification of the percentage of cells containing more than nine foci of (b) γH2AX (c) 53BP1 (d) phospho-ATM. For each condition, 45 fields and at least 500 cells were examined by Incell (GE healthcare). Data are presented as mean $\pm$ SEM, n = 3 replicates.

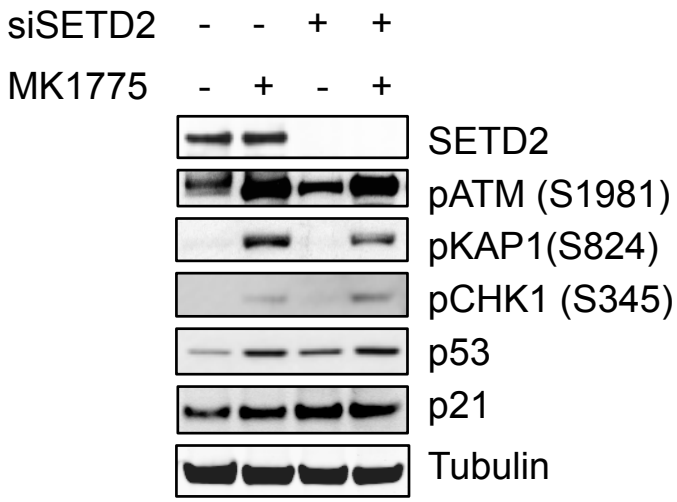


Figure 6.2: SETD2 depletion does not impede DNA damage response after WEE1 inhibition. Western blotting analysis of protein levels in U2OS cells transfected with non-targeting or SETD2 siRNA 48 hours prior to treatment with DMSO or MK1775 (200nM) for 24 hours.

conversion by a reporter assay in fission yeast. Similarly, Jha and Strahl observed that plasmid re-ligation efficiency was significantly increased by set2 deletion in budding yeast, which was almost entirely dependent on Rad51. In addition, loss of Set2 leads to increased resection, as measured by RPA recruitment in G1. These observations together suggest that loss of Set2 increases HR, and by deduction, it is required for NHEJ. A piece of direct evidence for Set2 in NHEJ came from (Pai et al., 2014), where Set2 deletion reduced Ku recruitment and/or retention at a DSB.

How can one explain the differences: why does the depletion of yeast Set2 impair NHEJ, while the depletion of human SETD2 impairs HR?

In search for the explanation, one needs to first look at the fundamental differences between human SETD2 and yeast Set2. Yeast Set2 is required for setting

all three forms of methyl-H3K36, thus Set2 deletion abolishes of all three states of H3K36 methylation: H3K36me, H3K36me2 and H3K36me3. However, human SETD2 is a trimethyltransferase, which only affects the levels of H3K36me3.

Therefore, to understand the functional differences between yeast and human H3K36 methylation, one needs to directly compare the same methylation state. This can be achieved by either (1) reducing only the H3K36me3 modification in yeast, leaving H3K36me and H3K36me2 unaffected, then comparing with human SETD2; or (2) reducing all three forms of H3K36 methylation (H3K36me, me2 and me3) in human cells then compare with yeast Set2.

While it is unclear how to specifically modify H3K36me3 in yeast, a publication on human SETMAR (a methyltransferase that catalyses H3K36me and H3K36me2) may provide a clue (Fnu et al., 2011). They showed that H3K36me2 catalysed by SETMAR (Metnase) promoted DSB repair through NHEJ. Importantly, in Figure 4, they over-expressed two mutant histone H3 (H3R36 or H3A36) which could not be methylated (neither mono- or di- nor tri-methylated). When all three forms of H3K36 methylation was reduced, they saw a reduction in the recruitment of both KU70 and NBS1 to the DSB site. KU70 is a bona fide NHEJ factor, while NBS1 complex facilities DSB repair predominantly by HR in vertebrates. Thus simultaneous reduction of all three forms of H3K36 methylation reduces both NHEJ and HR (which make sense).

So, a reason why deletion of yeast Set2 impairs NHEJ while depletion of human SETD2 impairs HR is because yeast Set2 is required for setting all three

forms of methyl-H3K36, and therefore the changes in histone modification are more equivalent to H3A36 (instead of SETD2). Therefore the expected phenotype for Set2 deletion is reduced NHEJ (and reduced HR). However, while Set2 deletion reduced NHEJ, it did not seem to reduce HR, probably because LEDGF was not evolutionarily conserved, thus the resection machineries can still be recruited in the absence of H3K36me3.

6.2 Potential interplay between SETD2's role in HR and DNA replication

Chapter 3 described a role for SETD2 in homologous recombination (HR) repair of DNA double-stranded breaks (DSBs) and Chapter 4 described a role for SETD2 in deoxynucleotide (dNTP) synthesis. Therefore three questions will be discussed in this section:

Subsection 6.2.1: do the two functions of SETD2 (HR and dNTP synthesis) originate from the same molecular mechanism?

Subsection 6.2.2: can SETD2's role in HR contribute to its synthetic lethal interaction with the WEE1 inhibitor?

Subsection 6.2.3: can SETD2's role in dNTP synthesis contribute to HR?

6.2.1 Do the two functions originate from the same molecular mechanism?

Chapter 3 showed that SETD2 (and H3K36me3) contributed to HR by facilitating DSB end resection. The mechanism is supported directly by multiple pieces of experimental evidence: (1) co-immunoprecipitation (co-IP) experiments showed that H3K36me3 directly interacts with LEDGF; (2) chromatin immunoprecipitation (ChIP) experiments showed that SETD2 knockdown reduced chromatin retention of LEDGF; (3) micro-irradiation experiments showed that SETD2 knockdown reduced recruitment of CtIP (resection factor) to the DSB site; (4) an *in vivo* resection assay showed that SETD2 knockdown reduced the amount of single-stranded DNA (resection product) in the proximity to the DSB site.

Chapter 4 showed that SETD2 (and H3K36me3) contributed to dNTP synthesis by promoting the transcription of the ribonucleotide-reductase subunit RRM2. The mechanism is also supported by direct experiment evidence: (1) quantitative reverse transcription polymerase chain reaction (qRT-PCR) and Western blotting showed that SETD2 knockdown reduced the levels of RRM2 mRNA and protein; (2) dNTP measurements showed that SETD2 knockdown reduced the dNTP pool size; (3) ChIP experiments showed that SETD2 knockdown reduced the recruitment of transcription initiation factors (TAFs) and RNA polymerase II to the promoter of the *E2F1* gene; (4) Cell viability measurements showed that the toxicity from SETD2 knockdown could be completely suppressed by expressing

exogenous RRM2.

BrdU experiments also showed that SETD2 knockdown did not significantly alter the cell cycle. Therefore the molecular changes described above are unlikely to be due to cell cycle alterations.

Recruitment of CtIP for DSB resection and activation of RRM2 gene transcription seems to be based on different molecular pathways. However, this does not exclude the possibility of crosstalk between the two pathways: the degree of resection may be regulated by cellular dNTP levels, and vice versa, RRM2 gene expression may be regulated by DSB resection. For example, earlier studies have shown that the reduction in dNTP levels by HU or thymidine stimulates HR (Lundin et al., 2003), and HR-deficient cells are hypersensitive to the treatment with HU or thymidine, suggesting that HR is required to repair collapsed forks generated by dNTP shortage (Petermann et al., 2010).

6.2.2 Can the role of SETD2 in HR contribute to the synthetic lethality?

One 'tricky' question that needs to be addressed is whether SETD2's role in HR (DNA repair) contributes to its synthetic lethal interaction with the WEE1, CHK1 and ATR inhibitors. And if so, how much does HR-deficiency contribute to the synthetic lethality compared to dNTP pool depletion.

Perhaps the simplest argument is: we cannot exclude the possibility that

the HR role of SETD2 is required for restart of stalled or collapsed replication forks generated by the combination of SETD2-depletion and MK1775 treatment. However, the HR role is likely to be secondary compared to the role in dNTP synthesis, since dNTP depletion triggers fork stalling/collapsing. In other words, upon WEE1 inhibition, SETD2's function in RRM2 regulation is upstream of SETD2's function in HR.

The best supporting evidence for the argument above comes from the viability data collected from BRCA2-deficient and -proficient isogenic cell lines challenged with the WEE1 or ATR inhibitors. BRCA2-deficient (HR-deficient) cells are not more sensitive to WEE1 or ATR inhibitors than BRAC2-proficient cells, despite their acute sensitivity to the PARP inhibitor (Fig 6.3).

However, for the sake of completion, here I also discuss the evidence supporting the idea that HR-deficiency contributes to the sensitivity towards the WEE1, CHK1 or ATR inhibitors.

Cell viability measurements showed that RAD51 and BLM siRNA knockdown sensitises U2OS cells to WEE1 and CHK1 inhibitors (Fig 6.4). This finding is partially in agreement with a recent presentation in the NCRI (National Cancer Research Institute) conference (2013), which showed that in an siRNA screen, knockdown of genes in the HR or the Fanconi anaemia (FA) pathway sensitises cells to the WEE1 inhibitor MK1775. However the difference between my experiments and the other group's is that they used p53-defective cells, which are already hypersensitive to the WEE1 inhibitors.

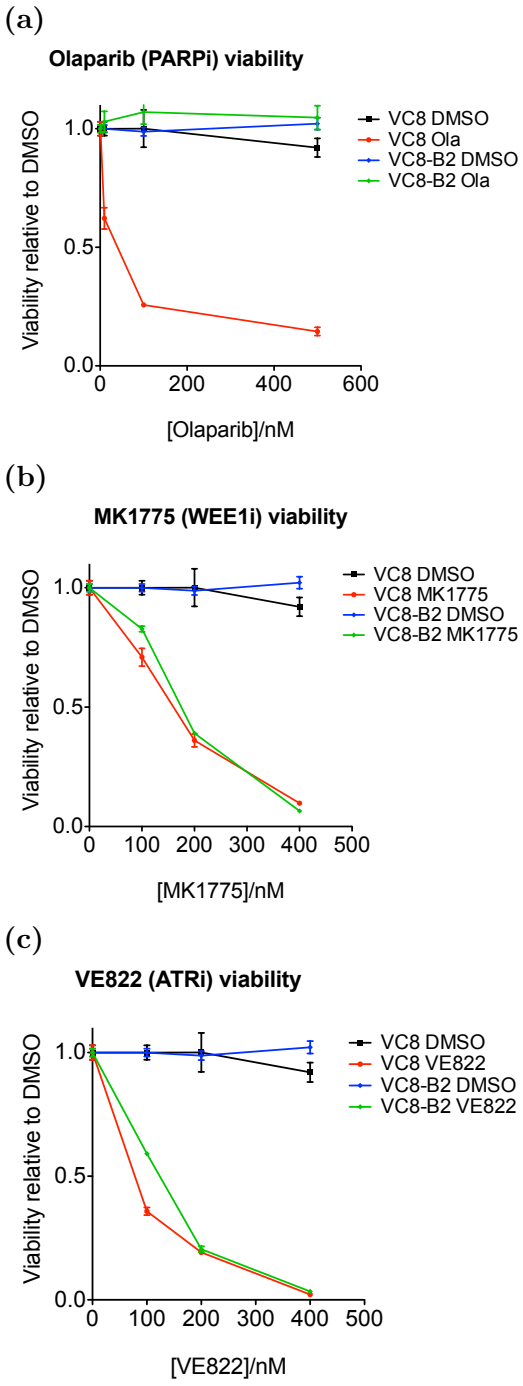
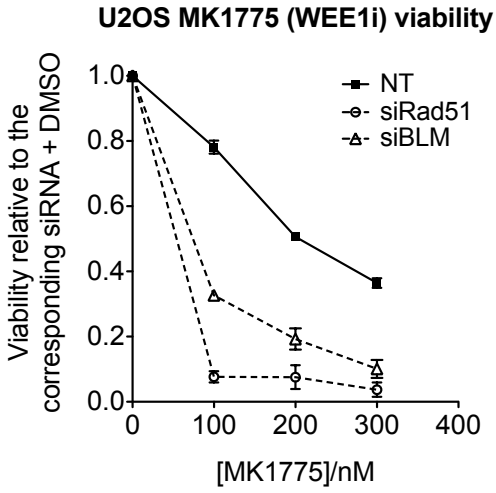


Figure 6.3: BRAC2-deficient cells are not more sensitive to the WEE1 or ATR inhibitors than BRCA2-proficient cells. Viability of VC8 (BRCA2-deficient) and VC8-B2 (BRCA2-proficient) isogenic cell lines were measured by Resazurin five days after a single treatment with (a) PARP inhibitor Olaparib, (b) WEE1 inhibitor MK1775 and (c) ATR inhibitor VE822 at the indicated concentrations. Data are presented as mean ± SEM, n = 3 replicates.

(a)



(b)

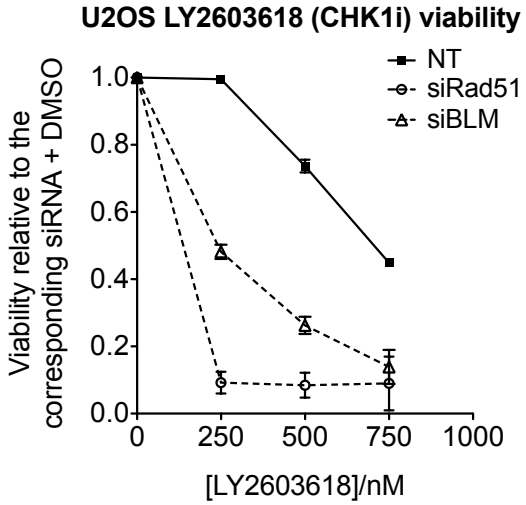


Figure 6.4: RAD51 or BLM depletion sensitises cells to MK1775 and LY2603618. U2OS cells were transfected with non-targeting siRNAs (NT) or RAD51 siRNAs (siRAD51) or BLM siRNAs (siBLM). 48 hours after transfection, cells were treated with DMSO or MK1775 (the WEE1 inhibitor) or LY2603618 (the CHK1 inhibitor) for five days and cell viability was measured by Resazurin. For each knockdown condition, viability was normalised to the viability of cells transfected with the same siRNA but treated with DMSO instead of the inhibitors (thus siRNA toxicity was accounted for). Data are presented as mean ± SEM, n = 2 replicates.

In addition, strictly speaking, RAD51 and BLM are not the ideal candidates to test for the contribution from the HR pathway, since they both exhibit other functions in response to replication stress, which may be independent from their function in HR. RAD51 plays a dual role in replication stress: it is responsible for both restarting stalled replication forks (by fork reversal) as well as repairing collapsed forks (by HR) (Petermann et al., 2010). BLM facilitates fork restart by its helicase activity, but it also inhibits new origin firing in response to replication stress as well as suppressing the aberrant formation of recombination intermediates (Petermann and Helleday, 2010).

Therefore, based on the data presented here and the existing literature, one cannot say that SETD2's function in HR alone is enough to cause its synthetic lethal interaction with the WEE1 inhibitors.

6.2.3 Can the role of SETD2 in dNTP production contribute to its function in HR?

Chapter 4 showed that SETD2 knockdown reduces the transcription of RRM2, leading to a reduction in the dNTP pool size. Since the homology-directed synthesis step of HR requires dNTP, it is worth considering whether SETD2's role in RRM2 contributes to HR.

If dNTP synthesis contributes to HR, how much does it contribute? To answer this, one needs to know how much decrease in dNTP would abolish HR. While it

is difficult to control the exact amount of dNTPs in living cells, a cellular-extract system enabled a more precise measurement: Lehman and Carroll suggested that dNTP is required for the completion of recombination (homology-directed synthesis), but not for the resection step. When individual dNTP levels fell from 0.5mM to 0.1mM, homologous recombination became inefficient, and a side reaction produced end-joined products (Lehman and Carroll, 1991).

How do the findings in the cell-free system translate to the cellular system? Other literature estimated that in cycling human cells, the average concentration of dNTP is around 0.5mM (Jamburuthugoda et al., 2008). We and others (D'Angiolella et al., 2012) have shown that RRM2 depletion leads to 3-fold changes in global dATP and dGTP levels. Therefore, changes in RRM2 do have the potential to affect HR through dNTP levels. In addition, given that RRM2 is recruited to the nucleus to supply dNTP locally at DNA damage sites, RRM2 depletion may lead to an even greater reduction of dNTP at the damage site.

We have demonstrated that SETD2 also directly affects the resection step of HR (Pfister et al., 2014), a step that does not require dNTP and occurs prior to the homology-directed synthesis step. Therefore SETD2 may contribute to HR in two ways: pre-synpatic (resection) and post-synpatic (homology-directed synthesis). To test how much SETD2's role in dNTP contributes to HR, one can compare the HR efficiency between siSETD2 and siSETD2+exogenous deoxyribonucleosides. If SETD2 affects dNTP in the HR process, siSETD2+deoxyribonucleosides should rescue the reduction in HR.

6.3 Additional ways to make use of this synthetic lethal interaction

From a clinical perspective, the synthetic lethal interaction described in Chapters 4 and 5 has suggested a potential monotherapy that involves treating H3K36me3-deficient cancers with either WEE1 inhibitors, CHK1 inhibitors or ATR inhibitors.

Cell viability measurements suggested that the potential monotherapy provides a 5 to 10-fold sensitisation effect towards SETD2-deficient cancer cells. It is therefore desirable to increase the 'therapeutic window' by enhancing the inhibitor efficacy (preferably without increasing normal tissue toxicity).

Therefore this section will provide some experimental evidence showing that the efficacy can potentially be increased by the following reagents:

Subsection 6.3.1: DNA damaging agents;

Subsection 6.3.2: DNA damage response (DDR) inhibitors;

Subsection 6.3.3: DNA replication inhibitors;

Subsection 6.3.4: In addition to patients with H3K36me3-deficient cancers, is there any other patient population that could benefit from this synthetic lethal interaction?

6.3.1 Enhancing the efficacy by increasing DNA damage

The rationale for combining the kinase inhibitors with DNA damaging agents in this case is as follows: (1) the kinase inhibitors induced DNA damage in SETD2-deficient cells, which leads to cell death. If the levels of DNA damage is further increased, would it push more SETD2-deficient cells into apoptosis?

Ionising radiation (IR) was chosen as the source of DNA damage because it can be better directed to the tumour compared to other chemotherapeutic agents. Cell viability measurement showed that low doses of IR enhanced the efficacy of low doses of the WEE1 inhibitor MK1775 more significantly in SETD2-deficient cells than in SETD2-proficient cells. For SETD2-deficient A498 cells, the viability after MK1775 (100nM) was 73%; after MK1775 (100nM) plus IR (2Gy) was 40% (45% reduction from MK1775 only). However, for SETD2-proficient RCC4 cells, cell viability after MK1775 (100nM) was 82%; after MK1775 (100nM) and IR (2Gy) was 68% (17% reduction from MK1775 only) (Fig 6.5a). The viability after MK1775 treatment was higher than that presented in Chapter 4 because the inhibitor was washed off after 24 hours in this experiment (instead of wash off after 72 hours in Chapter 4).

Next, the radio-sensitisation effect by MK1775 was estimated from the viability data. For A498 cells, cell killing by 2Gy plus 100nM MK1775 is as effective as 8Gy alone, suggesting a 4-fold radio-sensitisation effect by MK1775 (Fig 6.5a, red line). However, for RCC4 cells, cell killing by 2Gy plus 100nM MK1775 is

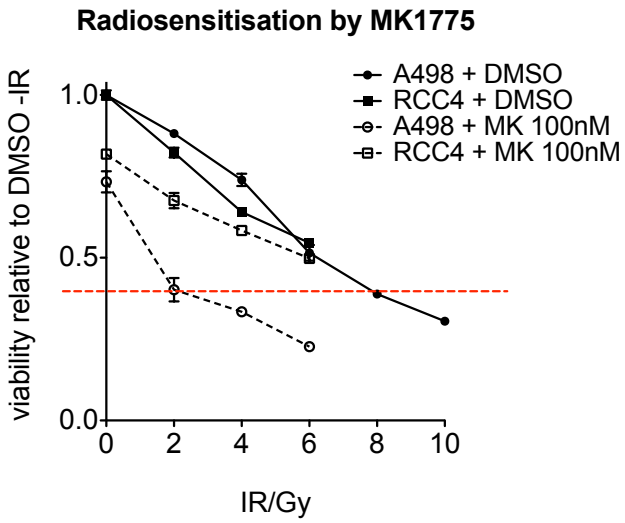
less effective than 4Gy alone, suggesting a less dramatic radio-sensitisation effect in SETD2-proficient cells.

Likewise, low doses of IR significantly enhanced the efficacy of low doses of the CHK1 inhibitor LY2603618 in SETD2-deficient cells. For SETD2-deficient A498 cells, cell viability after LY2603618 (250nM) was 57%; after LY2603618 (250nM) plus IR (2Gy) was 25% (56% reduction). However, for SETD2-proficient RCC4 cells, cell viability after LY2603618 (250nM) was 100%; after LY2603618 (250nM) and IR (2Gy) was 84% (16% reduction) (Fig 6.5b).

The radio-sensitisation effect by CHK1 inhibitor on SETD2-deficient A498 is higher than 5-fold (2Gy plus 250nM LY2603618 is more effective than 10Gy alone), while there is very little radio-sensitisation effect on SETD2-proficient RCC4 (Fig 6.5b).

Previous publications suggested that WEE1 inhibitor MK1775 sensitises p53-deficient cells to IR (Bridges et al., 2011; Sarcar et al., 2011; Caretti et al., 2013), but it was a little surprising that it also sensitises SETD2-deficient cells to IR. In attempt to understand why, DSBs were measured by γH2AX foci. γH2AX foci showed that similar levels of damage was induced regardless of SETD2 status or MK1775 treatment (IR 2h). However, the levels of DSBs are higher after MK1775 treatment, and even higher after combining SETD2 knockdown and MK1775 (IR 16 – 48 hours) (Fig 6.6). Given that forced activation of CDK1 via WEE1 inhibition impairs homologous recombination (Krajewska et al., 2013), it is possible that SETD2's role in DNA repair may also be required to repair the

(a)



(b)

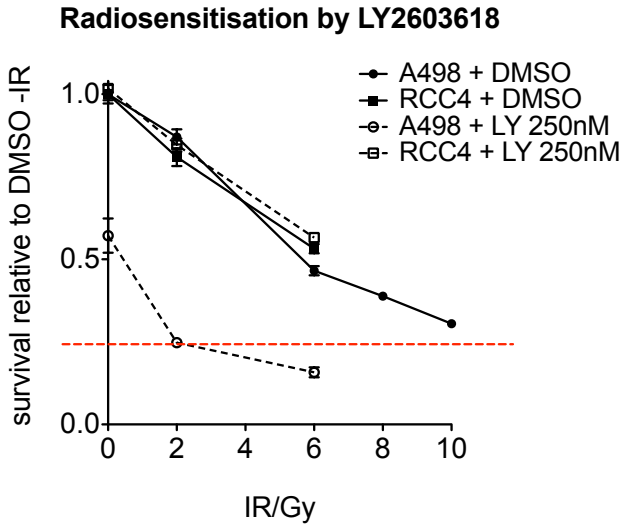


Figure 6.5: WEE1 and CHK1 inhibitors sensitise SETD2-deficient cells to radiation. SETD2-wildtype RCC4 cells and SETD2-deficient A498 cells are treated with either DMSO or WEE1 inhibitor MK1775 (100nM) or CHK1 inhibitor LY2603618 (250nM). Cells are then left unirradiated or irradiated with increasing dose of IR. Cell viability was measured five days after the treatment. Data are presented as mean ± SEM, n = 3 independent experiments.

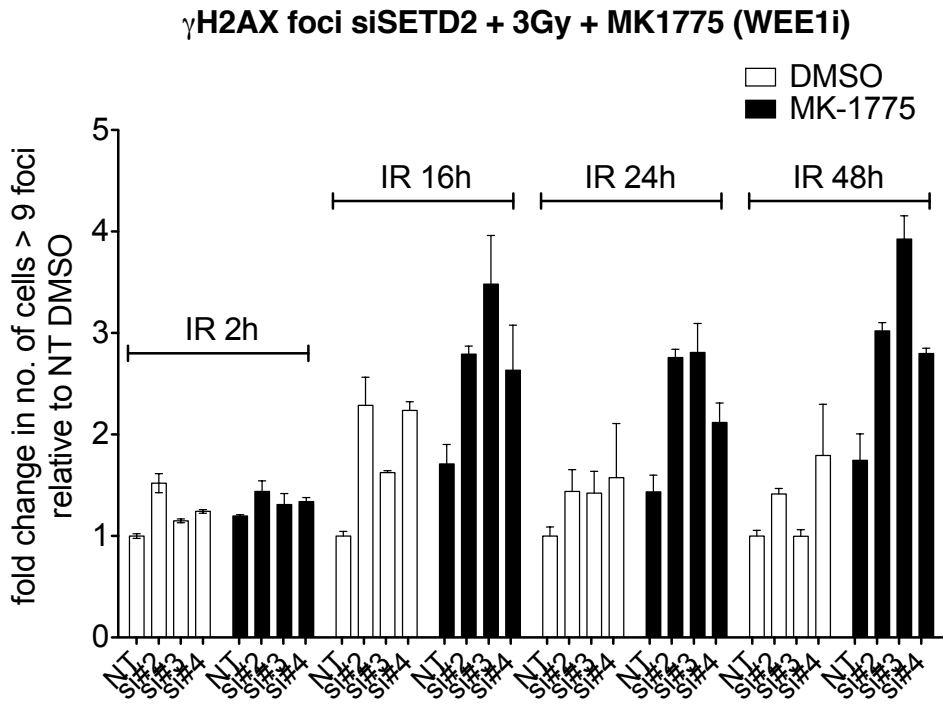


Figure 6.6: MK1775 enhances DNA damage in SETD2-deficient cells after radiation. U2OS cells were transfected with SETD2 siRNAs (si#2, si#3 and si#4). 48 hours after transfection, cells were treated with DMSO or MK1775 (200nM) with or without IR (3Gy). Cells were fixed with 4% PFA at indicated times and stained with anti-γH2AX antibody. γH2AX foci were analysed by Incell. Data are presented as mean ± SEM, n = 3 replicates.

DSBs after IR, especially after MK1775-induced HR inhibition.

In conclusion, this observation could potentially make the current synthetic lethal interaction more attractive to clinical trials for three reasons: (1) The combinational therapy can improve the efficacy of the monotherapy (either chemo- or radiotherapy alone). (2) The combination requires a lower dose of the kinase inhibitors, and thus may reduce the toxicity of the monotherapy. (3) It may be more likely to be implemented when the control group are receiving IR

or the inhibitors instead of a placebo. Thus it is more likely to reach patients that are still in their early stage of treatment, not just patients that have shown refraction/resistance to several therapies.

In addition to IR, current literature has suggested that WEE1, CHK1 or ATR inhibitors can sensitive cancer cells to various DNA damaging agents (mainly reported as through inhibiting G2 arrest). A few are listed here as examples: (1) the WEE1 inhibitor MK1775 potentiated the cytotoxic effects of pemetrexed, doxorubicin, camptothecin, and mitomycin C (in p53-negative cells) (Hirai et al., 2010); (2) the CHK1 inhibitor Gö6976 enhanced cell death in response Cisplatin (Thompson et al., 2012); and (3) the ATR inhibitor VE821 sensitised cells to cisplatin, topotecan, gemcitabine, and the PARP inhibitor veliparib (Huntoon et al., 2013).

6.3.2 Enhancing the efficacy by inhibiting the DDR response

Chapter 4 showed that in SETD2-deficient cells, the WEE1 inhibitor MK1775 induced massive DNA damage (both single-stranded and double-stranded), which activated the DNA damage response through ATM and ATR. Therefore inhibiting ATM on top of MK1775 is expected to inhibit DNA repair, thus enhancing the levels of DNA damage and cell death.

In the absence of DNA damage, the ATM inhibitor exhibits very little cyto-

toxicity. Since WEE1 inhibition did not induce much DNA damage in SETD2-proficient cells, it was hypothesised that combining the WEE1 inhibitor and the ATM inhibitor would specifically enhance toxicity towards SETD2-deficient cancer cells, leaving normal tissue unharmed. To test this, cell viability was measured in U2OS and A498 cells.

It was found that combining the ATM inhibitor with a low dose of WEE1 inhibitor (MK1775, 100nM) reduced A498 viability by 69% from MK1775 alone. However, the same combination only reduced U2OS viability by 25% from MK1775 alone (Fig 6.7).

This sensitisation effect by the ATM inhibitor is expected to hold for ATR and CHK1 inhibitors based on current literature. ATR inhibitors were reported to sensitise cells deficient in ATM or p53 after treatment with DNA-damaging agents (Reaper et al., 2011). The CHK1 inhibitor was shown to exhibit a synergistic effect with the ATM inhibitor specifically in cells deficient in FANCF (a DNA repair protein) (Chen et al., 2009).

6.3.3 Enhancing the efficacy by increasing replication stress

Apart from DNA damage, replication stress is another key factor that kills SETD2-deficient cells upon treatment with the WEE1, CHK1 or ATR inhibitors (Chapter 4 and 5). Since increasing DNA damage increased the efficacy of the inhibitors, DNA replication inhibitors were also expected to increase the efficacy.

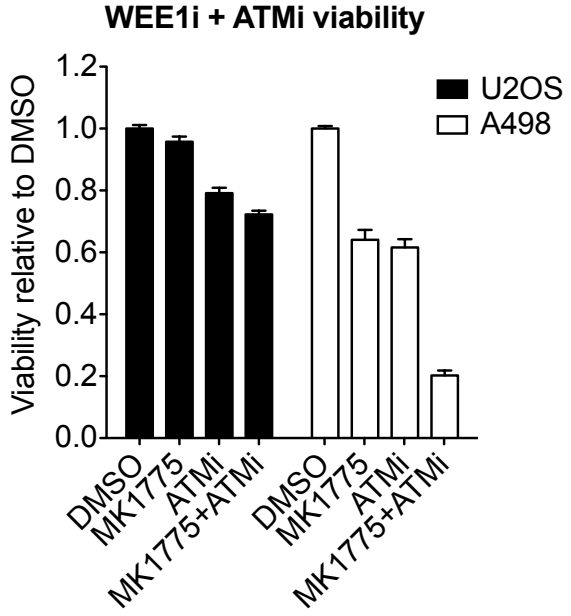


Figure 6.7: Viability of U2OS or A498 cells five days after treatment with DMSO, the ATM inhibitor KU55933 (10μM), the WEE1 inhibitor MK1775 (100nM) or a combination of KU55933 (10μM) and MK1775 (100nM).

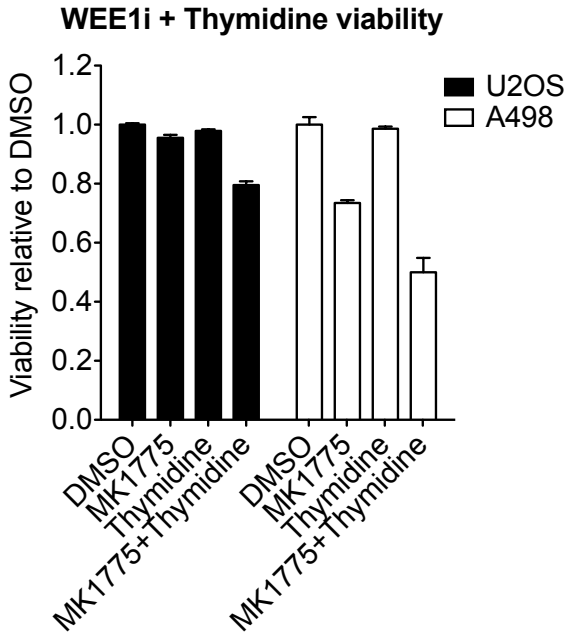


Figure 6.8: Viability of U2OS or A498 cells five days after treatment with DMSO, Thymidine (25μM), the WEE1 inhibitor MK1775 (100nM) or a combination of Thymidine (25μM) and MK1775 (100nM).

Thymidine was known to slow the progression of replication forks by depleting cellular pools of dCTP, and a high concentration of thymidine (4mM) triggers DNA damage response dependent on both ATM and ATR (Bolderson et al., 2004). Here, a non-toxic concentration of thymidine (25μM) was used in combination with the WEE1 inhibitor MK1775 (Fig 6.8) and cell viability was measured.

While a low dose of thymidine alone was not toxic to either U2OS or A498 cells, the combination of thymidine and the WEE1 inhibitor MK1775 reduced U2OS viability by 16%, and A498 viability by 32%.

The sensitisation effect of replication inhibitors was also documented in the

current literature. Here are a few examples: (1) CHK1 depletion increased cell death after treatment with replication inhibitors such as excess thymidine, hydroxyurea, and camptothecin (Rodriguez and Meuth, 2006); and (2) WEE1 inhibitors sensitised p53-deficient cells to 5-FU (a thymidylate synthase inhibitor) (Hirai et al., 2010).

6.3.4 Treating ATR, CHK1 or WEE1-deficient cancers with SETD2 inhibitors

The siRNA studies showed that not only the inhibitors, but also the depletion of WEE1/CHK1/ATR, can kill SETD2-deficient cells. Therefore, one could hypothesise that perhaps the synthetic lethality interaction could be reversed: i.e., could cancer cells that are deficient in WEE1, CHK1 or ATR be selectively killed by a SETD2 inhibitor?

Recent crystal structure analysis of the SET domain of SETD2 has enabled the development of SETD2 inhibitors. A group has demonstrated that N-propyl sinefungin (Pr-SNF) selectively interacted and inhibited the catalytically active form of SETD2 (Zheng et al., 2012).

The existence of a SETD2 inhibitor provides the opportunity to treat cancers deficient in ATR, CHK1 or WEE1 – if such cancers exist. Unlike ATM and CHK2, which are frequently mutated in cancers, the loss-of-function mutations in ATR, CHK1 or WEE1 are hardly found naturally, reflecting their essential

cellular functions. However, according to the Sanger COSMIC project, down-regulation of these genes does exist in several types of cancers, as summarised in Table 6.1.

Further analysis of Table 6.1 reveals that for each cancer type, over-expression of these genes is more common than under-expression. The only exception is ovarian cancer, where *WEE1* under-expression is much more frequent than over-expression. Also, the under-expression of *CHK1* and *ATR* is more frequent in this cancer type than in others. Therefore, if the SETD2 inhibitor ever becomes an intervention for cancer treatment, ovarian cancer may be an initial candidate target.

6.4 Future directions

In addition to the ideas mentioned previously in this chapter, this section will consider some interesting questions that could be addressed in the future. Some of them could be clinically relevant while others aim to explore the fast-growing field of chromatin biology.

6.4.1 How does H3K36me3 control transcriptional activation?

Chapter 4 showed that SETD2 regulates the transcription of E2F1 and RRM2 (supported by the qRT-PCR data and Western blotting analysis). In addition,

(a)

Tissue	WEE1 over expression	WEE1 under expression
Large intestine	8.85	1.3
Breast	5.93	0.66
Lung	5.67	0
Kidney	5.13	0
Central nervous system	4.1	0.51
Haematopoietic and lymphoid	4.05	0
Ovary	1.09	13.32

(b)

Tissue	CHK1 over expression	CHK1 under expression
Lung	10.76	0
Breast	5.93	0
Kidney	5.83	0
Large intestine	4.69	1.3
Haematopoietic and lymphoid	4.62	0.58
Endometrium	3.52	0
Ovary	0.54	1.09

(c)

Tissue	ATR over expression	ATR under expression
Ovary	19.02	3.26
Lung	17.44	3.34
Endometrium	9.62	0.7
Breast	7.91	1.98
Central nervous system	5.13	0.51
Kidney	3.73	0.47
Haematopoietic and lymphoid	1.16	1.73

Table 6.1: Frequency of over and under expression of *WEE1*, *CHK1* and *ATR* genes in various cancer types. Data obtained from the COSMIC project by Sanger Institute. (a) http://cancer.sanger.ac.uk/cosmic/gene/analysis?ln=WEE1#dist (b) http://cancer.sanger.ac.uk/cosmic/gene/analysis?ln=CHEK1#dist (c) http://cancer.sanger.ac.uk/cosmic/gene/analysis?ln=ATR#dist

SETD2-dependent H3K36me3 regulates transcription initiation by its presence at the promoter and by recruiting transcription initiation factors and RNA polymerase II (supported by the ChIP-qPCR data). This is in agreement with the genome-wide ChIP-mass spectrometry data, which showed that a large number of TAFs bind to H3K36me3 (Vermeulen et al., 2010).

This finding is nevertheless a little surprising because H3K36me3 is previously known to be present at the gene bodies of the transcribed genes (especially towards the 3' end), in order to recruit histone deacetylases to condense the transcribed chromatin. However, for certain gene promoters, H3K36me3 does co-localise with H3K4me3 (a marker of the active promoter) and H3K27ace (a marker of active transcription), according to the UCSC database (website URL: genome.ucsc.edu). Moreover, a very recent paper on murine Setd2 showed that H3K36me3 is present at the promoter of the Fgfr3 gene and regulates Fgfr3 transcription initiation (Zhang et al., 2014).

If SETD2 regulates gene transcription, how many genes are affected? From Chapter 3 we know that SETD2 depletion does not affect the expression of the major DNA repair genes (RAD51, BRCA2, RAD50, CtIP, MRE11, RPA32 and KU80). From Chapter 4 we know that SETD2 depletion does not affect the expression of RRM1, CyclinF, 53R2 and most of E2F family members (E2F3, E2F4, E2F6, E2F7).

Therefore, what should we expect to see if a RNA-seq or a microarray was performed in H3K36me3-proficient v.s. H3K36me3-deficient isogenic cell lines?

Given that H3K36me3 levels peak at G1 and early S-phase, and disappear in G2, could SETD2 depletion affect the genes normally transcribed in G1 and S? A brief *in-silico* search in the UCSC database did not reveal any correlation between the H3K36me3 co-localisation with H3K27ace and the genes it regulates. For example, H3K36me3 is present at the promoters of both RRM1 (not regulated by H3K36me3) and RRM2 (regulated by H3K36me3) genes. Therefore the transcription regulation by H3K36me3 does not seem to be entirely dependent on the presence of H3K36me3 at the promoter: there seems to be a second layer of control. Could it be H3K36me3-binding factors or the surrounding histone modifications that are regulated by the cell cycle?

6.4.2 Is RRM2 the entire story?

Chapters 4 and 5 suggested that the target of the synthetic lethality is RRM2: SETD2 depletion reduces *RRM2* transcription while CDK1 hyper-activity (due to WEE1, CHK1 or ATR inhibition) degrades RRM2 proteins. Therefore cells suffer from critically low levels of RRM2 and dNTP, and arrest infinitely in S-phase until MUS81 creates DNA double-stranded breaks and triggers cell death.

While the story is straightforward and strongly supported by experimental evidence, one may wish to explore the full complexity of this synthetic lethality. Some of the alternative functions and pathways will be discussed here, with the hope that this synthetic lethal interaction may keep us and the science community

entertained for a while, just as the PARP and BRCA story did.

One piece of evidence that indicates there may be additional mechanisms that contribute to this synthetic lethal interaction is the sensitivity towards the RNR inhibitor Hydroxyurea. Upon hydroxyurea treatment, the difference in IC50 values between A498 and U2OS is less than 2-fold (compared to 5-10 fold after treatment with the WEE1, CHK1 or ATR inhibitors) (Fig 6.9a). Similarly, inhibiting DNA synthesis by the DNA polymerase alpha inhibitor Aphidicolin (APH) did not selectively kill SETD2-deficient A498 cells (Fig 6.9b).

How can we explain the lack of selective killing by HU compared to the inhibitors of WEE1, CHK1 or ATR? One clue is that HU is unable to induce a large amount of DNA double-stranded breaks, and that it is does not cause more DNA damage in SETD2-deficient cells compared to SETD2-proficient cells. An alkaline comet assay (which measures both single-stranded and double-stranded DNA breaks) showed that HU induced a similar amount of DNA damage in the control and SETD2-knockdown cells (Fig 6.12a). A neutral comet assay (which measures mainly double-stranded DNA breaks) showed that in SETD2-deficient cells, HU induced much lower levels of DNA double-stranded breaks compared to the CHK1 and ATR inhibitors (Fig 6.12b). The data suggest that it may be possible that CDK1 activity has additional implications apart from depleting dNTP pools (and all those implications together are toxic to SETD2-deficient cells).

The other clue is the mild effect on dCTP, dTTP and dGTP levels by HU

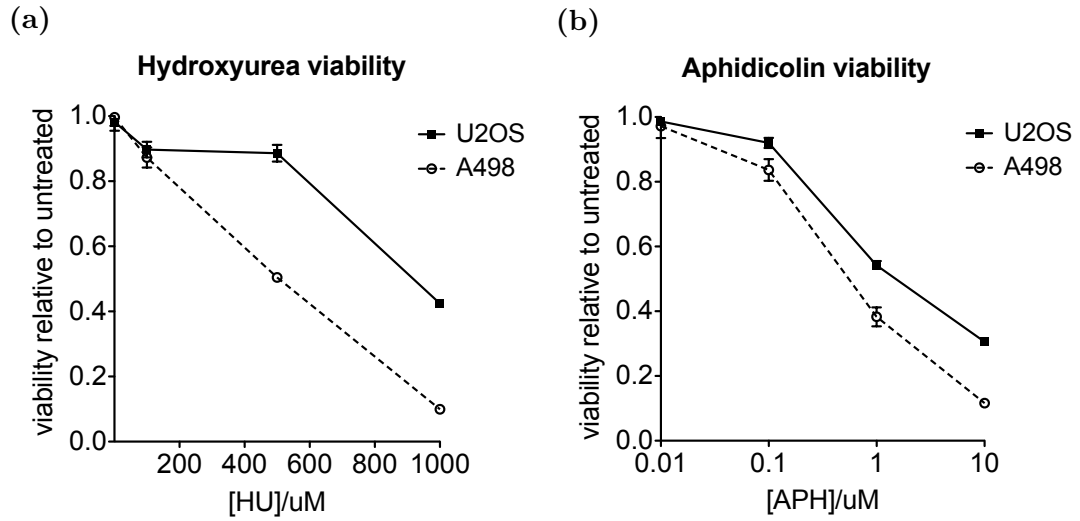


Figure 6.9: Hydroxyurea and Aphidicolin showed very little selectivity towards SETD2-deficient cells. SETD2-wildtype U2OS cells and SETD2-deficient A498 cells were treated with either Hydroxyurea (HU) or Aphidicolin (APH) at indicated concentrations. Cell viability was measured five days after the treatment. Data are presented as mean SEM, n = 3 replicates.

compared to the inhibitors. Measurements of dNTP pool size suggested that although dATP was significantly reduced by HU, the other three dNTPs were not. Previous publications also support this view: a group showed that although HU prevented the increase of the dNTP pool at G1/S, it did not exhaust any of the four dNTPs, probably because HU triggers a feedback mechanism that inhibits replication when dNTP falls below a critical threshold (Koç et al., 2004).

In addition to the clues obtained by comparing to HU, here two additional functions of WEE1 (CHK1 and ATR) are discussed.

(1) Origin firing

WEE1, CHK1 and ATR were known to suppress unscheduled origin firing (even in the absence of replication stress) (Sø rensen and Syljuå sen, 2012; Beck

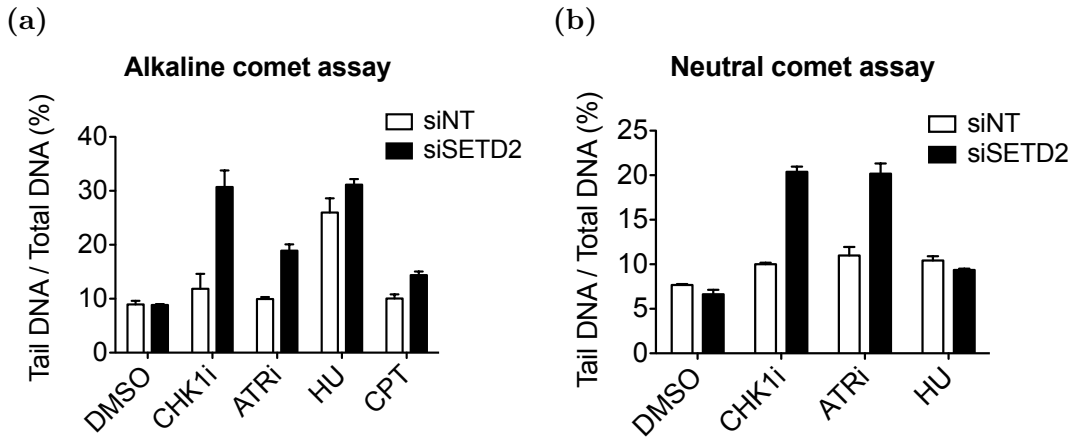


Figure 6.10: Hydroxyurea induces single-stranded DNA breaks but not double-stranded breaks. U2OS cells were transfected with either non-targeting siRNA or SETD2 siRNA 72 hours prior to treatment with either DMSO, the CHK1 inhibitor LY2603618 (500nM), the ATR inhibitor VE821 (2.5μM) or Hydroxyurea (2mM) for 48 hours. (a) Alkaline comet assay which measures both single-stranded and double-stranded DNA breaks. (b) Neutral comet assay which measures mainly double-stranded DNA breaks. Data are presented as mean SEM, n = 2 independent experiments.

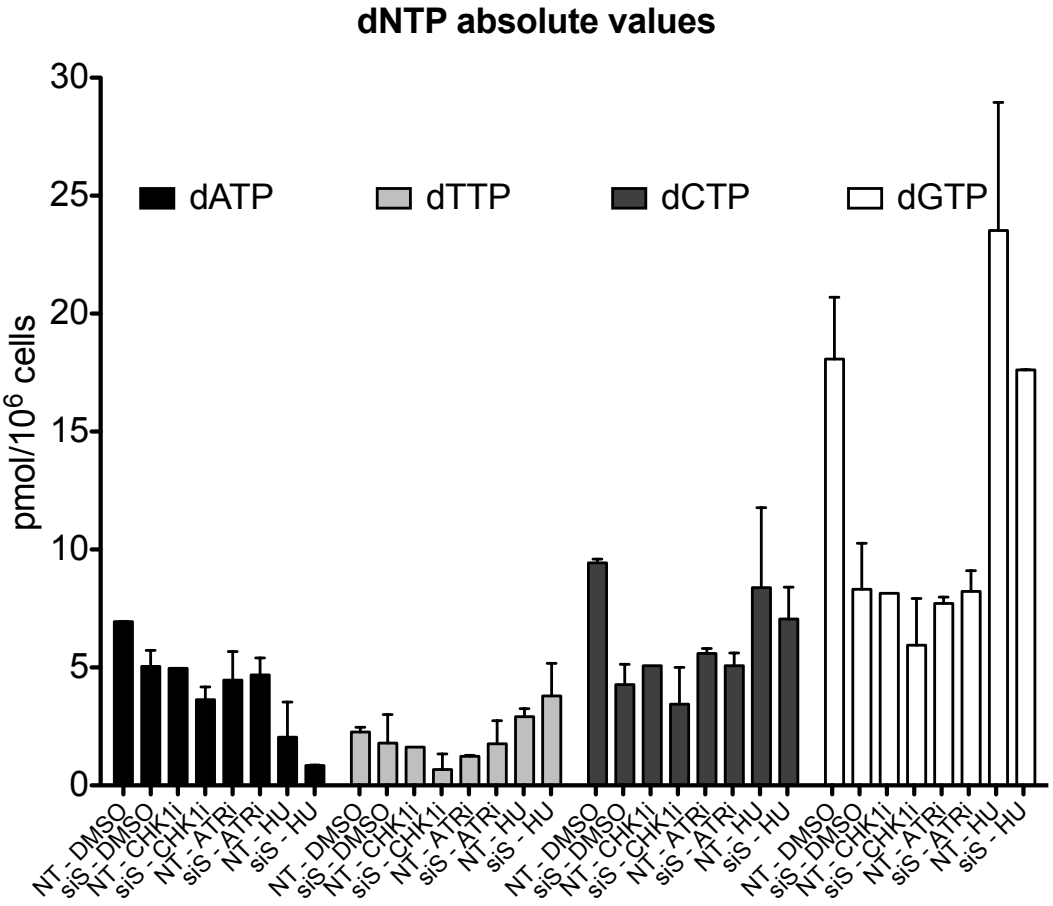


Figure 6.11: SETD2 and CHK1/ATR affect the production of dATP, dGTP and dCTP, while HU only affects the levels of dATP. U2OS cells were transfected with either non-targeting siRNA or SETD2 siRNA 72 hours prior to treatment with either DMSO, the CHK1 inhibitor LY2603618 (500nM), the ATR inhibitor VE821 (2.5μM) or Hydroxyurea (2mM) for 24 hours. Data are presented as mean SEM, n = 2 independent experiments. (While dATP should be the highest, for some reason the absolute value did not reflect that, probably due to measuring techniques. However, the relative fold-changes are consistent.)

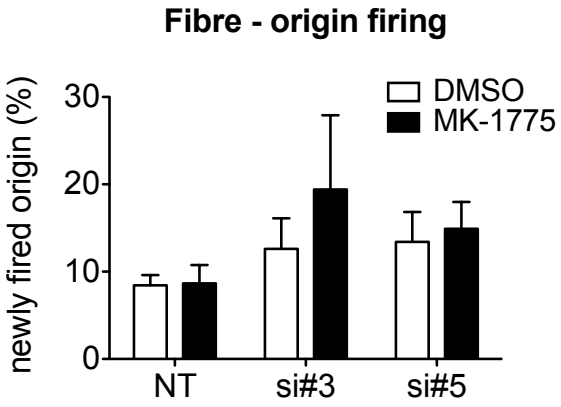


Figure 6.12: The WEE1 inhibitor increases origin firing in SETD2-deficient cells. U2OS cells were transfected with either non-targeting siRNA or SETD2 siRNAs (si#3 and si#5) 72 hours prior to treatment with either DMSO or the WEE1 inhibitor MK1775 (200nM) for 24 hours. Data are presented as mean SEM, n = 2 independent experiments.

et al., 2012). Excessive origin firing was shown to reduce the dNTP pool and cause DNA replication stress. In an attempt to assess the degree of excessive origin firing, the DNA fibre assay was used. DNA fibre analysis showed that MK1775 may have a tendency (although the p-value was not significant) to increase origin firing specifically in SETD2-deficient cells.

However, this analysis was done with the fact in mind that DNA fibre is not the best way to measure origin firing. A method involving DNA combing and measuring inter-origin distance may be better.

(2) G2/M checkpoint

Chapter 4 showed that unlike for p53-deficient cells, the mitotic population in SETD2-deficient cells did not increase after treatment with the WEE1 inhibitor MK1775. However, given the significant increase in DNA damage, and the fact

that WEE1 is a critical G2/M checkpoint kinase, raises the question whether they might carry un-repaired DNA damage in the small proportion of cells that did enter mitosis.

Micronuclei are DNA bodies outside the nucleus and are formed during anaphase from lagging acentric chromosome or chromatid fragments caused by mis-repair of DNA breaks or un-repaired DNA breaks (Fenech and Crott, 2002). Therefore if the increased DNA damage is carried into mitosis, micronuclei can form in the cell cycle that follows. Analysis of DAPI staining showed that MK1775 treatment dramatically increased the formation of micronuclei, even in SETD2-proficient cells. In SETD2-deficient cells, the incidence of micronuclei is a bit higher (Fig 6.13). The analysis also confirmed that the mitotic population was not increased by MK1775 (even slightly reduced). Therefore one might think that the role of MK1775 is not solely to push S-phase cells into mitosis, nor is it solely to generate DNA damage.

Another way to measure DNA damage carried over to the next cell cycle is the analysis of 53BP1 foci in G1. Consistent with micronuclei, immunofluorescence experiments showed that MK1775 increased the proportion of cells containing 53BP1 foci in G1-phase in SETD2-proficient cells, which becomes even higher in SETD2-deficient cells (Fig 6.14). 53BP1 foci is a marker for DNA double-stranded breaks (DSBs). Further analysis of the staining pattern revealed that CyclinA-positive cells (the S-G2 population) hardly stained for 53BP1 foci, suggesting that most DSBs exist in the G1 population (or perhaps most DSBs are

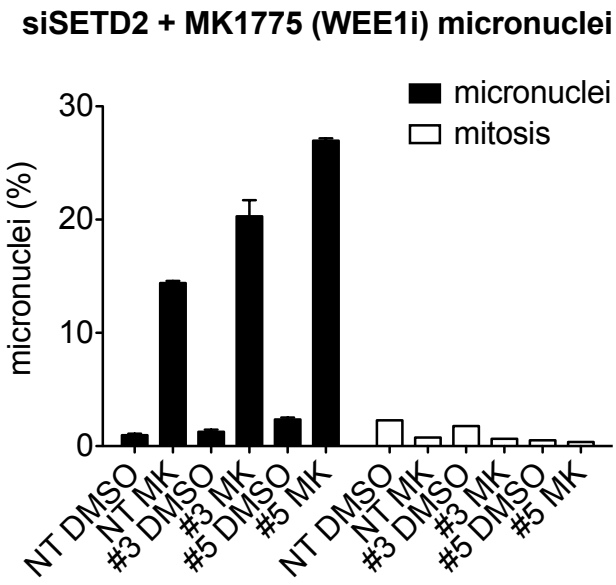


Figure 6.13: The WEE1 inhibitor MK1775 induces micronuclei more effectively in SETD2-depleted cells. U2OS cells were transfected with non-targeting siRNA (NT) or SETD2 siRNAs (si#3 and si#5) 48 hours prior to DMSO or MK1775 (200nM) treatment for 48 hours. Cells were fixed with 4% PFA, stained with DAPI and the percentage of cells exhibiting micronuclei or undergoing mitosis was analysed by Incell (GE healthcare). Data are presented as mean ± SEM, n = 3 replicates.

generated through mitosis?) (Fig 6.14).

Based on the preliminary data and current literature, one can attempt an answer to the question 'Is there anything beyond RRM2?'. It appears that (in addition to RRM2) the WEE1, CHK1 and ATR inhibitors may contribute to this synthetic lethal interaction through: (1) allowing critical depletion of dNTP by either (a) inhibiting the feedback mechanism that usually prevents dNTP depletion, or (b) increasing unscheduled origin firing even in the presence of replication stress; (2) evasion of the G2/M checkpoint, allowing cells containing un-repaired DNA damage (generated by replication stress) to enter mitosis, resulting in massive double-stranded breaks in the next cell cycle.

6.4.3 Other combinational therapies

Section 6.3 described several methods that can potentially enhance the efficacy of the WEE1 inhibitor MK1775 towards SETD2-deficient cells (e.g., increasing DNA damage, inhibiting ATM and increasing replication stress). Here some other combinations tested will be analysed.

PARP inhibitor

The PARP inhibitors were known to selectively kill HR-deficient cells. Given that SETD2 is involved HR, one would expect that SETD2-deficient cells are hypersensitive to the PARP inhibitor Olaparib. However, surprisingly SETD2-deficient cells are not hypersensitive to Olaparib (at least compared to the WEE1,

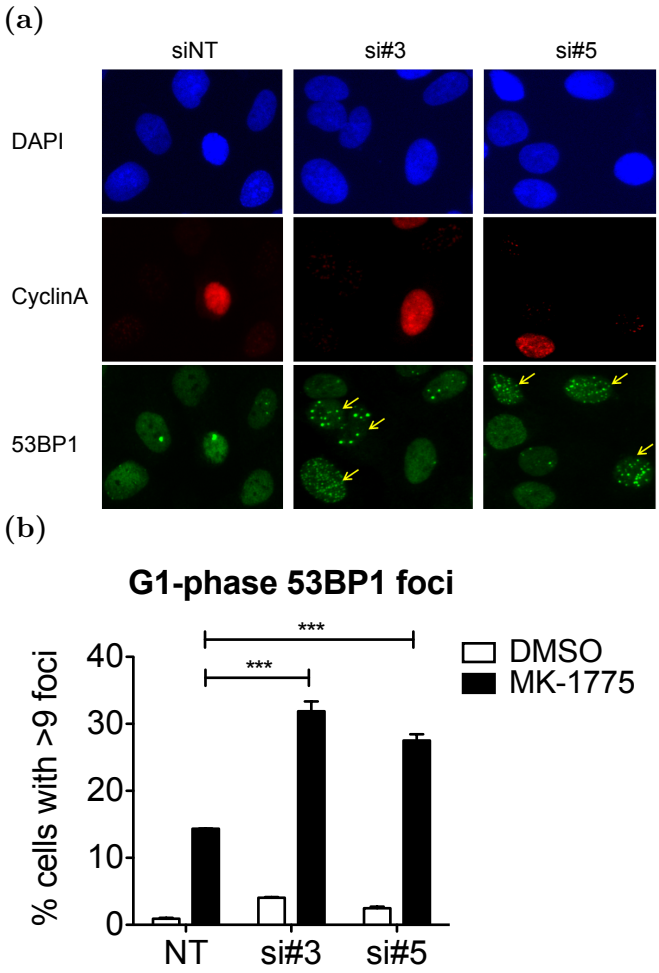


Figure 6.14: The WEE1 inhibitor MK1775 causes extensive DNA double-stranded breaks in the G1 population. (a) Immunofluorescence analysis of 53BP1 foci in the CyclinA negative (G1-phase) population in U2OS transfected with non-targeting or SETD2 siRNAs (si#3 and si#5) 48 hours prior to treatment with DMSO or MK1775 (200nM) for 48 hours. (b) Qualification of percentage of cells containing more than nine 53BP1 foci per nucleus. Data are presented as mean ± SEM, n = 3 independent experiments.

CHK1 or ATR inhibitors) (Fig 6.15a). Also, combining Olaparib with the WEE1 inhibitor MK1775 did not increase the efficacy of MK1775 either (Fig 6.15b).

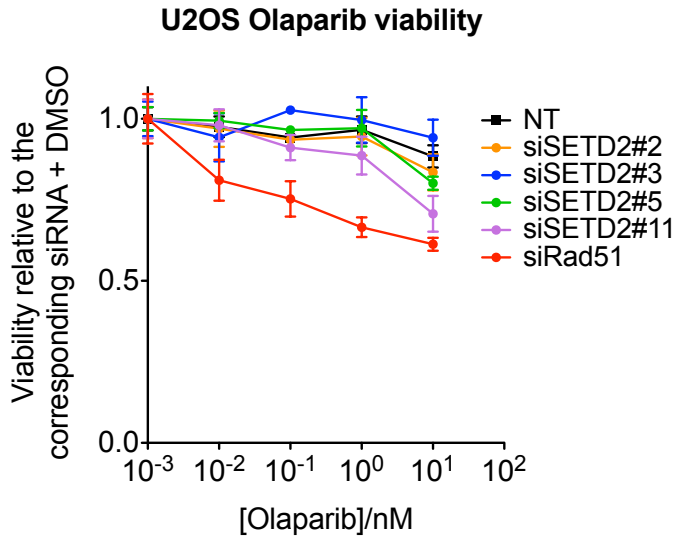
Why does not Olaparib sensitise SETD2-deficient cells to the WEE1 inhibitor? A classic view was that PARP functions in base excision repair of DNA single-stranded breaks caused by oxidative damage (and alkylating agents or ionising radiation); and that in the absence of PARP and HR factors, unprepared single-stranded breaks become double-stranded breaks during replication. One possibility could be that the type of DNA damage generated by replication stress (due to WEE1 inhibition) is different from those repaired by PARP. Thus PARP is dispensable in this synthetic lethal interaction.

CDC25 inhibitor

Interestingly, during the search for sensitisers, one inhibitor stood out as it specifically sensitises SETD2-proficient cells to the WEE1 inhibitor MK1775. Cell viability measurements showed that while the CDC25 inhibitor is not very toxic to either U2OS or A498 cells, it becomes much more toxic towards SETD2-proficient U2OS cells when combined with the WEE1 inhibitor MK1775. Surprisingly, for SETD2-deficient A498 cells, the combination was not more toxic than MK1775 alone (Fig 6.16).

If it holds true, this finding would have two implications: (1) the efficacy of the WEE1 inhibitor can be enhanced by the CDC25 inhibitor (provided that the cancer is not deficient in H3K36me3); (2) it suggests that CDC25 and SETD2

(a)



(b)

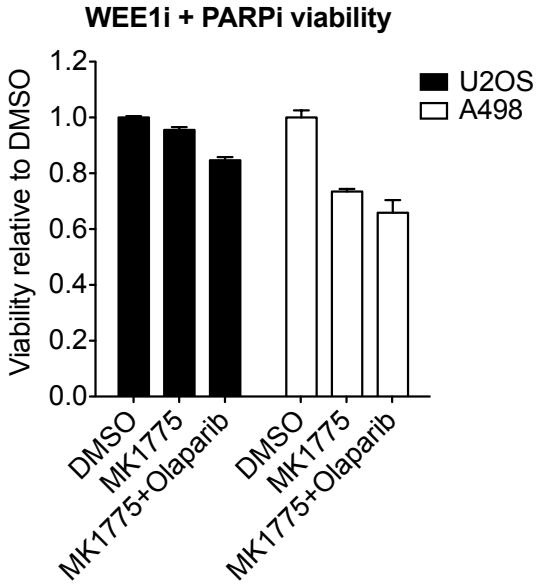


Figure 6.15: SETD2-deficient cells are not sensitised by PARP inhibitor Olaparib. (a) U2OS cells were transfected with non-targeting siRNAs, SETD2 siRNAs or RAD51 siRNAs 48 hours prior to treatment with DMSO or Olaparib at indicated concentrations. Cell viability was measured by Resazurin five days after inhibitor treatment. (b) Viability of U2OS or A498 cells five days after treatment with DMSO, the WEE1 inhibitor MK1775 (100nM) or a combination of the WEE1 inhibitor (100nM) and the PARP inhibitor Olaparib (200nM).

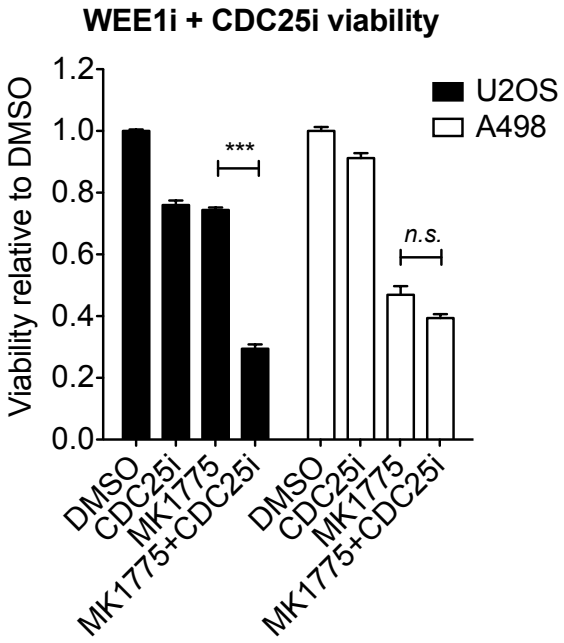


Figure 6.16: Viability of U2OS or A498 cells three days after treatment with DMSO, the CDC25 inhibitor (5μM), the WEE1 inhibitor MK1775 (200nM) or a combination of the CDC25 inhibitor (5μM) and MK1775 (200nM).

are somehow involved in the same pathway or regulate a shared target.

CDC25 family members are responsible for the dephosphorylation of Tyrosine 15 and Threonine 14 of CDK1 (and CDK2), which leads to CDK activation and cell cycle progression. Could SETD2 have any role in CDK regulation? A Western blot has came into the picture: it showed that SETD2 knockdown reduced phosphorylation of CDK1 at Tyrosine 15 (Fig 6.17). However, this hypothesis needs to be tested more rigorously to exclude the possibility of an indirect effect.

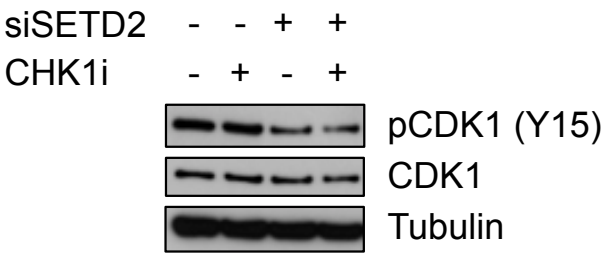


Figure 6.17: SETD2 knockdown may have reduced the phosphorylation of CDK1 at Tyrosine 15. U2OS cells were transfected with non-targeting siRNA or SETD2 siRNA 72 hours prior to DMSO or CHK1 inhibitor LY2603618 (500nM) treatment for 24 hours. Samples were treated and harvested by me and the Western blotting was performed by Ms Giulia Orlando.

6.4.4 Do the kinases work through the same mechanism?

In Chapter 5, WEE1, CHK1 and ATR were grouped together as they all selectively kill H3K36me3-deficient cells. While they have many similarities, they are also very different.

While the inhibition (either by siRNA or inhibitors) of all three kinases induced similar phenotypes in SETD2-deficient cells (S-phase arrest, increased DNA damage and apoptosis) (as shown in Chapter 5), they did exhibit synergistic effects when combined. For example, when WEE1 siRNA is combined with CHK1 siRNA, cell viability was further reduced (Fig 6.18a). Also, when the WEE1 inhibitor is combined with the CHK1 inhibitor, the S-phase arrest became more severe: even fewer cells could incorporate BrdU (Fig 6.18b). However, when the ATR inhibitor is combined with the CHK1 inhibitor, the effect is less obvious (Fig 6.19). A possible explanation is that upon DNA damage in S-phase, CHK1 and ATR are involved in the intra S-phase checkpoint as well as in the G2/M

checkpoint, while WEE1 is only involved in the G2/M checkpoint.

6.4.5 Which kinase has the best therapeutic potential?

The IC_{50} values suggest that *in vitro*, the effective concentrations for the existing inhibitors of WEE1 (MK1775), CHK1 (LY2603618), and ATR (VE822) are all within a nano-molar range for H3K36me3-deficient cells (A498, K36M, KDM4A over-expression or SETD2 knockdown cells). Given that all three inhibitors induce a similar amount of the non-replicating population, and a similar amount of DNA damage, it is difficult to tell which one should take priority when exploring their therapeutic potential for SETD2-deficient cancer patients.

However, another aspect to consider is the consistency between the different small molecule inhibitors of the same kinase. Apart from MK1775, other WEE1 inhibitors showed less selective killing of H3K36me3-deficient cells (data not shown). This is likely because the other molecules are poorer inhibitors of WEE1 (which may explain why MK1775 is currently the only WEE1 inhibitor in clinical trials). Therefore, if this intervention focuses on the WEE1 inhibitor, there will be only one molecule (and one pharmaceutical company) available.

All three CHK1 inhibitors tested in this thesis (LY2603618, AZD7762 and Gö6976) behave consistently on H3K36me3-deficient cells. However, a drawback of the CHK1 inhibitors is that currently CHK1-specific inhibitors are rare – most inhibitors are CHK1/CHK2 inhibitors. Likewise, ATR-specific inhibitors are rare,

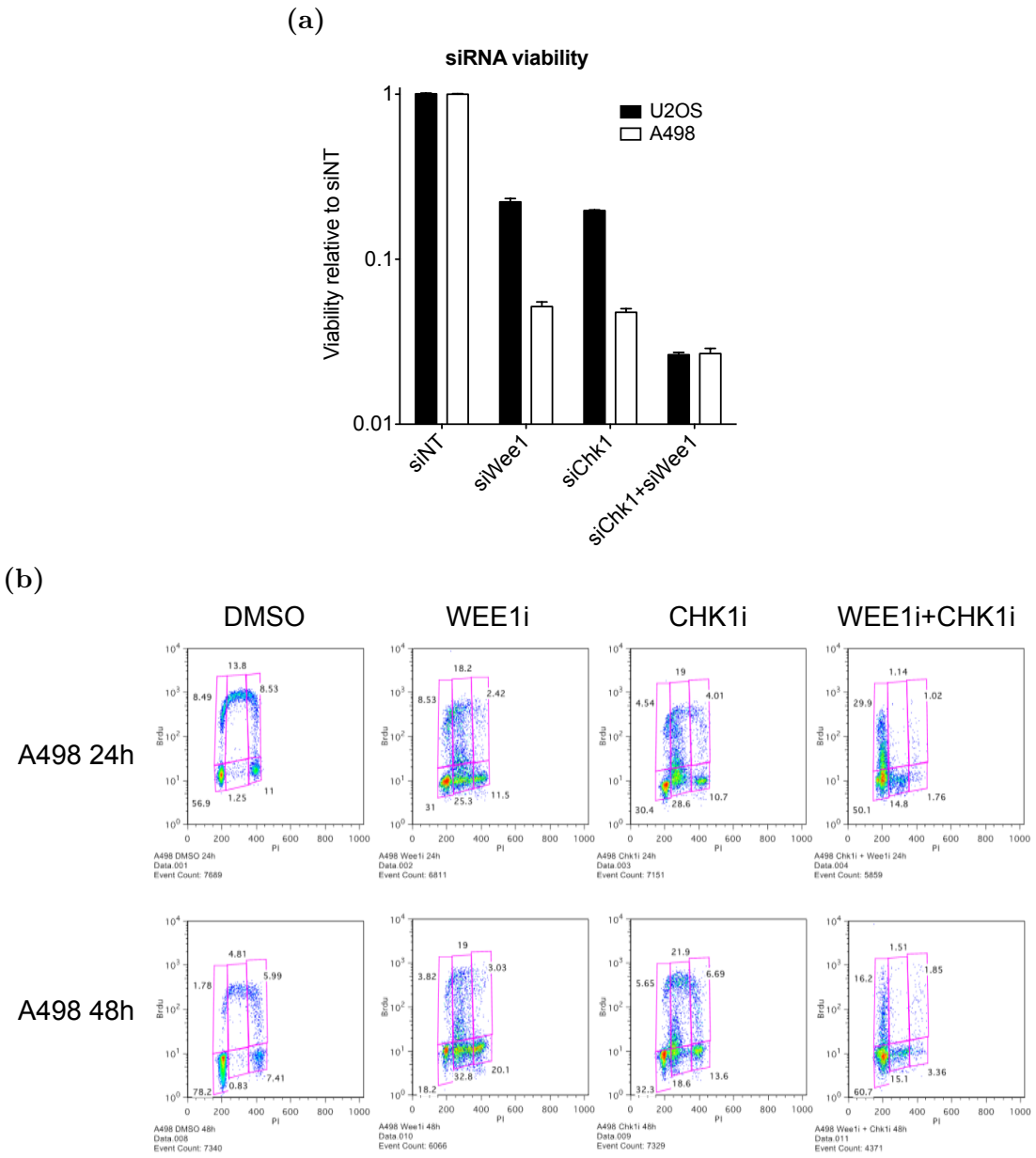


Figure 6.18: Combined inhibition of WEE1 and CHK1 induces a more severe phenotype. (a) Viability of U2OS or A498 cells treated with indicated siRNAs for five days. (b) BrdU cell cycle analysis of A498 cells after treatment with indicated inhibitors for 24 or 48 hours.

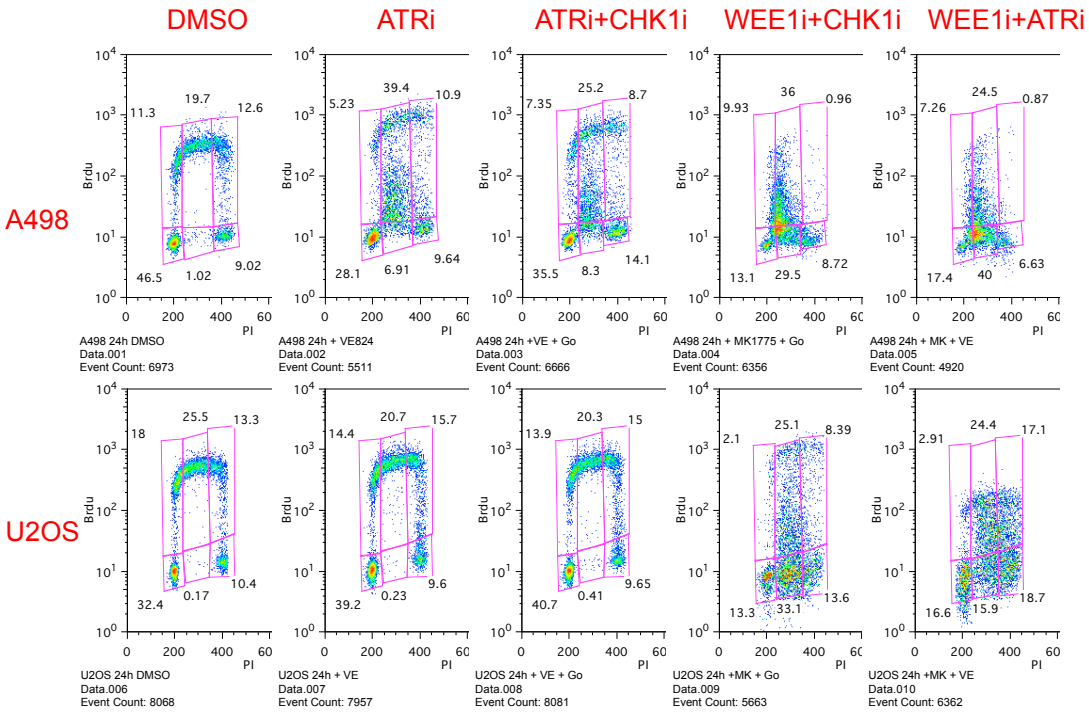


Figure 6.19: Combined inhibition of WEE1 and ATR (but not combined inhibition of CHK1 and ATR) induces a more severe phenotype. BrdU cell cycle analysis of U2OS or A498 cells after treatment with indicated inhibitors for 24 hours.

as most inhibitors are ATR/ATM inhibitors.

6.4.6 The resistance mechanism

Many targeted therapies fail to cure patients due to the mutator phenotype of the cancer cells, and the heterogeneity within individual tumours. Cancers can evolve resistance mechanisms much faster than it takes for a drug to flow through the development process. Therefore it is important to understand, and to attempt to overcome, drug resistance, even before a clinical trials starts.

This work has described several rescue mechanisms, including CDK1 inhibition, MUS81 depletion, and RRM2 over-expression. To help kickstart the search for methods to prevent or target these mutations, it would be important to understand how cancers can acquire mutations that increase RRM2 or dNTP production, or reduce CDK1 activity. If a screen is carried out to search for resistance mechanisms, then mutations in these pathways are expected.

The rescue mechanisms found in this project also suggest that CDK1 inhibitors (which are in clinical development) should not be used in conjunction with WEE1, CHK1 or ATR inhibitors.

6.4.7 How can these discoveries serve patients?

Before treating cancer patients with the inhibitors, it is necessary to determine whether or not the cancer is deficient in SETD2 or H3K36me3. The presence of

H3K36me3-deficiency indicates that the patient will benefit from treatment using a WEE1 inhibitor, a CHK1 inhibitor or an ATR inhibitor.

H3K36me3 deficiency can be determined in several ways in a clinical setting:

(1) A decreased amount of H3K36me3 can be detected by immunohistochemistry, Western blotting, mass spectrometry or FACS on a cancer biopsy.

(2) A decreased amount of the SETD2 protein, or an increased amount of KDM4 proteins, can be measured with immunohistochemistry, Western blotting, mass spectrometry or FACS.

(3) A decreased amount of SETD2 mRNA, or an increased amount of KDM4 mRNAs, can be measured by qRT-PCR or microarrays.

(4) A mutation in the SETD2 gene can be determined by DNA or RNA sequencing.

(5) A chromosome 3 abnormality, such as chromosome 3p deletion or rearrangement, can be identified using cytogenetic analysis such as giemsa banding, fluorescence *in situ* hybridisation (FISH), or comparative genomic hybridisation.

Methods (3–5) can be applied on cancer biopsies as well as on the cancer cells circulating in the blood of the patient. In addition, the RNA-based method may be applied on the urinary or blood exosomes. The DNA-based methods may be carried out on circulating free DNA in the blood.

Other biomarkers can also be used to predict the outcome. These include RRM2 levels, dNTP levels, CDK1 levels or endogenous DNA damage levels.

6.4.8 SETD2 and cancer stem cells

Cancer stem cells, like normal stem cells, exhibit a unique epigenetic landscape from differentiated cells. The epigenetic modifications (both DNA and chromatin modifications) maintain the self-renewal and pluripotency of the stem cells. SETD2, as a chromatin modifying enzyme, may be involved in stem cell or cancer stem cell maintenance.

Indeed, recent work shows that in the presence of a genetic lesion, downregulation of SETD2 promotes the self-renewal potential of leukaemia stem cells (Zhu et al., 2014). One way to maintain stemness is to inhibit differentiation. To this end, a recent report on murine Setd2 suggests that H3K36me3 is critical for the endodermal differentiation and Setd2 deletion-blocked differentiation of mouse embryonic stem cells (mESCs) (Zhang et al., 2014). These findings suggest that SETD2-deficiency could be an enabling characteristic of cancer stem cells, and that targeting SETD2-deficient cells may help to eliminate cancer stem cells from the tumour mass.

6.5 Summary

In summary, this thesis has ascribed two novels functions to H3K36me3: (1) it is required for the accurate repair of DNA double-stranded breaks; and (2) it is involved in the transcriptional regulation of RRM2, a gene that is essential for dNTP synthesis during DNA replication.

This work also opens many interesting opportunities for future studies. The perhaps most promising that have been touched upon in the section above are: (1) the potential interplay between DNA repair and DNA replication; (2) possible combinational therapies involving WEE1, CHK1 and ATR inhibitors; and (3) the role of H3K36me3 in transcriptional control (and its potential contribution to cancer stemness).

Finally, from a broader perspective, this work has reported a new therapy for cancer based on the concept of synthetic lethality – thus providing a less toxic and more effective treatment, as it specifically targets cancer cells. Since the inhibitors used to target H3K36me3-deficiency (WEE1, CHK1 and ATR) are in clinical trials, and H3K36me3-deficiency is frequently observed in multiple cancers (in some cancers it accounts for over 50% of the patient population), patients with cancers deficient in H3K36me3 could potentially benefit from treatment with these inhibitors. Thus the findings in this thesis could be of immediate relevance to clinicians and cancer patients.

Chapter 7

Appendix

The two published publications that were produced as part of my DPhil are included below.

OPEN ACCESS
CellPress

Cell Reports
Article

SETD2-Dependent Histone H3K36 Trimethylation Is Required for Homologous Recombination Repair and Genome Stability

Sophia X. Pfister,[1] Sara Ahrabi,[1] Lykourgos-Panagiotis Zalmas,[2] Sovan Sarkar,[1] François Aymard,[3,4] Csanád Z. Bachrati,[5] Thomas Helleday,[6] Gaëlle Legube,[3,4] Nicholas B. La Thangue,[2] Andrew C.G. Porter,[7] and Timothy C. Humphrey[1,*]
[1]CRUK MRC Oxford Institute for Radiation Oncology, Department of Oncology, University of Oxford, Oxford OX3 7DQ, UK
[2]Laboratory of Cancer Biology, Department of Oncology, University of Oxford, Oxford OX3 7DQ, UK
[3]Laboratoire de Biologie Cellulaire et Moléculaire du Contrôle de la Prolifération, Université de Toulouse, Université Paul Sabatier, 31062 Toulouse, France
[4]CNRS, Laboratoire de Biologie Cellulaire et Moléculaire du Contrôle de la Prolifération, 31062 Toulouse, France
[5]School of Life Sciences, University of Lincoln, Lincoln LN6 7TS, UK
[6]Science for Life Laboratory, Division of Translational Medicine and Chemical Biology, Department of Medical Biochemistry and Biophysics, Karolinska Institutet, 171 21 Stockholm, Sweden
[7]Gene Targeting Group, Centre for Haematology, Imperial College Faculty of Medicine, London W12 0NN, UK
*Correspondence: timothy.humphrey@oncology.ox.ac.uk
http://dx.doi.org/10.1016/j.celrep.2014.05.026
This is an open access article under the CC BY-NC-ND license (http://creativecommons.org/licenses/by-nc-nd/3.0/).

SUMMARY

Modulating chromatin through histone methylation orchestrates numerous cellular processes. SETD2-dependent trimethylation of histone H3K36 is associated with active transcription. Here, we define a role for H3K36 trimethylation in homologous recombination (HR) repair in human cells. We find that depleting SETD2 generates a mutation signature resembling RAD51 depletion at I-SceI-induced DNA double-strand break (DSB) sites, with significantly increased deletions arising through microhomology-mediated end-joining. We establish a presynaptic role for SETD2 methyltransferase in HR, where it facilitates the recruitment of C-terminal binding protein interacting protein (CtIP) and promotes DSB resection, allowing Replication Protein A (RPA) and RAD51 binding to DNA damage sites. Furthermore, reducing H3K36me3 levels by overexpressing KDM4A/JMJD2A, an oncogene and H3K36me3/2 demethylase, or an H3.3K36M transgene also reduces HR repair events. We propose that error-free HR repair within H3K36me3-decorated transcriptionally active genomic regions promotes cell homeostasis. Moreover, these findings provide insights as to why oncogenic mutations cluster within the H3K36me3 axis.

INTRODUCTION

DNA double-stranded breaks (DSBs) are potentially lethal lesions if unrepaired, and their misrepair can give rise to genome instability, a hallmark of cancer (Jeggo and Lavin, 2009). To maintain genome stability in response to such lesions, cells employ either homologous recombination (HR) or nonhomologous end-joining (NHEJ) pathways to repair DSBs. HR is initiated by 5′ end resection to generate a 3′ single-stranded DNA (ssDNA) overhang. Resection is a two-step process initiated by removing a short oligonucleotide through the activities of the Mre11-Rad50-Nbs1 (MRN) complex and CtIP. Extensive resection is performed by Exo1 or DNA2-BLM in conjunction with Replication Protein A (RPA), which binds ssDNA and removes secondary structures (Sugiyama et al., 1998; Symington and Gautier, 2011). This, in turn, leads to RAD51 nucleofilament formation, which promotes strand invasion of a homologous chromatid, leading to accurate repair (Heyer et al., 2010). During classical NHEJ (C-NHEJ), the broken ends are rapidly bound and protected by the Ku70/Ku80 heterodimer, which acts as a platform to recruit the DNA-PK catalytic subunit (DNA-PKcs). Damaged ends are then processed and subsequently joined by the Ligase 4 (Lig4), XRCC4, XLF complex in a template-independent manner, which can lead to inaccurate repair (Lieber, 2010). DSBs may also be repaired through alternative end-joining pathways, such as microhomology-mediated end-joining (MMEJ), which do not require Ku or Lig4. Like HR, MMEJ is initiated by resection, and end-joining is mediated through annealing of short direct repeats of microhomology. MMEJ leads to deletions and is frequently associated with chromosomal rearrangements (McVey and Lee, 2008).

DSB repair is further facilitated through chromatin modification by chromatin remodeling complexes, by incorporation of histone variants, and by histone modification (Smeenk and van Attikum, 2013). Histone H3K36 dimethylation has recently been proposed to facilitate NHEJ, where Metnase (SETMAR) directly mediates H3K36 dimethylation near the break site, leading to recruitment and stabilization of NBS1 and Ku70 (Fnu et al., 2011). Histone H3K36 is also trimethylated, which in mammalian cells is performed uniquely by the SETD2/HYPB methyltransferase (Edmunds et al., 2008). H3K36me3 is associated with transcriptional elongation and is found in gene coding regions,

peaking at 3′ ends (Edmunds et al., 2008). SETD2-dependent H3K36 trimethylation facilitates a number of processes within the cell, including splicing, repression of intragenic transcripts, and chromatin accessibility (Li et al., 2013; Wagner and Carpenter, 2012). *SETD2* is also mutated in a number of cancer types, including breast, lung, acute lymphoblastic leukemia, clear cell renal cell carcinoma, and glioma, supporting its role as a tumor suppressor (Al Sarakbi et al., 2009; Dalgliesh et al., 2010; Fontebasso et al., 2013; Newbold and Mokbel, 2010; Zhang et al., 2012). SETD2-dependent H3K36 trimethylation has recently been shown to regulate DNA mismatch repair (Li et al., 2013). However, SETD2-deficient cancers exhibit a wide range of mutations, including insertions, deletions (indels), and chromosomal aberrations (Sato et al., 2013; Zhu et al., 2014), suggesting an additional role for SETD2 in genome stability.

Additionally, H3K36 methylation is regulated by the KDM4/JMJD2 family of histone demethylases. These contain JmjN-JmjC and tandem-Tudor domains that specifically remove the tri- and dimethyl forms of both H3K9 and H3K36, with preference for the trimethyl form being observed in the case of KDM4A/JMJD2A (Couture et al., 2007; Klose et al., 2006; Whetstine et al., 2006). KDM4 family proteins are frequently overexpressed in cancers and are associated with poor patient survival (Berry and Janknecht, 2013; Black et al., 2013).

Here, we investigate the role of SETD2-dependent H3K36me3 in maintaining genome stability. We establish a role for H3K36me3 in HR repair by facilitating resection. In addition, we define a role for SETD2 and RAD51 in maintaining genome stability through suppressing MMEJ at break sites.

RESULTS

SETD2 Suppresses Break-Induced Mutations

Tumor suppressors can suppress carcinogenesis by preventing genome instability, a hallmark of cancer. To investigate the impact of loss of SETD2, a tumor suppressor, on genome stability following DSB induction, we developed an I-SceI-induced loss of function assay (HPRT$^+$:I-SceI). Intron-encoded endonuclease 1 from *Saccharomyces cerevisiae* (I-SceI) is a rare-cutting endonuclease that has no predicted recognition site in the mammalian genome (Jasin, 1996). An I-SceI recognition sequence was inserted into the endogenous *HPRT* exon 6 in HT1080 (fibrosarcoma) cells. The I-SceI site maintains the HPRT reading frame and makes only a single amino acid change that does not impair the function of HPRT (Figure 1A). Following I-SceI induction, inaccurate DSB repair generates HPRT-negative mutants, which can be selected for using 6-thioguanine (6-TG), and indels can be detected by PCR amplification using primers flanking the break site (Figure 1A). Following small interfering RNA (siRNA) knockdown and I-SceI induction, the frequency of HPRT loss (mutation frequency) in SETD2-depleted cells was 1.65%, significantly higher ($p = 0.0014$) than that of nontargeting controls (1.1%). These findings resembled those in RAD51-depleted cells in which the frequency of HPRT loss was also significantly increased to 1.88% ($p = 0.0022$) compared to nontargeting controls (Figure 1B). SETD2 and RAD51 codepletion (siS+SiR) also significantly increased the mutation frequency to 1.52% ($p = 0.037$), which was similar to the frequency observed following either SETD2 or RAD51 depletion (Figure 1B). We confirmed that I-SceI protein expression and cleavage efficiency were the same in cells transfected with either control siRNA or SETD2 siRNA (Figures S1A–S1C). In addition, *HPRT* gene transcription was not affected by SETD2 knockdown, as shown by quantitative RT-PCR (qRT-PCR) of spliced and unspliced HPRT mRNA (Figures S1D and S1E). Therefore, the mutation frequency in this system is likely to be directly associated with misrepair of the DSB at the I-SceI site.

Further, we studied the mutation patterns across the break site of 30 individually isolated HPRT-negative clones from each background by PCR amplification and sequencing. HPRT-negative clones from cells treated with nontargeting control siRNA indicated the presence of microdeletions of 2–5 bp, consistent with DSB repair by C-NHEJ. Larger microdeletions were also observed that were associated with regions of microhomology located either side of the break site, consistent with DSB repair through MMEJ (Figures 1C and S1F).

Sequence analysis indicated that SETD2-depleted cells exhibited a significant increase in average deletion length (11 bp, $p < 0.0001$) compared to control cells (5 bp) (Figures 1C and 1D). RAD51-depleted cells exhibited a further significant increase in the average deletion length (22 bp, $p = 0.014$) (Figures 1C and 1D). RAD51 and SETD2 codepletion generated deletion lengths (an average of 8 bp) comparable to those observed following SETD2 knockdown, which in turn was significantly higher than the nontargeting control ($p = 0.026$) (Figures 1C and 1D). Insertions at the HPRT break site were also detected. However, the frequency and size of the insertions was not significantly altered between SETD2-depleted cells, SETD2/RAD51 codepleted and nontargeting controls.

We next examined the mechanism for misrepair in cells exhibiting deletions. We found that the frequency of microhomology-mediated end-joining (MMEJ) was significantly increased in SETD2 and RAD51-depleted cells ($p < 0.05$) (Figures 1E and S1G). This suggested that HR-deficient cells use MMEJ as an alternative repair mechanism, which gives rise to a mutation signature of sequence loss between regions of microhomology. These results support a role for SETD2 in tumor suppression by maintaining genome stability through preventing deleterious mutations arising in response to DSBs. These findings further identify a similar break-induced mutation signature between SETD2- and RAD51-depleted cells, suggesting an early role for SETD2 in HR repair.

SETD2 Is Required for Homologous Recombination Repair

To test the role for SETD2 in DSB repair, we depleted SETD2 in U2OS and HeLa cells using two independent siRNAs and measured the clonogenic survival following exposure to DNA-damaging agents. SETD2 knockdown significantly reduced survival after treatment with mitomycin C (MMC), camptothecin (CPT), or ionizing radiation (IR) in U2OS cells and HeLa cells compared to nontargeting controls (Figures 2A and S2A). These results identify a role for SETD2 in the cellular response to DNA damage and are consistent with a role for SETD2 in DSB repair.

SETD2 knockdown was validated by western blotting (Figure 2B). Western blotting also showed that SETD2 knockdown

OPEN ACCESS
CellPress

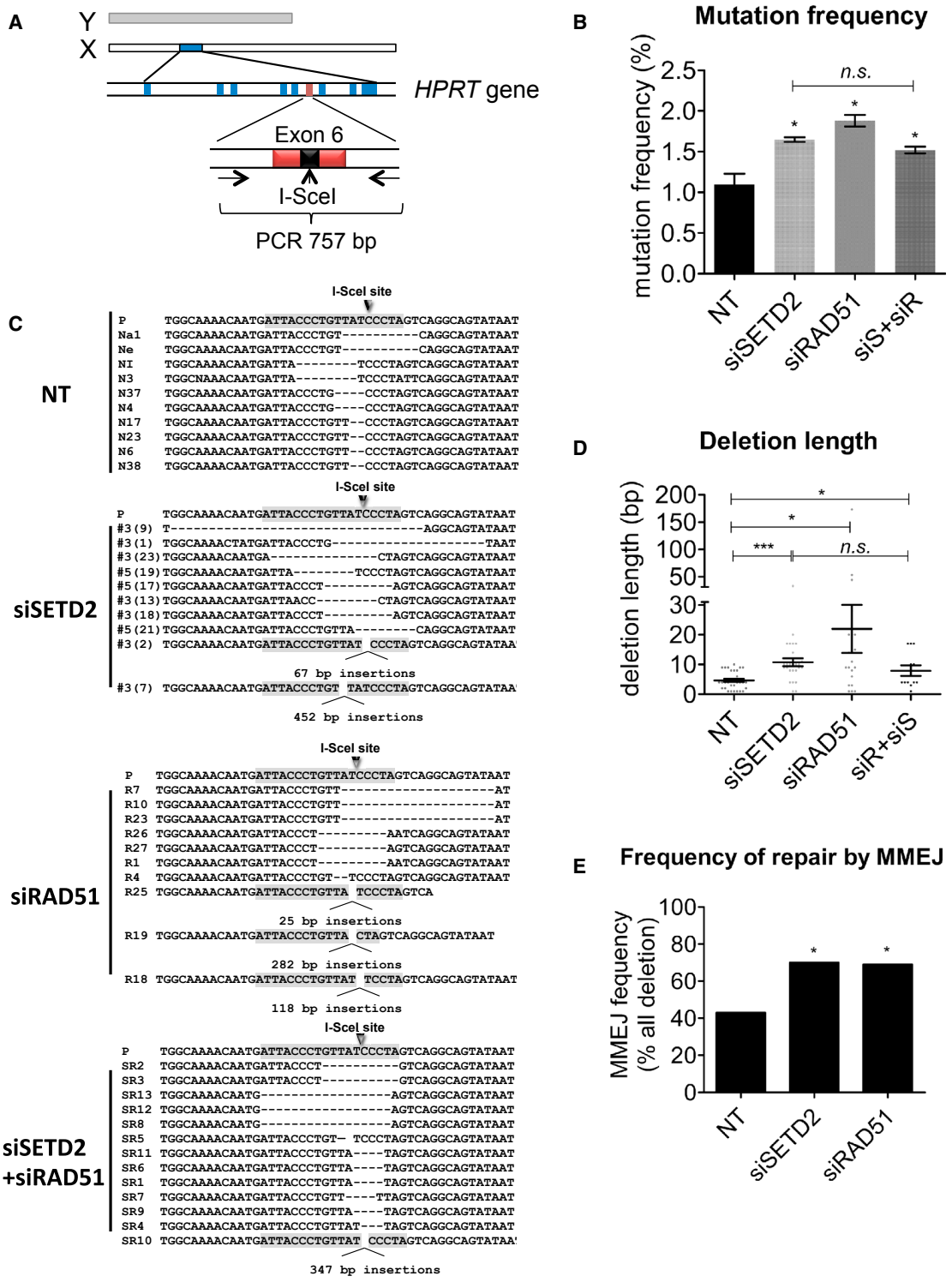


Figure 1. SETD2- and RAD51-Depleted Cells Exhibit a Common Break-Induced Mutation Signature

(A) Schematic map of the HPRT$^+$:I-SceI assay, where arrows indicate PCR primers used to amplify genomic DNA to allow sequencing across the break site (see Supplemental Experimental Procedures).

(B) Mutation frequency of nontargeting control (NT), SETD2-depleted, RAD51-depleted, and SETD2/RAD51-codepleted cells (siS+siR) after I-SceI induced DSB. Error bars represent SEM and *p < 0.05; n.s., not significant.

(legend continued on next page)

significantly reduced global levels of H3K36me3, confirming SETD2 as the major H3K36me3 methyltransferase in human cells (Figure 2B). Because RAD51 is more likely to be affected among DNA repair genes by siRNA off-target effects (Adamson et al., 2012), we also confirmed that SETD2 knockdown by siRNA did not affect the RAD51 protein levels (Figure 2B). We confirmed that SETD2 knockdown had no effect on the expression of major HR proteins, including BRCA2, RAD50, CtIP, MRE11, and RPA and the NHEJ protein KU80 (Figure S2B). We also observed no changes to the cell cycle after SETD2 knockdown (Figure S2C).

Both MMC and CPT induce S phase-specific DSBs, which are predominantly repaired by HR (Arnaudeau et al., 2001; Moynahan et al., 2001). To test a possible role for SETD2 in HR repair, we used a well-characterized GFP-based reporter for HR (DR-GFP). The HR reporter contains an I-SceI recognition sequence, which upon I-SceI expression is cleaved to generate a DSB. DSB repair by HR using a direct repeat within the reporter cassette as a template results in an intact GFP gene (Figure 2C)(Pierce et al., 1999). SETD2 knockdown by two independent siRNAs significantly reduced HR repair of an I-SceI induced DSB by 67%–77% compared to nontargeting control cells ($p < 0.0003$) (Figure 2D). As a control for the HR reporter, knockdown of RAD51 reduced HR activity by 97% ($p < 0.0001$), whereas DNA-PKcs inhibitor NU7441 had no effect on HR (Figure 2D). In contrast, SETD2 knockdown had no effect on repair of an I-SceI induced DSB in an NHEJ reporter (IRES-TK-EGFP) in which joining of two I-SceI sites separated by a thymidine kinase gene (TK) results in GFP expression (Figures 2E and 2F)(Ogiwara et al., 2011). As a control, RAD51 had no effect on the same NHEJ reporter, whereas the DNA-PK inhibitor NU7441 reduced NHEJ activity by 98% ($p < 0.0001$) (Figure 2F). These results identify a role for SETD2 in HR repair.

An Early Role for SETD2 in Homologous Recombination

To further investigate the role of SETD2 in DSB repair, we examined the rate of repair following IR. We used γH2AX foci as a marker of DNA damage and found that following exposure to 5 Gy IR, SETD2 knockdown significantly delayed removal of γH2AX foci at 48 hr ($p < 0.003$) compared to nontargeting controls, supporting a role for SETD2 in efficient DSB repair (Figure 3A). We next investigated the effect of SETD2 depletion on the recruitment of HR repair proteins following DNA damage. SETD2 knockdown resulted in significantly reduced RAD51 foci formation 4 and 8 hr after exposure to IR compared to nontargeting controls ($p < 0.0013$) (Figure 3B). SETD2 knockdown also significantly reduced RAD51 foci formation after exposure to CPT ($p < 0.05$) (Figure S2D).

We also examined the effect of SETD2 depletion on RPA recruitment, where we induced DSBs in S phase cells using CPT or MMC. A significant reduction in RPA foci formation was observed after CPT or MMC treatment following SETD2 knockdown compared to nontargeting controls ($p < 0.023$) (Figures 3C and S2E). SETD2 knockdown leads to reduced H3K36me3 in the nuclei as confirmed by costaining the cells with antibodies against H3K36me3 and RPA (Figure S2F). Together, these findings support a role for SETD2 in promoting HR through facilitating recruitment of RPA and RAD51 to DNA damage sites.

To further confirm the impact of SETD2 loss on the recruitment of HR factors to the site of DSBs, we performed chromatin immunoprecipitation (ChIP) near the I-SceI site in the DR-GFP cassette (Figure S3A). The I-SceI site is located within the DR-GFP cassette under the control of the highly active CMV promoter, and thus H3K36me3, which is associated with active transcription, is predicted to be present throughout the cassette. After induction of DSBs by I-SceI, no change in H3K36me3 or SETD2 levels was detected proximal or distal to the break site after 8, 24, or 48 hr following I-SceI transfection (Figure S3B). The results were also quantified by ChIP-qPCR (Figure S3C). Although other groups also observed no changes to H3K36me3 level after DSB, globally (Fnu et al., 2011) or locally at the break site (Pei et al., 2011; Aymard et al., 2014), we were surprised by the lack of reduction in H3K36me3 or SETD2 knowing that regional transcriptional silencing has been observed at sites of DSBs (Shanbhag et al., 2010). We speculate that the unexpected maintenance of H3K36me3 at the DSB site by SETD2 may serve as an anchor to mediate HR repair.

We monitored recruitment of major HR factors to the DSB site in the ChIP system. RPA and RAD51 were recruited to the DSB site, resulting in increased binding to the "up" site 18 hr after I-SceI transfection, compared to uncut controls (Figure 3D). SETD2 depletion substantially reduced the recruitment of RPA and RAD51 after the I-SceI cut (Figure 3D). SETD2 protein depletion was validated by western blotting (Figure S3D), and was further confirmed by the absence of SETD2 or H3K36me3 at the break site (Figure 3D). These findings are consistent with the RPA and RAD51 foci data, indicating that SETD2 is required to recruit RPA and RAD51 to DSB sites. Together, these findings confirm a presynaptic role for SETD2 in facilitating HR repair of DSBs.

H3K36me3 Is Required for Homologous Recombination Repair

To investigate if the methyltransferase activity of SETD2 is required for its role in HR, we generated two doxycycline-inducible U2OS cell lines, where either a wild-type *SETD2* cDNA or a methyltransferase-dead *SETD2* cDNA was inserted behind a Tet operator in the genome of U2OS cells. Upon addition of doxycycline to the cell culture medium, the Tet operator was derepressed and the wild-type or mutant SETD2 was expressed. Both cDNA constructs were mutated so that they are refractory to SETD2 siRNA#3. The methyltransferase-dead SETD2 was

(C) Representative sequence alignments of the above-mentioned PCR products in nontargeting control (NT), SETD2-depleted, RAD51-depleted, and SETD2/RAD51-codepleted backgrounds, respectively.

(D) Average length of deletions (bp) in different backgrounds, where each dot represents an independent clone. The lines represent mean and SEM, *$p < 0.05$, ***$p < 0.001$.

(E) Frequency of repair by MMEJ in deletion mutants isolated from different backgrounds. p values calculated by statistical analysis "difference between proportions," *$p < 0.05$. See also Figure S1.

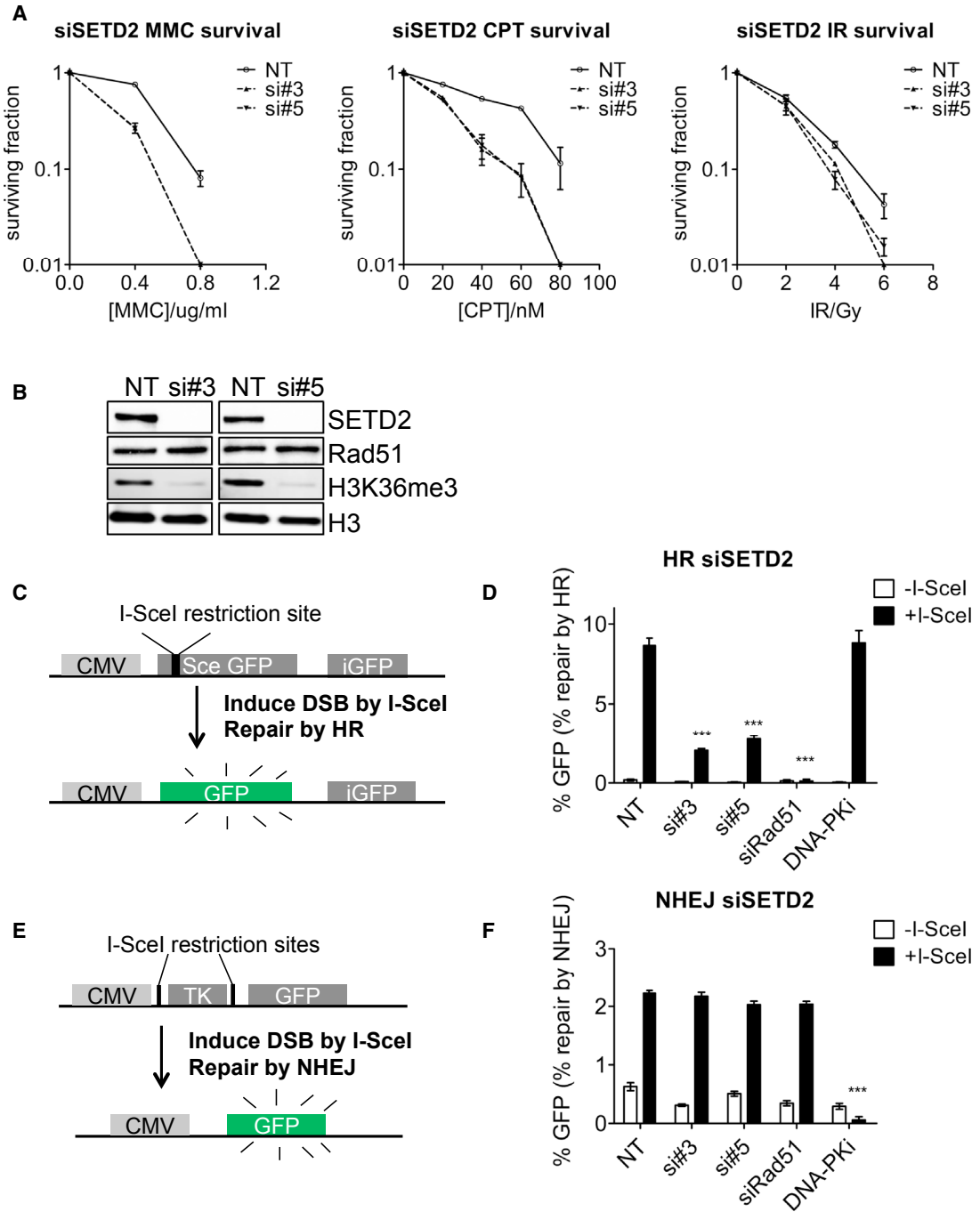


Figure 2. SETD2 Is Required for Homologous Recombination

(A) Clonogenic survival of SETD2 knockdown (si#3 and si#5) or nontargeting control (NT) U2OS cells treated with indicated concentrations of MMC, CPT, and IR. Error bars show SEM from three independent experiments.

(B) Western blots showing levels of SETD2, RAD51, and H3K36me3 72 hr after siRNA transfection.

(C) Schematic map of the DR-GFP cassette for assessing HR efficacy.

(D) HR repair efficacy of reporter cells treated with nontargeting control siRNA (NT), SETD2 siRNAs (si#3 and si#5), RAD51 siRNA (siRad51), or DNA-PK inhibitor NU7441 (Axon), indicated by the percentage of GFP-positive cells. Error bars show SEM from three independent experiments. ***$p < 0.001$.

(E) Schematic map of the NHEJ cassette.

(F) NHEJ repair efficacy of reporter cells treated with nontargeting control siRNA (NT), SETD2 siRNAs (si#3 and si#5), RAD51 siRNA (siRAD51), or DNA-PK inhibitor NU7441, indicated by the percentage of GFP-positive cells. Error bars show SEM from three independent experiments. ***$p < 0.001$. See also Figure S2.

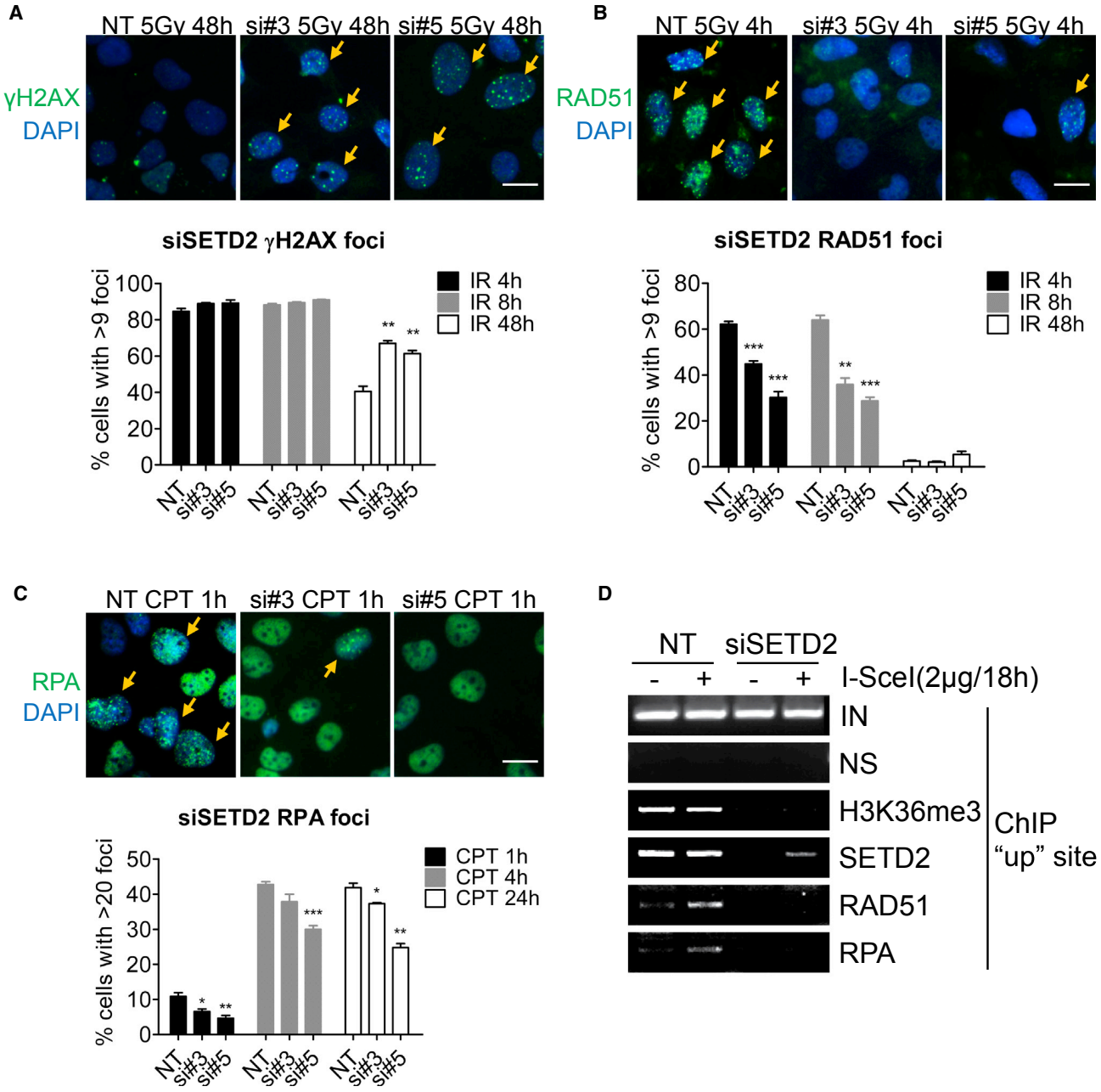


Figure 3. SETD2 Is Required for the Recruitment of RPA and RAD51

(A and B) γH2AX (A) or RAD51 (B) foci formation at indicated times after IR (5 Gy) in U2OS cells treated with nontargeting control siRNA (NT) or SETD2 siRNAs (si#3 and si#5). Error bars represent SEM from three independent experiments.

(C) RPA32 foci formation at indicated times after treatment with CPT (10 μM) in U2OS cells transfected with control siRNA (NT) or SETD2 siRNAs (si#3 and si#5). Representative fluorescent images are shown; scale bar, 20 μm. For each condition, 45 fields and at least 500 cells were examined by Incell (GE Healthcare). Error bars show SEM from three independent experiments. ***$p < 0.001$, **$p < 0.01$, *$p < 0.05$.

(D) ChIP analysis on DR-GFP U2OS cells transfected with nontargeting control (NT) or SETD2 siRNA for 72 hr, followed by transfection of either vector or I-SceI plasmid for a further 18 hr, as indicated. ChIP on the "up" DNA site of the DR-GFP cassette was performed on the lysate using antibodies against nonspecific Ig (NS), H3K36me3 (Abcam), SETD2 (Abcam), RAD51 (Santa Cruz Biotechnology), or RPA (Millipore); inputs (IN) are also indicated.

See also Figures S2 and S3.

mutated at two amino acid residues located within the catalytic site of the SET domain, which are conserved with yeast Set2. The corresponding mutations in yeast were shown to abolish the methyltransferase activity (Rea et al., 2000;Strahl et al., 2002) (Figure 4A). Both arginine (R) and cysteine (C) residues were mutated in the methyltransferase-dead (MD) cDNA by

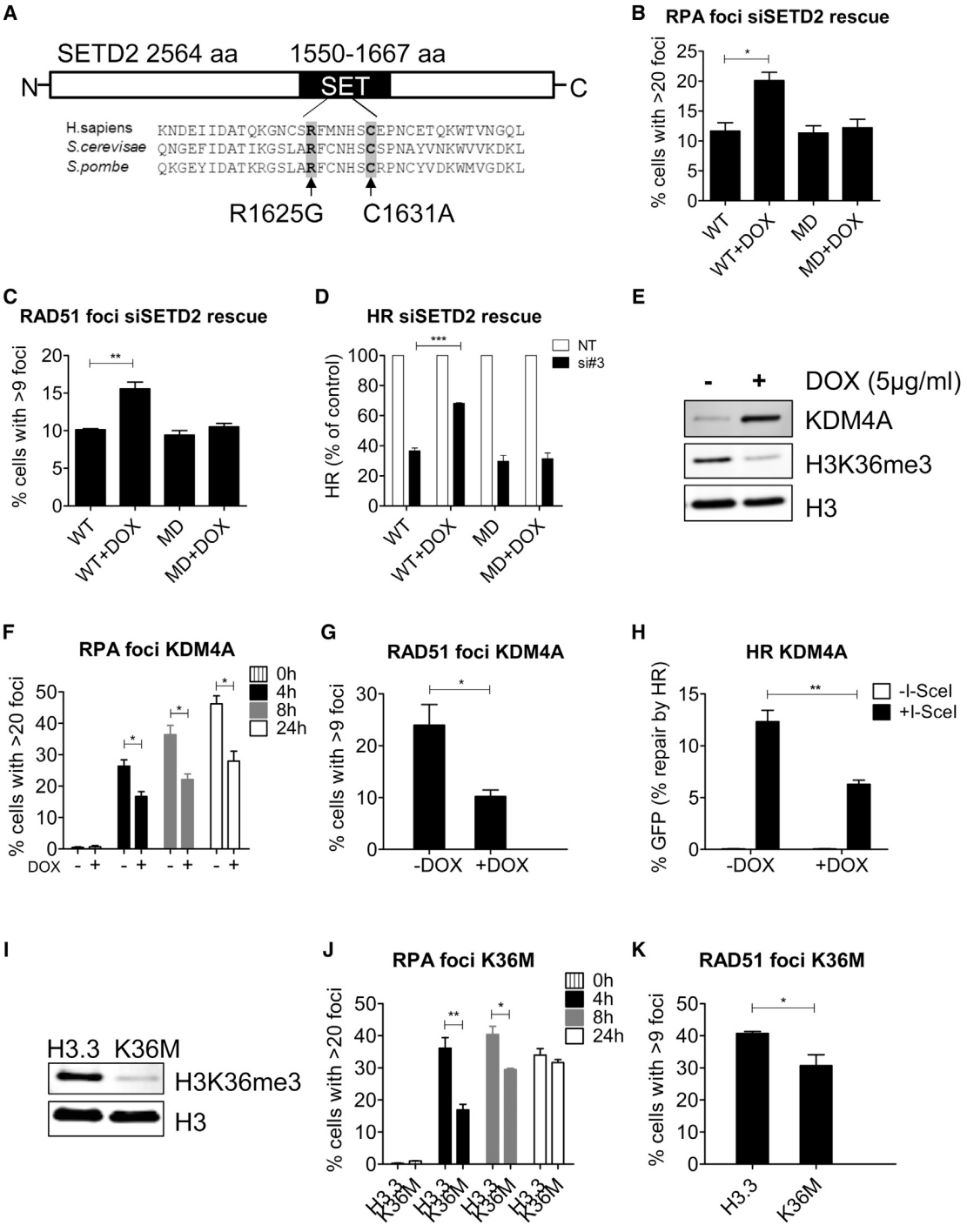


Figure 4. H3K36me3 Is Required for Efficient HR Repair

(A) Schematic map showing site-directed mutagenesis for abolishing the methyltransferase activity of SETD2, with both R and C residues mutated simultaneously. Sequence alignment of human SETD2 and *Saccharomyces cerevisiae* Set2 and *Schizosacchromyces pombe* Set2 amino acid sequences reveals evolutionarily conserved residues that reside in the SET domain.

(B) RPA32 foci formation at 2 hr after treatment with CPT (10 μM) in cells transfected with SETD2 siRNA. WT: T-REx U2OS clone (see Experimental Procedures) with wild-type *SETD2* cDNA integrated but not expressing exogenous SETD2. WT+DOX: the same WT clone expressing exogenous wild-type SETD2. MD: T-REx U2OS clone with methyltransferase-dead mutant *SETD2* cDNA integrated but not expressing exogenous SETD2. MD+DOX: the same MD clone expressing exogenous mutant SETD2. Error bars show SEM from three independent experiments, *p < 0.05.

(legend continued on next page)

site-directed mutagenesis (see Supplemental Experimental Procedures). Western blot analysis confirmed that doxycycline-induced expression of wild-type SETD2 could restore the level of H3K36me3 after siSETD2 treatment, whereas expression of methyltransferase-dead SETD2 could not restore the level of H3K36me3 (Figure S4A).

We depleted endogenous SETD2 with siRNA#3 and examined the rescue of the phenotype by the two constructs. Although the wild-type construct increased foci formation of RPA and RAD51 after DNA damage in siSETD2 cells, the methyltransferase-dead mutant did not (Figures 4B and 4C). This is consistent with the observation that the wild-type construct partially restored HR efficiency whereas the methyltransferase-dead (MD) mutant did not (Figure 4D). Five to six clones containing each construct were independently isolated and tested. All WT clones were able to restore HR efficiency, but none of the MD clones showed rescue (Figures S4B and S4C).

The observation that the methyltransferase-dead SETD2 mutant could not rescue HR efficiency suggested that H3K36me3 is required for efficient HR. To test this further, we used SETD2-independent approaches to disrupt H3K36me3 levels. First, we overexpressed KDM4A, an oncogene and a demethylase specific for tri- and dimethylated histone H3K36 and H3K9, predicting that overexpression of KDM4A would reduce the level of H3K36me3 and thus impair HR. Therefore, a doxycycline-inducible KDM4A-expression U2OS cell line was generated. Upon addition of doxycycline, KDM4A was overexpressed, which led to a global reduction in H3K36me3 levels (Figure 4E). We then compared the recruitment of the HR factors in this cell line with or without KDM4A overexpression. We found that KDM4A overexpression inhibited the formation of RPA and RAD51 foci after DNA damage (Figures 4F and 4G). Accordingly, KDM4A overexpression also reduced HR efficiency as assessed by the HR reporter ($p = 0.0078$) (Figure 4H). Using the same cell line without *KDM4A* cDNA integration, we found that doxycycline itself had no effect on HR efficiency of U2OS cells (Figure S4D). These findings indicate that overexpression of the oncogene KDM4A significantly reduces levels of H3K36me3 and HR.

Second, we utilized a dominant-negative mutation in the histone *H3.3* gene (*H3.3K36M*) that was recently shown to reduce H3K36me3 specifically without affecting other histone methylations (Lewis et al., 2013). Accordingly, in cells expressing the mutant *H3.3K36M* transgene, global levels of H3K36me3 were depleted compared to the wild-type H3.3 control (Figure 4I). Cells expressing H3.3K36M also exhibited delayed RPA and RAD51 foci formation following DNA damage (Figures 4J and 4K), consistent with similar delays seen in KDM4A overexpressing cells or SETD2-depleted cells. Neither KDM4A overexpression nor H3.3K36M expression affected cell cycle progression as assessed by BrdU incorporation (Figures S4E and S4F), thus excluding the possibility that the reduction in RPA, RAD51 foci formation and HR efficacy was due to cell cycle effects. The common feature of all three different systems (SETD2 knockdown and rescue, KDM4A overexpression, and H3.3K36M expression) was the reduction in the recruitment of HR proteins and HR efficiency associated with reduced H3K36me3. Together these findings confirm a role for H3K36me3 in HR.

SETD2 Promotes DSB End Resection

Lens epithelium-derived growth factor p75 (LEDGF) binds to H3K36me3 constitutively through its PWWP domain. Upon DNA damage LEDGF recruits CtIP, which facilitates the resection step during HR repair (Daugaard et al., 2012). Accordingly, we were able to coprecipitate LEDGF and H3K36me3, independently of DNA damage in U2OS cells (Figure 5A). LEDGF binding to chromatin was reduced upon SETD2 depletion, consistent with preferential binding of LEDGF to H3K36me3 (Eidahl et al., 2013), and was DSB independent (Figure 5B). We predicted that the reduced LEDGF binding following SETD2 depletion would reduce recruitment of CtIP upon damage. We therefore used micro-irradiation to induce localized DSBs and studied the recruitment of CtIP using a U2OS cell line expressing GFP-tagged CtIP (Sartori et al., 2007). We found CtIP to be localized to sites of DNA damage marked by γH2AX (Figure 5C). In contrast, SETD2 knockdown resulted in reduced recruitment of CtIP to the DNA damage site as marked by γH2AX (Figure 5C). If SETD2 facilitates HR through LEDGF binding and CtIP recruitment, we would expect SETD2 to be epistatic with CtIP. Indeed, codepletion of SETD2 and CtIP (siC+siS) showed the same level of reduction in HR as CtIP-depletion alone (Figures 5D and S5A).

(C) RAD51 foci formation at 4 hr after IR (5 Gy) in cells transfected with SETD2 siRNA. The clones used are the same as in (B). Error bars show SEM from three independent experiments, $^{**}p < 0.01$.

(D) HR efficacy in cells transfected with NT or SETD2 siRNA. The clones used are the same as in (B); error bars show SEM from three independent experiments, $^{***}p < 0.001$.

(E) Western blot showing levels of KDM4A, H3K36me3 and H3 following KDM4A induction with 5 μg/ml doxycycline (DOX) for 72 hr in the KDM4A T-REx U2OS cells (see Experimental Procedures).

(F) RPA32 foci formation at indicated time after 2 hr CPT (10 μM) treatment in KDM4A T-REx cells treated with or without 5 μg/ml doxycycline (DOX). Error bars show SEM from three independent experiments, $^{*}p < 0.05$.

(G) RAD51 foci formation 8 hr after IR (5 Gy) in KDM4A T-REx cells treated with or without 5 μg/ml doxycycline (DOX). Error bars show SEM from three independent experiments. $^{*}p < 0.05$.

(H) HR repair efficacy in KDM4A T-REx DR-GFP U2OS cells treated with or without 5 μg/ml doxycycline (DOX). Error bars show SEM for three independent experiments. $^{**}p < 0.01$.

(I) Western blot showing levels of H3K36me3 and H3 in U2OS cells with stably integrated *H3.3* (control) or *H3.3K36M* lentiviral construct (see Supplemental Experimental Procedures).

(J) RPA32 foci formation at indicated time after 2 hr CPT (10 μM) treatment in H3.3 or H3.3K36M stable expression cells. Error bars show SEM from three independent experiments.

(K) RAD51 foci formation 8 hr after IR (5 Gy) in H3.3 or H3.3K36M stable expression cells. Error bars show SEM for three independent experiments, $^{*}p < 0.05$. See also Figure S4.

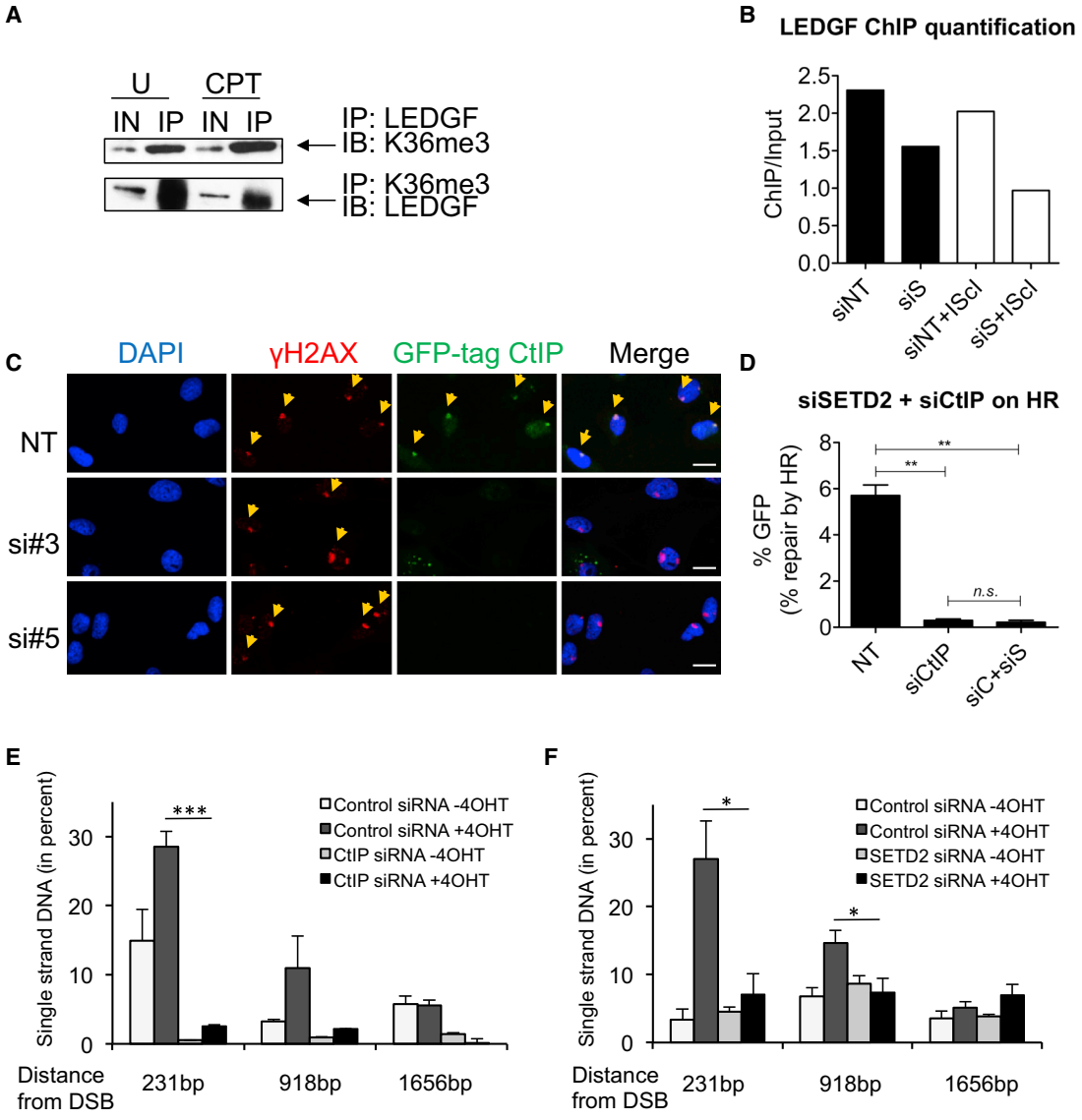


Figure 5. SETD2 Promotes HR through LEDGF/CtIP-Facilitated Resection

(A) Coimmunoprecipitation of LEDGF and H3K36me3 in the presence or absence of DNA damage. U2OS cells were left untreated (U) or treated with CPT (15 μM for 4 hr). Reciprocal co-IPs are shown.

(B) ChIP analysis of LEDGF binding to the DSB site before and after I-SceI induction in NT or SETD2 knockdown DR-GFP cells. siNT, control siRNA-treated cells before cut; siS, SETD2 siRNA-treated cells before cut; siNT+ISceI, control siRNA-treated cells after cut; siS+ISceI: SETD2 siRNA-treated cells after cut. Numbers were quantified from one ChIP-PCR experiment and show LEDGF-ChIP over input.

(C) Microirradiation showing CtIP recruitment to the damage site in U2OS cells treated with nontargeting control siRNA (NT) or SETD2 siRNAs (si#3 and si#5). Fluorescent images were acquired using a confocal microscope (Zeiss); scale bars, 20 μm.

(D) HR efficacy (as measured by GFP reporter assay as in Figure 2D) in cells transfected with control siRNA (NT) or CtIP siRNA (siCtIP) or both CtIP and SETD2 siRNA (siC+siS). Error bars show SEM from three independent experiments, **p < 0.01, n.s. not significant.

(E) CtIP depletion impedes resection at an AsiSI induced DSB. DNA was extracted from 4OHT-treated or untreated DIvA cells, transfected with control or CtIP siRNA, as indicated. Resection was analyzed, using a protocol detailed in Zhou et al. (2014), at an AsiSI-induced DSB reported to be repaired by a RAD51-dependent pathway (DSB-II in Aymard et al., 2014). The mean and SEM (n = 4, technical replicate) of a representative experiment are presented.

(F) SETD2 depletion impedes resection at an AsiSI induced DSB. DNA was extracted from 4OHT-treated or untreated DIvA cells, transfected with control or SETD2 siRNA, as indicated. Same as in (E) except that cells were transfected with a siRNA directed against SETD2. The mean and SEM (n = 4, technical replicate) of a representative experiment are presented. See also Figure S5.

These findings are consistent with the hypothesis that SETD2-dependent H3K36me3 promotes recruitment of CtIP by LEDGF to break sites.

Reduced CtIP recruitment, together with the reduced RPA foci formation following SETD2 depletion, suggested that SETD2-dependent H3K36 trimethylation might promote DSB resection.

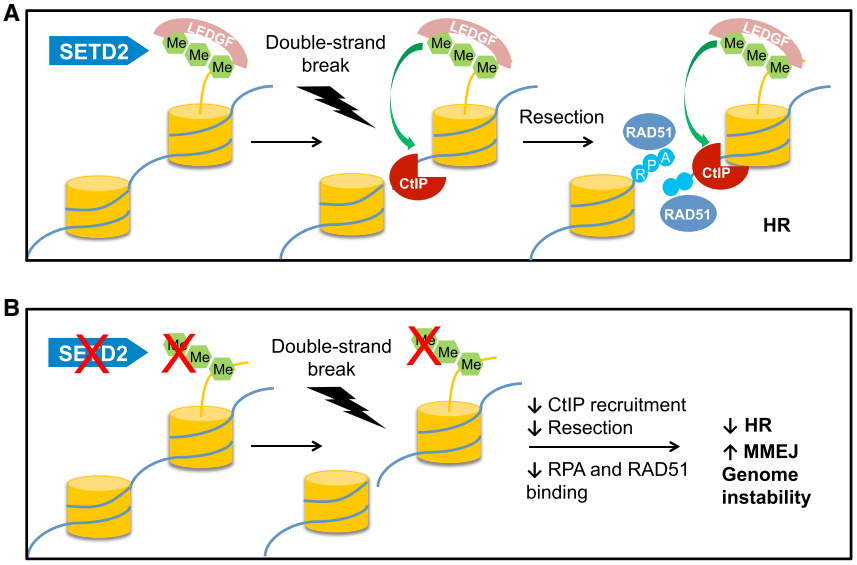


Figure 6. Model for the Role of SETD2-Dependent H3K36me3 in HR and Genome Stability

(A) SETD2-dependent H3K36 trimethylation constitutively recruits LEDGF to chromatin. Following DNA double-strand break, LEDGF recruits CtIP, thereby promoting resection, facilitating RPA and RAD51 recruitment.

(B) In the absence of H3K36 trimethylation, lack of LEDGF chromatin association results in reduced recruitment of CtIP after double-strand breaks, impairing resection and HR, leading to elevated levels of MMEJ and genome instability.

To directly measure resection, we used an in vivo resection assay (Zhou et al., 2014) in which levels of ssDNA were assessed at increasing distances from a specific DSB induced by the AsiSI restriction enzyme, which was found to recruit RAD51 (Iacovoni et al., 2010; Aymard et al., 2014). Following DSB induction (+4OHT), ssDNA was readily detected 231 bp from the AsiSI break site (DSB-II in Aymard et al., 2014) and at reduced levels further from the break site. Following CtIP depletion, ssDNA levels were significantly reduced at 231 bp ($p = 2.2 \times 10^{-5}$) and 918 bp ($p = 0.057$) from the break site compared to control siRNAs (Figure 5E). Following SETD2 depletion, ssDNA levels were also significantly reduced at 231 bp ($p = 0.021$) and 918 bp ($p = 0.037$) from the break site compared to control siRNAs (Figure 5F), and SETD2 depletion did not affect DSB induction at this site as assayed by XRCC4 ChIP (Figure S5B), thus confirming a role for SETD2 in facilitating DSB resection.

DISCUSSION

The *SETD2* gene encoding the H3K36 trimethyltransferase is among the most mutated in human cancers (Lawrence et al., 2014). Yet, how SETD2 functions to suppress the genome instability frequently observed in SETD2-deficient cancer cells is unknown (Sato et al., 2013; Zhu et al., 2014). Here, we describe a role for SETD2-dependent H3K36 trimethylation in facilitating error-free DSB repair and genome stability through efficient HR. Our data support a model in which LEDGF is constitutively anchored to H3K36me3-decorated chromatin through its PWWP domain. Upon DNA damage, chromatin-bound LEDGF recruits CtIP, which promotes resection—an essential step in HR repair (Figure 6A). In the absence of SETD2-dependent H3K36me3, the chromatin association of LEDGF is compromised, and DNA damage-induced CtIP recruitment is impaired, leading to reduced resection and HR and an increase in error-prone MMEJ and subsequent genome instability (Figure 6B). Our data do not, however, exclude the possibility that other H3K36me3 binding factors may also contribute to efficient HR.

The involvement of H3K36me3 in HR raises the question as to whether this histone mark is DSB inducible or preset to determine the choice of repair pathways. We did not detect any appreciable increase in H3K36me3 levels at the break site following I-SceI induction. These findings are consistent with previous observations indicating that H3K36me3 levels do not change following DNA damage, either globally (Fnu et al., 2011) or locally (Aymard et al., 2014; Pei et al., 2011). Given that SETD2-dependent H3K36 trimethylation strongly correlates with actively transcribed regions of the genome (Edmunds et al., 2008; Yoh et al., 2008), our findings thus support a spatial link between HR and transcriptionally active, H3K36me3 decorated regions of the genome. Indeed, because HR repair is usually error free, this would be expected to protect genome integrity following DSB induction or replication fork collapse at such sites, which would be important in maintaining cell homeostasis.

Genome-wide sequencing has suggested certain mutation signatures are associated with specific cancer types (Alexandrov et al., 2013) but lacks the power to identify driver mutations that give rise to that mutation signature. Here, we use a system to determine the impact of individual gene dysfunction on mutation patterns arising during the repair of a single DSB. We show that, by depleting SETD2 or RAD51 HR proteins, DSB induction leads to significantly increased mutation frequencies associated with deletions within six cell cycles (5 days). These findings identify a role for SETD2, like RAD51, in suppressing break-induced mutations. Further mechanistic analysis indicated that deletions arising from SETD2 or RAD51 depletion resulted from a significant increase in error-prone MMEJ. We propose that MMEJ arises from failed HR. SETD2 loss results in partial resection, short ssDNA 3′ ends and reduced RPA foci. These partially resected ends are insufficient to promote efficient HR and are no longer substrates for C-NHEJ. Instead, these partially resected ends become substrates for MMEJ. Similarly, following RAD51 depletion, whereas resection proceeds normally, HR is blocked presynaptically, resulting in the accumulation of longer unrepaired resected ends. Such ends are no longer substrates for C-NHEJ, and, because HR cannot proceed, the ends are instead

rejoined by MMEJ. Extensive resection following RAD51 loss facilitates annealing between regions of microhomology further from the break site, thus leading to larger deletions than those observed for SETD2. The observations that HR was significantly reduced whereas C-NHEJ was unchanged following SETD2 or RAD51 depletion are consistent with this model. Together, these findings suggest a role for HR in maintaining genome stability through suppression of MMEJ. This "real-time" mutation study can therefore provide important insights into how loss of these genes contributes to somatic mutation and intratumor heterogeneity, and it highlights the importance of HR repair genes in maintaining genome stability.

SETD2 is a tumor suppressor and its loss is an important step in the progression of a number of cancer types (Dalgliesh et al., 2010; Fontebasso et al., 2013; Gerlinger et al., 2012). Our findings provide mechanistic insights into how SETD2 functions as a tumor suppressor. Moreover, all three Tudor domain-containing KDM4/JMJD2 proteins (A, B, and C) are frequently overexpressed in various cancers, including breast, colorectal, lung, and prostate (Berry and Janknecht, 2013). Our findings predict that overexpression of these KDM4 family members causes genome instability and tumorigenesis through loss of H3K36me3-mediated HR repair. The identification of a role for H3K36me3 in facilitating HR repair, in addition to its recently described role in mismatch repair (Li et al., 2013), establishes the H3K36me3 chromatin mark as an important functional node for maintaining genome stability.

EXPERIMENTAL PROCEDURES

I-SceI-Inducible HPRT Mutation Assay

The reporter HT1080 cell line with a functional but I-SceI-cleavable *HPRT* gene was generated by inserting an 18 bp I-SceI recognition site into exon 6 of the *HPRT* gene using gene targeting. Reporter cells were transfected with the *I-SceI* plasmid 48 hr after siRNA knockdowns. The cells were allowed to repair in a nonselective medium for 5 days before seeding and selecting for HPRT-negative cells using 6-TG (15 μg/ml).

The mutation frequency was calculated as the number of HPRT-negative colonies divided by number of cells plated, after correcting for plating efficiency. To determine the mutation sequence, individual single-cell colonies were isolated, and genomic DNA spanning the DSB junction was PCR-amplified using the primers flanking the I-SceI site. Sequence alignment of the PCR products was conducted using the DNA Data Bank of Japan (DDBJ) ClustalW program.

In Vivo DNA End Resection Assay

DIvA cells (DSB Inducible via AsiSI [Aymard et al., 2014]) were transfected with siRNA using the Cell Line Nucleofactor kit V (Amaxa) according to the manufacturer's instructions. Forty-eight hours after siRNA transfection, cells were treated or not with 300 nM of 4-hydroxytamoxifen (4OHT) (Sigma; H7904) for 4 hr. DNA was purified using QIAGEN DNeasy kit. Single-stranded DNA generated at an AsiSI-induced DSB was analyzed using the procedure described in Zhou et al. (2014), with the modifications described in Supplemental Experimental Procedures. The percentage of ssDNA was calculated with the following equation: $ssDNA\% = 1/(2^{(\Delta Ct-1)} + 0.5) \times 100$, where ΔCt is calculated by subtracting the Ct obtained from mock-digested sample from the BanI-digested sample.

Generation of Inducible KDM4A Overexpression Cell Lines

U2OS-Flp-In/T-REx cells express the Tet repressor and contain a single Flp-In site (Gordon et al., 2009). U2OS-Flp-In/T-REx/DRGFP cells were generated by integrating the pDR-GFP expression plasmid (Pierce et al., 1999) into the U2OS-Flp-In/T-REx cells. The *KDM4A* cDNA (Genecopoeia) was cloned into the pDESTfrtto destination vector by a Gateway LR reaction (Life Technologies). U2OS-Flp-In/T-REx or U2OS-Flp-In/T-REx/DRGFP cells were cotransfected with the resulting *KDM4A* destination plasmid and pOG44 (Invitrogen). Stable clones that express the KDM4A protein under the control of the T-REx system were subjected to the treatments indicated.

Data Analysis

Data points from individual assays represent mean ± SEM. Statistical significance between two conditions was assessed by a two-tailed unpaired t test. $^*p < 0.05$, $^{**}p < 0.01$, $^{***}p < 0.001$, and n.s. represents $p \geq 0.05$.

Full details of all other experimental procedures are given in the Supplemental Experimental Procedures.

SUPPLEMENTAL INFORMATION

Supplemental Information includes Supplemental Experimental Procedures and five figures and can be found with this article online at http://dx.doi.org/10.1016/j.celrep.2014.05.026.

AUTHOR CONTRIBUTIONS

S.X.P., S.A., L.-P.Z., S.S., and F.A. designed and performed experiments. The HPRT$^+$:I-SceI assay was developed by A.C.G.P. The FLIP-IN cells and plasmids were developed by C.Z.B., T.C.H., A.C.G.P., T.H., N.B.L.T., and G.L. supervised the work. T.C.H. and S.X.P. wrote the manuscript with discussion and input from all authors. Experiments in Figure 1 were performed by S.A., with technology developed by A.C.G.P.; Figure 2 was performed by S.X.P. and S.A.; Figure 3 was performed by S.X.P. and L.-P.Z.; Figure 4 was performed by S.S. and S.X.P., with technology developed by C.Z.B.; Figure 5 was performed by S.S., L.-P.Z., S.X.P., and F.A.; Figure 6 was produced by S.X.P. Experiments in Figure S1 were performed by S.A. and S.S.; Figure S2 was performed by S.X.P. and S.A.; Figure S3 was performed by L.-P.Z.; Figure S4 was performed by S.X.P. and S.S.; Figure S5 was performed by F.A. and S.X.P.

ACKNOWLEDGMENTS

We thank David Allis for the *H3.3* and *H3.3K36M* lentiviral vectors; Catherine Millar for the U2OS-Flp-In/T-REx cell line; Atsushi Shibata and Hideaki Hogiwara for the NHEJ reporter cell line; Wojciech Niedzwiedz for the siRNAs against CtIP; and Annika Baude and Jiri Lukas for CtIP-GFP U2OS cells. We thank Mick Woodcock for helping with FACS analysis and Fereydoon Ahrabi for statistical analysis. We thank Peter McHugh and Valentine Macaulay for helpful discussions. This research was supported by the Medical Research Council (C.Z.B., T.H., S.S., T.C.H. grant R066538 and R19583), (L.-P.Z., N.B.L.T. grant ANRUBT00); Cancer Research UK (S.A. grant C5255/A15935) (L.-P.Z., N.L.T. grant 300/A13058); the Clarendon Scholarship (S.A., S.X.P.); the BBSRC (A.C.G.P. grant BB/H003371/1 and C.Z.B. grant BB/K019597/1); the Agence Nationale pour la Recherche (G.L. grant ANR-09-JCJC-0138); Association Contre le Cancer (G.L., F.A.); and the Torsten and Söderberg Foundation (T.H.).

Received: December 20, 2013
Revised: April 16, 2014
Accepted: May 12, 2014
Published: June 12, 2014

REFERENCES

Adamson, B., Smogorzewska, A., Sigoillot, F.D., King, R.W., and Elledge, S.J. (2012). A genome-wide homologous recombination screen identifies the RNA-binding protein RBMX as a component of the DNA-damage response. Nat. Cell Biol. *14*, 318–328.

Al Sarakbi, W., Sasi, W., Jiang, W.G., Roberts, T., Newbold, R.F., and Mokbel, K. (2009). The mRNA expression of SETD2 in human breast cancer: correlation with clinico-pathological parameters. BMC Cancer *9*, 290.

Alexandrov, L.B., Nik-Zainal, S., Wedge, D.C., Aparicio, S.A., Behjati, S., Biankin, A.V., Bignell, G.R., Bolli, N., Borg, A., Børresen-Dale, A.L., et al.; Australian Pancreatic Cancer Genome Initiative; ICGC Breast Cancer Consortium; ICGC MMML-Seq Consortium; ICGC PedBrain (2013). Signatures of mutational processes in human cancer. Nature *500*, 415–421.

Arnaudeau, C., Lundin, C., and Helleday, T. (2001). DNA double-strand breaks associated with replication forks are predominantly repaired by homologous recombination involving an exchange mechanism in mammalian cells. J. Mol. Biol. *307*, 1235–1245.

Aymard, F., Bugler, B., Schmidt, C.K., Guillou, E., Caron, P., Briois, S., Iacovoni, J.S., Daburon, V., Miller, K.M., Jackson, S.P., and Legube, G. (2014). Transcriptionally active chromatin recruits homologous recombination at DNA double-strand breaks. Nat. Struct. Mol. Biol. *21*, 366–374.

Berry, W.L., and Janknecht, R. (2013). KDM4/JMJD2 histone demethylases: epigenetic regulators in cancer cells. Cancer Res. *73*, 2936–2942.

Black, J.C., Manning, A.L., Van Rechem, C., Kim, J., Ladd, B., Cho, J., Pineda, C.M., Murphy, N., Daniels, D.L., Montagna, C., et al. (2013). KDM4A lysine demethylase induces site-specific copy gain and rereplication of regions amplified in tumors. Cell *154*, 541–555.

Couture, J.F., Collazo, E., Ortiz-Tello, P.A., Brunzelle, J.S., and Trievel, R.C. (2007). Specificity and mechanism of JMJD2A, a trimethyllysine-specific histone demethylase. Nat. Struct. Mol. Biol. *14*, 689–695.

Dalgliesh, G.L., Furge, K., Greenman, C., Chen, L., Bignell, G., Butler, A., Davies, H., Edkins, S., Hardy, C., Latimer, C., et al. (2010). Systematic sequencing of renal carcinoma reveals inactivation of histone modifying genes. Nature *463*, 360–363.

Daugaard, M., Baude, A., Fugger, K., Povlsen, L.K., Beck, H., Sørensen, C.S., Petersen, N.H., Sorensen, P.H., Lukas, C., Bartek, J., et al. (2012). LEDGF (p75) promotes DNA-end resection and homologous recombination. Nat. Struct. Mol. Biol. *19*, 803–810.

Edmunds, J.W., Mahadevan, L.C., and Clayton, A.L. (2008). Dynamic histone H3 methylation during gene induction: HYPB/Setd2 mediates all H3K36 trimethylation. EMBO J. *27*, 406–420.

Eidahl, J.O., Crowe, B.L., North, J.A., McKee, C.J., Shkriabai, N., Feng, L., Plumb, M., Graham, R.L., Gorelick, R.J., Hess, S., et al. (2013). Structural basis for high-affinity binding of LEDGF PWWP to mononucleosomes. Nucleic Acids Res. *41*, 3924–3936.

Fnu, S., Williamson, E.A., De Haro, L.P., Brenneman, M., Wray, J., Shaheen, M., Radhakrishnan, K., Lee, S.H., Nickoloff, J.A., and Hromas, R. (2011). Methylation of histone H3 lysine 36 enhances DNA repair by nonhomologous end-joining. Proc. Natl. Acad. Sci. USA *108*, 540–545.

Fontebasso, A.M., Schwartzentruber, J., Khuong-Quang, D.A., Liu, X.Y., Sturm, D., Korshunov, A., Jones, D.T., Witt, H., Kool, M., Albrecht, S., et al. (2013). Mutations in SETD2 and genes affecting histone H3K36 methylation target hemispheric high-grade gliomas. Acta Neuropathol. *125*, 659–669.

Gerlinger, M., Rowan, A.J., Horswell, S., Larkin, J., Endesfelder, D., Gronroos, E., Martinez, P., Matthews, N., Stewart, A., Tarpey, P., et al. (2012). Intratumor heterogeneity and branched evolution revealed by multiregion sequencing. N. Engl. J. Med. *366*, 883–892.

Gordon, W.R., Vardar-Ulu, D., L'Heureux, S., Ashworth, T., Malecki, M.J., Sanchez-Irizarry, C., McArthur, D.G., Histen, G., Mitchell, J.L., Aster, J.C., and Blacklow, S.C. (2009). Effects of S1 cleavage on the structure, surface export, and signaling activity of human Notch1 and Notch2. PLoS ONE *4*, e6613.

Heyer, W.D., Ehmsen, K.T., and Liu, J. (2010). Regulation of homologous recombination in eukaryotes. Annu. Rev. Genet. *44*, 113–139.

Iacovoni, J.S., Caron, P., Lassadi, I., Nicolas, E., Massip, L., Trouche, D., and Legube, G. (2010). High-resolution profiling of gammaH2AX around DNA double strand breaks in the mammalian genome. EMBO J. *29*, 1446–1457.

Jasin, M. (1996). Genetic manipulation of genomes with rare-cutting endonucleases. Trends Genet. *12*, 224–228.

Jeggo, P., and Lavin, M.F. (2009). Cellular radiosensitivity: how much better do we understand it? Int. J. Radiat. Biol. *85*, 1061–1081.

Klose, R.J., Yamane, K., Bae, Y., Zhang, D., Erdjument-Bromage, H., Tempst, P., Wong, J., and Zhang, Y. (2006). The transcriptional repressor JHDM3A demethylates trimethyl histone H3 lysine 9 and lysine 36. Nature *442*, 312–316.

Lawrence, M.S., Stojanov, P., Mermel, C.H., Robinson, J.T., Garraway, L.A., Golub, T.R., Meyerson, M., Gabriel, S.B., Lander, E.S., and Getz, G. (2014). Discovery and saturation analysis of cancer genes across 21 tumour types. Nature *505*, 495–501.

Lewis, P.W., Müller, M.M., Koletsky, M.S., Cordero, F., Lin, S., Banaszynski, L.A., Garcia, B.A., Muir, T.W., Becher, O.J., and Allis, C.D. (2013). Inhibition of PRC2 activity by a gain-of-function H3 mutation found in pediatric glioblastoma. Science *340*, 857–861.

Li, F., Mao, G., Tong, D., Huang, J., Gu, L., Yang, W., and Li, G.M. (2013). The histone mark H3K36me3 regulates human DNA mismatch repair through its interaction with MutSα. Cell *153*, 590–600.

Lieber, M.R. (2010). The mechanism of double-strand DNA break repair by the nonhomologous DNA end-joining pathway. Annu. Rev. Biochem. *79*, 181–211.

McVey, M., and Lee, S.E. (2008). MMEJ repair of double-strand breaks (director's cut): deleted sequences and alternative endings. Trends Genet. *24*, 529–538.

Moynahan, M.E., Cui, T.Y., and Jasin, M. (2001). Homology-directed dna repair, mitomycin-c resistance, and chromosome stability is restored with correction of a Brca1 mutation. Cancer Res. *61*, 4842–4850.

Newbold, R.F., and Mokbel, K. (2010). Evidence for a tumour suppressor function of SETD2 in human breast cancer: a new hypothesis. Anticancer Res. *30*, 3309–3311.

Ogiwara, H., Ui, A., Otsuka, A., Satoh, H., Yokomi, I., Nakajima, S., Yasui, A., Yokota, J., and Kohno, T. (2011). Histone acetylation by CBP and p300 at double-strand break sites facilitates SWI/SNF chromatin remodeling and the recruitment of non-homologous end joining factors. Oncogene *30*, 2135–2146.

Pei, H., Zhang, L., Luo, K., Qin, Y., Chesi, M., Fei, F., Bergsagel, P.L., Wang, L., You, Z., and Lou, Z. (2011). MMSET regulates histone H4K20 methylation and 53BP1 accumulation at DNA damage sites. Nature *470*, 124–128.

Pierce, A.J., Johnson, R.D., Thompson, L.H., and Jasin, M. (1999). XRCC3 promotes homology-directed repair of DNA damage in mammalian cells. Genes Dev. *13*, 2633–2638.

Rea, S., Eisenhaber, F., O'Carroll, D., Strahl, B.D., Sun, Z.W., Schmid, M., Opravil, S., Mechtler, K., Ponting, C.P., Allis, C.D., and Jenuwein, T. (2000). Regulation of chromatin structure by site-specific histone H3 methyltransferases. Nature *406*, 593–599.

Sartori, A.A., Lukas, C., Coates, J., Mistrik, M., Fu, S., Bartek, J., Baer, R., Lukas, J., and Jackson, S.P. (2007). Human CtIP promotes DNA end resection. Nature *450*, 509–514.

Sato, Y., Yoshizato, T., Shiraishi, Y., Maekawa, S., Okuno, Y., Kamura, T., Shimamura, T., Sato-Otsubo, A., Nagae, G., Suzuki, H., et al. (2013). Integrated molecular analysis of clear-cell renal cell carcinoma. Nat. Genet. *45*, 860–867.

Shanbhag, N.M., Rafalska-Metcalf, I.U., Balane-Bolivar, C., Janicki, S.M., and Greenberg, R.A. (2010). ATM-dependent chromatin changes silence transcription in cis to DNA double-strand breaks. Cell *141*, 970–981.

Smeenk, G., and van Attikum, H. (2013). The chromatin response to DNA breaks: leaving a mark on genome integrity. Annu. Rev. Biochem. *82*, 55–80.

Strahl, B.D., Grant, P.A., Briggs, S.D., Sun, Z.W., Bone, J.R., Caldwell, J.A., Mollah, S., Cook, R.G., Shabanowitz, J., Hunt, D.F., and Allis, C.D. (2002). Set2 is a nucleosomal histone H3-selective methyltransferase that mediates transcriptional repression. Mol. Cell. Biol. *22*, 1298–1306.

Sugiyama, T., New, J.H., and Kowalczykowski, S.C. (1998). DNA annealing by RAD52 protein is stimulated by specific interaction with the complex of replication protein A and single-stranded DNA. Proc. Natl. Acad. Sci. USA *95*, 6049–6054.

Symington, L.S., and Gautier, J. (2011). Double-strand break end resection and repair pathway choice. Annu. Rev. Genet. *45*, 247–271.

Wagner, E.J., and Carpenter, P.B. (2012). Understanding the language of Lys36 methylation at histone H3. Nat. Rev. Mol. Cell Biol. *13*, 115–126.

OPEN
ACCESS
CellPress

Whetstine, J.R., Nottke, A., Lan, F., Huarte, M., Smolikov, S., Chen, Z., Spooner, E., Li, E., Zhang, G., Colaiacovo, M., and Shi, Y. (2006). Reversal of histone lysine trimethylation by the JMJD2 family of histone demethylases. Cell *125*, 467–481.

Yoh, S.M., Lucas, J.S., and Jones, K.A. (2008). The Iws1:Spt6:CTD complex controls cotranscriptional mRNA biosynthesis and HYPB/Setd2-mediated histone H3K36 methylation. Genes Dev. *22*, 3422–3434.

Zhang, J., Ding, L., Holmfeldt, L., Wu, G., Heatley, S.L., Payne-Turner, D., Easton, J., Chen, X., Wang, J., Rusch, M., et al. (2012). The genetic basis of early T-cell precursor acute lymphoblastic leukaemia. Nature *481*, 157–163.

Zhou, Y., Caron, P., Legube, G., and Paull, T.T. (2014). Quantitation of DNA double-strand break resection intermediates in human cells. Nucleic Acids Res. *42*, e19.

Zhu, X., He, F., Zeng, H., Ling, S., Chen, A., Wang, Y., Yan, X., Wei, W., Pang, Y., Cheng, H., et al. (2014). Identification of functional cooperative mutations of SETD2 in human acute leukemia. Nat. Genet. *46*, 287–293.

7. Cheong, C.G. & Hall, T.M.T. *Proc. Natl. Acad. Sci. USA* **103**, 13635–13639 (2006).
8. Choudhury, R., Tsai, Y.S., Dominguez, D., Wang, Y. & Wang, Z. *Nat. Commun.* **3**, 1147 (2012).
9. Cooke, A., Prigge, A., Opperman, L. & Wickens, M. *Proc. Natl. Acad. Sci. USA* **108**, 15870–15875 (2011).
10. Ozawa, T., Natori, Y., Sato, M. & Umezawa, Y. *Nat. Methods* **4**, 413–419 (2007).
11. Tilsner, J. *et al. Plant J.* **57**, 758–770 (2009).
12. Wang, Y., Cheong, C.G., Hall, T.M.T. & Wang, Z. *Nat. Methods* **6**, 825–830 (2009).
13. Gerber, A.P., Herschlag, D. & Brown, P.O. *PLoS Biol.* **2**, E79 (2004).
14. Opperman, L., Hook, B., DeFino, M., Bernstein, D.S. & Wickens, M. *Nat. Struct. Mol. Biol.* **12**, 945–951 (2005).
15. Miller, M.T., Higgin, J.J. & Hall, T.M.T. *Nat. Struct. Mol. Biol.* **15**, 397–402 (2008).
16. Wang, Y., Opperman, L., Wickens, M. & Hall, T.M.T. *Proc. Natl. Acad. Sci. USA* **106**, 20186–20191 (2009).
17. Campbell, Z.T. *et al. Cell Reports* **1**, 570–581 (2012).
18. Zhu, D., Stumpf, C.R., Krahn, J.M., Wickens, M. & Hall, T.M.T. *Proc. Natl. Acad. Sci. USA* **106**, 20192–20197 (2009).
19. Qiu, C. *et al. J. Biol. Chem.* **287**, 6949–6957 (2012).
20. Koh, Y.Y. *et al. RNA* **17**, 718–727 (2011).

SET-ting the stage for DNA repair

Deepak K Jha, Sophia X Pfister, Timothy C Humphrey & Brian D Strahl

Mechanisms of DNA damage repair within actively transcribed genes are poorly understood. Five new reports shed light on the contributions of chromatin to this process by uncovering roles for histone H3 Lys36 methylation, a post-translational modification previously linked to transcription elongation, in the control of DNA-damage signaling and double strand break repair.

© 2014 Nature America, Inc. All rights reserved.

Eukaryotic cells experience a plethora of DNA lesions, the most severe form being a DNA double-strand break (DSB), which can result in chromosomal rearrangements or cell death. DSBs can be caused by endogenous events (for example, meiotic DSBs or replication through single-stranded nicks) and exogenous agents (for example, exposure to gamma radiation)[1]. Cells respond to DSBs by activating the DNA-damage response (DDR), which performs a number of functions including delaying the cell cycle to facilitate DNA repair. In mammalian cells, induction of DSBs activates the ATM and ATR (Tel1 and Mec1 in budding yeast) kinase signaling cascades resulting in phosphorylation of downstream substrates such as histone H2A.X (H2A in yeast) and 53BP1 (Rad9 in yeast)[2]. Two major pathways, nonhomologous end joining (NHEJ) and homologous recombination (HR), repair the majority of DSBs[3], and pathway choice is contingent on whether DSB ends are resected or not. This is dependent on the balance between factors promoting NHEJ (Ku, 53BP1 and RIF1) and resection (CtIP, MRN, EXO1, BLM and DNA2)[3], which is in turn influenced by chromatin structure and the phase of the cell cycle in which DNA damage occurs[3].

An emerging theme is the critical part that chromatin plays in multiple aspects of the cellular response to DSBs[4]. Methylation of histone H3 Lys36 (H3K36) is a post-translational modification conserved in eukaryotes from yeast to humans. In yeast, Set2 is the sole methyltransferase that catalyzes H3K36 mono-, di- and trimethylation (to form H3K36me1, H3K36me2 and H3K36me3, respectively), whereas its human ortholog, SETD2, catalyzes formation of only H3K36me3 (ref. 5). Through an association with the hyperphosphorylated, elongating form of RNA polymerase II (RNAPII), Set2 (SETD2) is recruited to the bodies of actively transcribed genes, where it catalyzes H3K36 methylation. One major function of Set2-mediated H3K36 di- and trimethylation in budding yeast is the recruitment and activation of a histone deacetylase complex (Rpd3S) as well as an ATP-dependent chromatin-remodeling complex (Isw1b)[5]. These complexes function in the wake of elongating RNAPII to maintain chromatin integrity by creating a compact chromatin environment restrictive to intragenic or 'cryptic' transcription. In human cells, H3K36me2 formation catalyzed by SETMAR (Metnase) has been implicated in NHEJ[6]. H3K36me3 formation catalyzed by SETD2 also prevents cryptic transcription[5] and regulates alternative splicing[7] and mismatch repair[8]. Five recent papers[9–13] further expand the known functions of Set2 (SETD2) and H3K36 methylation by demonstrating their involvement in DDR and DSB repair. Here, we draw evidence from these five publications to compare and contrast the emerging roles of yeast Set2 and human SETD2 in three main aspects of DSB repair—DDR and repair-pathway choice as well as the link between transcription and DNA repair.

Two of the aforementioned studies, Carvalho *et al.*[10] and Jha and Strahl[11], support roles for yeast Set2 and human SETD2 in DNA damage–checkpoint activation. Using budding yeast as a model system, Jha and Strahl[11] show that loss of H3K36 methylation resulting from Set2 deletion (*set2Δ*) leads to reduced phosphorylation of histone H2A Ser129 and Rad53, thus signifying attenuated DNA damage–checkpoint activation. Similarly, using human clear cell renal cell carcinoma (ccRCC) cell lines, Carvalho *et al.*[10] show that activation of DDR is defective in SETD2-deficient or SETD2-depleted cells, as measured by reduced ATM activation, γ-H2AX, delayed 53BP1 recruitment to DNA-damage sites, decreased p53 stabilization and downstream activation of p21 (ref. 10), the major cyclin-dependent kinase inhibitor that is required for DNA damage–dependent cell-cycle arrest. These findings are consistent with a reported role for Set2 in checkpoint activation in fission yeast[14], and they indicate that Set2 (SETD2) affects a very early aspect of DNA-damage sensing.

In two yeast model systems, both Jha and Strahl[11] (in budding yeast) and Pai *et al.*[12] (in fission yeast) show that Set2 promotes NHEJ (**Fig. 1a**). Jha and Strahl[11] show that deletion of *SET2* or mutation of H3K36 is sensitive to DSBs induced by phleomycin, radiation or a homothalic (HO) endonuclease. In the case of fission yeast, Pai *et al.*[12] show that Set2 promotes Ku recruitment and/or retention at a DSB. Using a minichromosome-based DSB repair assay, they show that loss of Set2 substantially increases the frequency of gene conversion, thus suggesting that Set2 inhibits

Deepak K. Jha and Brian D. Strahl are at the Department of Biochemistry and Biophysics, University of North Carolina at Chapel Hill, North Carolina, USA, and Brian D. Strahl is also at the Lineberger Comprehensive Cancer Center, University of North Carolina at Chapel Hill, North Carolina, USA. Sophia X. Pfister and Timothy C. Humphrey are at the Cancer Research UK and Medical Research Council Oxford Institute for Radiation Oncology, Department of Oncology, University of Oxford, Oxford, UK.
e-mail: timothy.humphrey@oncology.ox.ac.uk or brian_strahl@med.unc.edu

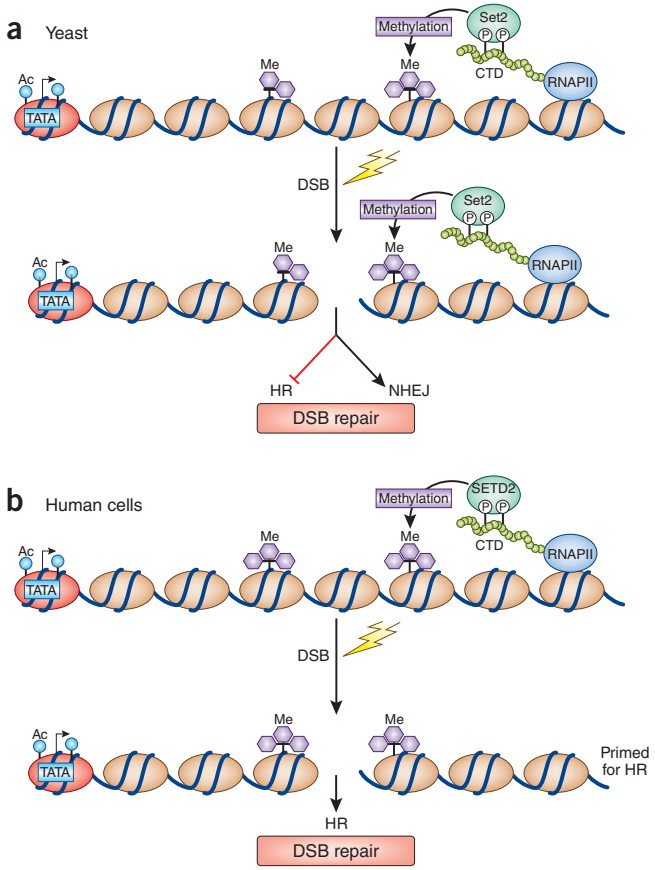


Figure 1 H3K36 methylation functions in DSB sensing and repair. (**a**) In the context of transcribing RNAPII, yeast Set2 catalyzes all forms of H3K36 methylation (mono-, di- and trimethylation). Set2 methylation contributes to transcription elongation by recruiting deacetylases and ATP-dependent remodeling complexes to maintain chromatin integrity. Five recent reports[9–13] identify a new role for Set2 in DSB repair. In budding and fission yeast, Set2 is recruited to sites of DSBs in an RNAPII-dependent manner. H3K36 methylation regulates DNA-integrity-checkpoint activation, chromatin architecture at DSBs and repair-pathway choice (preference for NHEJ). P denotes phosphorylation. (**b**) In human cells, preexisting H3K36me3 marks generated by SETD2 during transcription are used to anchor LEDGF, which in turn recruits CtIP after DSB induction to promote DNA end resection and repair of the DSB via HR. The lightning bolt indicates a DNA-damage event generating a DSB, and red nucleosomes indicate the +1 nucleosome at the 5′ end of genes, which typically contains the H2A variant H2A.Z (Htz1) and is marked by histone acetylation. CTD, C-terminal domain.

HR. Similarly, Jha and Strahl[11] observed that when a linearized plasmid was transformed into *set2*Δ cells, religation efficiency was significantly increased and was almost entirely dependent on Rad51, an HR component. This suggests that loss of Set2 favors repair via HR. Consistently with these observations, these yeast studies indicate that loss of Set2 results in a relatively open chromatin structure, as measured by chromatin immunoprecipitation (ChIP) of acetylated histone H4, Htz1 (the yeast homolog of the mammalian H2A variant H2A.Z) and micrococcal nuclease digestion. This in turn increases resection kinetics (as measured by loss of input DNA signal, increased recruitment of RPA by ChIP in G1-arrested cells and increased RPA recruitment by immunofluorescence), indicating that loss of Set2 promotes recruitment of the HR repair machinery.

These yeast studies also reveal that H3K36 modification influences repair-pathway choice. Pai *et al.*[12] demonstrate an antagonistic relationship between H3K36me3 and acetylated H3K36 (H3K36ac) by showing that deletion of Set2 increases the level of H3K36ac and reduces NHEJ. Conversely, deletion of the H3K36 acetyltransferase Gcn5 increases the level of H3K36me3 and reduces HR. Collectively, these results suggest that Set2 and Gcn5 compete to modify H3K36, creating a 'chromatin switch' between NHEJ and HR. Furthermore, they show that H3K36me levels are high in G1 and that H3K36ac levels are high in S-G2, and the cell-cycle distribution of these histone modifications conforms to the preferred repair pathway in each cell-cycle phase: NHEJ in G1 and HR in S-G2.

In contrast to the above findings, human SETD2 is required for HR (**Fig. 1b**). Using a well-established GFP reporter system in which repair of an I-SceI endonuclease–induced DSB by HR generates an intact GFP gene, Aymard *et al.*[9], Carvalho *et al.*[10] and Pfister *et al.*[13] show that short interfering RNA–mediated depletion of SETD2 results in reduced HR. Loss of SETD2 also reduces the formation of RPA foci[13] and RAD51 foci[10,13] and the recruitment of RAD51 to DSBs, as measured by ChIP[9,13]. Moreover, SETD2 depletion reduces DSB end resection, as shown by an *in vivo* assay measuring single-stranded DNA generated by the resection machinery in the vicinity of a DSB[13]. Together, the Aymard *et al.*[9] and Pfister *et al.*[13] studies support a model in which SETD2-dependent H3K36me3 anchors lens epithelium–derived growth factor p75 (LEDGF) to chromatin through its PWWP domain. After DSB induction, chromatin-bound LEDGF recruits the resection enzyme CtIP, which in turn promotes resection and recruitment of RAD51. However, Carvalho *et al.*[10] found that RAD51 recruitment was reduced without defects in resection[10].

In contrast to the observations in human cells, both yeast papers[11,12] show that Set2 and H3K36 methylation negatively regulate DNA end resection. One reason for the apparent discrepancy could arise from the possibility that in the absence of SETD2, reduced damage-induced γ-H2AX phosphorylation may lead to reduced 53BP1 recruitment, thereby permitting resection[3], a result alluded to in Carvalho *et al.*[10] However, resection in mammalian cells is compromised by the additional requirement for SETD2 to recruit CtIP, in a LEDGF-dependent manner[9,13]. In yeast, loss of Set2 may similarly reduce Rad9 (53BP1) recruitment through reduced H2A phosphorylation or other checkpoint-dependent events, thus permitting resection. Nevertheless, LEDGF is not evolutionarily conserved in budding and fission yeast. Thus, in yeast, in contrast to mammalian cells, Sae2 (CtIP) may be recruited to DSB sites independently of Set2, thereby promoting efficient resection and HR. In addition, Set2 in yeast catalyzes mono-, di- and trimethylation of H3K36, whereas human SETD2 catalyzes only H3K36 trimethylation. Therefore, the differences between yeast and human cells could also be a result of different methylation states having different, perhaps even opposing, functions after DSBs are formed. Indeed, human H3K36me2 promotes NHEJ, whereas H3K36me3 promotes HR[6]. Moreover, SETD2 is substantially larger than the yeast Set2 proteins, with an extended uncharacterized N terminus that may have unique functions in the repair process.

The demonstrated role of Set2 (SETD2) in DNA repair raises the question of whether

© 2014 Nature America, Inc. All rights reserved.

H3K36me3 levels increase in response to DNA damage. In the two yeast systems, H3K36me3 rapidly accumulated at the site of DSBs[11,12], but in human cells, no increase in SETD2 or H3K36me3 was observed at DSB sites[9,10,13], thus suggesting that H3K36me3 levels are preset, presumably by prior transcription, and may be sufficient for downstream functions in DSB repair. Indeed, Aymard *et al.*[9] show that, in human cells, HR preferentially repairs transcriptionally active regions. They used a rare-cutting endonuclease (AsiSI) to generate around 150 DSBs across the genome, which were then subdivided into RAD51- or XRCC1-enriched DSBs by ChIP-sequencing[9]. RAD51 enrichment implied the use of HR, whereas XRCC1 enrichment suggested that the DSB was being repaired by NHEJ. Surprisingly, RAD51-enriched DSBs tended to occur in transcriptionally active regions, and this preference was lost when transcription was abolished by addition of the transcriptional inhibitor DRB. Conversely, reactivating a repressed gene directed DSB repair toward HR. Given that H3K36me3 is correlated with transcription frequency and gene length in yeast, it will be interesting to investigate how DSBs are repaired in genes of varying lengths and transcription rates in human cells.

Additional support for a transcription-coupled function for Set2 and H3K36 methylation is provided by Jha and Strahl[11]. By using a truncated form of Set2 that inhibits its interaction with RNAPII, these authors demonstrate that Set2 association with RNAPII is critical for its DNA-repair function. Furthermore, Jha and Strahl[11] observed a substantial reduction in the protein levels of Set2 and RNAPII after DSB induction, and they found this reduction to be proteasome dependent. Why RNAPII and Set2 are degraded after DSB induction remains unclear, but the requirement to prevent transcription around a DSB to allow for DNA repair events might offer a plausible explanation. The interaction of Set2 with RNAPII is conserved in human cells as well, thus raising the intriguing possibility that the role defined for H3K36 methylation in DSB signaling and repair could be intertwined with transcription elongation in all organisms. Further studies are needed to elucidate how transcription-dependent H3K36 methylation regulates DSB repair.

The identification of a role for H3K36me3 in HR in human cells contrasts with a previous report, which showed that SETMAR (Metnase)-mediated H3K36me2 promotes DSB repair through NHEJ[6]. The distinct repair pathways associated with H3K36 dimethylation (NHEJ) and trimethylation (HR) suggest the tantalizing prospect that, in mammalian cells as in yeast, H3K36 modification contributes to choice of DSB repair pathway, albeit via different histone marks. However, studies by Pfister *et al.*[13] show that depleting SETD2-dependent H3K36 trimethylation results in reduced HR, whereas NHEJ remains unchanged. The authors inferred the pathways mediating DSB repair by inducing a break within the *HPRT* gene by using I-SceI and sequencing the repair products. Surprisingly, depleting either SETD2 or RAD51 resulted in a substantial increase in microdeletions, with break junctions being associated with regions of microhomology (2–4 bp) on either side of the break site. These findings suggest that HR genes may suppress microhomology-mediated end joining (MMEJ), a repair process dependent on short stretches of microhomology[15]. Microdeletions also frequently occur in cancer cells, and the observation that SETD2 loss increases the incidence of microdeletions has repercussions for tumorigenesis in cancers such as ccRCC, in which SETD2 is frequently mutated[16].

If H3K36me functions in DSB repair, this histone mark would be expected to help to maintain genome integrity. In agreement with this hypothesis, Putnam *et al.*[17] have shown that the *SET2* gene of budding yeast genetically interacts with genes that suppress gross chromosomal rearrangement (such as *MRE11* and *RAD9*), thereby reinforcing the idea that loss of Set2 might contribute to chromosomal abnormalities. Furthermore, and outside of DSB repair, Li *et al.*[8] have shown that H3K36 trimethylation by SETD2 also contributes to DNA mismatch repair in an MSH6-dependent manner. The authors found that MSH6 is recruited to chromatin via interaction of its PWWP domain with H3K36me3, and that it aids in repairing nucleotide mismatches. The identification of roles for SETD2 and H3K36me3 in DDR, DSB repair and mismatch repair provide new mechanistic insights into how SETD2 may function as a tumor suppressor.

Some outstanding issues relating to Set2 (SETD2) and genome stability raised by these studies include: (i) What is the mechanism by which SETD2 promotes DNA-damage-checkpoint activation? (ii) Is there any correlation between transcription rate or gene length and the repair proficiency of DSBs induced in gene bodies? (iii) What is the mechanistic basis and significance of RNAPII degradation after DSB induction? (iv) What is the contribution of SETD2 (and H3K36me3) loss–dependent MMEJ to chromosomal aberrations in tumorigenesis? Although many mechanistic questions remain, these recent findings clearly define H3K36me as a critically important and evolutionarily conserved chromatin mark in maintaining genome stability. Future work to further define how Set2 (SETD2) contributes to DNA repair in the context of transcription will be needed to illuminate its role in this process as well as in human disease.

COMPETING FINANCIAL INTERESTS
The authors declare no competing financial interests.

1. Hoeijmakers, J.H. *N. Engl. J. Med.* **361**, 1475–1485 (2009).
2. Polo, S.E. & Jackson, S.P. *Genes Dev.* **25**, 409–433 (2011).
3. Chapman, J.R., Taylor, M.R. & Boulton, S.J. *Mol. Cell* **47**, 497–510 (2012).
4. Papamichos-Chronakis, M. & Peterson, C.L. *Nat. Rev. Genet.* **14**, 62–75 (2013).
5. Venkatesh, S. & Workman, J.L. *Wiley Interdiscip. Rev. Dev. Biol.* **2**, 685–700 (2013).
6. Fnu, S. *et al. Proc. Natl. Acad. Sci. USA* **108**, 540–545 (2011).
7. Luco, R.F. *et al. Science* **327**, 996–1000 (2010).
8. Li, F. *et al. Cell* **153**, 590–600 (2013).
9. Aymard, F. *et al. Nat. Struct. Mol. Biol.* **21**, 366–374 (2014).
10. Carvalho, S. *et al. eLife* **3**, e02482 (2014).
11. Jha, D.K. & Strahl, B.D. *Nat. Commun.* **5**, 3965 (2014).
12. Pai, C.C. *et al. Nat. Commun.* **5**, 4091 (2014).
13. Pfister, S.X. *et al. Cell Reports* **7**, 2006–2018 (2014).
14. Kim, H.S., Rhee, D.K. & Jang, Y.K. *Biochem. Biophys. Res. Commun.* **368**, 419–425 (2008).
15. Symington, L.S. & Gautier, J. *Annu. Rev. Genet.* **45**, 247–271 (2011).
16. Lawrence, M.S. *et al. Nature* **505**, 495–501 (2014).
17. Putnam, C.D. *et al. Proc. Natl. Acad. Sci. USA* **109**, E3251–E3259 (2012).

© 2014 Nature America, Inc. All rights reserved.

Bibliography

Aarts, M., Sharpe, R., Garcia-Murillas, I., Gevensleben, H., Hurd, M. S., Shumway, S. D., Toniatti, C., Ashworth, A. and Turner, N. C. (2012). Forced mitotic entry of S-phase cells as a therapeutic strategy induced by inhibition of WEE1. Cancer Discov. *2*, 524–539.

Adamson, B., Smogorzewska, A., Sigoillot, F. D., King, R. W. and Elledge, S. J. (2012). A genome-wide homologous recombination screen identifies the RNA-binding protein RBMX as a component of the DNA-damage response. Nat. Cell Biol. *14*, 318–328.

Ahn, J., Urist, M. and Prives, C. (2004). The Chk2 protein kinase. DNA Repair *3*, 1039–47.

Al-minawi, A. Z., Saleh-gohari, N. and Helleday, T. (2008). The ERCC1/XPF endonuclease is required for efficient single-strand annealing and gene conversion in mammalian cells. Nucleic Acids Res. *36*, 1–9.

Al Sarakbi, W., Sasi, W., Jiang, W. G., Roberts, T., Newbold, R. F. and Mokbel, K. (2009). The mRNA expression of SETD2 in human breast cancer: correlation with clinico-pathological parameters. BMC Cancer *9*, 290.

Arnaudeau, C., Lundin, C. and Helleday, T. (2001). DNA double-strand breaks associated with replication forks are predominantly repaired by homologous recombination involving an exchange mechanism in mammalian cells. J. Mol. Biol. *307*, 1235–1245.

Aymard, F., Bugler, B., Schmidt, C. K., Guillou, E., Caron, P., Briois, S., Iacovoni, J. S., Daburon, V., Miller, K. M., Jackson, S. P. and Legube, G. (2014). Transcriptionally active chromatin recruits homologous recombination at DNA double-strand breaks. Nat. Struct. Mol. Biol. *21*, 366–74.

Barber, L. J., Youds, J. L., Ward, J. D., McIlwraith, M. J., O'Neil, N. J., Petalcorin, M. I. R., Martin, J. S., Collis, S. J., Cantor, S. B., Auclair, M., Tissenbaum, H., West, S. C., Rose, A. M. and Boulton, S. J. (2008). RTEL1 Maintains Genomic Stability by Suppressing Homologous Recombination. Cell *135*, 261–271.

Bartek, J., Lukas, C. and Lukas, J. (2004). Checking on DNA damage in S phase. Nat. Rev. Mol. Cell Biol. *5*, 792–804.

Barton, O., Naumann, S. C., Diemer-Biehs, R., Künzel, J., Steinlage, M., Conrad, S., Makharashvili, N., Wang, J., Feng, L., Lopez, B. S., Paull, T. T., Chen, J., Jeggo, P. A. and Löbrich, M. (2014). Polo-like kinase 3 regulates CtIP during DNA double-strand break repair in G1. J. Cell Biol. *206*, 877–94.

Beck, H., Nähse-Kumpf, V., Larsen, M. S., O'Hanlon, K. A., Patzke, S., Holmberg, C., Mejlvang, J., Groth, A., Nielsen, O., Syljuå sen, R. G. and Sø rensen, C. S. (2012). Cyclin-dependent kinase suppression by WEE1 kinase protects the genome through control of replication initiation and nucleotide consumption. Mol. Cell Biol. *32*, 4226–4236.

Begg, A. C., McNally, N. J., Shrieve, D. C. and Kärcher, H. (1985). A method to measure the duration of DNA synthesis and the potential doubling time from a single sample. Cytometry *6*, 620–626.

Berry, W. L. and Janknecht, R. (2013). KDM4/JMJD2 histone demethylases: epigenetic regulators in cancer cells. Cancer Res. *73*, 2936–42.

Bolderson, E., Scorah, J., Helleday, T., Smythe, C. and Meuth, M. (2004). ATM is required for the cellular response to thymidine induced replication fork stress. Hum. Mol. Genet. *13*, 2937–2945.

Bommi-Reddy, A., Almeciga, I., Sawyer, J., Geisen, C., Li, W., Harlow, E., Kaelin, W. G. and Grueneberg, D. A. (2008). Kinase requirements in human cells: III. Altered kinase requirements in VHL-/- cancer cells detected in a pilot synthetic lethal screen. Proc. Natl. Acad. Sci. U.S.A. *105*, 16484–16489.

Bouwman, P. and Jonkers, J. (2012). The effects of deregulated DNA damage signalling on cancer chemotherapy response and resistance. Nat. Rev. Cancer *12*, 587–98.

Bridges, K. A., Hirai, H., Buser, C. A., Brooks, C., Liu, H., Buchholz, T. A., Molkentine, J. M., Mason, K. A. and Meyn, R. E. (2011). MK-1775, a novel wee1 kinase inhibitor, radiosensitizes p53-defective human tumor cells. Clin. Cancer Res. *17*, 5638–5648.

Bryant, H. E., Schultz, N., Thomas, H. D., Parker, K. M., Flower, D., Lopez, E., Kyle, S., Meuth, M., Curtin, N. J. and Helleday, T. (2005). Specific killing of BRCA2-deficient tumours with inhibitors of poly(ADP-ribose) polymerase. Nature *434*, 913–917.

Calvo, E., Chen, V. J., Marshall, M., Ohnmacht, U., Hynes, S. M., Kumm, E., Diaz, H. B., Barnard, D., Merzoug, F. F., Huber, L., Kays, L., Iversen, P.,

Calles, A., Voss, B., Lin, A. B., Dickgreber, N., Wehler, T. and Sebastian, M. (2014). Preclinical analyses and phase I evaluation of LY2603618 administered in combination with Pemetrexed and cisplatin in patients with advanced cancer. Invest. New Drugs *32*, 955–68.

Caretti, V., Hiddingh, L., Lagerweij, T., Schellen, P., Koken, P. W., Hulleman, E., van Vuurden, D. G., Vandertop, W. P., Kaspers, G. J. L., Noske, D. P. and Wurdinger, T. (2013). WEE1 kinase inhibition enhances the radiation response of diffuse intrinsic pontine gliomas. Mol. Cancer Ther. *12*, 141–50.

Carvalho, S., Raposo, A. C., Martins, F. B., Grosso, A. R., Sridhara, S. C., Rino, J., Carmo-Fonseca, M. and De Almeida, S. F. (2013). Histone methyltransferase SETD2 coordinates FACT recruitment with nucleosome dynamics during transcription. Nucleic Acids Res. *41*, 2881–2893.

Carvalho, S., Vítor, A. C., Sridhara, S. C., Martins, F. B., Raposo, A. C., Desterro, J. M., Ferreira, J. and de Almeida, S. F. (2014). SETD2 is required for DNA double-strand break repair and activation of the p53-mediated checkpoint. Elife *3*, e02482.

Chabes, A. and Thelander, L. (2000). Controlled protein degradation regulates ribonucleotide reductase activity in proliferating mammalian cells during the normal cell cycle and in response to DNA damage and replication blocks. J. Biol. Chem. *275*, 17747–17753.

Chabes, A. L., Björklund, S. and Thelander, L. (2004). S Phase-specific transcription of the mouse ribonucleotide reductase R2 gene requires both a proximal repressive E2F-binding site and an upstream promoter activating region. J. Biol. Chem. *279*, 10796–10807.

Chan, D. A. and Giaccia, A. J. (2011). Harnessing synthetic lethal interactions in anticancer drug discovery. Nat. Rev. Drug Discov. *10*, 351–364.

Chen, C. C., Kennedy, R. D., Sidi, S., Look, A. T. and D'Andrea, A. (2009). CHK1 inhibition as a strategy for targeting Fanconi Anemia (FA) DNA repair pathway deficient tumors. Mol. Cancer *8*, 24.

Ciccia, A. and Elledge, S. J. (2010). The DNA damage response: making it safe to play with knives. Mol. Cell *40*, 179–204.

Cimprich, K. A. and Cortez, D. (2008). ATR: an essential regulator of genome integrity. Nat. Rev. Mol. Cell Biol. *9*, 616–627.

Dalgliesh, G. L., Furge, K., Greenman, C., Chen, L., Bignell, G., Butler, A., Davies, H., Edkins, S., Hardy, C., Latimer, C., Teague, J., Andrews, J., Barthorpe, S., Beare, D., Buck, G., Campbell, P. J., Forbes, S., Jia, M., Jones,

D., Knott, H., Kok, C. Y., Lau, K. W., Leroy, C., Lin, M. L., McBride, D. J., Maddison, M., Maguire, S., McLay, K., Menzies, A., Mironenko, T., Mulderrig, L., Mudie, L., O'Meara, S., Pleasance, E., Rajasingham, A., Shepherd, R., Smith, R., Stebbings, L., Stephens, P., Tang, G., Tarpey, P. S., Turrell, K., Dykema, K. J., Khoo, S. K., Petillo, D., Wondergem, B., Anema, J., Kahnoski, R. J., Teh, B. T., Stratton, M. R. and Futreal, P. A. (2010). Systematic sequencing of renal carcinoma reveals inactivation of histone modifying genes. Nature *463*, 360–363.

D'Angiolella, V., Donato, V., Forrester, F. M., Jeong, Y. T., Pellacani, C., Kudo, Y., Saraf, A., Florens, L., Washburn, M. P. and Pagano, M. (2012). Cyclin F-mediated degradation of ribonucleotide reductase M2 controls genome integrity and DNA repair. Cell *149*, 1023–1034.

Daugaard, M., Baude, A., Fugger, K., Povlsen, L. K., Beck, H., Sø rensen, C. S., Petersen, N. H. T., Sorensen, P. H. B., Lukas, C., Bartek, J., Lukas, J., Rohde, M. and Jäättelä, M. (2012). LEDGF (p75) promotes DNA-end resection and homologous recombination. Nat. Struct. Mol. Biol. *19*, 803–10.

David, S. S., O'Shea, V. L. and Kundu, S. (2007). Base-excision repair of oxidative DNA damage. Nature *447*, 941–950.

de Haro, L. P., Wray, J., Williamson, E. A., Durant, S. T., Corwin, L., Gentry, A. C., Osheroff, N., Lee, S. H., Hromas, R. and Nickoloff, J. A. (2010). Metnase promotes restart and repair of stalled and collapsed replication forks. Nucleic Acids Res. *38*, 5681–5691.

DeGregori, J., Kowalik, T. and Nevins, J. R. (1995). Cellular targets for activation by the E2F1 transcription factor include DNA synthesis- and G1/S-regulatory genes. Mol. Cell Biol. *15*, 4215–4224.

Do, K., Doroshow, J. H. and Kummar, S. (2013). Wee1 kinase as a target for cancer therapy. Cell Cycle *12*, 3159–64.

Duns, G., van den Berg, E., van Duivenbode, I., Osinga, J., Hollema, H., Hofstra, R. M. and Kok, K. (2010). Histone methyltransferase gene SETD2 is a novel tumor suppressor gene in clear cell renal cell carcinoma. Cancer Res. *70*, 4287–4291.

Edmunds, J. W., Mahadevan, L. C. and Clayton, A. L. (2008). Dynamic histone H3 methylation during gene induction: HYPB/Setd2 mediates all H3K36 trimethylation. EMBO J *27*, 406–420.

Eidahl, J. O., Crowe, B. L., North, J. A., McKee, C. J., Shkriabai, N., Feng, L., Plumb, M., Graham, R. L., Gorelick, R. J., Hess, S., Poirier, M. G., Foster,

M. P. and Kvaratskhelia, M. (2013). Structural basis for high-affinity binding of LEDGF PWWP to mononucleosomes. Nucleic Acids Res. *41*, 3924–3936.

Esashi, F., Christ, N., Gannon, J., Liu, Y., Hunt, T., Jasin, M. and West, S. C. (2005). CDK-dependent phosphorylation of BRCA2 as a regulatory mechanism for recombinational repair. Nature *434*, 598–604.

Farmer, H., McCabe, N., Lord, C. J., Tutt, A. N. J., Johnson, D. A., Richardson, T. B., Santarosa, M., Dillon, K. J., Hickson, I., Knights, C., Martin, N. M. B., Jackson, S. P., Smith, G. C. M. and Ashworth, A. (2005). Targeting the DNA repair defect in BRCA mutant cells as a therapeutic strategy. Nature *434*, 917–921.

Fenech, M. and Crott, J. W. (2002). Micronuclei, nucleoplasmic bridges and nuclear buds induced in folic acid deficient human lymphocytes - Evidence for breakage-fusion-bridge cycles in the cytokinesis-block micronucleus assay. Mutat. Res. *504*, 131–136.

Fnu, S., Williamson, E. A., De Haro, L. P., Brenneman, M., Wray, J., Shaheen, M., Radhakrishnan, K., Lee, S. H., Nickoloff, J. A. and Hromas, R. (2011). Methylation of histone H3 lysine 36 enhances DNA repair by nonhomologous end-joining. Proc. Natl. Acad. Sci. U.S.A. *108*, 540–545.

Fontebasso, A. M., Schwartzentruber, J., Khuong-Quang, D. A., Liu, X. Y., Sturm, D., Korshunov, A., Jones, D. T., Witt, H., Kool, M., Albrecht, S., Fleming, A., Hadjadj, D., Busche, S., Lepage, P., Montpetit, A., Staffa, A., Gerges, N., Zakrzewska, M., Zakrzewski, K., Liberski, P. P., Hauser, P., Garami, M., Klekner, A., Bognar, L., Zadeh, G., Faury, D., Pfister, S. M., Jabado, N. and Majewski, J. (2013). Mutations in SETD2 and genes affecting histone H3K36 methylation target hemispheric high-grade gliomas. Acta Neuropathol. *125*, 659–669.

Franken, N. A., Rodermond, H. M., Stap, J., Haveman, J. and van Bree, C. (2006). Clonogenic assay of cells in vitro. Nat. Protoc. *1*, 2315–2319.

Gao, Y. G., Yang, H., Zhao, J., Jiang, Y. J. and Hu, H. Y. (2014). Autoinhibitory structure of the WW domain of HYPB/SETD2 regulates its interaction with the proline-rich region of huntingtin. Structure *22*, 378–386.

Gerlinger, M., Rowan, A. J., Horswell, S., Larkin, J., Endesfelder, D., Gronroos, E., Martinez, P., Matthews, N., Stewart, A., Tarpey, P., Varela, I., Phillimore, B., Begum, S., McDonald, N. Q., Butler, A., Jones, D., Raine, K., Latimer, C., Santos, C. R., Nohadani, M., Eklund, A. C., Spencer-Dene, B., Clark, G., Pickering, L., Stamp, G., Gore, M., Szallasi, Z., Downward, J., Futreal, P. A. and Swanton, C. (2012). Intratumor heterogeneity and branched evolution revealed by multiregion sequencing. N. Engl. J. Med. *366*, 883–892.

Grant, G. D., Brooks, L., Zhang, X., Mahoney, J. M., Martyanov, V., Wood, T. A., Sherlock, G., Cheng, C. and Whitfield, M. L. (2013). Identification of cell cycle-regulated genes periodically expressed in U2OS cells and their regulation by FOXM1 and E2F transcription factors. Mol. Biol. Cell *24*, 3634–3650.

Hakimi, A. A., Chen, Y. B., Wren, J., Gonen, M., Abdel-Wahab, O., Heguy, A., Liu, H., Takeda, S., Tickoo, S. K., Reuter, V. E., Voss, M. H., Motzer, R. J., Coleman, J. A., Cheng, E. H., Russo, P. and Hsieh, J. J. (2013). Clinical and Pathologic Impact of Select Chromatin-modulating Tumor Suppressors in Clear Cell Renal Cell Carcinoma. Eur. Urol. *63*, 848–854.

Hanada, K., Budzowska, M., Davies, S. L., van Drunen, E., Onizawa, H., Beverloo, H. B., Maas, A., Essers, J., Hickson, I. D. and Kanaar, R. (2007). The structure-specific endonuclease Mus81 contributes to replication restart by generating double-strand DNA breaks. Nat. Struct. Mol. Biol. *14*, 1096–1104.

Hanahan, D. and Weinberg, R. A. (2011). Hallmarks of cancer: the next generation. Cell *144*, 646–74.

Hartlerode, A. J. and Scully, R. (2009). Mechanisms of double-strand break repair in somatic mammalian cells. Biochem. J. *423*, 157–168.

Helleday, T. (2011). The underlying mechanism for the PARP and BRCA synthetic lethality: clearing up the misunderstandings. Mol. Oncol. *5*, 387–93.

Hirai, H., Arai, T., Okada, M., Nishibata, T., Kobayashi, M., Sakai, N., Imagaki, K., Ohtani, J., Sakai, T., Yoshizumi, T., Mizuarai, S., Iwasawa, Y. and Kotani, H. (2010). MK-1775, a small molecule Wee1 inhibitor, enhances anti-tumor efficacy of various DNA-damaging agents, including 5-fluorouracil. Cancer Biol. Ther. *9*, 514–522.

Hochegger, H., Dejsuphong, D., Fukushima, T., Morrison, C., Sonoda, E., Schreiber, V., Zhao, G. Y., Saberi, A., Masutani, M., Adachi, N., Koyama, H., de Murcia, G. and Takeda, S. (2006). Parp-1 protects homologous recombination from interference by Ku and Ligase IV in vertebrate cells. EMBO J *25*, 1305–1314.

Hu, M., Sun, X. J., Zhang, Y. L., Kuang, Y., Hu, C. Q., Wu, W. L., Shen, S. H., Du, T. T., Li, H., He, F., Xiao, H. S., Wang, Z. G., Liu, T. X., Lu, H., Huang, Q. H., Chen, S. J. and Chen, Z. (2010). Histone H3 lysine 36 methyltransferase Hypb/Setd2 is required for embryonic vascular remodeling. Proc. Natl. Acad. Sci. U.S.A. *107*, 2956–2961.

Huen, M. S. Y., Sy, S. M. H. and Chen, J. (2010). BRCA1 and its toolbox for the maintenance of genome integrity. Nat. Rev. Mol. Cell Biol. *11*, 138–148.

Huntoon, C. J., Flatten, K. S., Wahner Hendrickson, A. E., Huehls, A. M., Sutor, S. L., Kaufmann, S. H. and Karnitz, L. M. (2013). ATR inhibition broadly sensitizes ovarian cancer cells to chemotherapy independent of BRCA status. Cancer Res. *73*, 3683–3691.

Iacovoni, J. S., Caron, P., Lassadi, I., Nicolas, E., Massip, L., Trouche, D. and Legube, G. (2010). High-resolution profiling of gammaH2AX around DNA double strand breaks in the mammalian genome. EMBO J *29*, 1446–1457.

Ibragimova, I., Maradeo, M. E., Dulaimi, E. and Cairns, P. (2013). Aberrant promoter hypermethylation of PBRM1, BAP1, SETD2, KDM6A and other chromatin-modifying genes is absent or rare in clear cell RCC. Epigenetics *8*, 486–493.

Jackson, S. P. and Bartek, J. (2010). The DNA-damage response in human biology and disease. Nature *461*, 1071–1078.

Jamburuthugoda, V. K., Santos-Velazquez, J. M., Skasko, M., Operario, D. J., Purohit, V., Chugh, P., Szymanski, E. A., Wedekind, J. E., Bambara, R. A. and Kim, B. (2008). Reduced dNTP binding affinity of 3TC-resistant M184I HIV-1 reverse transcriptase variants responsible for viral infection failure in macrophage. J. Biol. Chem. *283*, 9206–9216.

Jeggo, P. and Lavin, M. F. (2009). Cellular radiosensitivity: how much better do we understand it? Int. J. Radiat. Biol. *85*, 1061–1081.

Jha, D. K., Pfister, S. X., Humphrey, T. C. and Strahl, B. D. (2014). SET-ting the stage for DNA repair. Nat. Struct. Mol. Biol. *21*, 655–657.

Jha, D. K. and Strahl, B. D. (2014). An RNA polymerase II-coupled function for histone H3K36 methylation in checkpoint activation and DSB repair. Nat. Commun. *5*, 3965.

Jiricny, J. (2006). The multifaceted mismatch-repair system. Nat. Rev. Mol. Cell Biol. *7*, 335–346.

Johnson, D. G., Schwarz, J. K., Cress, W. D. and Nevins, J. R. (1993). Expression of transcription factor E2F1 induces quiescent cells to enter S phase. Nature *365*, 349–352.

Klose, R. J., Yamane, K., Bae, Y., Zhang, D., Erdjument-Bromage, H., Tempst, P., Wong, J. and Zhang, Y. (2006). The transcriptional repressor JHDM3A demethylates trimethyl histone H3 lysine 9 and lysine 36. Nature *442*, 312–316.

Koç, A., Wheeler, L. J., Mathews, C. K. and Merrill, G. F. (2004). Hydroxyurea Arrests DNA Replication by a Mechanism that Preserves Basal dNTP Pools. J. Biol. Chem. *279*, 223–230.

Kohn, E. A., Yoo, C. J. and Eastman, A. (2003). The protein kinase C inhibitor Gö6976 is a potent inhibitor of DNA damage-induced S and G2 cell cycle checkpoints. Cancer Res. *63*, 31–35.

Krajewska, M., Heijink, a. M., Bisselink, Y. J. W. M., Seinstra, R. I., Silljé, H. H. W., de Vries, E. G. E. and van Vugt, M. a. T. M. (2013). Forced activation of Cdk1 via wee1 inhibition impairs homologous recombination. Oncogene *32*, 3001–8.

Lawrence, M. S., Stojanov, P., Mermel, C. H., Robinson, J. T., Garraway, L. A., Golub, T. R., Meyerson, M., Gabriel, S. B., Lander, E. S. and Getz, G. (2014). Discovery and saturation analysis of cancer genes across 21 tumour types. Nature *505*, 495–501.

Ledermann, J., Harter, P., Gourley, C., Friedlander, M., Vergote, I., Rustin, G., Scott, C. L., Meier, W., Shapira-Frommer, R., Safra, T., Matei, D., Fielding, A., Spencer, S., Dougherty, B., Orr, M., Hodgson, D., Barrett, J. C. and Matulonis, U. (2014). Olaparib maintenance therapy in patients with platinum-sensitive relapsed serous ovarian cancer: A preplanned retrospective analysis of outcomes by BRCA status in a randomised phase 2 trial. Lancet Oncol. *15*, 852–861.

Lehman, C. W. and Carroll, D. (1991). Homologous recombination catalyzed by a nuclear extract from Xenopus oocytes. Proc. Natl. Acad. Sci. U.S.A. *88*, 10840–10844.

Lewis, P. W., Müller, M. M., Koletsky, M. S., Cordero, F., Lin, S., Banaszynski, L. A., Garcia, B. A., Muir, T. W., Becher, O. J. and Allis, C. D. (2013). Inhibition of PRC2 activity by a gain-of-function H3 mutation found in pediatric glioblastoma. Science *340*, 857–861.

Li, B., Jackson, J., Simon, M. D., Fleharty, B., Gogol, M., Seidel, C., Workman, J. L. and Shilatifard, A. (2009). Histone H3 lysine 36 dimethylation (H3K36me2) is sufficient to recruit the Rpd3s Histone deacetylase complex and to repress spurious transcription. J. Biol. Chem. *284*, 7970–7976.

Li, F., Mao, G., Tong, D., Huang, J., Gu, L., Yang, W. and Li, G. M. (2013). The histone mark H3K36me3 regulates human DNA mismatch repair through its interaction with MutSα. Cell *153*, 590–600.

Li, M., Phatnani, H. P., Guan, Z., Sage, H., Greenleaf, A. L. and Zhou, P. (2005). Solution structure of the Set2-Rpb1 interacting domain of human Set2 and its interaction with the hyperphosphorylated C-terminal domain of Rpb1. Proc. Natl. Acad. Sci. U.S.A. *102*, 17636–17641.

Lieber, M. R. (2010). The mechanism of double-strand DNA break repair by the nonhomologous DNA end-joining pathway. Annu. Rev. Biochem. *79*, 181–211.

Liu, S., Opiyo, S. O., Manthey, K., Glanzer, J. G., Ashley, A. K., Amerin, C., Troksa, K., Shrivastav, M., Nickoloff, J. A. and Oakley, G. G. (2012a). Distinct roles for DNA-PK, ATM and ATR in RPA phosphorylation and checkpoint activation in response to replication stress. Nucleic Acids Res. *40*, 10780–10794.

Liu, X., Shi, Y., Maag, D. X., Palma, J. P., Patterson, M. J., Ellis, P. A., Surber, B. W., Ready, D. B., Soni, N. B., Ladror, U. S., Xu, A. J., Iyer, R., Harlan, J. E., Solomon, L. R., Donawho, C. K., Penning, T. D., Johnson, E. F. and Shoemaker, A. R. (2012b). Iniparib nonselectively modifies cysteine-containing proteins in tumor cells and is not a Bona Fide PARP inhibitor. Clin. Cancer Res. *18*, 510–523.

Loeb, L. A. and Monnat, R. J. (2008). DNA polymerases and human disease. Nat. Rev. Genet. *9*, 594–604.

Lucio-Eterovic, A. K., Singh, M. M., Gardner, J. E., Veerappan, C. S., Rice, J. C. and Carpenter, P. B. (2010). Role for the nuclear receptor-binding SET domain protein 1 (NSD1) methyltransferase in coordinating lysine 36 methylation at histone 3 with RNA polymerase II function. Proc. Natl. Acad. Sci. U.S.A. *107*, 16952–16957.

Lundin, C., Schultz, N., Arnaudeau, C., Mohindra, A., Hansen, L. T. and Helleday, T. (2003). RAD51 is involved in repair of damage associated with DNA replication in mammalian cells. J. Mol. Biol. *328*, 521–535.

Mahaney, B. L., Meek, K. and Lees-Miller, S. P. (2009). Repair of ionizing radiation-induced DNA double-strand breaks by non-homologous end-joining. Biochem. J. *417*, 639–650.

Martín, Y., Domínguez-Kelly, R. and Freire, R. (2011). Novel insights into maintaining genomic integrity: Wee1 regulating Mus81/Eme1. Cell Div. *6*, 21.

Mateo, J., Ong, M., Tan, D. S. P., Gonzalez, M. a. and de Bono, J. S. (2013). Appraising iniparib, the PARP inhibitor that never was–what must we learn? Nat. Rev. Clin. Oncol. *10*, 688–96.

Matsuoka, S., Ballif, B. A., Smogorzewska, A., McDonald, E. R., Hurov, K. E., Luo, J., Bakalarski, C. E., Zhao, Z., Solimini, N., Lerenthal, Y., Shiloh, Y., Gygi, S. P. and Elledge, S. J. (2007). ATM and ATR substrate analysis reveals extensive protein networks responsive to DNA damage. Science *316*, 1160–1166.

McGowan, C. H. and Russell, P. (1995). Cell cycle regulation of human WEE1. EMBO J *14*, 2166–2175.

McVey, M. and Lee, S. E. (2008). MMEJ repair of double-strand breaks (director's cut): deleted sequences and alternative endings. Trends Genet. *24*, 529–38.

Meek, K., Dang, V. and Lees-Miller, S. P. (2008). DNA-PK: the means to justify the ends? Adv. Immunol. *99*, 33–58.

Michels, J., Vitale, I., Saparbaev, M., Castedo, M. and Kroemer, G. (2013). Predictive biomarkers for cancer therapy with PARP inhibitors. Oncogene *33*, 3894–3907.

Mordes, D. A. and Cortez, D. (2008). Activation of ATR and related PIKKs. Cell Cycle *7*, 2809–12.

Motycka, T. A., Bessho, T., Post, S. M., Sung, P. and Tomkinson, A. E. (2004). Physical and Functional Interaction between the XPF/ERCC1 Endonuclease and hRad52. J. Biol. Chem. *279*, 13634–13639.

Moynahan, M. E., Cui, T. Y. and Jasin, M. (2001). Homology-directed DNA repair, mitomycin-C resistance, and chromosome stability is restored with correction of a Brca1 mutation. Cancer Res. *61*, 4842–4850.

Nakanishi, K., Taniguchi, T., Ranganathan, V., New, H. V., Moreau, L. A., Stotsky, M., Mathew, C. G., Kastan, M. B., Weaver, D. T. and D'Andrea, A. D. (2002). Interaction of FANCD2 and NBS1 in the DNA damage response. Nat. Cell Biol. *4*, 913–920.

Neshat, M. S., Mellinghoff, I. K., Tran, C., Stiles, B., Thomas, G., Petersen, R., Frost, P., Gibbons, J. J., Wu, H. and Sawyers, C. L. (2001). Enhanced sensitivity of PTEN-deficient tumors to inhibition of FRAP/mTOR. Proc. Natl. Acad. Sci. U.S.A. *98*, 10314–10319.

Newbold, R. F. and Mokbel, K. (2010). Evidence for a tumour suppressor function of SETD2 in human breast cancer: a new hypothesis. Anticancer Res. *30*, 3309–3311.

Nordlund, P. and Reichard, P. (2006). Ribonucleotide reductases. Annu. Rev. Biochem. *75*, 681–706.

Ogiwara, H., Ui, A., Otsuka, A., Satoh, H., Yokomi, I., Nakajima, S., Yasui, A., Yokota, J. and Kohno, T. (2011). Histone acetylation by CBP and p300 at double-strand break sites facilitates SWI/SNF chromatin remodeling and the recruitment of non-homologous end joining factors. Oncogene *30*, 2135–2146.

Olive, P. L. and Banáth, J. P. (2006). The comet assay: a method to measure DNA damage in individual cells. Nat. Protoc. *1*, 23–29.

Origanti, S., Cai, S.-r., Munir, A. Z., White, L. S. and Piwnica-Worms, H. (2012). Synthetic lethality of Chk1 inhibition combined with p53 and/or p21 loss during a DNA damage response in normal and tumor cells. Oncogene *32*, 577–588.

Pai, C. C., Deegan, R. S., Subramanian, L., Gal, C., Sarkar, S., Blaikley, E. J., Walker, C., Hulme, L., Bernhard, E., Codlin, S., Bähler, J., Allshire, R., Whitehall, S. and Humphrey, T. C. (2014). A histone H3K36 chromatin switch coordinates DNA double-strand break repair pathway choice. Nat. Commun. *5*, 4091.

Parker, L. L. and Piwnica-Worms, H. (1992). Inactivation of the p34cdc2-cyclin B complex by the human WEE1 tyrosine kinase. Science *257*, 1955–1957.

Parsons, J. L., Tait, P. S., Finch, D., Dianova, I. I., Edelmann, M. J., Khoronenkova, S. V., Kessler, B. M., Sharma, R. A., McKenna, W. G. and Dianov, G. L. (2009). Ubiquitin ligase ARF-BP1/Mule modulates base excision repair. EMBO J *28*, 3207–3215.

Patel, A. G., De Lorenzo, S. B., Flatten, K. S., Poirier, G. G. and Kaufmann, S. H. (2012). Failure of iniparib to inhibit poly(ADP-ribose) polymerase in vitro. Clin. Cancer Res. *18*, 1655–1662.

Pei, H., Zhang, L., Luo, K., Qin, Y., Chesi, M., Fei, F., Bergsagel, P. L., Wang, L., You, Z. and Lou, Z. (2011). MMSET regulates histone H4K20 methylation and 53BP1 accumulation at DNA damage sites. Nature *470*, 124–128.

Petermann, E. and Helleday, T. (2010). Pathways of mammalian replication fork restart. Nat. Rev. Mol. Cell Biol. *11*, 683–687.

Petermann, E., Orta, M. L., Issaeva, N., Schultz, N. and Helleday, T. (2010). Hydroxyurea-Stalled Replication Forks Become Progressively Inactivated and Require Two Different RAD51-Mediated Pathways for Restart and Repair. Mol. Cell *37*, 492–502.

Pfister, S. X., Ahrabi, S., Zalmas, L. P., Sarkar, S., Aymard, F., Bachrati, C. Z., Helleday, T., Legube, G., La Thangue, N. B., Porter, A. C. and Humphrey, T. C. (2014). SETD2-Dependent Histone H3K36 Trimethylation Is Required for Homologous Recombination Repair and Genome Stability. Cell Rep. *7*, 2006–2018.

Pierce, A. J., Johnson, R. D., Thompson, L. H. and Jasin, M. (1999). XRCC3 promotes homology-directed repair of DNA damage in mammalian cells. Genes Dev. *13*, 2633–2638.

Pires, I. M., Olcina, M. M., Anbalagan, S., Pollard, J. R., Reaper, P. M., Charlton, P. a., McKenna, W. G. and Hammond, E. M. (2012). Targeting radiation-resistant hypoxic tumour cells through ATR inhibition. Br. J. Cancer *107*, 291–9.

Prevo, R., Fokas, E., Reaper, P. M., Charlton, P. A., Pollard, J. R., McKenna, W. G., Muschel, R. J. and Brunner, T. B. (2012). The novel ATR inhibitor VE-821 increases sensitivity of pancreatic cancer cells to radiation and chemotherapy. Cancer Biol. Ther. *13*, 1072–1081.

Pryde, F., Jain, D., Kerr, A., Curley, R., Mariotti, F. R. and Vogelauer, M. (2009). H3 k36 methylation helps determine the timing of cdc45 association with replication origins. PLoS One *4*, e5882.

Puyol, M., Martín, A., Dubus, P., Mulero, F., Pizcueta, P., Khan, G., Guerra, C., Santamaría, D. and Barbacid, M. (2010). A Synthetic Lethal Interaction between K-Ras Oncogenes and Cdk4 Unveils a Therapeutic Strategy for Non-small Cell Lung Carcinoma. Cancer Cell *18*, 63–73.

Rea, S., Eisenhaber, F., O'Carroll, D., Strahl, B. D., Sun, Z. W., Schmid, M., Opravil, S., Mechtler, K., Ponting, C. P., Allis, C. D. and Jenuwein, T. (2000). Regulation of chromatin structure by site-specific histone H3 methyltransferases. Nature *406*, 593–599.

Reaper, P. M., Griffiths, M. R., Long, J. M., Charrier, J.-D., Maccormick, S., Charlton, P. A., Golec, J. M. C. and Pollard, J. R. (2011). Selective killing of ATM- or p53-deficient cancer cells through inhibition of ATR. Nat. Chem. Biol. *7*, 428–430.

Regairaz, M., Zhang, Y. W., Fu, H., Agama, K. K., Tata, N., Agrawal, S., Aladjem, M. I. and Pommier, Y. (2011). Mus81-mediated DNA cleavage resolves replication forks stalled by topoisomerase I-DNA complexes. J. Cell. Biol. *195*, 739–749.

Rodriguez, R. and Meuth, M. (2006). Chk1 and p21 cooperate to prevent apoptosis during DNA replication fork stress. Mol. Biol. Cell *17*, 402–412.

Sarcar, B., Kahali, S., Prabhu, A. H., Shumway, S. D., Xu, Y., Demuth, T. and Chinnaiyan, P. (2011). Targeting radiation-induced G(2) checkpoint activation with the Wee-1 inhibitor MK-1775 in glioblastoma cell lines. Mol. Cancer Ther. *10*, 2405–14.

Sartori, A. A., Lukas, C., Coates, J., Mistrik, M., Fu, S., Bartek, J., Baer, R., Lukas, J. and Jackson, S. P. (2007). Human CtIP promotes DNA end resection. Nature *450*, 509–514.

Sato, Y., Yoshizato, T., Shiraishi, Y., Maekawa, S., Okuno, Y., Kamura, T., Shimamura, T., Sato-Otsubo, A., Nagae, G., Suzuki, H., Nagata, Y., Yoshida, K., Kon, A., Suzuki, Y., Chiba, K., Tanaka, H., Niida, A., Fujimoto, A., Tsunoda, T., Morikawa, T., Maeda, D., Kume, H., Sugano, S., Fukayama, M., Aburatani, H., Sanada, M., Miyano, S., Homma, Y. and Ogawa, S. (2013). Integrated molecular analysis of clear-cell renal cell carcinoma. Nat. Genet. *45*, 860–7.

Shaheen, M., Williamson, E., Nickoloff, J., Lee, S.-H. and Hromas, R. (2010). Metnase/SETMAR: a domesticated primate transposase that enhances DNA repair, replication, and decatenation. Genetica *138*, 559–66.

Shanbhag, N. M., Rafalska-Metcalf, I. U., Balane-Bolivar, C., Janicki, S. M. and Greenberg, R. A. (2010). ATM-Dependent chromatin changes silence transcription in cis to dna double-strand breaks. Cell *141*, 970–981.

Sherman, P. A. and Fyfe, J. A. (1989). Enzymatic assay for deoxyribonucleoside triphosphates using synthetic oligonucleotides as template primers. Anal. Biochem. *180*, 222–226.

Shimada, M., Niida, H., Zineldeen, D. H., Tagami, H., Tanaka, M., Saito, H. and Nakanishi, M. (2008). Chk1 Is a Histone H3 Threonine 11 Kinase that Regulates DNA Damage-Induced Transcriptional Repression. Cell *132*, 221–232.

Shimura, T., Torres, M. J., Martin, M. M., Rao, V. A., Pommier, Y., Katsura, M., Miyagawa, K. and Aladjem, M. I. (2008). Bloom's syndrome helicase and Mus81 are required to induce transient double-strand DNA breaks in response to DNA replication stress. J. Mol. Biol. *375*, 1152–1164.

Simsek, D., Brunet, E., Wong, S. Y. W., Katyal, S., Gao, Y., McKinnon, P. J., Lou, J., Zhang, L., Li, J., Rebar, E. J., Gregory, P. D., Holmes, M. C. and Jasin, M. (2011). DNA ligase III promotes alternative nonhomologous end-joining during chromosomal translocation formation. PLoS Genet. *7*.

Sirbu, B. M., Couch, F. B. and Cortez, D. (2012). Monitoring the spatiotemporal dynamics of proteins at replication forks and in assembled chromatin using isolation of proteins on nascent DNA. Nat. Protoc. *7*, 594–605.

Sirbu, B. M., Couch, F. B., Feigerle, J. T., Bhaskara, S., Hiebert, S. W. and Cortez, D. (2011). Analysis of protein dynamics at active, stalled, and collapsed replication forks. Genes Dev. *25*, 1320–1327.

Smeenk, G. and van Attikum, H. (2013). The chromatin response to DNA breaks: leaving a mark on genome integrity. Annu. Rev. Biochem. *82*, 55–80.

Sø rensen, C. S. and Syljuå sen, R. G. (2012). Safeguarding genome integrity: The checkpoint kinases ATR, CHK1 and WEE1 restrain CDK activity during normal DNA replication. Nucleic Acids Res. *40*, 477–486.

Strahl, B. D., Grant, P. A., Briggs, S. D., Sun, Z.-W., Bone, J. R., Caldwell, J. A., Mollah, S., Cook, R. G., Shabanowitz, J., Hunt, D. F. and Allis, C. D. (2002). Set2 is a nucleosomal histone H3-selective methyltransferase that mediates transcriptional repression. Mol. Cell Biol. *22*, 1298–1306.

Sun, X. J., Wei, J., Wu, X. Y., Hu, M., Wang, L., Wang, H. H., Zhang, Q. H., Chen, S. J., Huang, Q. H. and Chen, Z. (2005). Identification and characterization of a novel human histone H3 lysine 36-specific methyltransferase. J. Biol. Chem. *280*, 35261–35271.

Suzuki, K., Yamauchi, M., Oka, Y., Suzuki, M. and Yamashita, S. (2011). Creating localized DNA double-strand breaks with microirradiation. Nat. Protoc. *6*, 134–139.

Thompson, R., Meuth, M., Wol, P., Zhu, Y. and Danson, S. (2012). Treatment with the Chk1 inhibitor Gö6976 enhances cisplatin cytotoxicity in SCLC cells. Int. J. Oncol. *40*, 194–202.

Toledo, L. I., Murga, M., Zur, R., Soria, R., Rodriguez, A., Martinez, S., Oyarzabal, J., Pastor, J., Bischoff, J. R. and Fernandez-Capetillo, O. (2011). A cell-based screen identifies ATR inhibitors with synthetic lethal properties for cancer-associated mutations. Nat. Struct. Mol. Biol. *18*, 721–727.

Van Linden, A. a., Baturin, D., Ford, J. B., Fosmire, S. P., Gardner, L., Korch, C., Reigan, P. and Porter, C. C. (2013). Inhibition of Wee1 sensitizes cancer cells to antimetabolite chemotherapeutics in vitro and in vivo, independent of p53 functionality. Mol. Cancer. Ther. *12*, 2675–84.

Venkatesh, S. and Workman, J. L. (2013). Set2 mediated H3 lysine 36 methylation: regulation of transcription elongation and implications in organismal development. Wiley Interdiscip. Rev. Dev. Biol. *2*, 685–700.

Vermeulen, M., Eberl, H. C., Matarese, F., Marks, H., Denissov, S., Butter, F., Lee, K. K., Olsen, J. V., Hyman, A. A., Stunnenberg, H. G. and Mann, M. (2010). Quantitative interaction proteomics and genome-wide profiling of epigenetic histone marks and their readers. Cell *142*, 967–980.

Wagner, E. J. and Carpenter, P. B. (2012). Understanding the language of Lys36 methylation at histone H3. Nat. Rev. Mol. Cell Biol. *13*, 115–126.

Wang, M., Wu, W., Wu, W., Rosidi, B., Zhang, L., Wang, H. and Iliakis, G. (2006). PARP-1 and Ku compete for repair of DNA double strand breaks by distinct NHEJ pathways. Nucleic Acids Res. *34*, 6170–6182.

Weiss, G. J., Donehower, R. C., Iyengar, T., Ramanathan, R. K., Lewandowski, K., Westin, E., Hurt, K., Hynes, S. M., Anthony, S. P. and McKane, S. (2013). Phase I dose-escalation study to examine the safety and tolerability of LY2603618, a checkpoint 1 kinase inhibitor, administered 1 day after pemetrexed 500 mg/m(2) every 21 days in patients with cancer. Invest. New Drugs *31*, 136–44.

Wells, J., Graveel, C. R., Bartley, S. M., Madore, S. J. and Farnham, P. J. (2002). The identification of E2F1-specific target genes. Proc. Natl. Acad. Sci. U.S.A. *99*, 3890–3895.

Whetstine, J. R., Nottke, A., Lan, F., Huarte, M., Smolikov, S., Chen, Z., Spooner, E., Li, E., Zhang, G., Colaiacovo, M. and Shi, Y. (2006). Reversal of Histone Lysine Trimethylation by the JMJD2 Family of Histone Demethylases. Cell *125*, 467–481.

Williams, R. S., Williams, J. S. and Tainer, J. A. (2007). Mre11-Rad50-Nbs1 is a keystone complex connecting DNA repair machinery, double-strand break signaling, and the chromatin template. Biochem. Cell Biol. *85*, 509–520.

Wojewódzka, M., Buraczewska, I. and Kruszewski, M. (2002). A modified neutral comet assay: Elimination of lysis at high temperature and validation of the assay with anti-single-stranded DNA antibody. Mutat. Res. *518*, 9–20.

Wold, M. S. (1997). Replication protein A: a heterotrimeric, single-stranded DNA-binding protein required for eukaryotic DNA metabolism. Annu. Rev. Biochem. *66*, 61–92.

Xie, L., Pelz, C., Wang, W., Bashar, A., Varlamova, O., Shadle, S. and Impey, S. (2011). KDM5B regulates embryonic stem cell self-renewal and represses cryptic intragenic transcription. EMBO J *30*, 1473–1484.

Xie, P., Tian, C., An, L., Nie, J., Lu, K., Xing, G., Zhang, L. and He, F. (2008). Histone methyltransferase protein SETD2 interacts with p53 and selectively regulates its downstream genes. Cell Signal *20*, 1671–1678.

Yang, H., Ye, D., Guan, K. L. and Xiong, Y. (2012). IDH1 and IDH2 mutations in tumorigenesis: Mechanistic insights and clinical perspectives. Clin. Cancer Res. *18*, 5562–5571.

You, Z. and Bailis, J. M. (2010). DNA damage and decisions: CtIP coordinates DNA repair and cell cycle checkpoints. Trends Cell Biol. *20*, 402–409.

Yun, M. H. and Hiom, K. (2009). CtIP-BRCA1 modulates the choice of DNA double-strand-break repair pathway throughout the cell cycle. Nature *459*, 460–463.

Zalmas, L. P., Coutts, A. S., Helleday, T. and Thangue, N. B. L. (2013). E2F-7 couples DNA damage-dependent transcription with the DNA repair process. Cell Cycle *12*, 3037–3051.

Zhang, J., Ding, L., Holmfeldt, L., Wu, G., Heatley, S. L., Payne-Turner, D., Easton, J., Chen, X., Wang, J., Rusch, M., Lu, C., Chen, S. C., Wei, L., Collins-Underwood, J. R., Ma, J., Roberts, K. G., Pounds, S. B., Ulyanov, A., Becksfort, J., Gupta, P., Huether, R., Kriwacki, R. W., Parker, M., McGoldrick, D. J., Zhao, D., Alford, D., Espy, S., Bobba, K. C., Song, G., Pei, D., Cheng, C., Roberts, S., Barbato, M. I., Campana, D., Coustan-Smith, E., Shurtleff, S. A., Raimondi, S. C., Kleppe, M., Cools, J., Shimano, K. A., Hermiston, M. L., Doulatov, S., Eppert, K., Laurenti, E., Notta, F., Dick, J. E., Basso, G., Hunger, S. P., Loh, M. L., Devidas, M., Wood, B., Winter, S., Dunsmore, K. P., Fulton, R. S., Fulton, L. L., Hong, X., Harris, C. C., Dooling, D. J., Ochoa, K., Johnson, K. J., Obenauer, J. C., Evans, W. E., Pui, C. H., Naeve, C. W., Ley, T. J., Mardis, E. R., Wilson, R. K., Downing, J. R. and Mullighan, C. G. (2012). The genetic basis of early T-cell precursor acute lymphoblastic leukaemia. Nature *481*, 157–163.

Zhang, Y., Xie, S., Zhou, Y., Xie, Y., Liu, P., Sun, M., Xiao, H., Jin, Y., Sun, X., Chen, Z., Huang, Q. and Chen, S. (2014). H3K36 Histone Methyltransferase Setd2 Is Required for Murine Embryonic Stem Cell Differentiation toward Endoderm. Cell Rep. *8*, 1989–2002.

Zheng, W., Ibáñez, G., Wu, H., Blum, G., Zeng, H., Dong, A., Li, F., Hajian, T., Allali-Hassani, A., Amaya, M. F., Siarheyeva, A., Yu, W., Brown, P. J., Schapira, M., Vedadi, M., Min, J. and Luo, M. (2012). Sinefungin derivatives as inhibitors and structure probes of protein lysine methyltransferase SETD2. J. Am. Chem. Soc. *134*, 18004–18014.

Zhou, Y., Caron, P., Legube, G. and Paull, T. T. (2014). Quantitation of DNA double-strand break resection intermediates in human cells. Nucleic Acids Res. *42*.

Zhu, X., He, F., Zeng, H., Ling, S., Chen, A., Wang, Y., Yan, X., Wei, W., Pang, Y., Cheng, H., Hua, C., Zhang, Y., Yang, X., Lu, X., Cao, L., Hao, L., Dong, L., Zou, W., Wu, J., Li, X., Zheng, S., Yan, J., Zhou, J., Zhang, L., Mi, S., Wang, X., Zhang, L., Zou, Y., Chen, Y., Geng, Z., Wang, J., Zhou, J., Liu, X., Wang, J., Yuan, W., Huang, G., Cheng, T. and Wang, Q.-F. (2014). Identification of functional cooperative mutations of SETD2 in human acute leukemia. Nat. Genet. *46*, 287–93.

Zou, L. and Elledge, S. J. (2003). Sensing DNA damage through ATRIP recognition of RPA-ssDNA complexes. Science *300*, 1542–1548.